AN INVESTIGATION OF THE HIGH PRESSURE ELECTRODELESS ARC IN AIR

DONALD D. HOLLISTER

Aeronutronic Division
Philco-Ford Corporation

Foreword

This report was prepared by the Aeronutronic Division of the Philco-Ford Corporation under USAF contract No. F33(615)-68C-1137.

The report summarizes the results of the work conducted from November 1967 to November 1968.

The original manuscript was submitted to the Air Force Flight Dynamics Laboratory in November 1968 under Philco-Ford Corporation publication number U-4484.

Mr. Donald D. Holister served as the principal investigator.

It is a pleasure to acknowledge the contributions of several colleagues to this work. The appendix on the hydromagnetic interaction was prepared in close collaboration with Dr. Paul G. Thiene, with whom many fruitful discussions of the phenomenology of the electrodeless arc were also held. Mr. Anthony F. Dugan supervised most of the numerical analysis. The programming was ably begun by Mr. Saul Kravitz and later completed by Mr. Lawrence Shultz, who also provided the useful machine plots of Appendix VI.

Several illuminating conversations with Dr. D. A. Cohen and Mr. Robert S. Wright cast the treatment of the radiation from the electrodeless arc into its present form. Recognition is due Dr. D. C. Garwood, without whose encouragement this study would never have been possible.

Special thanks are due Lt. Col. Donald Harney, USAF (Ret.), who provided exceptional guidance during the early phase of this study and who was always available for discussion of the many problems which arose during the study.

The Air Force Flight Dynamics Laboratory (FDMT) Project Engineer was Mr. Lawrence A. Walchli whose direction made a signal contribution to the scope and comprehensiveness of this work.

This Technical Report has been reviewed and is approved.

Philip P Antonatos

PHILIP P. ANTONATOS
Chief, Flight Mechanics Division
Air Force Flight Dynamics Laboratory

ABSTRACT

The equation of energy balance for the high pressure electrodeless arc in air is numerically integrated and agreement with the Thomson Eddy Current theory is found. Scaling laws are derived for purposes of engineering analysis and design. Conceptual designs for high pressure electrodeless and DC arc heaters are compared at the fifty megawatt level in a flowing plasma system. The electrodeless technique is found to be somewhat more efficient than the DC technique in this comparison.

CONTENTS

CONTENTS (Contd.)

CONTENTS

ILLUSTRATIONS

ILLUSTRATIONS (Contd.)

SECTION I

INTRODUCTION

A. PROGRAM OBJECTIVE AND SUMMARY OF RESULTS

The objective of this program is to determine the feasibility of utilizing RF (electrodeless) discharges to generate the reservoir conditions necessary for hyperenvironmental gas-dynamic test facilities, and to determine if the predicted performance of the electrodeless discharge significantly exceeds that of DC arc heaters.

In this study the equation of energy balance in an electrodeless arc was derived from the basic hydromagnetic conservation laws. Local thermodynamic equilibrium was shown to hold for the electrodeless arc in high pressure air. The effects on the discharge of the axial electric field of the induction solenoid were analyzed and shown to be of negligible importance in determining the overall energy balance within the discharge, and the Coulomb gauge was chosen only after a rigorous analysis.

Flow effects were treated in an argument based on the thermodynamics of irreversible processes in ionized gases. It was shown that the main effect of flow through a quasi-steady-state electrodeless arc was an enhanced power requirement that was proportional to the rate of weight flow. A possible hydromagnetic interaction between the magnetic field of the induction solenoid and the plasma flow field was theoretically treated, and shown to be negligibly small for all cases of practical interest.

The energy balance equation was shown to reduce to a form of the Elenbaas-Heller equation which included radiation transport. This equation was numerically integrated for the electrodeless arc in air for seventy-three cases within the following limits in pressure P, magnetic field B, and the frequency f of the magnetic field:

$$1 \text{ atm} \leq P \leq 30 \text{ atm}$$

$$1 \text{ gauss} \leq B_o \leq 1000 \text{ gauss}$$

$$10^5 \text{ cps} \leq f < 10^8 \text{ cps}$$

The results of the analysis were found to exhibit excellent quantitative agreement with a theory of the electrodeless discharge presented by J. J. Thomson[1,2], and verification[3] of this theory has been reported.[4]

The following conclusions were drawn from the theoretical study and the numerical analysis:

(1) The radius R of a stationary electrodeless arc is not determined by the diameter of its confinement vessel, but rather by the rate of entropy production within the discharge.

The condition for the existence of the electrodeless arc is thus:

$$\sqrt{2}\ R/\delta \approx 2.5$$

where δ is the electromagnetic "skin-depth" in the discharge.

(2) Verification of Thomson's theory permits the prediction[5] of the power requirement for the maintenance of any stationary electrodeless arc:

$$P_o = 3 \times 10^6\ B_o^2\ R^2\ f \text{ per unit length,}$$

(3) The power required to maintain an electrodeless arc in a flowing system is proportional to the weight flow rate through the arc, and is given by

$$P(u) = P_o + \dot{w}H,$$

where P is given in (2) above, $\dot{w}$ is the weight flow rate and H is the enthalpy of convection from the discharge.

The creation, for engineering purposes, of an analytical model of the electrodeless arc from the results of the numerical analysis was not necessary, once the validity of the Thomson model was established. A simple design scheme was derived from this model in which the a priori specification of the desired discharge pressure, plasma enthalpy, and weight flow rate is all that is necessary to perform a conceptual design study for an electrodeless plasma generator. The additional specification of discharge chamber radius and induction circuit Q (i.e., the ratio of inductive reactance to series resistance) then uniquely determines the

operating parameters and all pertinent design data for an electrodeless plasma production system.

Such a design study was performed for an electrodeless system operating near an optimum operating point of a high performance fifty megawatt DC arc heater. No attempt was made to optimize conditions for the electrodeless arc. Available data constrained the comparison to occur at pressures that were only approximately equal (i.e., DC arc 37 atm, electrodeless arc 30 atm), so the air flow through the electrodeless system was adjusted to provide a comparison at conditions that were heavily weighted in favor of the DC arc.

It was found that the electrodeless system produced a discharge efflux enthalpy 1.3 times that of the DC device. The overall efficiency of the electrodeless system (including nozzle loss) was shown to be 1.25 times that of the DC device at the operating point chosen for comparison.

B. DESCRIPTION OF THE ELECTRODELESS ARC DISCHARGE

The electrodeless discharge treated herein is a true gaseous arc discharge that occurs within the volume of a solenoid carrying high frequency current. The axially directed alternating magnetic field inside the solenoid induces an azimuthal electric field in accordance with Faraday's law, and azimuthal currents, driven by this field, ohmically heat the gas and maintain discharge ionization.

In the low pressure discharge limit (for example, a few torr), plasma electrons acquire large energies from both the solenoid electric

and magnetic fields, and escape from the discharge volume (i.e., runaway). This is reflected in the relatively high plasma potential and the large electron "temperature" which characterize[6] the non-equilibrium induced discharge at low pressures.

At pressures above a few millimeters the discharge tends to equilibrate, and for pressure $\gg$ 0.1 atmosphere, local thermodynamic equilibrium is established[7]. The axial electric field of the induction solenoid takes a negligible part in the discharge energy transport, and exceptionally large azimuthal currents flow in the plasma. In this high pressure limit one therefore speaks of the "thermal" electrodeless discharge.

The distinction should not be made that the low pressure induced discharge is a "glow" type of electrical discharge[8], however. Any magnetically induced discharge is an arc. The physics of the discharge, insofar as the mechanisms of discharge maintenance are concerned, does not change with pressure. The low pressure electrodeless discharge obeys the same physical laws as does the high pressure electrodeless discharge. The distinction is therefore one of amount, not of kind: the high pressure electrodeless discharge is in local thermodynamic equilibrium[7], the low pressure electrodeless discharge is not[9]. In this study both the high- and low-pressure magnetically induced electrodeless discharge shall be referred to as the "electrodeless arc".

C. AN HISTORICAL SURVEY OF THE DEVELOPMENT OF THE ELECTRODELESS ARC DISCHARGE

The first reported[10] observation of an electrodeless discharge was made in 1884 by W. Hittorf, who produced light in an evacuated tube when he

discharged a Leyden jar through a wire wrapped around the tube. Several years later[1], J. J. Thomson wrote a two-part research paper "On the Discharge of Electricity through Exhausted Tubes without Electrodes", which he prefaced as follows:

> "The following experiments, of which a short account was read before the Cambridge Philosophical Society last February, were originally undertaken to investigate the phenomena attending the discharge of Electricity through Gases when the conditions are simplified by confining the discharge throughout the whole of its course to the gas, instead of, as in ordinary discharge-tubes, making it pass from metallic or glass electrodes into the gas, and then out again from the gas into the electrodes."

In this work Thomson developed the theory of induction heating of metals; thirty-six years later[2] he applied this theory to "The Electrodeless Discharge through Gases", in what must now be recognized as the fundamental work in the field of electrodeless plasma production.

At the time, however, Thomson's work inspired considerable controversy among his colleagues. No less an authority than J. S. Townsend claimed that the electrodeless discharge was "electric" rather than "magnetic" in origin, and, on the heels of Thomson's publication, Townsend and Donaldson presented[11] their own theory of "Electrodeless Discharges" in which they managed to obtain almost total disagreement with the Thomson theory. MacKinnon later attempted[12] to resolve the controversy,

and was able to demonstrate that two kinds of electrodeless discharge exist: one of electric origin, and one of electromagnetic origin.

A careful theoretical study by Kunz[13] led to an attempt[14] by Tykocinski-Tykociner to perform an ambitious experiment designed to settle the problem for once and for all. Thomson's theory predicted that one of the effects of an electrodeless discharge would be a net decrease in the inductance of the solenoid producing the discharge. By placing the induction solenoid in the tuned circuit of a vacuum tube oscillator, Kunz and Tykocinski-Tykociner hoped to show an increase in the frequency of the oscillations because of the presence of the discharge. Likewise, by establishing a discharge with the axial electric field of the solenoid, the frequency of the oscillations would decrease because the effective capacitance of the tuned circuit is increased[15] by the presence of the discharge. It was therefore argued that the frequency of the oscillator producing the discharge could verify Thomson's theory.

The experimental observations yielded only a decrease in the oscillator frequency. Since this frequency decrease was significantly less than that predicted for the "H-" discharge, this was interpreted as proof of the presence of both the Thomson magnetic discharge and the Townsend electric discharge in the same apparatus, simultaneously.

The research of the next decade can be summarized by the work of Babat, in whose report[15] is found one of the best phenomenological descriptions ever published of the general properties of electrodeless discharges. It is significant to note that during the period encompassed by Babat's

research, Smith[16] was successful in magnetically inducing an electrodeless discharge in Hg vapor with low frequency current supplied by a motor generator.

Carruthers[17] observed a skin effect in low density induced discharges but did not attempt to compare his observations with induction plasma theory. Chuan[18] attempted* to capacitively excite an electrodeless discharge in a supersonic flow.

---

* It is important to note that the capacitive method of discharge induction is characterized by large voltages and small currents and, as shown in Appendix IV of this report, is definitely not suited to high-power plasma production. Capacitive plasmas more closely resemble the glow discharge than the arc. Significant power levels in any arc discharge necessarily require large currents because of the large conductivity of plasmas. Chuan's work was later extended by Carswel,[19] but neither researcher reported transferring appreciable powers to their plasmas. For high power application, such studies represent a strong argument in favor of the magnetically induced electrodeless arc discharge.

Thermonuclear technology continuously provided better plasma diagnostic techniques. With the advent of Scylla[20] and similar machines, the electrodeless discharge became the object of intense study throughout the world, and as a partial result of the new techniques, physical insight, which heretofore often had been lacking, was gained. Internal magnetic fields were measured.[21] Bolometers for measuring plasma energy losses were developed,[22] and direct measurements of the electrical conductivity of plasmas were reported.[23,24,25] Meanwhile, theory pertinent to the steady state induced discharge advanced. Eckert[26] investigated breakdown criteria and derived conditions for the transition from free to ambipolar diffusion in the low pressure electrodeless discharge[27]. Romig[28] included the effects of flow in the low pressure electrodeless arc diffusion problem, and Hollister extended Thomson's theory of the behavior of the magnetic induction within the induced discharge, and reported a partial experimental verification thereof.

Ionization phenomena in low density gas flows by induced discharges was studied by Barger, et al[29], who observed that a flowing discharge required more power than a stationary, but otherwise similar discharge. Later they attempted[30] to accelerate this plasma by means of a low frequency induced field.

Atmospheric pressure induction plasmas at the 10 KW level were studied by Reed[31], who reported the observation of exceptionally high* temperatures

*See Ref. 38.

in argon. The transition to high pressure discharge operation motivated Mironer's development[32] of a water-cooled metal discharge vessel to withstand the higher gas enthalpies obtained at atmospheric pressure.

During this period a considerable amount of research was being conducted in Europe and the Soviet Union. In connection with fusion studies, Alfven and his colleagues considered the problem of gaseous confinement, and proposed a novel method for the thermal insulation[33] of a thermonuclear plasma by an anular cylinder of plasma. Studies[34] of the initial ionization and low pressure breakdown in a pulsed electrodeless discharge were shown by Bobyrev and Fedyanin to be influenced by a skin effect. Bamberg and Dresvin's ambitious theoretical and experimental study[35] of the ring* discharge was erroneously interpreted as indicating the lack of a meaningful relationship between the skin effect in the discharge and the shape of the discharge but this study indicated also the need for a detailed theoretical treatment.

Construction of an intense (300 KW) electrodeless discharge from the discharge chamber wall was observed [36] by Raizer, et al. in a non-equilibrium ring discharge at low pressures. Dolgopolov and Stephanov treated ionic resonance effects theoretically[37], and discussed the possibility of magnetic resonance enhancement of the heating of high density plasmas. No experiments were reported, however, and it has not been established that such effects actually exist in the high pressure electrodeless arc discharge.

* See J. S. Thomson, Refs. 1-2.

More recently, a considerable number[38-45] of spectrographic measurements of electrodeless arc temperature and density distributions have been reported. Temperatures in the atmospheric induction plasma generally have appeared to be about 10,000° in argon and 7,000° in air. Of these, three deserve special attention. Goldfarb and Dresvin[38] found a significant error in Reed's[31] observations of the temperature distribution in an atmospheric discharge in argon (i.e., it was therefore no longer necessary to explain Reed's 16,000° central temperature peak). Donskoi, et al[42] improved the design of a water-cooled metal discharge chamber, and Dymshits and Koretskii[39] performed a comprehensive experimental study of the electrodeless arc in high pressure argon and reported the following highly significant observations:

(1) The discharge diameter and temperature are determined by neither the diameter of the discharge tube, nor the pressure, flow rate and velocity profile of the gas stream in it.

(2) The diameter of the plasma is inversely proportional to the root of the frequency, and satisfies the relation $d/\delta = 3.5$, where d is the discharge diameter and $\delta = [2/\sigma\mu\omega]^{\frac{1}{2}}$ is the "skin depth" in the discharge.

(3) The power transferred to an electrodeless discharge is proportional to the gas flow rate.

A year previous, a theoretical prediction of the first and second items above had been presented[5] on the basis of the Thomson theory of the electrodeless arc.

Discharges in noble gases were studied over a wide pressure range. Mitin and Fryadkin[46,47] reported electrodeless arc production at 20 atmospheres with less than a kilowatt of applied power. The effects on the discharge of various discharge chambers, including metal-walled chambers, have been investigated[48] by Donskoi, et al. Several studies of a general nature have also been reported.[49-52]

The efficiency of energy transfer to a low pressure electrodeless arc was experimentally treated[53] by Andrew, et al. who found that efficiencies of eighty percent are obtainable even at low pressures; agreement between experimental observations and predictions based on a short-circuited transformer model (e.g., the Thomson theory) was reported. Finally, the starting mechanism for the low pressure induced discharge was treated by Chandrakar and von Engel[54] who showed that the axial electric field of the induction solenoid provides the initial ionization from which breakdown and subsequent ring discharge formation is obtained.

Several attempts to solve the energy balance equation for the electrodeless arc have been reported. Gruzdev, et al[55] neglected flow and radiation, and attempted to successively approximate a balance between radial heat conduction and ohmic heating. This same group had earlier prepared a geometrical model of the electrodeless arc[56,57], and experimentally measured[58] the discharge energy balance.

Eckert[59] assumed a radiation-free form of the Elenbass-Heller energy equation, and obtained an analytical solution for the thermal electrodeless arc in argon.

The most ambitious analysis thus far reported is that of Soshnikov and Trekhov [7,60,61], who numerically integrated the Elenbaas-Heller equation. Their results do not yield a unique solution, however, and they report the use of a boundary condition[7] that is incorrect*, hence the value of this work is not clear at the present time.

An excellent theoretical-experimental study of the mechanisms of energy transfer in an electrodeless thermal plasma generator was reported by Freeman and Chase[8], who also freely discuss their laboratory techniques.

A circuit analysis recently reported by Sprouse[62] predicts values for power transfer and scaling that are in qualitative agreement with similar predictions from the Thomson theory. Thorpe reports[63] continuous operation of an electrodeless arc in several gases including air at atmospheric pressure, with power levels up to one megawatt.

---

*In the referenced work (Eq. (2), page 166) the imaginary component of the rf magnetic field at r = 0 is given as zero. It is shown in Section 2 of this report that this parameter is not only non-zero at r = 0, but must be negative. See also Eqn. (7), page 170 of reference 7 in which the plasma radiation loss is evaluated.

SECTION II

ANALYSIS OF THE ELECTRODELESS ARC

A. INTRODUCTION TO THE ANALYSIS

In general, the electrodeless technique of plasma generation has largely been limited to high-frequency operation in what has become known as the "ring" discharge. This discharge is observed when the high frequency axial magnetic field of a solenoid carrying high frequency currents induces azimuthal currents in an ionized gas. The resulting luminosity often appears (along the axis) as a bright ring, hence the name.

This was the discharge studied by Thomson. The physics of Thomson's low pressure "ring" discharge differs from the physics of the high pressure, high energy electrodeless arc only to the extent that the equilibration processes within the discharge occur at the lesser rate in the low pressure case (i.e., the n-collisional cross section for a given energy density depends on the local particle number density). This is recognized to be

a property of the discharge plasma, not of the discharge itself, and it follows that the collisional heating process in the high pressure electrodeless arc is not basically different from that in the low pressure ring discharge.

Thomson's model must therefore be applicable to the high pressure discharge. In this model the induction solenoid is of infinite extent, and the coaxial plasma is considered to be uniform and homogeneous, and a unit of length of this system is examined to quantitatively determine the "external" parameters (i.e., voltages, currents, power levels, etc.). The electrical analog for this model is given by a transformer that has its secondary winding shorted through a small resistance, as in Figure 1. Here L_1 represents the inductance of the solenoid inducing the discharge, R_1 accounts for circuit losses, M is determined by the geometry of the discharge inside the induction solenoid, and L_2 and R_2 refer respectively, to the inductance and resistance of the "gaseous turn" discharge plasma.

The impedance this circuit presents to its generator is given by

$$Z = \left[R_1 + \frac{\omega^2 M^2 R_2}{R_2^2 + \omega^2 L_2^2}\right] + j\omega \left[L_1 - \frac{\omega^2 M^2 L_2}{R_2^2 + \omega^2 L_2^2}\right]. \qquad (1)$$

If ionization is absent in the secondary (i.e., when there is no discharge) the resistance R_2 increases to infinity and no secondary current flows. The impedance of the circuit as seen by the generator is then

$$Z_o = R_1 + j\omega L_1. \qquad (2)$$

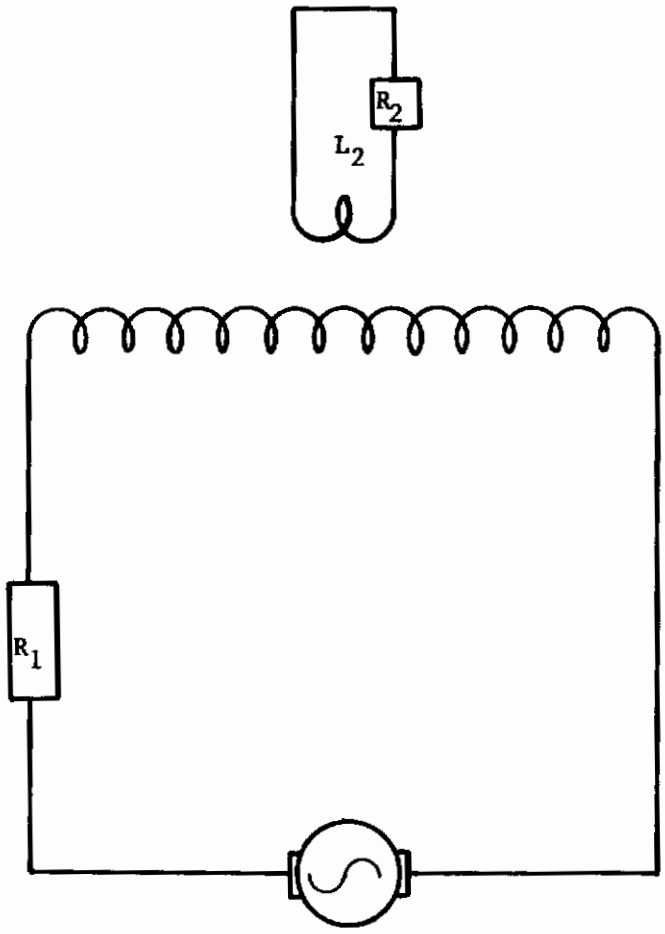

Figure 1. Equivalent Circuit of Electrodeless Plasma System.

Thus, ionization in the coupled circuit increases the overall resistance as seen by the generator, and for constant current the net losses increase (i.e., power is transferred to the gas). Additionally, ionization in the coupled circuit is seen to decrease the net inductive reactance of the circuit, and the overall effect of the discharge is to change both the real and the imaginary components of the circuit impedance.

B. THE THOMSON EDDY-CURRENT MODEL OF THE ELECTRODELESS ARC

Thomson's model was employed to relate the properties of the discharge plasma to the parameters L_2 and R_2 appearing in Eq. (1). This analysis is presented in full in Appendix I, where the following values for these parameters are derived:

$$L_2 = \frac{\pi R^2 N^2 \mu_o}{\ell}\left\{\left(\frac{2\delta}{\sqrt{2}R}\right)\frac{M_1(\sqrt{2}R/\delta)}{M_o(\sqrt{2}R/\delta)}\sin\left[\theta_1(\sqrt{2}R/\delta) - \theta_o(\sqrt{2}R/\delta) - \pi/4\right]\right\}, \quad (3)$$

$$R_2 = \frac{\pi R^2 N^2 \mu_o}{\ell}\omega\left\{\left(\frac{2\delta}{\sqrt{2}R}\right)\frac{M_1(\sqrt{2}R/\delta)}{M_o(\sqrt{2}R/\delta)}\cos\left[\theta_1(\sqrt{2}R/\delta) - \theta_o(\sqrt{2}R/\delta) - \pi/4\right]\right\}. \quad (4)$$

In these expressions R is the discharge radius, N/ℓ is the number of turns per unit length of the induction solenoid, $\delta = (2/\sigma\mu\omega)^{\frac{1}{2}}$ is the electromagnetic "skin depth" of a wave of angular frequency ω in a medium of electric conductivity σ, and the $M(\sqrt{2}R/\delta)$ functions are moduli of Bessel functions of the first kind with complex argument $(i^{3/2}\sqrt{2}R/\delta)$.

The power transferred to an electrodeless arc is given by the product of the mean square of the solenoid current and Eq. (4). This is found to be

$$P = \frac{1}{\mu_o} \cdot \omega B_o^2 f(\sqrt{2}R/\delta) \cdot \text{volume}, \qquad (5)$$

where $f(\sqrt{2}R/\delta)$ is the function within braces in Eq. (4), and B_o is the rms value of the applied magnetic field.

Maximization of Eq. (5) permits a determination of the conditions required for maximum power transfer to the discharge. These conditions obtain when the impedance presented by the plasma circuit equals the generator impedance. It was found that, to provide an impedance match, the physical size and electrical conductivity of the discharge must be related to the frequency of the applied magnetic field by

$$\frac{\sqrt{2}R}{\delta} = R\sqrt{\sigma\mu\omega} = 2.5 \qquad (6)$$

The existence criteria for the electrodeless arc were determined by examining the rate of entropy production in the discharge. This development is presented in Appendix II. In the case of the Thomson model it was found that the existence of the discharge is determined by Eq. (6) and that this condition is independent of flow through the discharge.

Thus, Eqns. (5) and (6) represent analytical scaling laws for the electrodeless arc discharge.

The importance of Eqn. (6) cannot be overemphasized: The electrodeless arc either adjusts its physical size and electrical conductivity in accordance with Eqn. (6) in order to absorb a maximum amount of power from the generator at the applied frequency, or the discharge ceases to exist. In the

Thomson model, this statement holds for all electrodeless arc discharges, and is seen to be independent of the gas in which the discharge is formed, the discharge pressure, the rate of flow through the discharge, and the physical size of the discharge vessel.

C. A DETAILED STUDY OF THE ENERGY BALANCE IN AN ELECTRODELESS ARC

The general equation of energy balance was rigorously derived from the basic continuum hydromagnetic equations. It was shown that this equation could be reduced to the Elenbaas-Heller energy equation by neglecting the effects of flow and viscosity in the analysis. A careful study of the consequences of this simplification showed that viscosity plays a minor role in determining the energy balance in an electrodeless arc discharge, and is indeed negligible; convective losses (i.e., flow effects), on the other hand, are not to be ignored.

1. DERIVATION OF EQUATION FOR NUMERICAL INTEGRATION

Existence criteria were established for the general electrodeless arc. Application of the thermodynamics of irreversible processes to this discharge yielded an existence condition for the actual discharge that was similar to that found for the Thomson model. It is shown in Appendix II that the discharge entropy production rate for an actual electrodeless arc is proportional to the flow rate, and the net power requirement for an actual electrodeless arc at constant pressure is given by:

$$P = P_o + \dot{w}H \tag{7}$$

where P_o is the zero flow power requirement, $\dot{w}$ is the weight flow rate through the electrodeless arc, and H is the enthalpy of convection from the electrodeless arc.

It was then established that, for all cases of interest in this study, both the magnetic Reynolds number and the hydromagnetic interaction parameter were significantly less than unity. Since the magnetic Reynolds number compares the rate of macroscopic motion of the discharge plasma with the rate of diffusion of the applied magnetic field through the plasma, while the hydromagnetic interaction parameter is determined by the ratio of the magnetic and dynamic pressures, both these characteristic dimensionless numbers having values less than unity indicates the absence of an appreciable hydromagnetic interaction in the flowing electrodeless arc. A theoretical treatment of the hydromagnetic interaction between the plasma flow field and the electromagnetic field in a model composed of a cylindrical plasma coaxial with an elementary loop of alternating current was conducted. The Green's function for this interaction is derived, presented and evaluated in Appendix III. From this study it was concluded that the induction field in an electrodeless arc is not appreciably disturbed by the flow.

The results of the theoretical treatment of the electrodeless arc entropy production, when taken with the results of the companion treatment of the electromagnetic-flow field interaction, show that the physical processes occurring within an electrodeless arc discharge are not determined by the gas flow through the discharge. Thus, in the convective reference frame a zero flow treatment of the discharge energy balance is valid, and this treatment will differ from that in the stationary reference frame by an amount determined by convective loss from the stationary discharge volume. In all

other respects the stationary electrodeless arc is identical to the flowing electrodeless arc in its energy balance mechanisms. The integration of the energy balance equation in the stationary reference frame thus differs from the integration of the energy balance equation in the fluid reference frame by a constant amount. That constant has been shown to equal the enthalpy of convection from the stationary discharge volume for the inviscid electrodeless arc discharge.

The energy balance equation was therefore evaluated in the fluid frame where it had the following form:

$$\frac{1}{r}\frac{d}{dr}\left(rK_c(T)\frac{dT}{dr}\right) - 4K_p(T)\tilde{\sigma}T^4 + \frac{1}{2}\omega^2\sigma(T)[A_r^2 + A_i^2] = 0, \qquad (8a)$$

for an optically thin plasma, and

$$\frac{1}{r}\frac{d}{dr}\left(r\tilde{K}(T)\frac{dT}{dr}\right) + \frac{1}{2}\omega^2\sigma(T)[A_r^2 + A_i^2] = 0. \qquad (8b)$$

for an optically thick plasma.

The complete derivation of these equations and all supporting analysis appears in Appendix IV of this report.

2. NUMERICAL INTEGRATION OF ENERGY BALANCE EQUATION

In Eqs. (8), $K_c(T)$, $K_p(T)$ and $\sigma(T)$ are respectively the coefficients of thermal conductivity including ambipolar diffusion, radiation absorption (Planck), and electrical conductivity, each coefficient being a known function of temperature and pressure for a given gas. The functions A refer to the real and imaginary components of the magnetic vector potential, and $\tilde{K}(T)$ is a modified coefficient of heat conductivity that is valid in

the optically thick (i.e., diffusion) regime of radiation transport:

$$\tilde{K}(T) \equiv K_c(T) + \frac{16}{3} \tilde{\sigma} \lambda_R(T) T^3, \tag{8c}$$

where λ_R is the Rosseland mean free absorption path length, also a function of temperature and pressure for a given gas, and $\tilde{\sigma}$ is the Stephen-Boltzmann constant.

The coefficients of thermal and electrical conductivity, the Rosseland mean free path, and other important data for this study were collected and tabulated as functions of temperature for air at one, three, ten and thirty atmospheres pressure. This tabulation appears in the print-out of the numerical analysis study under the heading, "Electrodeless Arc Vital Statistics".

Eq. (8a) was reduced to first order for numerical integration by taking a differential form of the heat conduction potential $S = rK_c(T) \frac{dT}{dr}$, and noting that $\vec{B} = \nabla \times \vec{A}$ to obtain:

$$\frac{dA_r}{dr} = B_r - \frac{A_r}{r}, \tag{9a}$$

$$\frac{dA_i}{dr} = B_i - \frac{A_i}{r}, \tag{9b}$$

$$\frac{dB_r}{dr} = - \omega\sigma(T) \mu_o A_i, \tag{9c}$$

$$\frac{dB_i}{dr} = \omega\sigma(T) \mu_o A_r, \tag{9d}$$

$$S = rK_c(T)\,\frac{dT}{dr}, \tag{9e}$$

and $$\frac{ds}{dr} = r\left[4\,\tilde{\sigma}\,K_p(T)\,T^4 - \frac{1}{2}\,\omega^2\sigma(T)(A_r^2 + A_i^2)\right]. \tag{9f}$$

These equations were programmed for integration by the Runge-Kutta* method and a computational sub-routine was provided to incorporate Eq. (8b) for cases where self-absorption of radiation by the discharge plasma takes place. Thus, for optically thick plasmas, Eqs. (9a-9d) remain unchanged, but Eqs. (9e) and (9f) become

$$S = \left[rK_c(T) + \frac{16}{3}\,\tilde{\sigma}\,T^3\,\lambda_R(T)\right]\frac{dT}{dr}, \tag{9e'}$$

$$\frac{ds}{dr} = -\frac{1}{2}\,r\omega^2\,\sigma(T)(A_r^2 + A_1^2). \tag{9f'}$$

Specific details of this program are given in Appendix V.

Solutions of Eqs. (9) were found for seventy-three individual cases within the bounds set by the following input limits:

$$1 \text{ atm} \leq \text{pressure} \leq 30 \text{ atm}$$

$$10^5 \text{ cps} \leq \text{frequency} \leq 10^8 \text{ cps}$$

$$1 \text{ gauss} \leq \text{magnetic field} \leq 1000 \text{ gauss}$$

For specified values of discharge pressure, applied field intensity and frequency, radial distributions were found for the following discharge

* Please see Appendix V.

parameters and their gradients:

Temperature: $T(r)$; $\frac{dT(r)}{dr}$

Real component of magnetic field: $B_r(r)$; $\frac{dB_r(r)}{dr}$

Imaginary component of magnetic field: $B_i(r)$; $\frac{dB_i(r)}{dr}$

Real component of magnetic vector potential: $A_r(r)$; $\frac{dA_r(r)}{dr}$

Imaginary component of magnetic vector potential: $A_i(r)$; $\frac{dA_i(r)}{dr}$

Heat conduction function: $S(r)$; $\frac{ds(r)}{dr}$

Additionally, radial distributions were computed for the following parameters:

Peak magnitude of magnetic field $B(r)$

Peak value of electric field $E(r)$

Peak value of electric current density $j(r)$

Rosseland mean free path $\lambda_R(r)$

Coefficient of heat conductivity $K_c(r)$

Coefficient of electrical conductivity $\sigma(r)$

Separate integrations were performed to obtain the following total values:

Total current/unit length induced in discharge

Total (ohmic) power consumed by discharge

Total power radiated from discharge

Fraction of total power radiated from discharge

Effective discharge radius

These data were tabulated in full in the print-out for the numerical analysis, and the radial temperature profiles for all cases treated in this study appear in Appendix VI of this report.

3. EVALUATION AND ANALYSIS OF DATA FROM NUMERICAL INTEGRATION

In order to perform the numerical integration, the following conditions on the field quantitites must be observed for r = 0:

$$B_r(0) > 0;\ B_i(0) < 0;\ \frac{dA_r}{dr}\Big|_{r=0} = \frac{1}{2}\ B_r(0);\ \frac{dA_i}{dr}\Big|_{r=0} = \frac{1}{2}\ B_i(0);$$

$$A_r(0) = A_i(0) = \frac{dB_r}{dr}\Big|_{r=0} = \frac{dB_i}{dr}\Big|_{r=0} = 0$$

Additionally, the boundary conditions on the applied field can be shown to require that for a radius $r^* > R$, where R is the discharge radius:

$$B_r(r^*) = B_o;\ B_i(r^*) = 0.$$

In this study it was found that the only values of the real and imaginary components of the axial magnetic induction capable of satisfying the above conditions that would also yield a balance of energy were essentially the same as those values derived from the eddy-current theory.

A fundamental prediction of the eddy current theory was shown to be that the physical size (i.e., the radius R) of the discharge depends on the electrical conducitivity of the discharge and the applied frequency according to

$$\sqrt{2}\ R/\delta = R\sqrt{\sigma\mu_o\omega} \approx 2.5,$$

where δ is the so-called "skin-depth" in the discharge plasma.

Arguments based on Steenbeck's principle of minimum entropy production support this equation, which has been experimentally observed to hold for the electrodeless arc in argon.[39]

In addition, the eddy-current theory predicts a definite relation between power dissipation, applied field, frequency, and size of the electrodeless arc discharge:

$$\text{power/unit length} = k\, B_o^2\, f\, R^2 \approx 3 \times 10^6\, B_o^2\, f\, R^2,$$

where B_o is the peak value of the applied field, and the constant k is evaluated for $\sqrt{2}\, R/\delta = 2.5$. It was found in the present study that this relation is quantitatively satisfied if the "radius" of the discharge is defined in terms of the radial position at which the incident magnetic field begins to suffer a change in its magnitude due to the presence of the plasma. This position is sufficiently near the "luminous" radius of the plasma (i.e., determined by the local plasma temperature), and to the radial position where the azimuthal currents vanish that either of these characteristic radii will suffice to define a "radius" within a relatively small constant value. This "effective" radius of the discharge is therefore interpreted as being the connecting link between the eddy current theory and an exact, rigorous solution of the energy balance equation for identical discharge conditions. The remarkable agreement between the two theoretical approaches is demonstrated in Figure 2, where the seventy-four points represent the seventy-three numerical evaluations described above, plus the only known reported[45] measurement of the radial temperature distribution in an electrodeless arc in air that also included sufficient

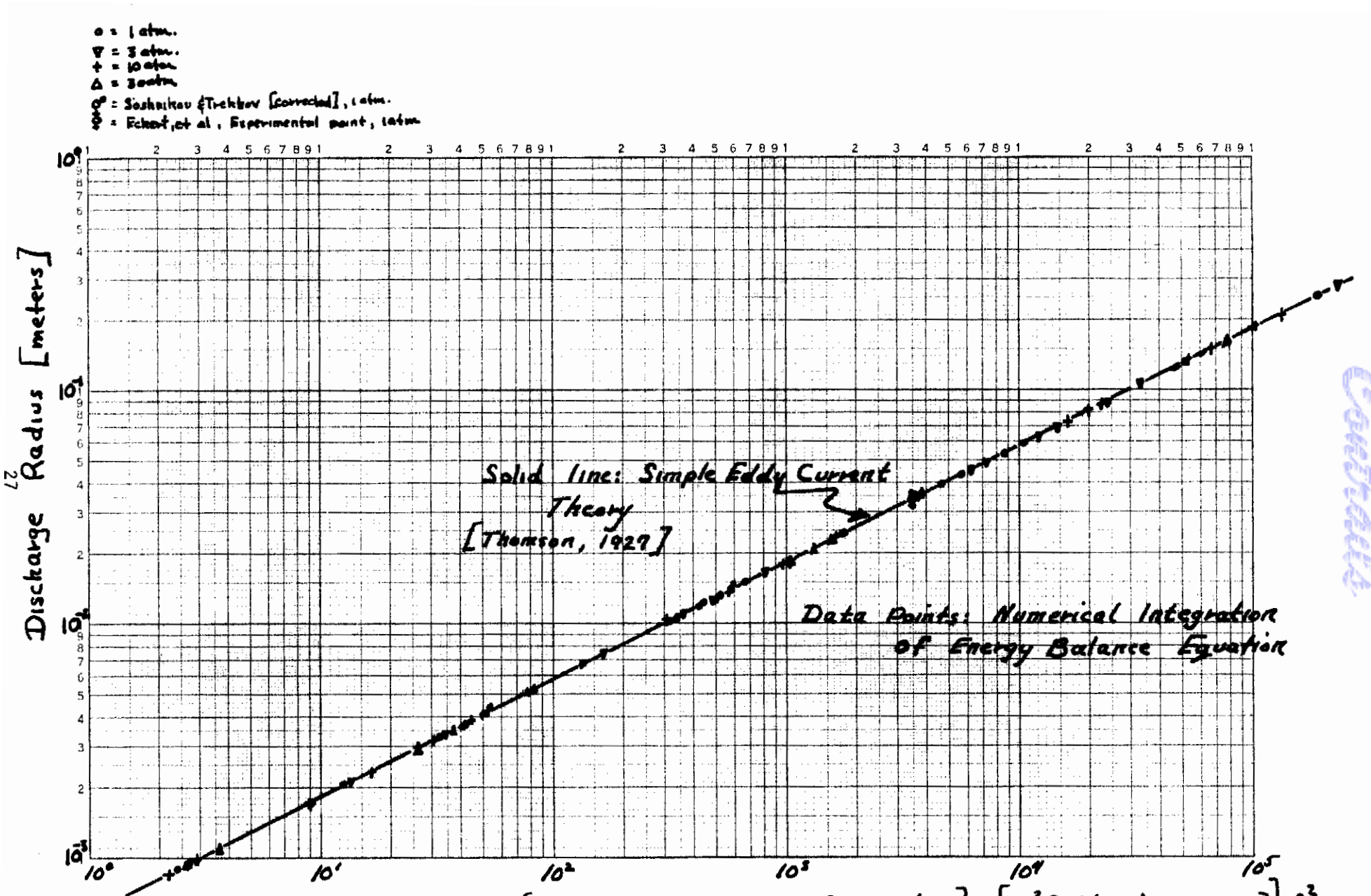

FIGURE 2.

information about induction coil size and shape, current and frequency to permit a meaningful comparison with theory.

The temperature profile observed in the referenced study is compared with the calculated temperature profile for identical discharge conditions in Figure 3A. The observed temperature peak is slightly less than five percent higher than the calculated value; this is believed to reflect a modification of the plasma temperature distribution function by the discharge tube wall. Since wall effects were suppressed in this analysis to assure the generality of the computed data, the calculated rise in the temperature profile is less than that observed. The observed deviation of theory from experiment in this respect is less than the reported experimental uncertainty, however. The observation therefore confirms the validity of the calculation for this particular case within the limits of this uncertainty (i.e., about seven percent) A machine plot of the computed temperature profile appears in Figure 3B.

The specific computation is presented below:

(a) Initial Conditions:

From Eckert, et al (J. Appl. Phys. 39, 1848 (1968), Figure 1), if the discharge tube diameter is 100 mm, the length of the induction solenoid is approximately 170 mm. The solenoid current was given as 40 amperes, and the solenoid has seven turns. The incident magnetic field is given by

$$B_o \approx \mu_o \frac{NI}{\ell} = \frac{12.54 \times 10^{-7} \times 7 \times 40}{0.170} = 20.7 \times 10^{-4} \text{ w/m}^2 = 20.7 \text{ gauss.}$$

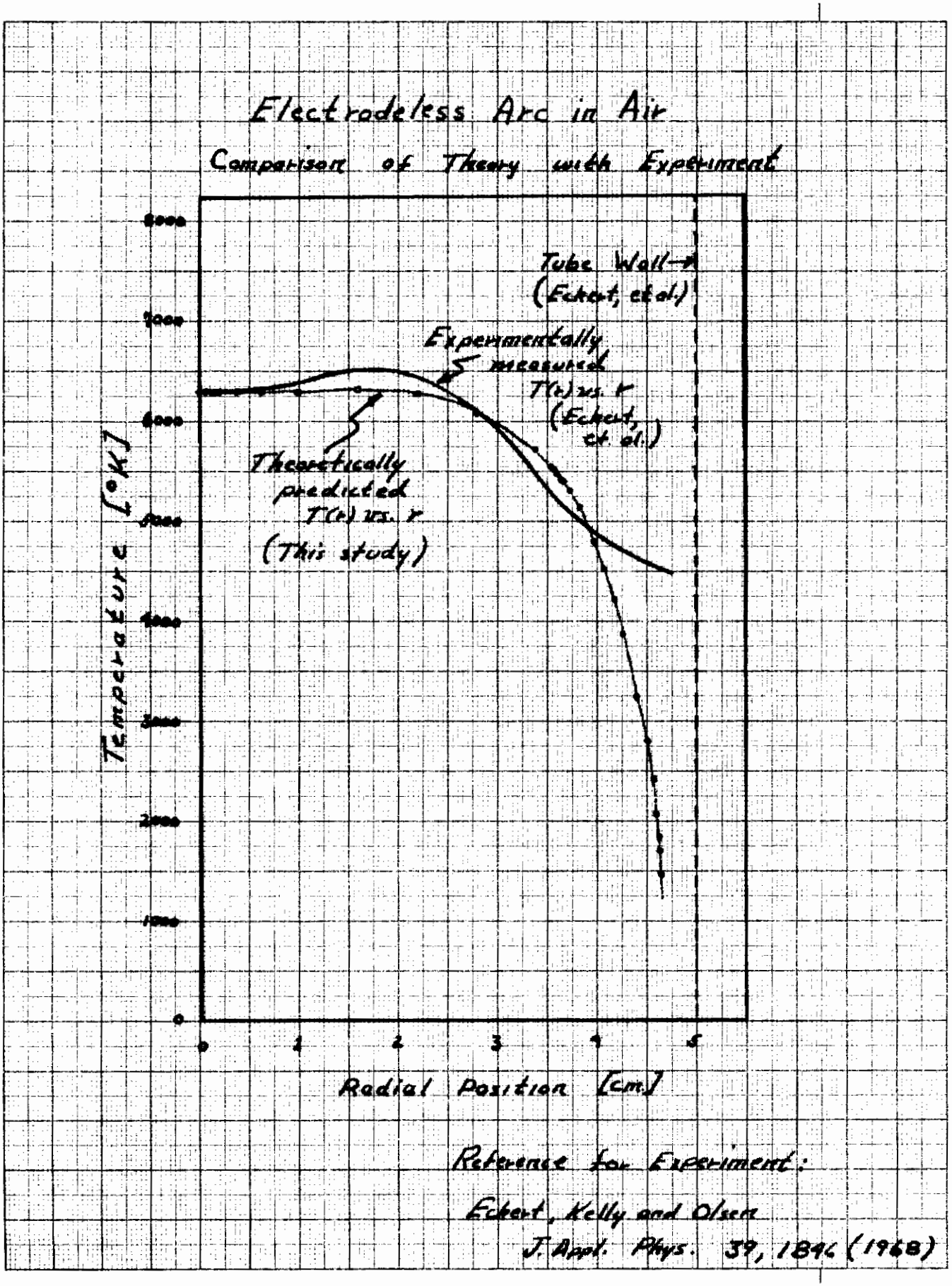

Figure 3A. Comparison of Theory with Experiment.

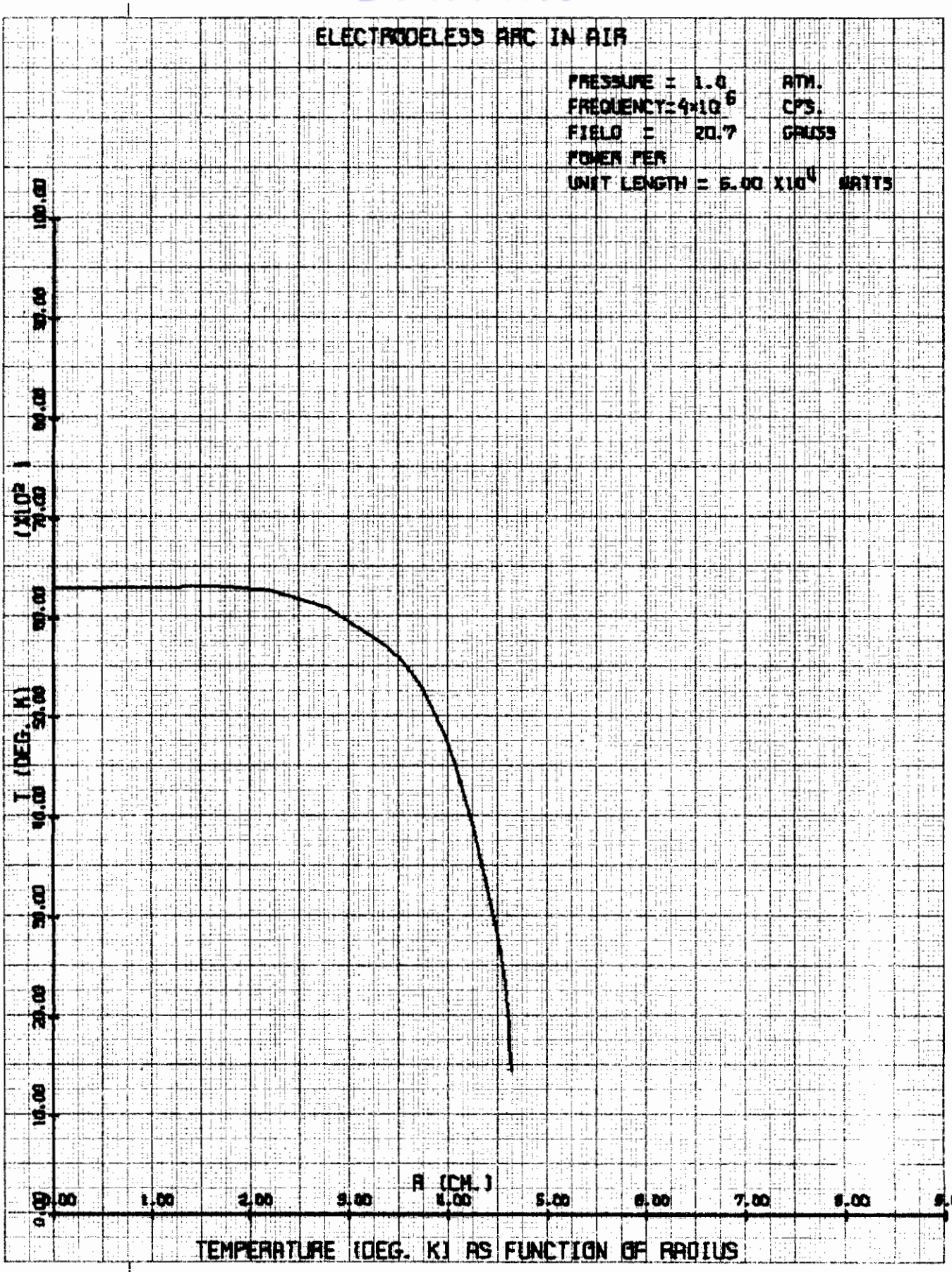

FIGURE 3B. THEORETICAL TEMPERATURE PROFILE

The initial conditions for the numerical analysis were as follows:

B_o = 20.7 gauss (computed above

T(0) = 6300°K (reported in publication)

P = 1 atmosphere (reported)

f = 4 x 10^6 cps (reported)

(b) Power dissipation:

Reported - 18 KW @ 60% efficiency = (i) 10.8 KW to discharge

(ii) 7.2 KW circuit loss

Computed - 60.45 KW/meter; for ℓ = 0.17 m this gives 10.3 KW dissipation.

(c) Comments:

The solenoid and solenoid-plasma geometry were not adequately described in the reference article. The initial condition for B_o for the numerical analysis is therefore a "best guess" approximation.

D. CONCLUSIONS FROM PHYSICAL STUDY

The immediate results of this study are as follows:

1. The "eddy current" theory of the electrodeless arc as proposed by Thomson is verified, subject to the definition of the discharge radius given above. Thus, the Thomson model is a valid analytical representation of the electrodeless arc discharge.

2. The electrodeless arc adjusts its physical size and internal temperature distribution in accordance with Steenbeck's principle

of minimum entropy production, hence:

3. The electrodeless arc discharge is scalable, the basic scaling laws being given by

$$\frac{\sqrt{2R}}{\delta} \approx 2.5$$

and

$$P/\ell = 3 \times 10^6 \, B_o^2 \, f \, R^2.$$

4. The effects of flow appear in a convective loss from the discharge volume. The power required to maintain a flowing discharge is

$$P = P_o + \dot{w}H.$$

These results are of considerable significance in terms of future engineering applications for the electrodeless arc because they show that the eddy current model of the electrodeless arc is perfectly valid for the purposes of engineering analysis. The specific energy balance solutions obtained in the numerical analysis give field and power requirements which show excellent agreement with equivalent parameter values obtained from the eddy current model. For purposes of analysis then, the two theories are equivalent, so long as their limits are not exceeded.

The eddy current theory gives correct values for "outside" observables such as total dissipation, discharge impedance, size, etc. Solutions of the energy balance equation yield correct values for the "inside" observables such as the distribution functions for temperature, current, magnetic field and the energy transport fluxes. These solutions also yield the relative contributions to the energy loss from thermal conductivity and radiation,

and they predict the physical size of the discharge and the net dissipation within the discharge.

The limits of the eddy current model are exceeded, for example, when the radiation flux is computed by means of this model. Likewise, the impedance the discharge presents to its generator cannot be calculated by means of the numerical analysis alone.

The presence of flow was shown not to be the dominant factor in the determination of the overall energy balance mechanisms for the electrodeless arc in high pressure air. In both the Thomson model and the numerical analysis it was found that the power required to maintain an electrodeless arc at a given set of operating conditions increases linearly with flow. The zero flow power requirement can be computed from either the eddy current model or from solutions for the energy balance equation, both of which are equivalent for power calculations. The addition of the flow equation to the basic scaling laws thus completes the analytical set required to perform meaningful engineering calculations for the scaling of the electrodeless arc discharge.

SECTION III

ENGINEERING DESIGN OF AN ELECTRODELESS ARC GENERATOR

A. INTRODUCTION

Technological exploitation of the electrodeless arc must be based on reliable calculations made within the framework of a valid model, if other than a cut-and-try type of engineering development of this discharge is desired.

Thomson's eddy-current theory provides such a model, and the validity of this model has been proven. The prescription of a design scheme for an electrodeless arc generator is justified, and the preparation of this scheme represents only a small extension of the preceding work.

B. BASIC DESIGN REQUIREMENTS

The basic requirement is stated in terms of a discharge pressure, the weight flow, and the enthalpy of the given working fluid. These values represent an operating point (i.e., the design point) of an electrodeless arc generator.

The following values will therefore be preassigned in any design study.

P (pressure)

$\dot{w}$ (weight flow rate)

H (enthalpy of flow)

Also, it is necessary that an a priori specification of the size of the discharge vessel be made. This is of no major consequence to the engineering analysis because of the size of the discharge has been shown to be independent of the size of the vessel in which the discharge is formed. In addition, electronic considerations will suggest the optimum Q (i.e., quality factor) for the particular application. Thus, the following parameters are assumed:

A (discharge vessel radius)

Q (circuit quality factor)

The definition of Q gives, for a series LR circuit

$$Q = \omega \frac{L}{\mathcal{R}},$$

where ω is the angular frequency of the current in the circuit, L is the coil inductance, and $\mathcal{R}$ is the series resistance. Values of L and $\mathcal{R}$ for the electrodeless arc are obtained from the eddy current theory:

$$L = \frac{\pi R^2 N^2 \mu_o}{\ell} \left\{ \frac{2}{x} \frac{M_1(x)}{M_o(x)} \sin \left[\theta_1(x) - \theta_o(x) - \pi/4\right] + \left(\frac{A^2}{R^2} - 1\right) \right\},$$

$$\mathcal{R} = \frac{\pi R^2 N^2 \mu_o}{\ell} \omega \left\{ \frac{2}{x} \frac{M_1(x)}{M_o(x)} \cos \left[\theta_1(x) - \theta_o(x) - \pi/4\right] \right\}.$$

For $x = \sqrt{2}\, R/\delta = 2.5$:

$$\frac{2}{x}\frac{M_1(x)}{M_o(x)} \sin\left(\theta_1(x) - \theta_o(x) - \pi/4\right) = \text{const} = g(\sqrt{2}R/\delta) \approx 0.62 ,$$

$$\frac{2}{x}\frac{M_1(x)}{M_o(x)} \cos\left(\theta_1(x) - \theta_o(x) - \pi/4\right) = \text{const} = f(\sqrt{2}R/\delta) \approx 0.38.$$

Then

$$Q = \omega \frac{L}{\tilde{\rho}} = \frac{g(\sqrt{2}R/\delta)}{f(\sqrt{2}R/\delta)} + \frac{A^2 - R^2}{f(\sqrt{2}R/\delta R^2)} = \frac{2.63\ A^2}{R^2} - 1 .$$

Thus

$$R = \sqrt{\frac{2.63\ A^2}{1 + Q}} \qquad (10)$$

gives the radius of the discharge that is required for the assigned circuit Q.

The preassigned values for the pressure and enthalpy of the discharge plasma are found in tables of the thermodynamic properties of the discharge gas. In the present study that gas is air and the thermodynamic properties of air are given, for example, by Fenter[64]. The temperature of the discharge that is obtained from the tables for the given pressure and enthalpy is equivalent to the reference temperature T_R that was introduced in the entropy production arguments* for the eddy current model. This is the "effective" discharge temperature. At the assigned discharge pressure, the discharge gas has a unique "effective" electrical conductivity that is determined by this discharge temperature. Thus, the effective electrical conductivity is determined by the preassigned pressure and enthalpy conditions:

* Please see Appendix II.

$$\sigma_{eff} = f(p,H). \tag{11}$$

The existence condition for the electrodeless arc states

$$\frac{\sqrt{2}R}{\delta} = R\sqrt{\sigma\mu_o\omega} \approx 2.5 . \tag{12a}$$

Therefore

$$f = \frac{7.93 \times 10^5}{\sigma_{eff} R^2} \tag{12b}$$

gives the frequency required to produce the specified discharge conditions in an impermeable plasma in which $\mu_o = 4\pi \times 10^{-7}$ henry/meter.

Solutions of the energy balance equation have been incorporated to map, for constant pressure, the field and frequency requirements for given values of discharge enthalpy and discharge radius for the pressures treated in the present study (i.e., 1-3-10-30 atm). These maps* appear in Figures (4-7) of this report. The zero-flow field requirement is obtained directly from the maps. It will be noticed that any stated pressure and enthalpy requirement yields a family of possible operating points, each point being determined by either the discharge radius, or the magnitude of the applied magnetic field, or the applied frequency. Thus, the required magnetic field is determined:

$$B = f(H, p, f, R,) \tag{13}$$

* The maps presented here were constructed by connecting the various data points by straight lines. Additional computations will be necessary to determine the fine structure of these curves.

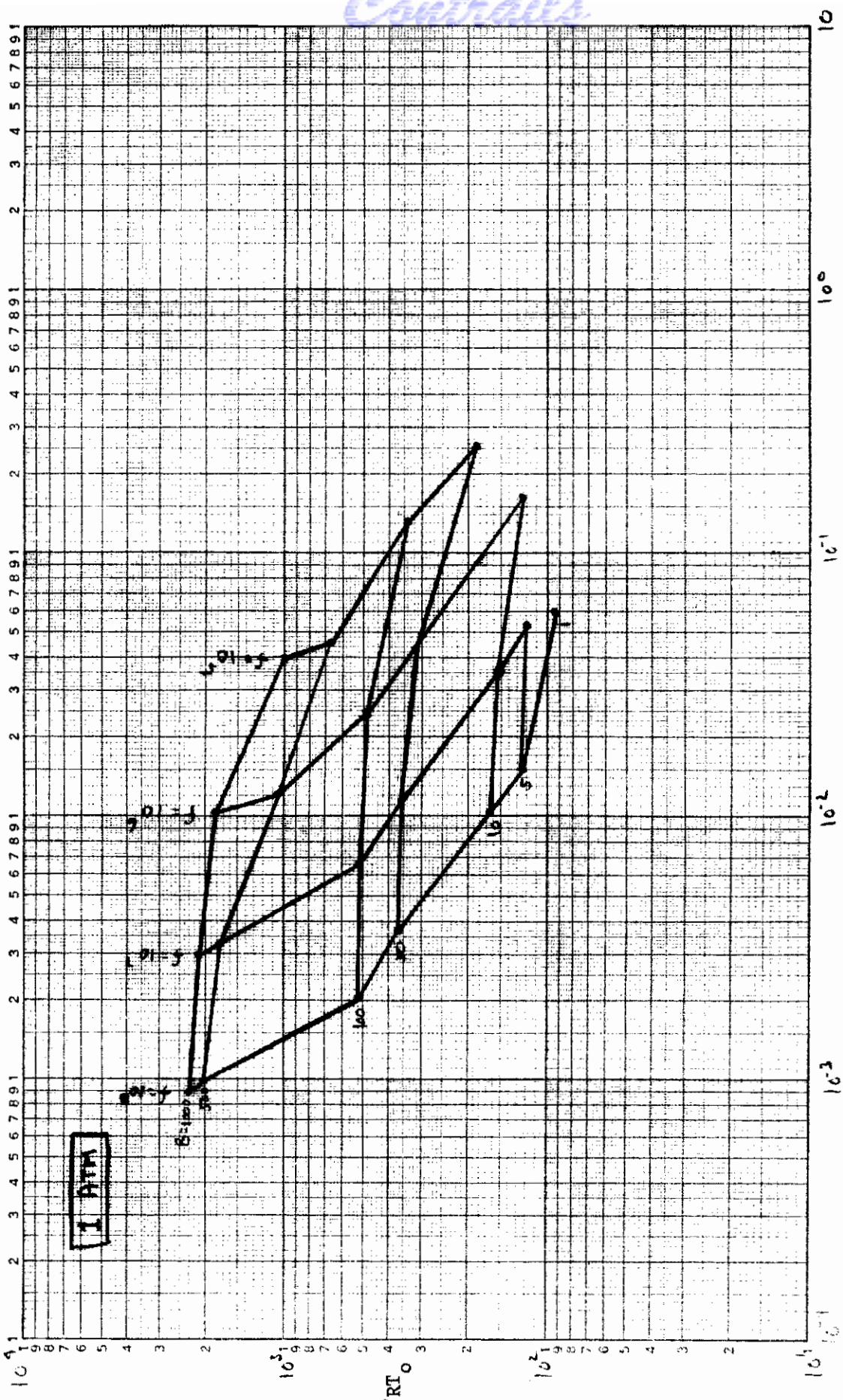

FIGURE 4. DISCHARGE ENTHALPY VERSUS DISCHARGE RADIUS (1 ATM)

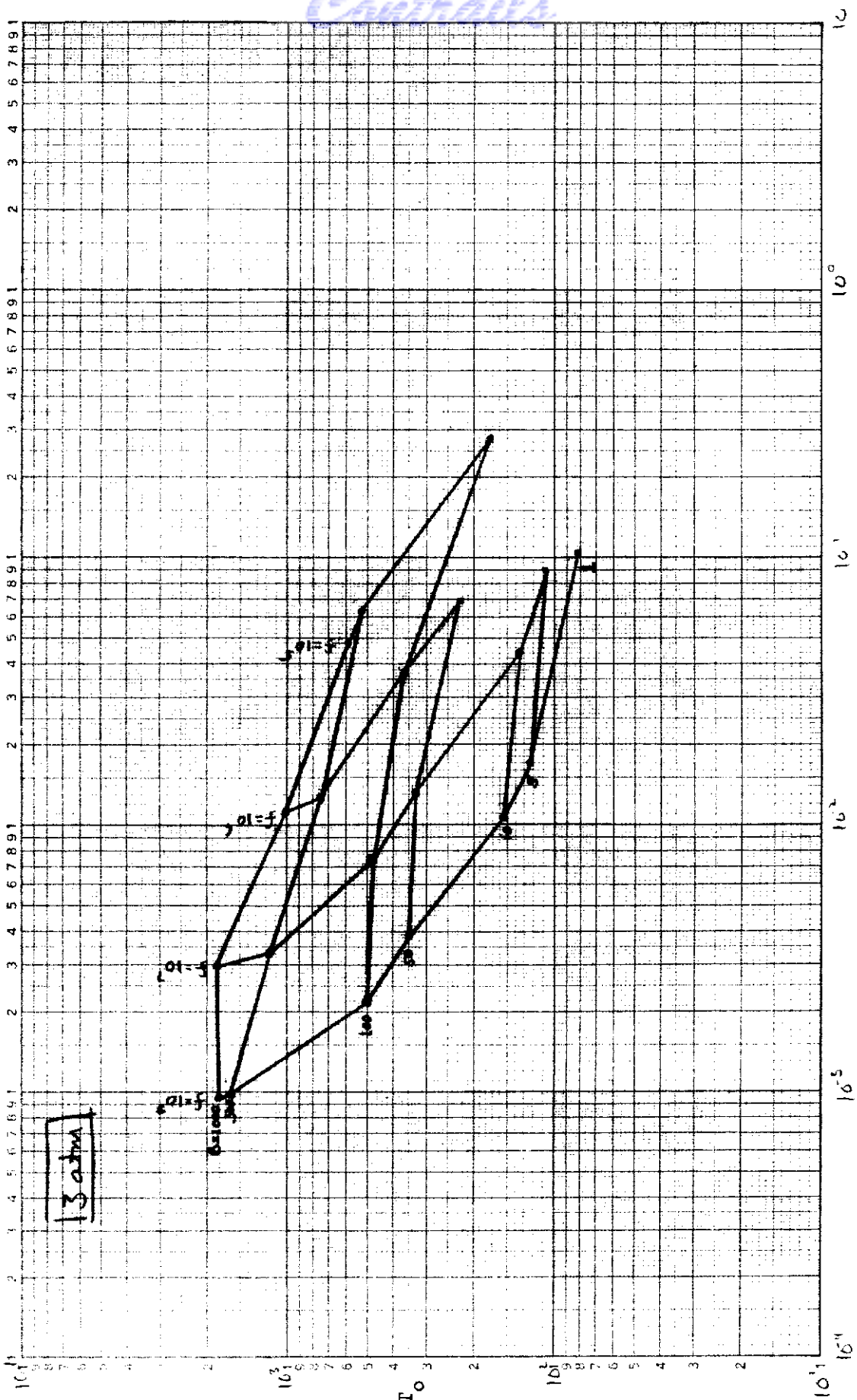

FIGURE 5. DISCHARGE ENTHALPY VERSUS DISCHARGE RADIUS (3 ATM)

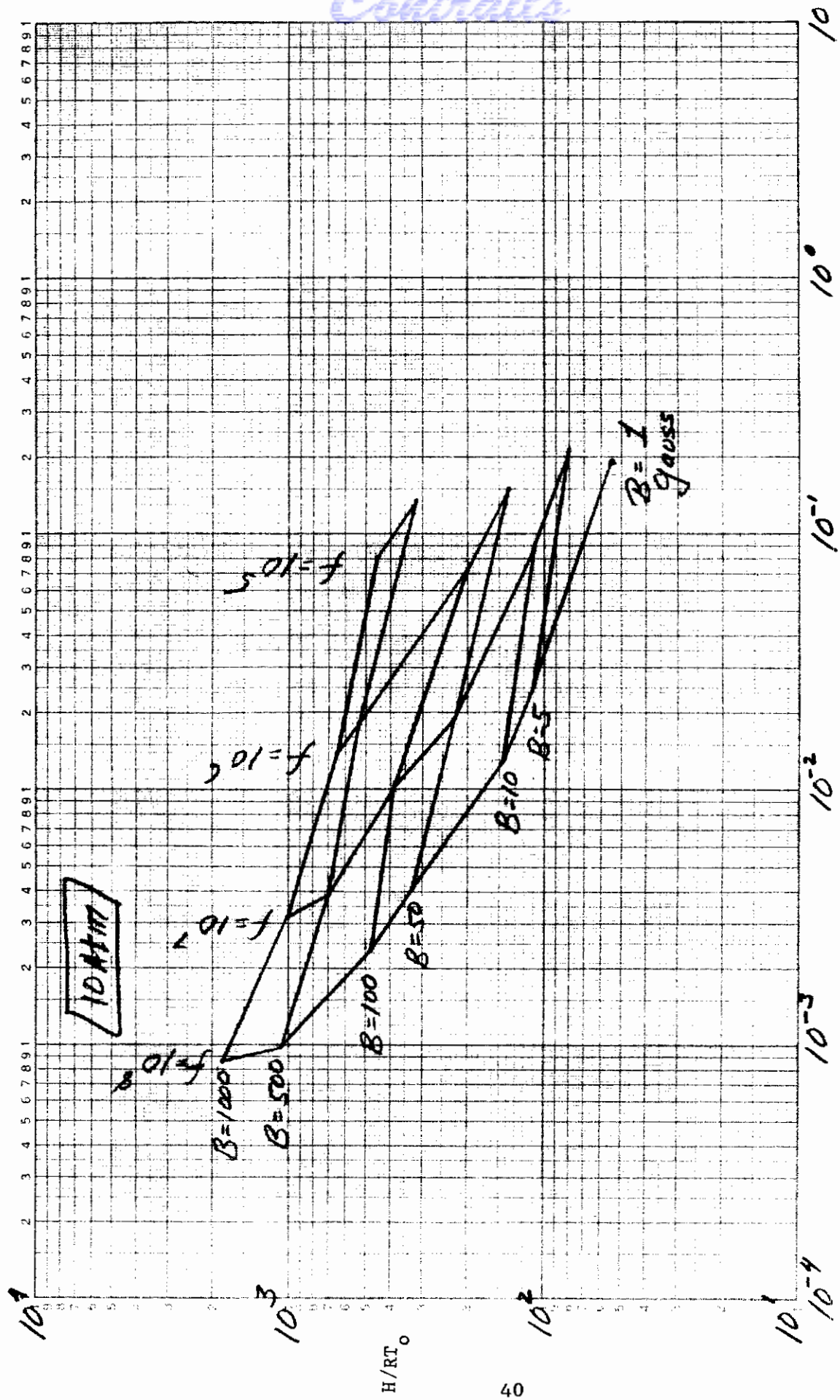

FIGURE 6. DISCHARGE ENTHALPY VERSUS DISCHARGE RADIUS (10 ATM)

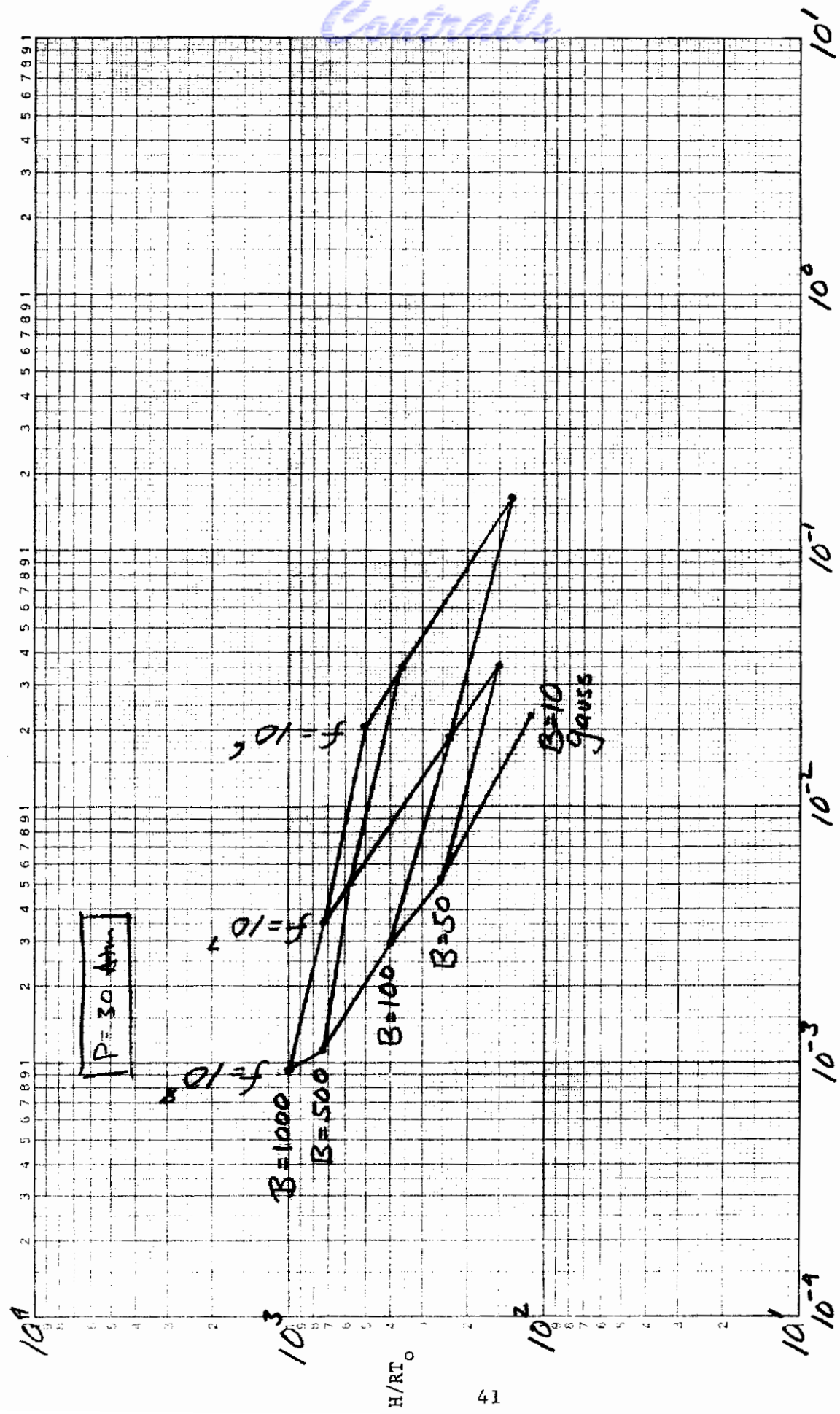

FIGURE 7. DISCHARGE ENTHALPY VERSUS DISCHARGE RADIUS (30 ATM)

The power per unit length required to produce the zero-flow discharge is given by

$$P/\ell = 3 \times 10^6 \, B^2 \, f \, R^2 \tag{14}$$

The power requirement for the flowing discharge is

$$P(u) = P_o + \dot{w}H \tag{15}$$

The zero-flow requirement is given by Eq. (14) and is mapped in Figs. (8-11). The product $\dot{w}H$ is formed and converted to the units of P_o. The sum of these gives the total power requirement. Since the discharge size has been fixed by the assumed value of the circuit Q, the magnitude of the applied field must be readjusted according to Eq. (14) to accommodate the increase in required power that accompanies the flow. The discharge size can also be varied, if this is desired.

C. AN ELEMENTARY DESIGN SCHEME

Assigned:

Pressure = p (atmospheres)

Weight flow rate = $\dot{w}$ (lbs/sec)

Bulk Enthalpy = H (BTU/lb)

Gas = Air

Requirements:

Circuit quality factor = Q (dimensionless)

Discharge vessel diameter = 2A (meters)

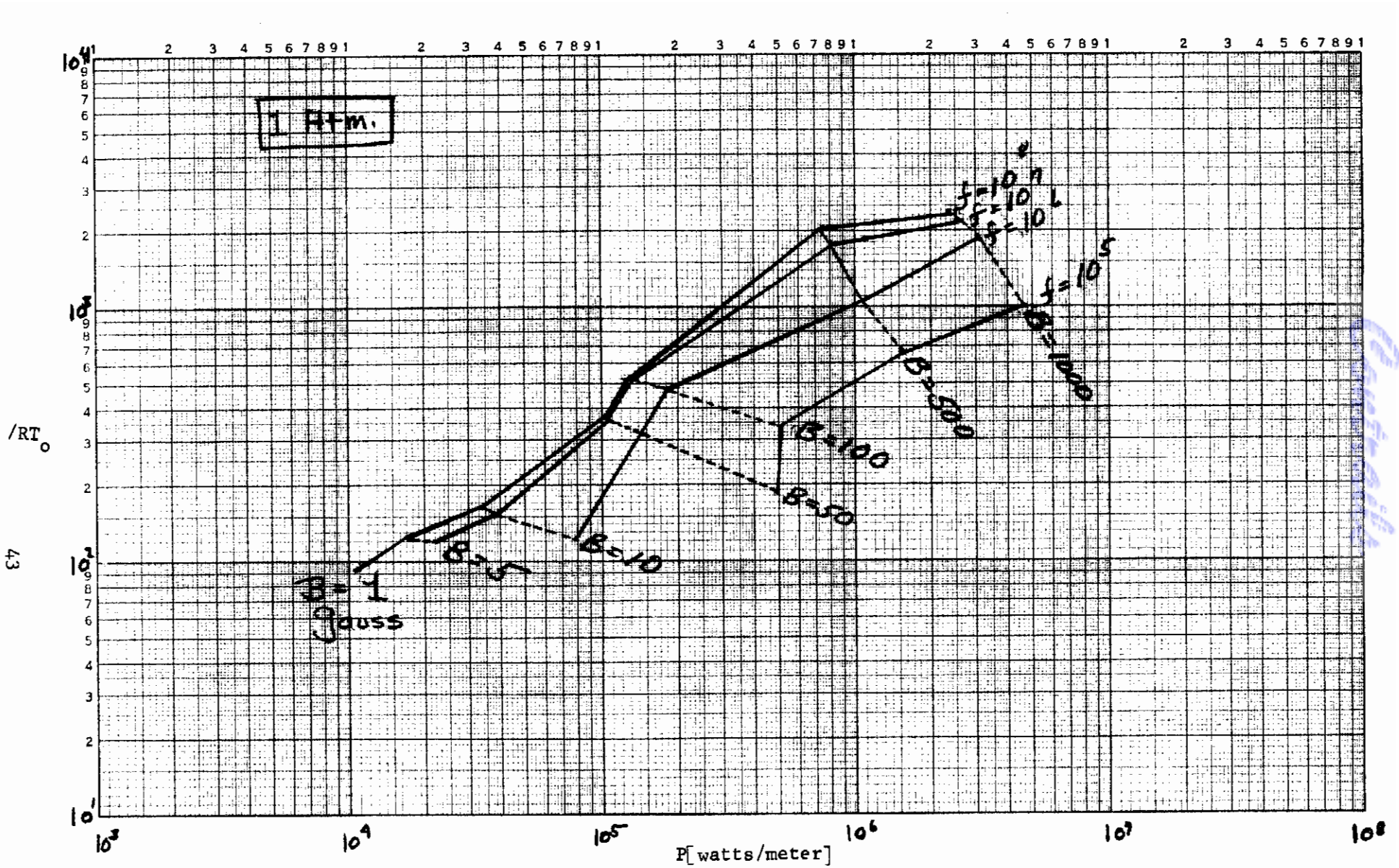

FIGURE 8. DISCHARGE ENTHALPY VERSUS POWER (1 ATM)

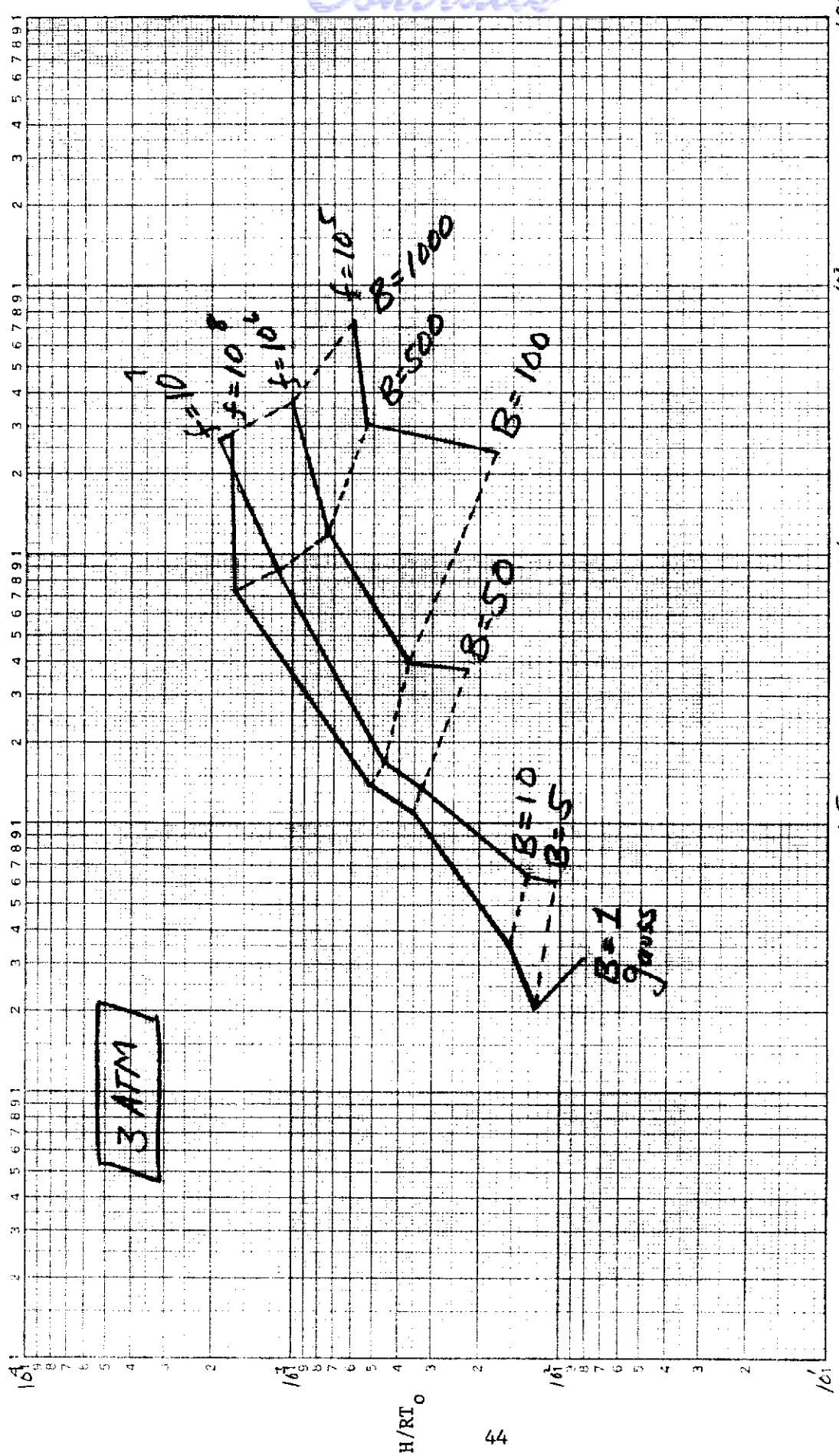

FIGURE 9. DISCHARGE ENTHALPY VERSUS POWER (3 ATM)

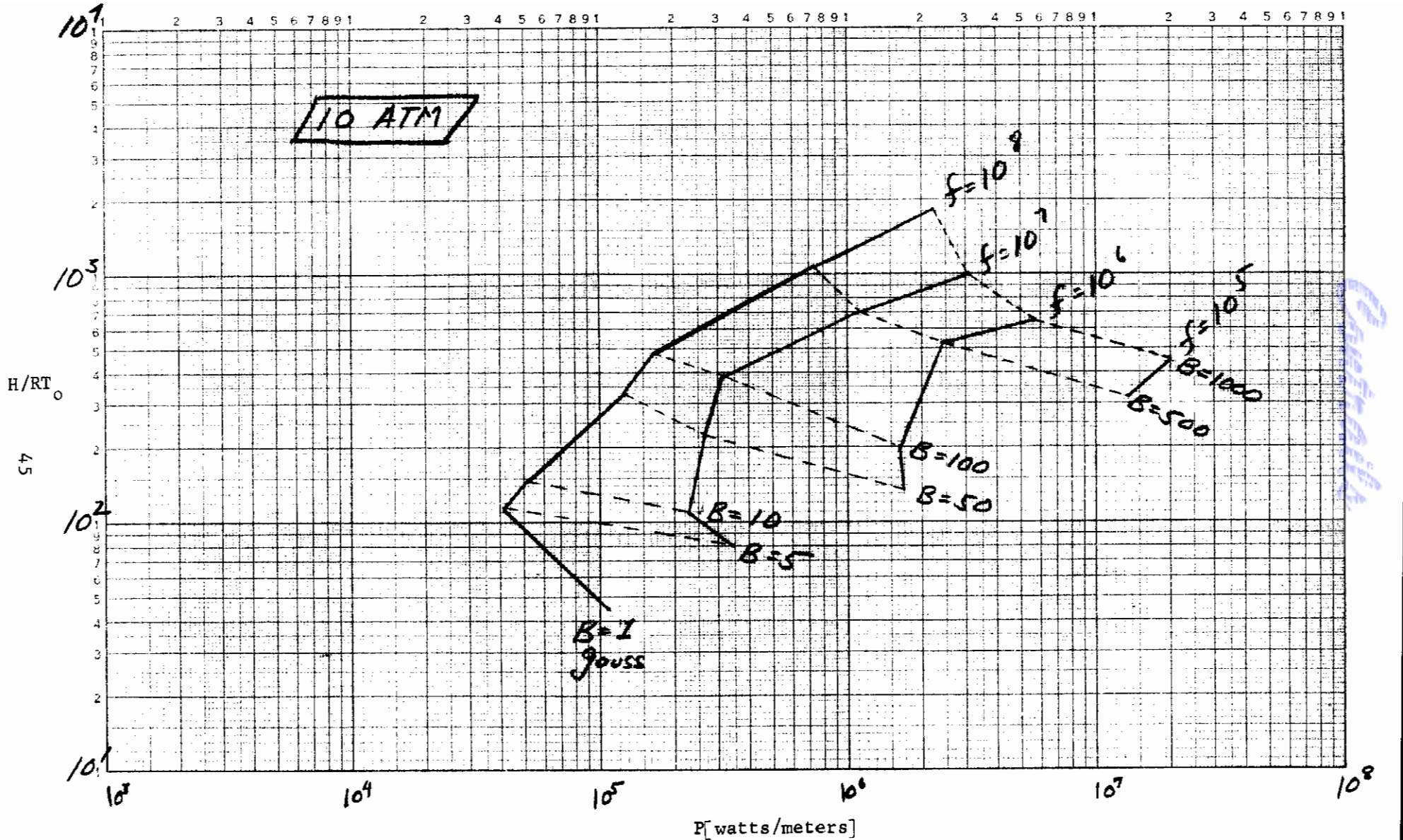

FIGURE 10. DISCHARGE ENTHALPY VERSUS POWER (10 ATM)

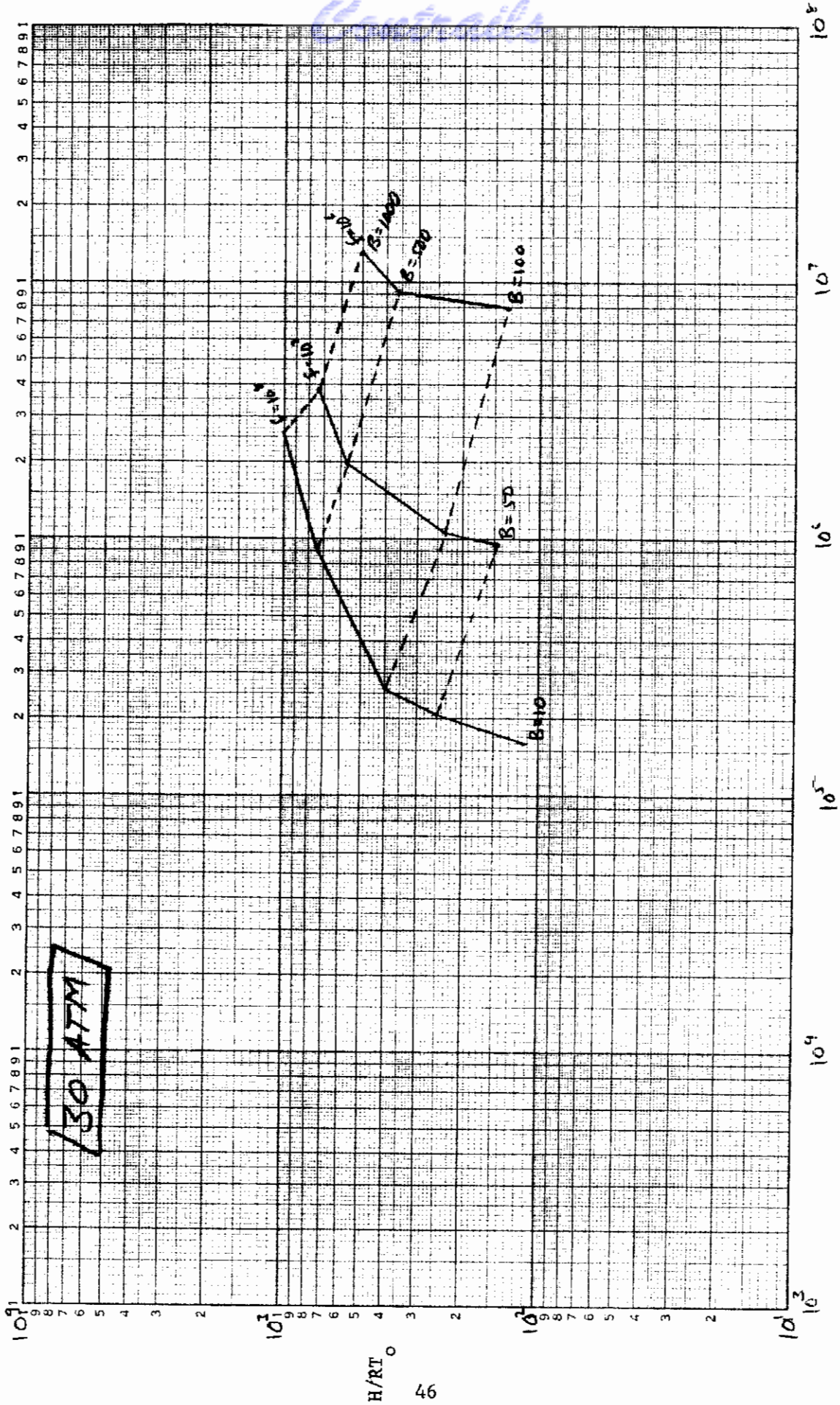

FIGURE 11. DISCHARGE ENTHALPY VERSUS POWER (30 ATM)

Design Scheme:

1. The discharge radius is given by Eq. (10):

$$R = \left[\frac{2.63A^2}{1 + Q}\right]^{1/2}$$

2. For the given pressure, the appropriate H vs R map is consulted. The frequency and applied field requirements are determined by the point (H,R) on this map.

3. The zero flow power (per unit length) is obtained from

$$P_o = 3 \times 10^6 \, B^2 \, R^2 \, f$$

4. The product $\dot{w}H$ is formed from the assigned operating conditions. This is converted to conventional power units by

$$\dot{w}H \text{ BTU/sec} - 1.058 \, \dot{w}H \text{ kilowatts}$$

5. The total power is found from the flow relation:

$$P_{total} = P_o + \dot{w}H$$

6. The final field requirement is computed from the scaling law

$$P/\ell = 3 \times 10^6 \, B^2 \, f \, R^2$$

This completes the selection of the basic design parameters.

D. A 50-MEGAWATT ELECTRODELESS ARC HEATER

The conceptual design procedure presented above can be employed to provide an estimate of comparison between the performance characteristics of the electrodeless arc and those of the DC arc in application as air heating

techniques. Such a comparison is somewhat arbitrary because the optimum operating conditions for a high performance DC heater are not necessarily the same as those of an electrodeless heater; hence, the ideal operating point for a DC device may not be ideal for a high frequency heater of similar power, or vice-versa. An arbitrary comparison nevertheless will be quite useful in developing a "feel" for the potential of the electrodeless arc, and can serve as a convenient starting point for future engineering development.

Scaling parameters for a high performance DC heater were developed from studies by Eschenbach, et al[65]. From the results of these studies, Smith and Doyle[66] were able to execute the conceptual design of a fifty-megawatt DC arc air heater and to predict the performance characteristics of this heater. These predictions are presented in Table I, where N is a scaling parameter[65] determined by the linear dimensions of the DC arc heater.

Similar data for an equivalent electrodeless arc air heater can be derived from the electrodeless arc design scheme. Ideally, the same operating point would be chosen for both cases. Unfortunately, however, adequate tabulations of the transport properties of air for pressures greater than thirty atmospheres were not available for inclusion in the numerical analysis of the electrodeless arc energy balance. The operating point of the sample electrodeless heater must therefore be chosen at the maximum evaluated

TABLE I

	N = 2 Actual Data	N = 7 Scaled Data
Arc voltage	4360	15,220
Arc current - amps	936	3,280
Power to heater - MW	4.08	50.00
Power to air - MW	2.14	26.25
Efficiency - percent	52.2	52.2
Air flow rate - lb/sec	0.511	6.260
Bulk air enthalpy - BTU/lb	2970	3,970
Heater chamber pressure - PSIA	550	550
Nozzle throat diameter - inches	0.525	1.835
ΔT cathode water - ^{o}F	65	65
Cathode water flow rate - gal/min	172	2,105
Cathode-nozzle loss - MW (%)	1.64(40)	20(40)
ΔT anode water - ^{o}F	25	25
Anode water flow rate - gal/min	72	882
Anode loss - MW (%)	0.264(6.5)	3.25(6.5)
ΔT swirl chamber water - ^{o}F	14	14
Swirl chamber water flow rate - gal/min	18.0	221
Swirl chamber loss - MW (%)	0.037(1.0)	0.50(1.0)
Total heat loss - MW (%)	1.941(47.5)	23.75(47.5)

pressure of thirty atmospheres (i.e., about twenty percent less than the pressure in the DC case).

The difference in pressures between the two cases is not considered to be of appreciable significance[67] because the thermodynamic properties of an air plasma at thirty atmospheres pressure are not appreciably different from the thermodynamic properties of the same air plasma at thirty-seven atmospheres pressure. The physical processes occurring in the one case must be nearly the same as those occurring in the other case. Clearly, however, the power requirement for any arc discharge at high pressures increases with pressure. To prevent an unfair bias in favor of the electrodeless arc for the comparison of the two techniques, the electrodeless arc operating point will therefore be further changed to accommodate both a larger mass flow and higher enthalpy than the DC arc comparison case. Rather than making an arbitrary choice for these parameters, the enthalpy will be taken at a known point (i.e., one that was calculated in the numerical analysis), and the air flow will be adjusted to give a total power requirement of 50 megawatts. A meaningful comparison is then possible for the power balances for the two cases, although the apparent advantage now stands completely with the DC arc.

The operating point assigned for this design is as follows:

P = Pressure = 30 atmospheres

H = Bulk air enthalpy = 5330 BTU/lb

$\dot{w}$ = weight flow rate = 8.7 lb/sec

Gas : air

The induction solenoid is assumed to have a diameter 2A of 0.127 meters and a length of one meter, and the Q of the induction circuit under load is taken at 7.43.

The effective radius of the discharge is derived from the expression for circuit Q:

$$R = \left[A^2/0.38\ (1 + Q)\right]^{\frac{1}{2}} = 3.55 \times 10^{-2} \text{ meters.}$$

In Figure 7 appeared an electrodeless arc map in which the bulk enthalpy of air at thirty atmospheres pressure is given as a function of discharge radius for various values of the applied magnetic field and frequency. These are the zero-flow values and they refer to the maintenance conditions for an electrodeless arc.

In the case of interest, $H/RT_o = 5330/35.58 = 1.5 \times 10^2$. Referring to Figure 7 it is seen that a field of 5×10^{-3} w/m^2 (= 50 gauss) and a frequency of 10^7 cps are required to produce a discharge of the proper size with the assigned bulk enthalpy.

The maintenance power P_o for these conditions is found from the second scaling law (or Fig. 11):

$$P_o = 3 \times 10^6\ B_o^2\ R^2\ f = 9.45 \times 10^5 \text{ watts.}$$

The enthalpy of convection is

$$\dot{w}H = 4.64 \times 10^4 \text{ BTU/sec} = 4.94 \times 10^7 \text{ watts.}$$

The total power requirement is obtained from the flow relation

$$P_{total} = P_o + \dot{w}H \approx 5 \times 10^7 \text{ watts.}$$

The transport losses for this case were computed in the numerical integration of the energy balance equation for the stated conditions:

$$P_{rad} = 7.87355 \times 10^{5} \text{ watts}$$

$$P_{cond} = 1.62221 \times 10^{5} \text{ watts.}$$

As before, the field required to transfer fifty megawatts to the flowing system is calculated from the second scaling law:

$$B = \left[P_{total} / 3 \times 10^{6} R^{2} f \right]^{\frac{1}{2}} = 3.63 \times 10^{-2} \text{ w/m}^{2}.$$

The circuit parameters are next calculated. The circuit Q under load is

$$Q = \omega L / \mathcal{R} = 7.43$$

Then

$$L = 1.18 \times 10^{-7} \mathcal{R} .$$

For fifty megawatts, the circulating current in the tuned circuit is found from

$$1/2 \; I^{2} \mathcal{R} = 5 \times 10^{7},$$

where I is the peak value of this current. Thus $I^{2}L = 11.8$.

The potential developed by the circulating current across the induction solenoid is L dI/dt. It is desirable for practical reasons not to permit this voltage to exceed 200 KV. Then

$$LI = 3.18 \times 10^{-3} \text{ (peak)}$$

Thus, in the tuned circuit the peak current is given by

$$K = \frac{I^{2}L}{IL} = \frac{11.8}{3.18 \times 10^{-3}} = 3.71 \times 10^{3} \text{ amperes}$$

and

$$L = \frac{3.18 \times 10^{-3}}{3.71 \times 10^{3}} = 8.58 \times 10^{-7} \text{ hy}$$

and

$$\mathcal{R} = \frac{L}{1.18 \times 10^{-7}} = \frac{8.57 \times 10^{-7}}{1.18 \times 10^{-7}} = 7.26 \text{ ohms.}$$

This resistance also equals $\omega\Delta L$, hence the unloaded inductance is

$$L_o = \frac{\mathcal{R}}{\omega} + L = 9.735 \times 10^{-7} \text{ hy.}$$

The unloaded solenoid inductance is simply

$$L_o = \frac{\mu_o N^2 \pi A^2}{\ell} .$$

Inserting the appropriate values, it is seen that eight turns are required to give the required inductance.

The high frequency (i.e. "skin") resistance of the solenoid is $nR_{\square}$, where $R_{\square}$ is the resistance per square unit of surface given by

$$R_{\square} = 1/\sigma\delta,$$

and n is the number of square units of conductor surface. For a solenoid of diameter D with N turns the total length is approximately $N\pi D$. If the solenoid is made of hollow tubing of diameter d, the square unit of surface has the dimensions $\pi d \cdot \pi d$. The number n of such squares on the solenoid is ND/d. The total resistance of the solenoid is then $ND/\sigma\delta d$. If the solenoid for the 50 MW electrodeless arc heater is wound from 2.54 centimeter diameter copper tubing its resistance is

$$R_{solenoid} = \frac{ND}{\sigma\delta d} = \frac{8 \times 12.7 \times 1.76 \times 10^{-8}}{3.16 \times 10^{-5} \times 2.54} = 2.33 \times 10^{-2}\ \Omega$$

where $\sigma_{cu} = (1/1.76 \times 10^{-8})\ \Omega^{-1}\ m^{-1}$, and δ is the skin depth in copper at the operational frequency of 10^7 cps (= 3.16×10^{-5} m).

The ohmic dissipation for the solenoid is calculated:

$$1/2\ I^2\ R_{solenoid} = 1.535 \times 10^5 \text{ watts.}$$

Finally, the heat loss to the expansion nozzle is estimated to be the same for an electrodeless arc as it is for an equivalent DC arc. The data for the DC arc indicate that 40 percent of the total power transferred to the gas is retransferred to the cathode-nozzle system[66]. The most conservative estimate for cathode losses is obtained by ignoring all cathode surface effects and simply assuming that the electronic and allied losses at the cathode are equal to those occurring at the anode (i.e., given in Ref. 66 as 6.5%). The nozzle loss is then the difference: 33.5 percent of the total power transferred to the gas is lost to the nozzle. Anode and cathode losses are, of course, absent in the electrodeless system.

The important parameters for the electrodeless arc system are presented in Table II. The two systems are compared in Table III.

TABLE II. TABULATION OF ELECTRODELESS ARC PARAMETERS

Pressure	30 atm
Bulk air enthalpy	5330 BTU/lb
Air flow rate	8.7 lb/sec
Power to air	33.8 Megawatts
Power to nozzle	16.3 Megawatts
Power radiated to wall	0.79 Megawatts
Power conducted to wall	0.16 Megawatts
Total heat loss	17.25 Megawatts
Efficiency of heater	65.5%
Discharge diameter	7.11 cm
Solenoid diameter	12.7 cm
Magnetic field/frequency	363 gauss/10^{7} cps
Solenoid: Inductance	9.735×10^{-7} Hy
Turns	8 - 1" dia Cu Tube
Resistance	2.23×10^{-2} ohms
Power loss	0.135 Megawatts
Capacitance	296 Pf
Circuit Q	7.43
Solenoid current	3.71×10^{3} peak amperes

TABLE III. COMPARISON OF DC AND ELECTRODELESS ARC HEATERS

	DC	Electrodeless
Arc voltage	15,220 volts	-
Arc current	3,280 amperes	-
Induction field	-	363 gauss
Frequency	-	10^7
Power to heater	50 MW	50 MW
Power to air	26.25 MW	33.8 MW
Efficiency	52.2 %	65.5 %
Air flow rate	6.26 lb/sec	8.70 lb/sec
Bulk air enthalpy	3970 BTU/lb	5330 BTU/lb
Heater chamber pressure	37.5 atm	30 atm
Nozzle-cathode loss	20 MW	16.3 MW
Anode loss	3.25 MW	0
Total heat loss	23.75 MW	17.25 MW

SECTION IV

COMMENTS ON THIS STUDY

A. PROJECT OBJECTIVE

As stated in Section I, the objective of this program was to determine the feasibility of utilizing the electrodeless arc discharge to generate the reservoir conditions necessary for hyperenvironmental gas-dynamic test facilities, and to determine if the predicted performance of the electrodeless discharge significantly exceeds that of the DC arc in the high pressure air heating applications.

These objectives have been met. It has been found that such application of the electrodeless arc is indeed feasible; moreover, in the specific example treated, the predicted performance of an air heater utilizing the electrodeless discharge was shown to be superior to that of an air heater power by a high voltage direct current arc discharge operated near the same set of conditions.

B. COMMENTS ON THE COMPARISON OF THE DC AND ELECTRODELESS ARCS

The performance characteristics of an electrodeless arc heater must be evaluated over the entire spectrum of operating points before a truly meaningful comparison with the high voltage direct current arc heater can be made. Such a comprehensive evaluation is not possible with the information gained during the present study alone. It is possible, however, to present qualitative evaluations of the trends indicated by this study, and to interpret these evaluations in terms of the projected overall performance characteristics of the electrodeless arc discharge. Such projected evaluations are necessarily speculative, but speculation based on thorough analysis is often of considerable value.

All DC arc devices have operating characteristics that can be described in terms of specific voltage-current relations. Such V-I characteristics are usually presented as a family of curves, any one of which is determined by the flow through the discharge or the discharge pressure, or some equivalent parameter. The slope of a VI curve (i.e., dV/dI) at an operating point is therefore equivalent to the impedance presented by the arc device to the current generator for the given flow conditions. Efficient transfer of power to the gas flowing through the discharge requires that this impedance equal (or nearly equal) the generator impedance, however. Thus, only a single point (actually a small interval) on a V-I characteristic curve represents an efficient condition of operation for a DC arc device. Changes in pressure or flow conditions are reflected in an impedance change that does not necessarily maintain the

discharge at an efficient operating point. Some latitude in parameter variation is offered by the use of ballasting techniques, but any such remedy consists more of matching the power source to the arc, rather than the reverse, and nevertheless tends to degrade the overall operational efficiency of the system.

The electrodeless arc was seen to match the impedance of its generator as a condition of its existence. Thus, this discharge is electrically efficient under all circumstances, and changes in pressure of flow can not degrade the electrical efficiency of the electrodeless arc. In an electrical sense the electrodeless arc is therefore the standard of comparison for efficiency.

The DC arc has a diameter D that depends[68,69] on the discharge pressure according to

$$D = (\text{const})P^{-\gamma}$$

where γ depends on the discharge current. An increase in discharge pressure thus decreases the discharge size. If the current is held constant, the discharge temperature must increase to provide for the increased current density, hence a greater fraction of the total power is thermally radiated from the arc with increasing pressure. At pressures of several atmospheres this radiation is of no major significance, but at elevated pressures, say several hundreds of atmospheres, radiation is known to dominate the energy loss from the arc, and represents the main source[70] of the confinement problems for high enthalpy, high pressure DC arc plasmas.

According to Stephens,[67] a significant increase in pressure is not favorable for high gas enthalpy generation in DC arc heaters, but is favorable toward high radiation energy generation.

In contrast, the electrodeless arc is an exceptionally flexible radiator. It has been shown that the electrodeless arc has a well defined radius that is determined by the arc conductivity and by the induction field frequency. This can immediately be seen by examining the radial temperature profiles for the electrodeless arc that are presented in Appendix VI to this report. Clearly, one can adjust the size of an electrodeless arc by adjusting the frequency of the induction field, as well as by adjusting the discharge pressure and/or the magnitude of the induction field. Thus, the electrodeless arc has an additional degree of freedom in its operation: the frequency. It is immediately obvious that, since radiation loss is enhanced by decreasing the size of the DC arc at constant current, the electrodeless arc can be made to be an excellent radiator (at a constant power and pressure) by an adjustment of the induction field frequency to decrease the discharge radius and maximize the discharge temperature. Likewise, if the enthalpy of the discharge gas is to be maximized (again at constant power and pressure) one adjusts the frequency of the induction field to obtain a larger discharge at a much lower temperature. This not only suppresses temperature radiation, but also permits the direct ohmic heating of the outer fringes of the discharge volume, and establishes a mechanism for a significant enhancement in the attainable efficiency in the production of high enthalpy flows at high pressures.

The fraction of the total power transferred to the stationary electrodeless arc that appears as a radiation loss is plotted against the discharge power in Figures (12-15) where a minimum is clearly indicated for each constant frequency family. This radiation fraction increases with pressure and power, and at high power levels apparently increases with decreasing frequency.

In the equivalent DC case similar curves would obtain; since the minimum point for each f = (const.) curve indicates the power level at which radial conduction dominates the transport processes. Only one curve would appear on a constant pressure graph in the DC case however, whereas the electrodeless arc would have a constant-pressure family of these relations, the total number consisting of as many members as there are useable frequencies.

A superficial examination of these curves suggests that, at some level of power the electrodeless arc, just as the DC arc, will radiate away all of its power, or at least enough of its power will be radiated that no further increase in discharge enthalpy is possible. This is probably a correct statement, but is not justified by a simple extrapolation of these radiation loss curves because at a sufficiently high temperature and pressure the number density of free electrons within the discharge becomes sufficiently great that self-absorption of temperature radiation occurs. The radiation fraction then becomes a surface effect where the surface is determined by the opacity of the discharge plasma.

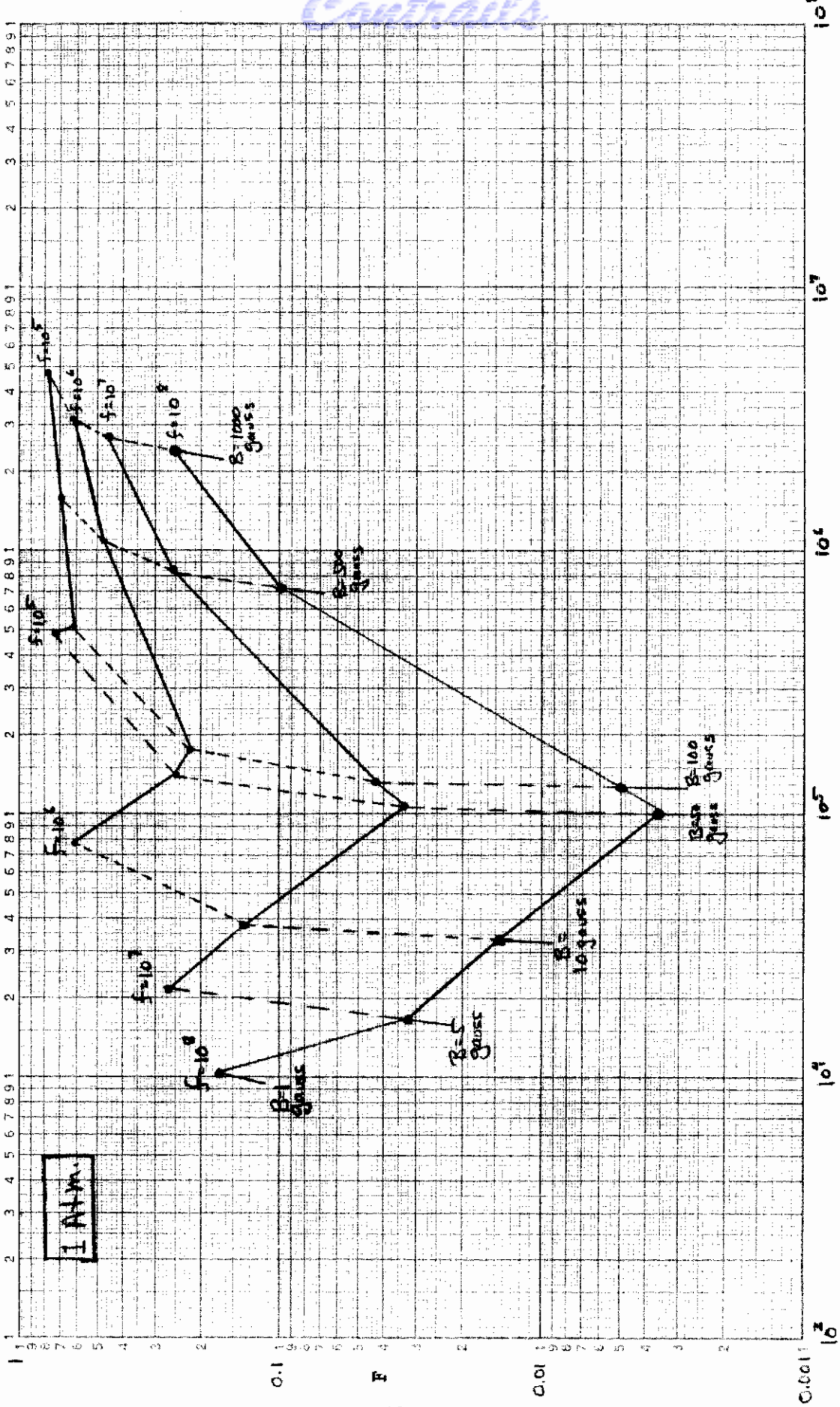

FIGURE 12. FRACTION OF TOTAL POWER RADIATED VS TOTAL POWER FOR STATIONARY DISCHARGES (1 ATM)

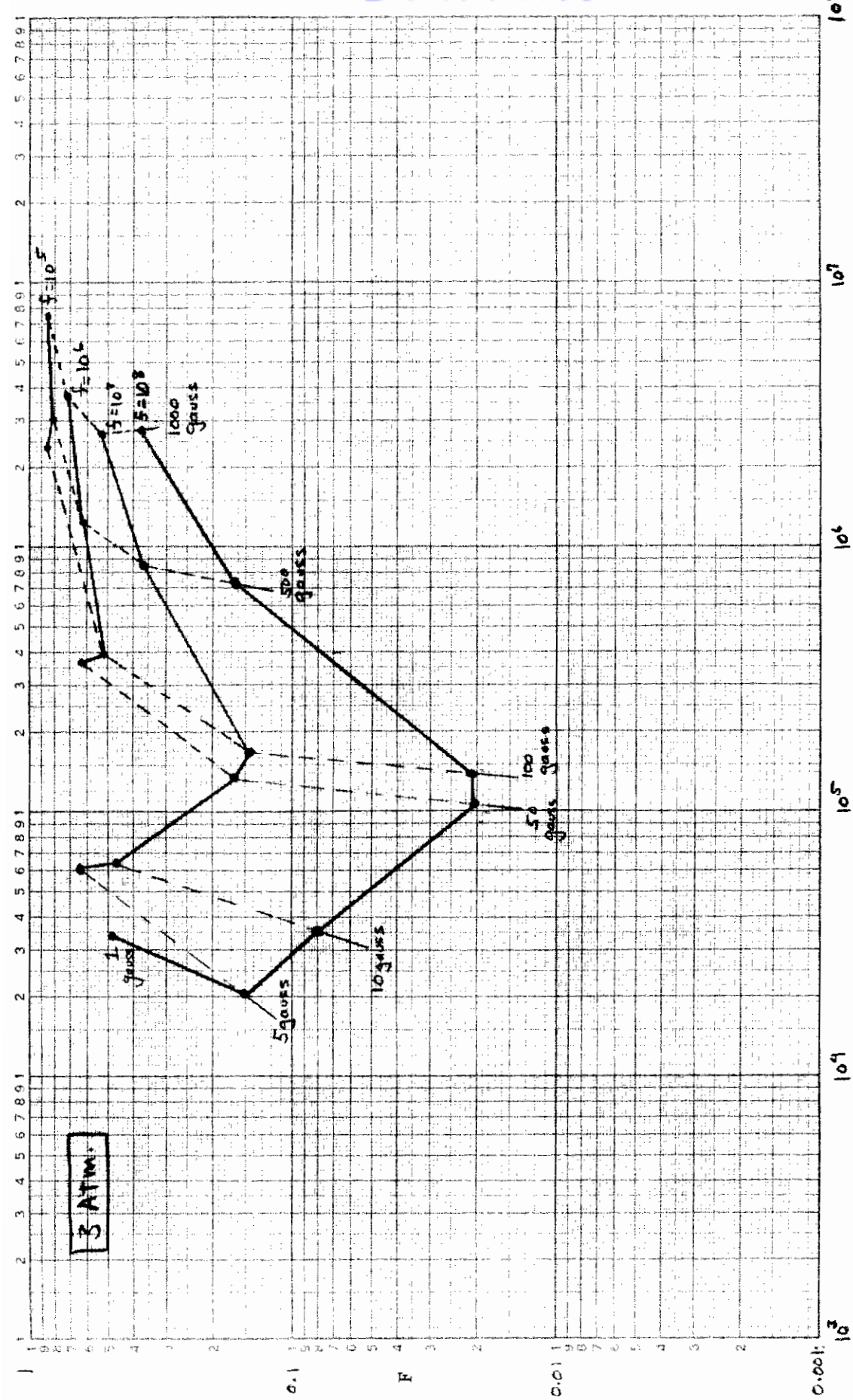

FIGURE 13. FRACTION OF TOTAL POWER RADIATED VS TOTAL POWER FOR STATIONARY DISCHARGES (3 ATM)

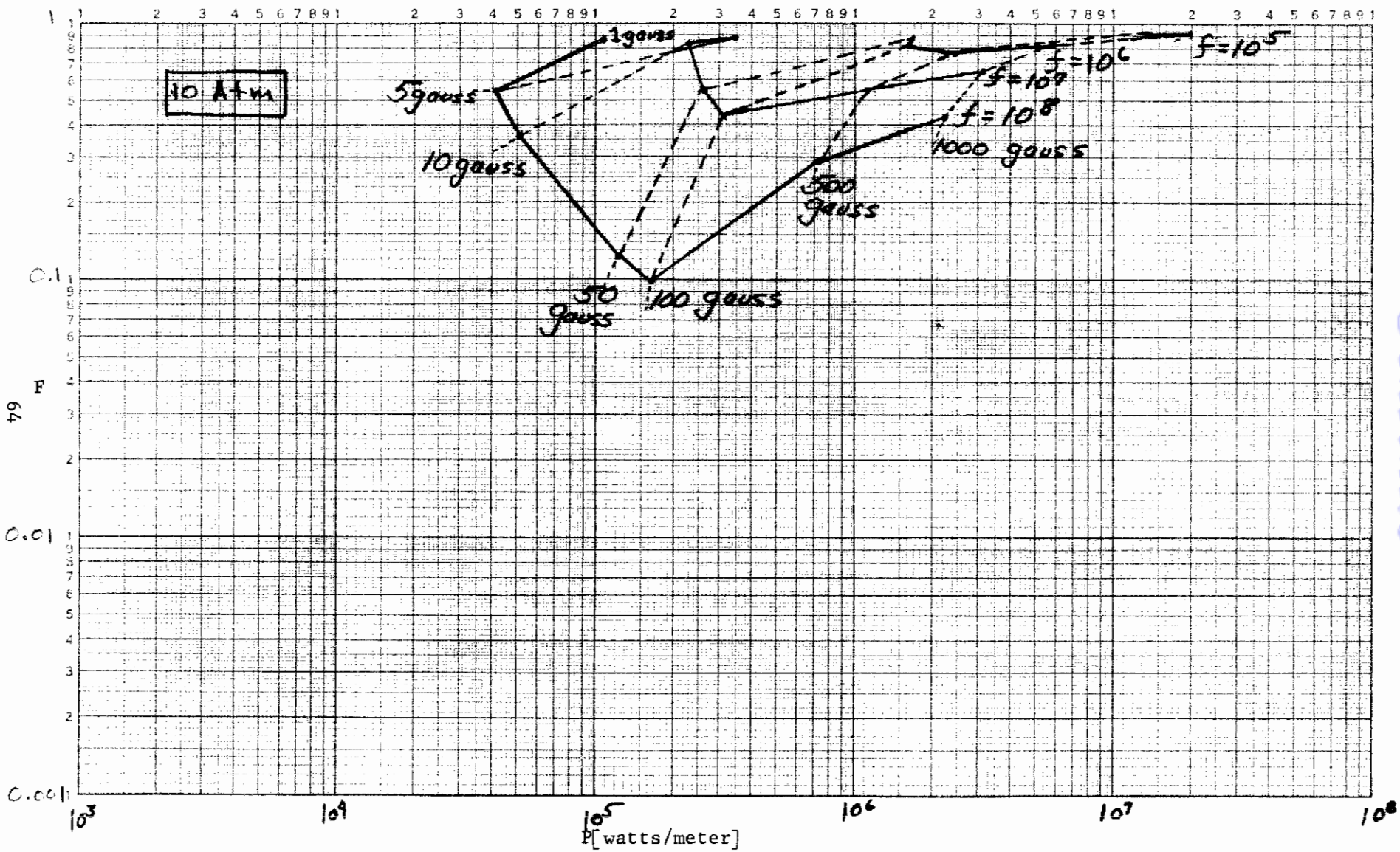

FIGURE 14. FRACTION OF TOTAL POWER RADIATED VS TOTAL POWER FOR STATIONARY DISCHARGES (10 ATM)

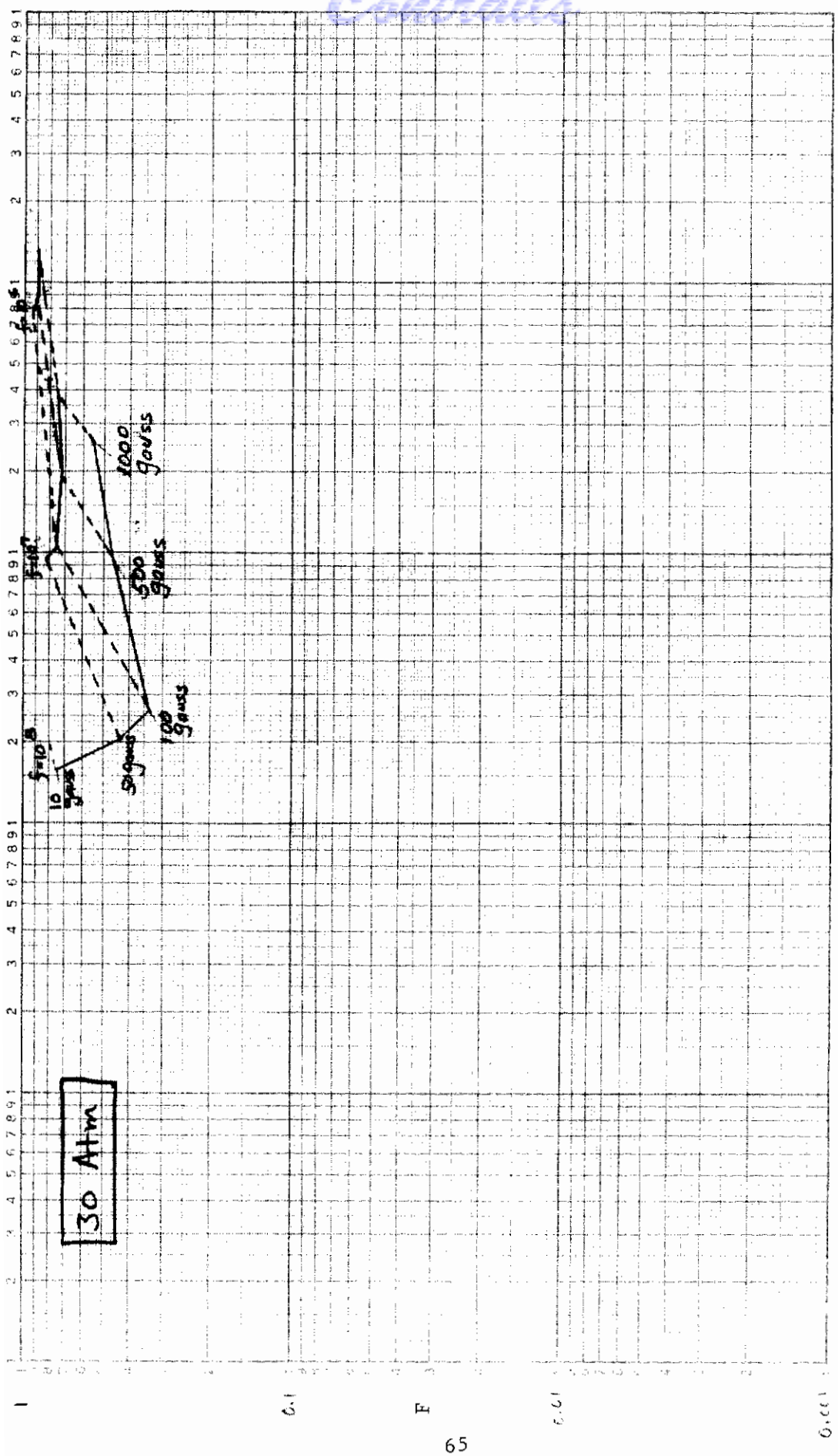

FIGURE 15. FRACTION OF TOTAL POWER RADIATED VS TOTAL POWER FOR STATIONARY DISCHARGES (30 ATM)

The discharge pressures treated in the present analysis were insufficient to allow self absorption to occur, hence this important effect does not appear in the families of radiation loss curves presented here.

The measure of discharge opacity of interest in this discussion is the Rosseland mean absorption coefficient or its reciprocal, the Rosseland mean free path. At high pressures (even at relatively low temperatures) this parameter governs radiation transport and will have a significant effect on both discharge enthalpy and radiation loss. For example, at a pressure of 1000 atmospheres a $10,000^{o}K$ plasma has a Rosseland mean free path of about two centimeters, and all the radiation from layers in the plasma deeper than two centimeters is effectively trapped within the discharge. The effect of this radiation trapping on the overall discharge efficiency is quite profound, since radiation is the dominant loss mechanism at the elevated temperatures and pressures of near-future interest. This important parameter is plotted in Figure 16 for several interesting pressures.

Taken together, the preceding comments present a hopeful picture for the future of high enthalpy plasma production in high pressure air, where the electrodeless arc produces a discharge that is constrained to absorb a maximum amount of power from its generator, and the size of the discharge is adjusted to maximize the trapping of radiation within the discharge.

An additional ramification of the electrodeless arc's additional degree of freedom is the suggestion that, since both the applied induction field

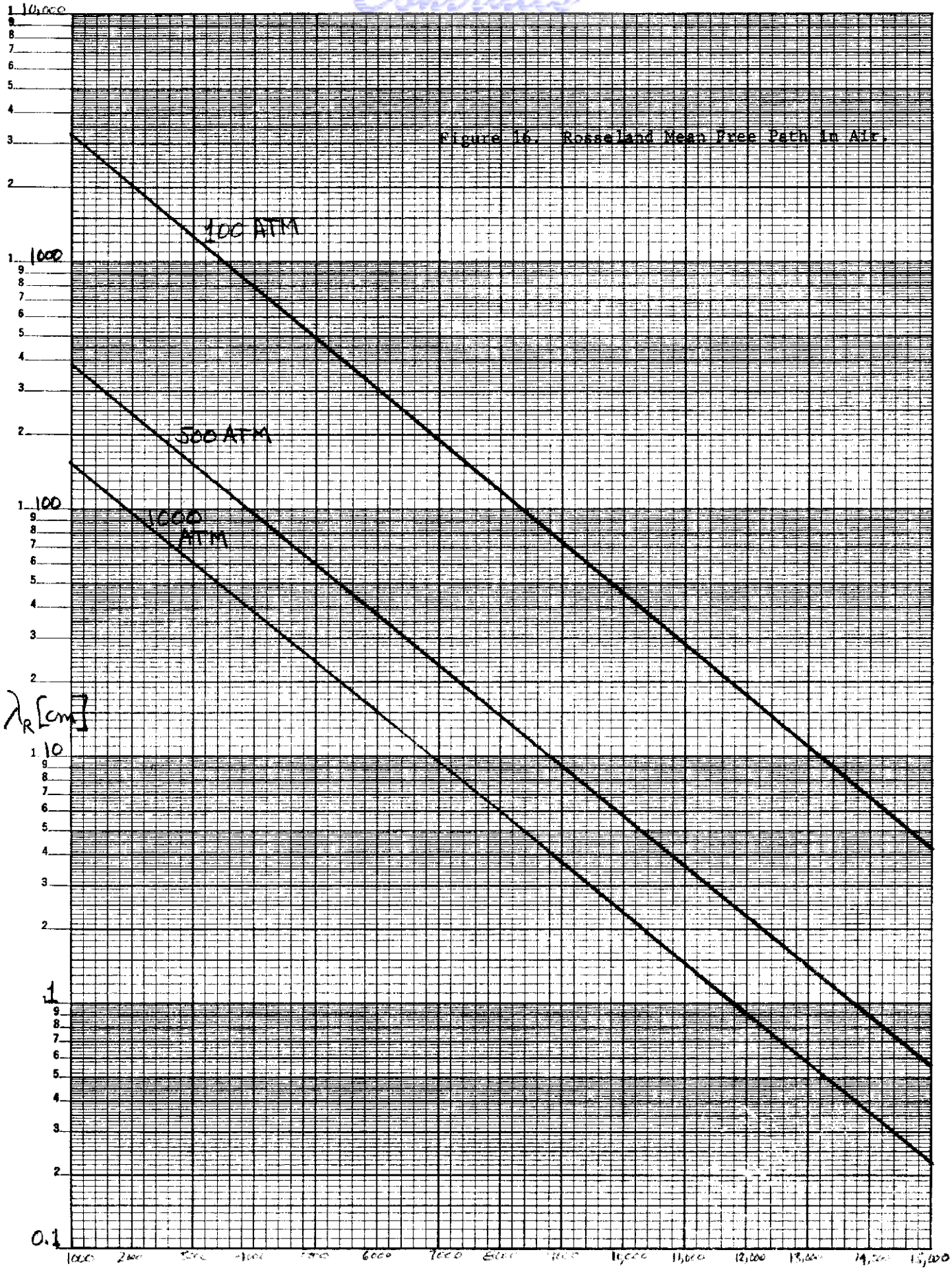

Figure 16. Rosseland Mean Free Path in Air.

and its frequency are adjustable, and since the flow through the discharge is adjustable, the simulation of large portions of an entire reentry trajectory may be an additional capability of the electrodeless arc heater[5].

The economics of high pressure plasma production have not been considered in this study. Several basic facts are available, however, that enable the economic comparison of the high voltage DC arc and the electrodeless arc, if only in the sense of a first approximation.

Facility costs are obviously the same for the electrodeless application as they are in the conventional approach. Also, the electrodeless device would most likely be designed around the same type of power supply as is the high voltage DC device, hence there is no difference in this respect. The only significant economic difference between the two approaches derives from the necessity for the production of high frequency oscillations to produce the electrodeless arc discharge. This represents a capital cost for electrodeless plasma production that must be borne in addition to all the costs of DC plasma production. Thus, the electrodeless arc requires apparatus that is more expensive watt-for-watt than that required for the high voltage DC arc.

It is not possible at this time to compare the cost of the enthalpy-watt (i.e., the power actually delivered to the flowing gas), because these data have not been assembled for this report. It is clear that the relative enthalpy-watt cost for the electrodeless arc would be reduced from the watt-for-watt cost because of the higher relative efficiency of the electrodeless arc. It is not clear at this time that any general cost-advantage for the electrodeless arc would (or could) result, however.

On the other hand, some specific results would obtain. Discharges involving small amounts of power (say, a few kilowatts or less) in low-pressure gases are probably less expensive to produce without electrodes than with electrodes because the fabrication costs for the DC arc heater alone are likely to exceed the total cost for the high frequency system.

At powers greater than a few kilowatts the cost of the radiofrequency generator dominates the capital picture (roughly $0.50/watt) and the DC arc generator is the obvious choice. Additionally, one must choose the DC device (i.e., economically) even at moderate power levels (say, up to several megawatts at this time) because the equipment costs for the electrodeless device at moderate power levels remain relatively high.

In the upper pressure and/or flow limits of the moderate power levels the cost advantage for the DC arc begins to suffer because of radiation loss (i.e., the enthalpy-watt cost increases), and the effects of electrode wear-and-tear are noticed in this "higher-performance" operational regime. At the ten-to-twenty megawatt level the enthalpy-watt cost advantage for the DC arc is expected to diminish for these reasons. Above about fifty megawatts, especially at high pressures, the enthalpy-watt cost advantage must belong to the electrodeless arc because of the excessive radiation loss from the DC arc.

REFERENCES

1. Thomson, J. J., Phil. Mag. S.5, 32, 321 (1891); S.5 32, 445 (1891).

2. Thomson, J. J., Phil. Mag. S.7, 4, 1128 (1927).

3. Francis, G., Ionization Phenomena in Gases, Academic Press, Inc., New York, 1960, p. 137.

4. Hollister, D. D., "On the Electrodeless Arc in High-Pressure Air," accepted for publication in Physics Letters, North-Holland Publishing Co., Amsterdam, The Netherlands.

5. Hollister, D. D., An Electrodeless Technique for Full Scale Simulation of the Reentry Environment, Proc. of Second Space Congress, Cocoa Beach, Fla., April, 1965; pp. 549-574.

6. Hollister, D. D., IEEE Trans. PTGAP, AP 13, 134 (1965).

7. Soshnikov, V. N., and Trekhov, E. S., High Temperature 4, 165 (1966).

8. Freeman, M. P., and Chase, J. D., J. Appl. Physics 39, 180 (1968).

9. Hollister, D. D., Bull. Amer. Phys. Soc. 7, 441 (1962).

10. Hittorf, W., Wied. Ann. 21, 137 (1884).

11. Townsend, J. S., and Donaldson, R. H., Phil. Mag. S.7, 5, 178 (1928).

12. MacKinnon, K. A., Phil. Mag. S.8,52, 605 (1929).

13. Kunz, Jakob, Phil. Mag. S.7, 13, 964 (1932).

14. Tykocinski-Tykociner, J. Phil. Mag. S.7, 13, 953 (1932).

15. Babat, G., J. Inst. Elect. Eng. (London) 94, 27 (1947).

16. Smith, C. G., Phys. Rev. 59, 997 (1941).

17. Carruthers, R., Appl. Sci. Res. 5, 135 (1955).

18. Chuan, R. L., Phys. Fluids, 1, 452 (1958).

19. Carswell, A. I., Rev. Sci. Instr. 34, 1015 (1963).

20. See, for example: Elmore, W. C., et al, Paper 15/p/356, Second U.N. International Conf. on the Peaceful Uses of Atomic Energy, Geneva, 1958; Kvartskhava, I.F., et al, Soviet Physics-Technical Physics 5, 1253 (1961); Andryuk, E. D., et al, Soviet Physics-Technical Physics 5, 497 (1960).

21. Majoda, F. C., and Sawyer, G. A., Phys. Fluids 6, 1195 (1963).

22. Gorelik, L. L., and Sinitsyn, V. V., Soviet Physics-Tech. Physics 9, 393 (1964).

23. Olson, R. A., and Lary, E. C., Rev. Sci. Instr. 33, 1350 (1962).

24. Hollister, D. D., AIAA Jour. 2, 1568 (1964).

25. Andryukhina, E. D., et al, Zhurn. Tek. Fiziki 30, 529 (1960).

26. Eckert, H. U., Bull. Amer. Phys., Soc. 5, 371 (1960).

27. Eckert, H. U. Jour. Appl. Phys. 33, 2780 (1962).

28. Romig, M. F., Phys. Fluids 3, 129 (1960).

29. Barger, R. L., Brooks, J. D., and Beasley, W. D., NASA TN D-431, Sept. 1960.

30. Barber, R. L., Brooks, J. D., and Beasley, W. D., NASA TN D-1004, Feb., 1962.

31. Reed, T. B., Jour. Appl. Phys. 32, 821 (1961).

32. Mironer, A., AIAA Jour. 1, 2638 (1963).

33. Alfven, H., and Smars, E., Nature 188, 801 (1960).

34. Bobyrev, N. A., and Fedyanin, O. I., Sov. Phys.-Tech. Phys. 6, 959 1962.

35. Bamberg, E. A., and Dresvin, S. V., Sov. Phys.-Tech. Phys. 8, 43 (1963).

36. Raizer, M. D., Frank, A. G., Kitzeva, V. F., Sov. Phys.-Tech. Phys. 8, 893 (1964).

37. Dolgopolov, V. V., and Stepanov, K. N., Sov. Phys.-Tech. Phys. 8, 893 (1964).

38. Gal'dfarb, V. M., and Dresvin, S. V., High Temperature 3, 303 (1965).

39. Dymshits, B. M., and Koretskii, Ya.P., Sov. Phys.-Tech. Phys. 9, 1294 (1966).

40. Johnston, P. D., Phys. Letters, 20, 499 (1966).

41. Hughes, D. W., and Wooding, E. R., Phys. Letters, 24A, 70 (1967).

42. Donskoi, A. V., Dresvin, S. U., and Ratnikov, D. G., High Temperature 3, 858 (1965).

43. Rovinskii, R. E., Gruzdev, V. A., Gutenmakher, T. M., and Sobolev, A. P., High Temperature, 5, 502 (1967).

44. Gol'dfarb, V. M., Donskoi, A. V., Dresvin, S. V., and Klubnikin, V. S., High Temperature 5, 495 (1967).

45. Eckert, H. V., Kelly, F. L., and Olsen, H. N., Jour. Appl. Phys. 39, 1846 (1968).

46. Mitin, R. V., and Pryadkin, K. K., Sov. Phys.-Tech. Phys. 10, 933 (1966).

47. Mitin, R. V., and Pryadkin, K. K., Sov. Phys.-Tech. Phys., 11, 672 (1966).

48. Donskoi, A. V., Dresvin, S. V., Voronin, K. K., and Volynets, F. K., High Temperature 3, 575 (1965).

49. Vagner, S. D., and Kyrlov, N. A., Sov. Phys.-Tech. Phys. 10, 1105 (1966).

50. El-Khalafawy, T. A., Souprunenko, V. A., Ternopole, A. M., and Bourham, M. A., Physics Letters, 29A, 233 (1967).

51. Bobyrev, N. A., Sov. Phys.-Tech. Phys., 11, 316 (1966).

52. Henderson, D. B., Phys. Fluids 10, 1962 (1967).

53. Andrew, S. I., Vanyukov, M. P., Egorova, A. A., and Sokolov, B. M., Sov. Phys.-Tech. Phys. 12, 910 (1968).

54. Chandrakar, K., and von Engel, A., Proc. Roy. Soc. 284A, 442 (1965).

55. Gruzdev, V. A., Rovinskii, R. E., and Sobolev, A. P., Zhur, Prik. Mekh. Tekh. Fiziki 1, 143 (1967).

56. Rovinskii, R. E., Belousova, L. E., and Gruzdev, V. A., High Temperature 4, 322 (1966).

57. Belousova, L. E., High Temperature 4, 472 (1966).

58. Rovinskii, R. E., Gruzdev, V. A., and Shirokova, I. P., High Temperature 4, 30 (1966).

59. Eckert, H. U., Analytical Solution of the Energy Balance Equation for Thermal Induction Plasmas in Argon, Presented at the AIAA Fluid and Plasma Dynamics Conference, L. A., California, June 1968.

60. Soshnikov, V. N., and Trekhov, E. S., High Temperature 4, 318 (1966).

61. Soshnikov, V. N., and Trekhov, E. S., High Temperature 5, 467 (1967).

62. Sprouse, J. A., Coupling Mechanism between RF Excited Coils and Conductive Media, Presented at the AIAA Fluid and Plasma Dynamics Conference, L.A., Calif., June 1968.

63. Thorpe, M., RF Plasma Simulation of Gas Core Reactor, Presented at AIAA Fluid and Plasma Dynamics Conference, June 1968.

64. Fenter, F. W., The Thermodynamic Properties of High Temperature Air, Chance-Vought Report No. RE-IR-14, Chance-Vought Research Center, Dallas, Texas, 28 June 1961.

65. Eschenbach, R. C., Skinner, G. M., and Arc Laboratory Staff, Development of Stable, High Power, High Pressure Arc Air Heaters for a Hypersonic Wind Tunnel, WADD Technical Report 61-100, July 1961.

66. Smith, R. T., and Doyle, J. P., A 50-Megawatt Arc Heater: Scaling Parameters and Performance Prediction. FDL TDR 64-91, August, 1964.

67. Stephens, E. D., Survey of High Pressure Electric Arc Technology, Presented at AIAA Fluid and Plasma Dynamics Conference, June 24-26, 1968.

68. Suits, C. G., J. Appl. Phys. 10, 730 (1939).

69. Cobine, J. D., Gaseous Conductors, Dover, New York, 1958, Chapter IX, Section 9.8.

70. Cann, G. L., Buhler, R. D., Harder, R. L., Moore, R. A., Basic Research on Gas Flows through Electric Arcs - Hot Gas Containment Limits, ARL Report 64-49, March 1964.

APPENDICES

APPENDIX I

THE THOMSON MODEL OF THE ELECTRODELESS ARC

In the Thomson model the discharge is analyzed by assuming that within the induction solenoid the field quantities vary in time as exp ($i\omega t$), and that in the coaxial discharge the electrical conductivity can be replaced by a uniform "effective" conductivity σ. Elimination of the time and electric field from Maxwell's equations then yields an equation for the magnetic flux density:

$$\nabla^2 \vec{B} - i\sigma\mu_o\omega \vec{B} + \omega^2\mu_o\epsilon_o \vec{B} = 0 \qquad (1)$$

In every case of practical interest the displacement term $|\omega^2\mu_o\epsilon_o\vec{B}|$ in Equation (1) will be negligibly small compared with the conductive term $|\sigma\mu_o\omega\vec{B}|$ (e.e. $\sigma \gg \omega\epsilon_o$). Furthermore, for the long solenoid the direction of the magnetic field is considered to be entirely axial; equation (1) is then written in cylindrical coordinates:

$$\frac{d^2B_z}{dr} + \frac{1}{r}\frac{dB_z}{dr} + i^3\sigma\mu\omega B_z = 0. \qquad (2)$$

This is recognized as a Bessel equation and has a solution

$$B_z(r) = C_1 J_o (\sqrt{\sigma\mu\omega}\, i^{3/2} r) + C_2 Y_o (\sqrt{\sigma\mu\omega}\, i^{3/2} r).$$

The constants C_1 and C_2 are evaluated by noting that, at $r = 0$ $B_z(0)$ is finite, hence $C_2 = 0$, and that at the outer extremity R of the discharge $B_z(R) = B_o$, the field of a long solenoid of N/ℓ turns per unit length which carries a current I. Thus

$$B_z(r) = B_o \frac{J_o (\sqrt{\sigma\mu\omega}\, i^{3/2} r}{J_o(\sqrt{\sigma\mu\omega}\, i^{3/2} R)}, \qquad (3)$$

where $B_o = \mu NI/\ell$, gives the radial distribution of the axial magnetic field in the induced electrodeless discharge.

The radial distribution of the induced current density is obtained from Ampere's circuital law and equation (3):

$$\vec{j}(r) = \frac{1}{\mu_o} (\nabla \times \vec{B}) = \hat{\phi} \frac{1}{\mu_o} \left[- \frac{\partial}{\partial r} B_z(r) \right].$$

This is evaluated:

$$\vec{j}(r) = i^{3/2} \sqrt{\sigma\mu\omega}\, \frac{B_o}{\mu_o} \frac{J_1 (\sqrt{\sigma\mu\omega}\, i^{3/2} r)}{J_o (\sqrt{\sigma\mu\omega}\, i^{3/2} R)} \hat{\phi} \qquad (4)$$

The total current per unit length in the discharge is obtained by integrating Equation (4) over the area normal to the direction of the current:

$$\frac{I}{\ell} = \int j(r) dr = \frac{B_o}{\mu_o} \left[1 - \frac{1}{J_o(\sqrt{\sigma\mu\omega}\, i^{3/2} R)} \right]. \qquad (5)$$

The azimuthal electric field is next obtained from Ohm's law and Equation (4):

$$E_\phi(r) = \frac{j_\phi(r)}{\sigma} = i^{3/2}\sqrt{\frac{\sigma\mu\omega}{\sigma\mu}}\, B_o \frac{J_1(\sqrt{\sigma\mu\omega}\, i^{3/2} r)}{J_o(\sqrt{\sigma\mu\omega}\, i^{3/2} R)}. \qquad (6)$$

The net power transferred into the plasma cylinder is given by the real part of the integral of the Poynting vector over the plasma surface

$$\text{Power} = \text{Re}\int(\vec{E} \times \vec{H}^*)\cdot\hat{n}\, dA$$

Thus

$$I_s^2 \mathcal{R} = \frac{\pi R^2 N^2 \mu_o}{\ell}\, \omega I_s^2 \left(\frac{2\delta}{\sqrt{2R}}\right) \frac{M_1(\sqrt{2}R|\delta)}{M_o(\sqrt{2}R|\delta)} \cos\left[\theta_1 - \theta_o - \pi/4\right], \qquad (7)$$

where $\mathcal{R}$ is the effective resistance of the plasma as seen by the generator, I_s is the current through the solenoid, R is the outer radius of the discharge, and the quantities designed by M are defined:

$$M_\nu(kx)\exp\left[i\theta_\nu(kx)\right] \equiv J_r\,(i^{3/2}kx)$$

For clarity the substitution $R\sqrt{\sigma\mu_o\omega} = \sqrt{2}R/\delta$ has been made, where $\delta = \left[2/\sigma\mu_o\omega\right]^{\frac{1}{2}}$ is the "skin depth" (i.e., the e-folding distance) of a wave of angular frequency ω into an impermeable medium of conductivity σ. The resistance $\mathcal{R}$ in Equation (7) is identical to the reflected series resistance in Equation (1) of Section II of this report. Thus

$$R_{\text{refl.}} = \mathcal{R} = \frac{\pi R^2 N \mu_o}{\ell}\, \omega \left(\frac{2\delta}{\sqrt{2R}}\right) \frac{M_1(\sqrt{2}R/\delta}{M_o(\sqrt{2}R/\delta)} \cos\left[\theta_1 - \theta_o - \pi/4\right]. \qquad (8)$$

The contribution of the plasma to the total system inductance is obtained from the imaginary part of the Poynting vector:

$$L_{Plasma} = \frac{\pi R^2 N^2 \mu_o}{\ell} \left(\frac{2\delta}{\sqrt{2}R} \right) \frac{M_1(\sqrt{2}R/\delta)}{M_o(\sqrt{2}R/\delta)} \sin \left[\theta_1 - \theta_o - \pi/4 \right].$$

The total system inductance includes a contribution from the part of the solenoid volume which does not contain the discharge. This is determined:

$$L_{Total} = \frac{\pi R^2 N^2 \mu_o}{\ell} \left(\frac{2\delta}{\sqrt{2}R} \right) \frac{M_1(\sqrt{2}R/\delta)}{M_o(\sqrt{2}R/\delta)} \sin \left[\theta_1 - \theta_o - \pi/4 \right] + \frac{\pi R^2 N^2 \mu_o}{\ell} \left(\frac{A^2}{R^2} - 1 \right), \quad (9)$$

where A is the radius of the solenoid. When multiplied by $j\omega$ this quantity equals the reactive term in Equation (1) of Section II of this report. Equation (7) is of the form

$$\text{Power/unit volume} = \frac{1}{\mu_o} \left[\omega B_o^2 \, f(\sqrt{2}R/\delta) \right] \quad (10)$$

where

$$f(\sqrt{2}R/\delta) \equiv \frac{2\delta}{\sqrt{2}R} \frac{M_1(\sqrt{2}R/\delta)}{M_o(\sqrt{2}R/\delta)} \cos \left[\theta_1 - \theta_o - \pi/4 \right]. \quad (11)$$

The quantity $f(\sqrt{2}R/\delta)$ is called the loss function for the electrodeless discharge and has a maximum value when $\sqrt{2}R/\delta \approx 2.5$. This is shown in Figure A1, where it can be seen that 2.5 is the value of $\sqrt{2}R/\delta$ for which a maximum amount of power is transferred from the solenoid to the coaxial plasma for a specified R and ω. In other words, the fact that the coaxial plasma absorbs the most power when $\sqrt{2}R/\delta \approx 2.5$ can be interpreted as the condition for an impedance match between the primary and secondary of the

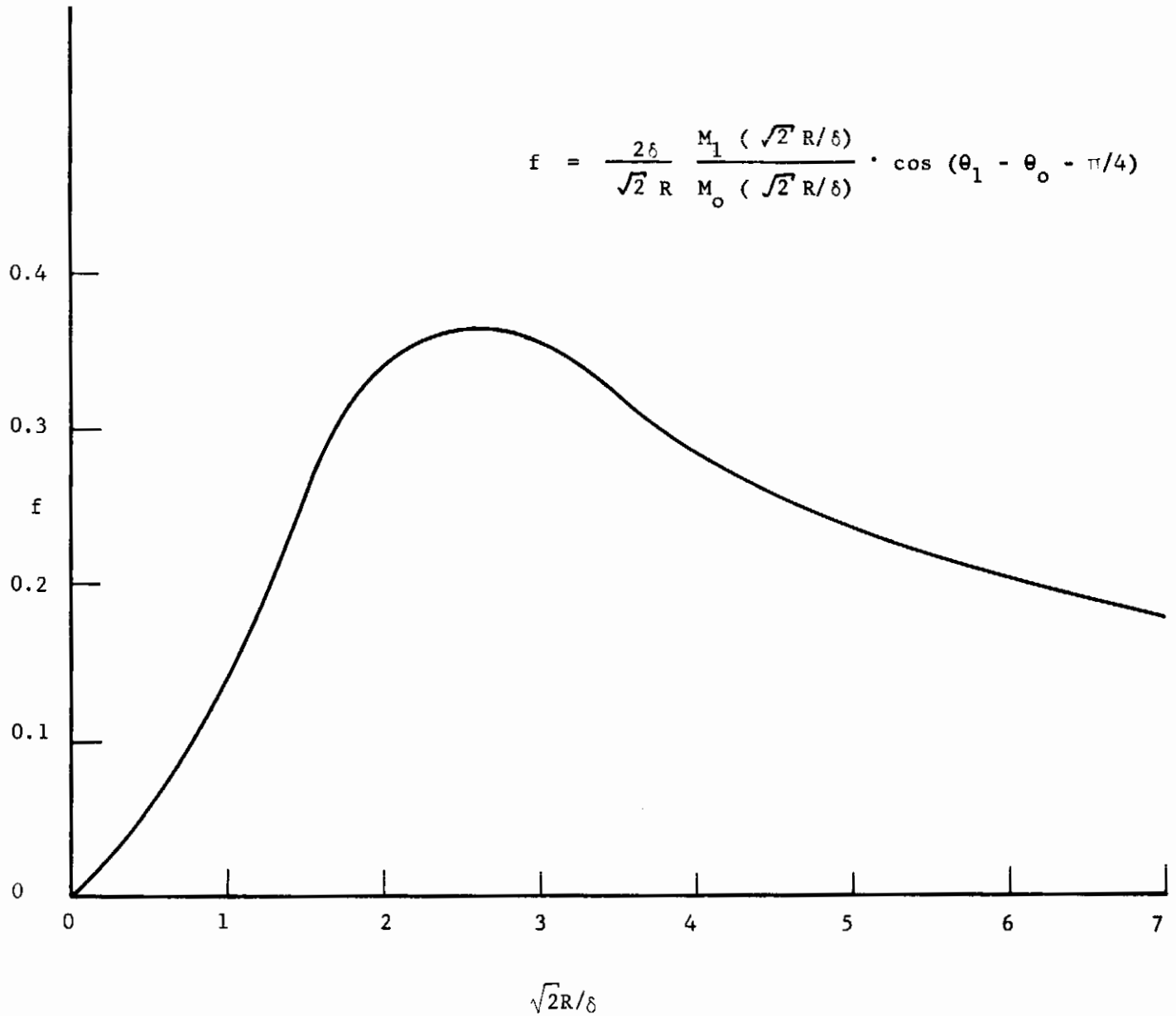

Figure 17 $f(\sqrt{2}R/\delta)$ as a function of $\sqrt{2}R/\delta$.

transformer presented earlier in Section II, Figure 1, hence as the condition for maximum operational efficiency of an induced discharge.

Since $\delta = \left[2/\sigma\mu_o\omega\right]^{\frac{1}{2}}$ this condition can be written

$$R\sqrt{\sigma\mu\omega} \approx 2.5 \qquad (12)$$

for maximum efficiency.

APPENDIX II

ENTROPY PRODUCTION AND POWER IN A FLOWING ELECTRODELESS ARC

In this development is made an appeal to the thermodynamics of irreversible processes in which the influence of flow on the rate of entropy production within the electrodeless arc is considered.

In this analysis a state of local thermodynamic equilibrium is assumed to exist in the discharge volume. The general conservation equation is written in terms of the specific entropy S in a fixed coordinate system:

$$\frac{\partial}{\partial t}(\rho S) + \nabla \cdot \vec{J}_s - \varphi_s = 0 \qquad (1)$$

where ρ is the mass density, $\vec{J}_s$ is the total entropy current density, φ_s denotes the rate of entropy production per unit volume, and all quantities are either scalar - or vector-point functions. Application of the principle of mass conservation to Eq. (1), and substitution of the convective derivative operator yields, after some manipulation:

$$\rho \frac{DS}{Dt} + \nabla \cdot \left[\vec{J}_s - \rho\vec{u}S\right] + S\vec{u} \cdot \nabla\rho = \varphi_s, \qquad (2)$$

where the quantity $\rho\vec{u}s$ is the convective current density of entropy.

Consider first the steady state, infinite, stationary electrodeless arc. In this case $\partial/\partial t$ and $\vec{u}$ vanish and Eqn. (2) becomes

$$\nabla \cdot \vec{J}_s = \varphi. \qquad (3)$$

The total entropy production rate Φ_T is found by integrating Eqn. (3) over the discharge volume. Application of Gauss' law then gives a relation between the flux and production rate of entropy:

$$\Phi_T = \int \vec{J}_s \cdot \hat{n}\, dA \qquad (4)$$

The energy balance in a stationary electrodeless arc is described by

$$\nabla \cdot \left[K_c (T)\vec{\nabla}T - q_{rad}\right] + \vec{j} \cdot \vec{E} = 0$$

which is recognized as the Elenbaas-Heller energy equation. It will also be recalled that in the electrodeless arc $\nabla \cdot \vec{j} = 0$. Finkelnburg and Maecker* have shown that, when applied to the thermal (i.e., equilibrated) arc discharge, the Elenbaas-Heller energy equation and the expression $\nabla \cdot \vec{j} = 0$ can be regarded as the Euler equations of the principle of minimum

---

* Finkelnburg, W., and Maecker, H., "Electric Arcs and Thermal Plasma," Handbuch der Physik XXII, Springer-Verlag, Berlin, 1956.

entropy production. Following Peters*, they derive the theorem of Guoy and Stodola**, which is verbally expressed as follows:

(Temperature of surroundings) x (Entropy production) = (Power dissipation).

This is written

$$\Phi_T = \frac{\text{Total Dissipation}}{T_R} = \frac{\int \vec{j} \cdot \vec{E}\, dV}{T_R} , \qquad (5)$$

where T_R is a boundary reference temperature. Thus, Eqn. (4) and Eqn. (5) can be combined to give

$$\int \vec{J}_s \cdot \hat{n}\, dA = \Phi_T = \frac{\int \vec{j} \cdot \vec{E} dV}{T_R} = \frac{I^2 \mathcal{R}}{T_R} , \qquad (6)$$

where I is the rms current in the induction solenoid and $\mathcal{R}$ is the resistance of the discharge reflected into the induction circuitry.

Finkelnburg and Maecker also show that the principle of increase of entropy is not the decisive law which determines the course of a thermodynamic process, but it is rather the tendency to have a minimum production of entropy which determines the process. This leads to an expression of Steenbeck's*** minimum entropy principle which, in the case of any thermal arc discharge simply states that the discharge is constrained to exist in a condition of minimum entropy production. Thus, from Steenbeck's principle is obtained

$$\delta \Phi_T = 0 \qquad (7)$$

---

* Peters, Th., Physik Verh. 6 (9), 173 (1955).

** Stodola, A., Steam and Gas Turbines, (in German) Berlin, 1924, (Ref. from Handbuch der Physik XXII).

***Steenbeck, M., Z. Physik 33, 809 (1932).

as a condition required for the existence of the high pressure electrodeless arc.

Let uniform flow be added to the system. The entropy production is obtained from Eqn. (2), where the steady state is again considered:

$$\rho\vec{u} \cdot \vec{\nabla}S + \nabla \cdot \vec{J}_s - \nabla \cdot \rho\vec{u}S + S\vec{u} \cdot \nabla\rho = \varphi_s. \tag{8}$$

But

$$\nabla \cdot \rho\vec{u}S = \rho S\nabla \cdot \vec{u} + \rho\vec{u} \cdot \nabla S + S\vec{u} \cdot \nabla\rho,$$

so Eqn. (8) becomes

$$\nabla \cdot \vec{J} - \rho S\nabla \cdot \vec{u} = \varphi_s. \tag{9}$$

But with uniform flow $\nabla \cdot \vec{u}$ vanishes, and Eqn. (9) reduces to Eqn. (3), which was previously evaluated. Thus, for the infinite, steady state electrodeless arc in a uniform flowing gas the entropy production rate is the same as in the absence of flow.

This does not imply that the power requirement is unchanged, however. Returning to Eqn. (3):

$$\nabla \cdot \vec{J}_s = \varphi_s.$$

It will be recalled the net entropy production Φ_T was found by evaluating the divergence of the entropy current density over the discharge volume. This integral was transformed to a surface integral by means of Gauss' theorem and presented as Eqn. (4). Gauss' theorem requires the integration to be performed over the entire enclosing surface, however. The zero flow case required

$$\vec{J}_s \cdot \hat{n} = \vec{J}_r \cdot \hat{\rho} + \vec{J}_\varphi \cdot \hat{\phi} + \vec{J}_z \cdot \hat{k} \equiv \vec{J}_r \cdot \hat{\rho},$$

since the axial and azimuthal contributions to the entropy current density vanish (i.e., $\vec{J}_\varphi \cdot \hat{\phi} = 0$ by symmetry, and $\vec{J}_z \cdot \hat{k} = 0$ because $\vec{J}_z = \rho\vec{u}S = 0$ in the absence of flow).

When flow is introduced $\vec{J}_\varphi \cdot \hat{\phi} = 0$, again by symmetry. However, it is clear that $\vec{J}_z \cdot \hat{k} \neq 0$ for $u_z \neq 0$. The integral of the axial entropy flux over the discharge area therefore does not vanish as in the zero flow case. In the uniform flow case the net entropy production per unit length has the same value as obtained for the zero flow case because in the former (flow) case the entropy current entering the unit length of the discharge volume just equals the entropy current leaving the unit length of discharge volume. This is written

$$\int_{A_1} \vec{J}_z \cdot \hat{k}\, dA_1 + \int_{A_2} \vec{J}_z \cdot \hat{k}\, dA_2 = 0,$$

since the unit vector $\hat{n}$ is everywhere directed outward such that its $\hat{k}$ component at A_1 is directed opposite its $\hat{k}$ component at A_2. The two integrals are equal and opposite, hence their sum is zero and the uniform flow is seen not to affect the net entropy production rate per unit length in an infinite electrodeless arc.

In the case of a non-infinite discharge with uniform flow the discharge volume is divided into three sections for analysis. These sections are the entrance region to the discharge volume, the exit region from the volume, and the discharge volume proper, which separates the end sections. This division forms a model which is composed of a uniform discharge volume bounded by regions of non-uniformity. The uniform region is identical to the case previously treated, and the entropy production rate in this part of the discharge is simply the rate previously computed times the number of unit lengths in the uniform discharge.

Near the solenoid end a characterization of the discharge similar to that preceding is very difficult because of the presence of large gradients in both the electromagnetic and the thermodynamic parameters.

In the steady state the rate of entropy production was given by Eqn. (9), which can be expanded to obtain

$$\frac{1}{r}\frac{\partial}{\partial r}\left(rJ_r\right) + \frac{\partial}{\partial z}J_z - \rho S\left[\frac{1}{r}\frac{\partial}{\partial r}\left(r\,u_r\right) + \frac{\partial u_z}{\partial z}\right] = \varphi_s . \qquad (10)$$

The formal integration of Eqn. (10) is beyond the scope of the present analysis, but an estimate of the net effect of this expression in the entropy production of the system can be made.

The first and third terms give the contribution to entropy production from the irreversible loss in heat from the system by radiation and conduction (viscosity effects have been neglected in this treatment). In magnitude such loss depends on the dissipation, including initial ionization. While not amenable to close estimation, it would appear that the mass average velocity cannot have an appreciable component in the radial direction, and the third term is approximately given by $-\int \rho S u_r \, 2\pi dr dz$. This is just the average contribution by radial convection. Likewise, the first term gives the total radial entropy flux. The sum of the first and third terms is apparently just the radial entropy flux from radiation and conduction sources, which, of course, includes a contribution from ionization and deionization. The second and fourth terms give the axial entropy flux in the transition region, also including the effects of ionization and deionization.

The effects of ionization and deionization on entropy production can be estimated by considering the total entropy production for ionization and deionization Φ_{ION} to be the sum over all particles of an average particulate entropy production rate φ_i:

$$\Phi_{ION} = \sum_n \varphi_i \tag{11}$$

Thus, averaging Eqn. (11) over all particles shows that the addition of flow to this system is accompanied by an increase in entropy production that is proportional to the particle flux (i.e., proportional to the flow). That ionization and deionization processes dominate entropy production in the transition region is clear because of the large difference between the breakdown energy requirement and that for the maintenance of an established discharge in the same gas. In the first approximation it can be assumed that the predominate entropy production "end effect" is due to ionization and/or deionization and is proportional to the mass flow rate:

$$\Phi_{ION} \propto \dot{m} = K \dot{m}$$

The total entropy production is therefore given by

$$\Phi_T = n\Phi_o + K \dot{m} \tag{12}$$

where Φ_o is the zero flow rate of entropy production per unit length in the electrodeless arc and n is the number of unit lengths in the uniform discharge column.

The Thomson model is amenable to this treatment. In the stationary state the entropy production takes a minimum value, thus $\delta\Phi$ vanishes and

$$\delta \frac{(\text{dissipation})}{T_R} = \delta\left(\frac{P}{T_R}\right) = \frac{1}{T_R}\ \delta P - \frac{P}{T_r^2}\ \delta T = 0$$

The dissipation per unit length in the Thomson model was given by

$$P = \frac{\pi}{\mu_o}\ \omega\ B_o^2\ R^2\ f\ (\sqrt{2}R/\delta),$$

where

$$f(\sqrt{2}R/\delta) \equiv \frac{2\delta}{\sqrt{2}R}\ \frac{M_1(\sqrt{2}R/\delta)}{M_o(\sqrt{2}R/\delta)}\ \cos\left[\ \theta_1(\sqrt{2}R/\delta)\ -\ \theta_o(\sqrt{2}R/\delta) - \pi/4\ \right].$$

A more convenient form for the dissipation expression is obtained by substituting $z = \sqrt{2}R/\delta = R\sqrt{\sigma\mu\omega}$ and $F(z) = (z/2)f(z)$ to give:

$$P = \frac{2\pi}{\mu_o^2}\ B^2\ z\ F(z)\ \sigma^{-1}.$$

For a fixed value of the applied magnetic field the variation is

$$\delta P = P\left[\ \frac{\delta z}{z} + \frac{\delta F}{F} - \frac{\delta\sigma}{\sigma}\ \right] = \frac{\partial P}{\partial z}\ dz,$$

where $\delta \equiv (\partial/\partial z)\ dz$. Then

$$\delta z = dz,$$

$$\delta F = \frac{\partial}{\partial z}\left(\frac{M_1(z)}{M_o(z)}\ \cos\left[\ \theta_1(z)\ -\ \theta_o(z)\ -\ \pi/4\ \right]\right) dz,$$

$$\delta\sigma = \frac{\partial}{\partial z}\left(\frac{z}{R}\right)^2\ \frac{1}{\mu\omega}\ dz.$$

Performing the indicated operations, one obtains

$$\delta P = P\left\{\frac{1}{z} - \frac{\left[\frac{1}{z}\frac{M_1(z)}{M_o(z)}\cos(\theta_1 - \theta_o - \pi/4) + \left(\frac{M_1}{M_o}\right)^2 \cos 2(\theta_1 - \theta_o - \frac{\pi}{4})\right]}{\frac{M_1}{M_o}\cos(\theta_1 - \theta_o - \frac{\pi}{4})} - \frac{2}{z}\right\} dz,$$

where

$$\frac{\partial M_1}{\partial z} = M_o(\sin\theta_1 - \theta_o - \tfrac{\pi}{4}) - \frac{M_1}{z} \quad ,$$

$$\frac{\partial M_o}{\partial z} = M_1 \cos\left[\theta_1 - \theta_o - \tfrac{\pi}{4}\right] ,$$

$$\frac{\partial \theta_1}{\partial z} = \frac{M_o}{M_1} \cos\left[\theta_1 - \theta_o - \tfrac{\pi}{4}\right],$$

$$\frac{\partial \theta_o}{\partial z} = \frac{M_1}{M_o} \sin\left[\theta_1 - \theta_o - \tfrac{\pi}{4}\right] .$$

Thus

$$\delta P = P\left[-\frac{2}{z} - \frac{M_1(z)}{M_o(z)} \frac{\cos 2(\theta_1 - \theta_o - \pi/4)}{\cos(\theta_1 - \theta_o - \pi/4)}\right] dz.$$

The existence of the electrodeless arc in the Thomson model is then determined by

$$\delta P = \frac{P}{T_R} \delta T.$$

The existence condition is thus written

$$\frac{2}{z} + \frac{M_1(z)}{M_o(z)} \frac{\cos 2\left[\theta_1 - \theta_o - \pi/4\right]}{\cos\left[\theta_1 - \theta_o - \pi/4\right]} = -\frac{1}{T}\frac{dT}{dz} \quad .$$

The condition for impedance match in the Thomson model of the electrodeless arc is given by

$$\frac{2}{z} + \frac{M_1(z)}{M_o(z)} \frac{\cos 2\left[\theta_1 - \theta_o - \pi/4\right]}{\cos\left[\theta_1 - \theta_o - \pi/4\right]} = 0.$$

Comparing the preceding two expressions one finds that the term $-\frac{1}{T}\frac{dT}{dz}$ is a concomitant of the discharge entropy production. This term is presented as a function of the argument $z = \sqrt{2}\ R/\delta$ in Figure A-2, where it is compared with the discharge resistance as a function of $z = \sqrt{2}\ R/\delta$, relative to that at conditions of "impedance match" (i.e., at $z = \sqrt{2}\ R/\delta = 2.5$). The existence condition is written

$$\delta\Phi = 0 = \frac{1}{T}\left[\delta P - \Phi\delta T\right].$$

In any open system $\Phi \geqslant 0$, hence δP has the same sense (i.e., sign) as δT, or δP vanishes. Thus,

$$\frac{\delta P}{\delta T} \geqslant 0$$

Consider a discharge operated with the argumement $z = \sqrt{2}\ R/\delta = 2.5$ such that the discharge absorbs the "maximum" power from its induction field. Let the effective temperature of the discharge plasma be T_o. Figure A-2 indicates that the entropy production function has zero value for this

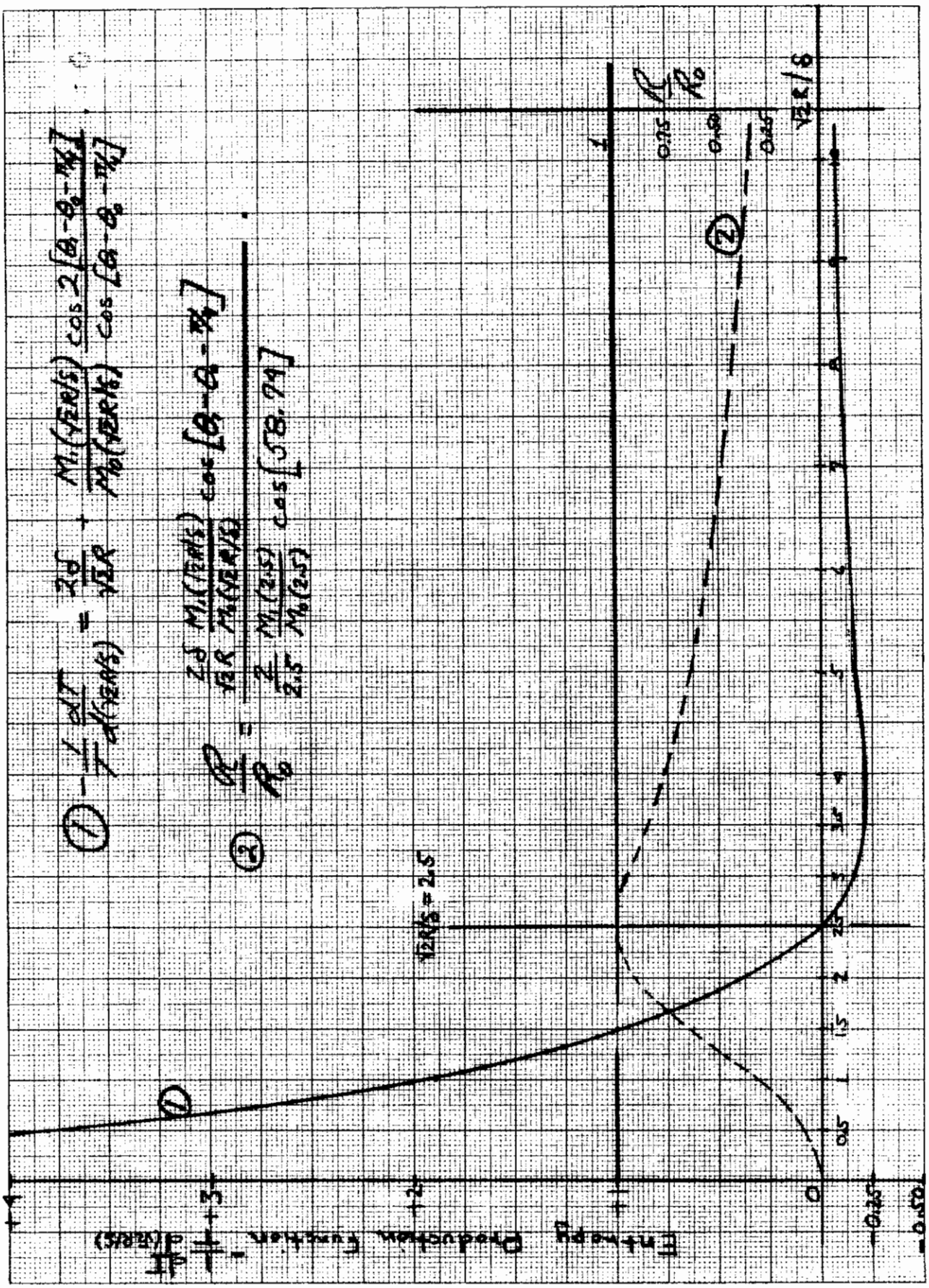

Figure 18 Entropy Production vs. $\sqrt{2}R/\delta$.

discharge. A variation δT in the discharge temperature is accompanied by a change in z such that

$$\frac{dz}{dT} = z\left[\frac{1}{R}\frac{dR}{dT} + \frac{1}{2\sigma}\frac{d\sigma}{dT}\right] .$$

If $dz/dT < 0$ the discharge is seen to absorb less power from the induction field and the entropy production of the discharge increases. If $dz/dT > 0$ the discharge again absorbs less power from the induction field, however the entropy production decreases. Since the entropy production for an impedance-matched discharge is minimum, a decrease in the production rate with temperature requires less than minimum discharge maintenance entropy production at the new temperature, which must be forbidden on thermodynamic grounds. Also, the decrease in z with temperature yields entropy production at the new temperature in excess of the minimum for discharge maintenance, as less power is absorbed by the discharge itself at this temperature. Since the power variation $\delta P \geq 0$, it must be that dz/dT vanishes always. Thus

$$\frac{1}{R}\frac{dR}{dT} = -\frac{1}{2\sigma}\frac{d\sigma}{dT} .$$

Also, a discharge apparently cannot exist for $z > 2.5$ since this requires a negative entropy production rate, and existence for $z < 2.5$ violates $\delta\Phi = 0$, hence must also be forbidden. Thus, for the Thomson model the condition for existence is

$$z = \sqrt{2}\, R/\delta = 2.5.$$

From Eqn. (9) it is immediately obvious that this argument is independent of the uniform flow through the discharge.

In the case of interest, the discharge entropy production is affected by the ionization and deionization at the ends by an amount that is constant in the first approximation. While not completely negligible, the "end effects" evidently do not dominate the problem, and are now neglected as a matter of convenience, with the reservation that hereafter the discharge column will be assumed to be of length $\gg$ diameter. For the Thomson model, the entropy production in the fluid reference frame was seen to be proportional to the power required to maintain the discharge, and the zero-flow scaling law $\sqrt{2}\ R/\delta = 2.5$ holds in both reference frames.

In the general case, within the fluid frame the energy balance is given by

$$Q_o = \int \vec{J}_o \cdot \vec{E}_o \, dV$$

where Q_o is the net loss from the discharge in the absence of flow.

In the stationary system the energy balance reads

$$\dot{w}H = \int \vec{J} \cdot \vec{E} \, dV - Q$$

where $\dot{w}H$ denotes the net enthalpy of convection from the discharge volume. Then

$$\int \vec{J} \cdot \vec{E} \, dV = \dot{w}H + Q$$

This heat loss Q was shown to be the same as Q_o in the zero flow case by application of Steenbeck's minimum entropy principle (the discharges are otherwise identical). This leads to

$$\int \vec{j} \cdot \vec{E}\, dV - \int \vec{j}_o \cdot E_o\, dV = \dot{w}H$$

which gives the power requirement for the flowing discharge. This can be written

$$P = P_o + \dot{w}H, \tag{13}$$

where P_o is the power required for maintenance of the zero flow electrodeless arc at a given pressure, and P is the power required for the maintenance of the same electrodeless arc with the addition of flow.

This problem has also been treated in the Soviet literature* for the channel model of the arc discharge. This treatment is abridged and presented below:

Neglecting friction and radiation loss, the energy balance becomes

$$\sigma E^2 + \frac{1}{r} \frac{\partial}{\partial r} \left(r\varkappa \frac{\partial T}{\partial r}\right) - \frac{\partial}{\partial z} \left(G_F J^*\right) = 0, \tag{14}$$

where G_F is the specific gas flow and J^* is the enthalpy of the retarded flow. Averaging Eqn. (14) over unit length, one can write

$$(1-\eta)\, \sigma E^2 R^2 + \frac{1}{\rho} \frac{d}{d\rho} \left(\rho \frac{dS}{d\rho}\right) = 0, \tag{15}$$

where η is a local "energy efficiency" defined as the fraction of the total power entering an elementary volume of the arc that goes to increase the total enthalpy of the gas passing through this volume, R is the radius of the channel and $\rho = r/R$ is the relative radius.

---

* Pustogarov, S. V., High Temperature, 4, 173 (1966).

For the conditions of the channel model it is shown that the presence of an axial gas flow characterized by the quantity η leads to an increase in the required power by a factor $(1 - \eta)^{-1}$. Under these conditions the radial temperature distribution and the heat flow to the wall remain the same as in the case $G_F = 0$. In a series of experimental measurements of arc characteristics with flow, the energy efficiency was found to be

$$\eta = \left(1 - \frac{Q_w}{EI}\right), \tag{16}$$

Since Q_w is held constant, Q_w/EI is just $P(o)/P(u)$, where $P(o)$ is the zero flow power requirement, and $P(u)$ is the power required for a given flow under otherwise identical conditions. Then

$$\eta = \left[1 - \frac{P(o)}{P(u)}\right] = \frac{\Delta P}{P(u)},$$

but

$$\int \vec{J}_1 \cdot \vec{E}_1 \, dV = P(u) = Q + \dot{w}H = \int \sigma \, E_1^2 \, dV$$

and

$$\int \vec{J}_o \cdot \vec{E}_o \, dV = P(o) = Q = \int \sigma \, E_o^2 \, dV$$

so

$$\eta = \frac{\dot{w}H}{P(o) + \dot{w}h}$$

and

$$P(u) = P(o) + \dot{w}H, \tag{17}$$

as before.

APPENDIX III

THE HYDROMAGNETIC INTERACTION

It is desired to determine the extent of the disturbance of the electromagnetic field by the plasma flow field in an electrodeless arc discharge. The Thomson eddy current model consists of an infinite solenoid of N/ℓ turns per unit length surrounding an infinite uniform plasma at rest. If the influence of a single turn of the solenoid on the system were known, the infinite solenoid model could be derived by superposition. If the single loop were to carry unit current, the analytical problem would be general. The solution for the spatial potential distribution of a unit source is the Green's function for that source. This function will be derived for the interesting case of a long uniform plasma flowing with uniform velocity along the axis of a single circular loop which carries unit current at a constant frequency. While this model has not yet been shown to describe the electrodeless arc, the presence or absence of a significant flow-induced disturbance of the induction field will determine whether or not it is physically valid to analytically extend a solution

of the first order, zero flow energy balance equation to include flow effects.

A. FORMULATION AND SOLUTION OF THE PROBLEM

The magnetic induction $\vec{B}$ can be derived from a vector potential $\vec{A}$. By definition

$$\vec{B} = \nabla \times \vec{A} \tag{1}$$

Additionally, the curl of the magnetic induction is given by

$$\nabla \times \vec{B} = \mu\left[\vec{j} + \epsilon \frac{\partial \vec{E}}{\partial t}\right], \tag{2}$$

where μ and ϵ are respectively the permeability and permittivity of the space at the point of interest, $\vec{j}$ is the current density and $\vec{E}$ is the electric field intensity at this point. If ψ is a local potential, and if $\vec{u}$ is the velocity with which the plasma moves relative to the source of the field quantities, the electric field intensity in the frame of the plasma is given by

$$\vec{E} = -\vec{\nabla}\psi - \frac{\partial \vec{A}}{\partial t} + \vec{u} \times \vec{B} \tag{3}$$

Eqns. (1-3) are now combined with Ohm's law to obtain

$$\nabla^2\vec{A} = \vec{\nabla}\left[\vec{\nabla} \cdot \vec{A} + (\sigma\mu + i\omega\epsilon)\psi\right] + (\omega^2\mu\epsilon - i\sigma\mu\omega)\vec{A} - \frac{i}{\omega}(\omega^2\mu\epsilon - i\sigma\mu\omega)\left[\vec{u}\times\vec{\nabla}\times\vec{A}\right] - \mu\vec{j}_{source} \tag{4}$$

where σ is the electrical conductivity of the plasma, $i\omega = \partial/\partial t$, and j_{source} is the source current density.

Substituting $-\kappa_o^2 n^2 = (\omega^2 \mu\varepsilon - i\sigma\mu\omega)$ into Eqn. (4), and choosing the Lorentz gauge $\nabla\cdot\vec{A} = -(i/\omega)\kappa_o^2 n^2 \Psi$ permits a simplification in the form of Eqn. (4):

$$\nabla^2\vec{A} + \kappa_o^2 n^2 \vec{A} - \frac{i}{\omega}\kappa_o^2 n^2 \left[\vec{u} \times (\vec{\nabla} \times \vec{A})\right] = -\mu\vec{j}_{source}. \qquad (5)$$

It is sufficient for the purpose of this analysis to consider only axial flow. When $\vec{u} = \hat{k}\, u_z$, the bracketed term on the left in Eqn. (5) is evaluated:

$$\left[\vec{u} \times (\vec{\nabla} \times \vec{A})\right] = -\hat{\phi}\, u_z \frac{\partial A}{\partial z}\varphi \qquad (6)$$

where axial and radial components of the vector potential vanish (i.e., radial and axial currents are suppressed in the electrodeless arc, hence $\vec{A}_r = \vec{A}_z = 0$).

Outside the plasma the electric conductivity vanishes. Inside the plasma the source current vanishes. Thus two regions exist, and Eqn. (5) in these regions is written:

$$\rho \leq R: \quad \hat{\phi}\left[\frac{1}{\rho}\frac{\partial}{\partial\rho}\left(\rho\frac{\partial}{\partial\rho}\right) - \frac{1}{\rho^2} + \kappa_o^2 n^2 + \frac{\partial^2}{\partial z^2} - \gamma\frac{\partial}{\partial z}\right]A_\varphi^{(i)} = 0, \qquad (7a)$$

$$\rho \geq R: \quad \hat{\phi}\left[\frac{1}{\rho}\frac{\partial}{\partial\rho}\left(\rho\frac{\partial}{\partial\rho}\right) - \frac{1}{\rho^2} + \kappa_o^2 + \frac{\partial^2}{\partial z^2}\right]A_\varphi^{(o)} = -\hat{\phi}\,\mu_o\, j_{source}, \qquad (7b)$$

where $\gamma = \sigma\mu u_z$, the plasma radius is denoted by R, the superscripts (i) and (o) refer to "inside" and "outside" the plasma, respectively, and ρ is the radial coordinate.

Solution of Eqns. (7) is obtained by finding the Green's function appropriate to this case. One observes that, for the single turn loop the source term can be replaced by a delta function at the source (i.e., primed) position.

The z-dependence in Eqns. (7) can be relegated to the k-plane via a Fourier transformation to give a set of linear equations in ρ:

$$\rho \leqslant R \left[\frac{d^2}{d\rho^2} + \frac{1}{\rho}\frac{d}{d\rho} + \left(\beta^2 - \frac{1}{\rho^2}\right)\right] G^{(i)}(\rho,k|\rho'z') = 0 \qquad (8a)$$

$$\rho \geqslant R \left[\frac{d^2}{d\rho^2} + \frac{1}{\rho}\frac{d}{d\rho} + \left(\alpha^2 - \frac{1}{\rho^2}\right)\right] G^{(o)}(\rho,k|\rho'z') = -\frac{e^{ikz'}}{2\pi\rho'}\delta(\rho-\rho'), \qquad (8b)$$

where $\alpha^2 = \kappa_o^2 - k^2$,

and $\beta^2 = \kappa_o^2 n^2 - i\gamma k - k^2$.

Closed form solutions for Eqns. (8) have been obtained for this boundary value problem. They are

$$\rho \geqslant R: \quad G^{(o)}(\rho,k|\rho',z') = \frac{i}{4} H_1(\alpha\rho') \left[J_1(\alpha\rho) - \Phi(k) H_1(\alpha\rho)\right] e^{ikz'}, \qquad (9a)$$

$$0 \leqslant \rho \leqslant R \quad G^{(i)}(\rho,k|\rho',z') = \frac{i}{4} H_1(\alpha\rho') J_1(\beta\rho)\theta(k) e^{ikz'}, \qquad (9b)$$

where the Hs are Bessel functions of the third kind, the Js are Bessel functions of the first kind, and $\Phi(k)$ and $\theta(k)$ are evaluated at the boundary $\rho = R$ to give

$$\Phi(k) = \frac{\alpha J_o(\alpha R) J_1(\beta R) - \beta J_o(\beta R) J_1(\alpha R)}{\alpha H_o(\alpha R) J_1(\beta R) - \beta J_o(\beta R) H_1(\alpha R)}, \qquad (10a)$$

$$\theta(k) = -\frac{\alpha J_o(\alpha R) H_1(\alpha R) - \alpha J_1(\alpha R) H_o(\alpha R)}{\alpha J_1(\beta R) H_o(\alpha R) - \beta J_o(\beta R) H_1(\alpha R)}. \qquad (10b)$$

The Green's function must be returned to real space by the inverse transform

$$G(\rho,z|\rho',z') = \frac{1}{2\pi}\int_{-\infty}^{\infty} G(\rho,k|\rho'z') e^{ikz} dk, \qquad (11)$$

for which the magnetic vector potential is obtained:

$$A(\underline{r}) = \mu_o \int G(\rho, z|\rho', z') j(\underline{r}') d\underline{r}'. \tag{12}$$

The effects of the plasma and the flow are now included in the evaluation of $A(\underline{r})$. If the field frequency is sufficiently low, displacement currents can be neglected and $\beta \to \left[k^2 + i\sigma\mu(\omega + uk)\right]^{\frac{1}{2}}$.

B. EVALUATION OF SOLUTIONS

Several cases shall now be examined.

Case 1: $\sigma \to 0$

In this case $\alpha = \beta = ik$

$$\Phi(1) \to \frac{ik(J_o J_1' - J_o' J_1)}{ik(J_1 H_o - J_o H_1)} = 0$$

$$\rho(k) \to \frac{-ik\,(J_o H_1 - J_1 H_o)}{ik\,(J_1 H_o - J_o H_1)} = 1$$

$$G^{(o)} \to \frac{i}{4} H_1(ik\rho') J_1(ik\rho) e^{ikz'} = G^{(i)}$$

$$\therefore \quad G^{(o,i)}(\rho, z|\rho', z') = \frac{1}{8\pi} \int_{-\infty}^{\infty} J_1(ik\rho) H_1(ik\rho') e^{-ik(z-z')} dk. \tag{13}$$

Noting that

$$J_1(ik\rho) \equiv i\, I_1(k\rho),$$

and

$$H_1(ik\rho') \equiv -\frac{2}{\pi} K_1(k\rho'),$$

Eqn. (13) is written

$$G^{(o,i)}(\rho, z|\rho' z') = \frac{1}{2\pi^2} \int_o^{\infty} I_1(k\rho) K_1(k\rho') \cos k(z-z') dk, \tag{14}$$

in which the integrand is seen to be an even function in k, hence $e^{-ik(z-z')}$ was replaced by cos k(z-z') and twice the integral was taken over semi-infinite limits.

The integral is contained in the table of integral transforms prepared by Erdelyi, et al.*

Case #2 $\sigma \to \infty$, $u = 0$.

In this case $\alpha \to ik$, $\beta \to i\left[k^2 + i\sigma\mu\omega\right]^{\frac{1}{2}}$

$$\Phi(k) \to 0$$

$$\Theta(k) \to 0$$

$$G^{(i)} \to 0$$

$$G^{(o)} \to \frac{i}{\pi}\int_{-\infty}^{\infty} J_1(ik\rho)H_1(ik\rho')e^{-ik(z-z')}\,dk,$$

as before.

The presence of an infinite conductor thus has no effect on the Green's function outside the cylinder. Within the conductor the Green's function vanishes.

Case #3 σ,u both finite.

In this case it is observed that Eqn. (9a) gives

$$G^{(o)}(\rho,k|\rho',z') = G_o^{(o)}(\rho,k|\rho'z') + \delta G^{(o)}\ (\rho,k|\rho',z';\sigma,u),$$

* Erdelyi, Magnus, Oberhettinger and Tricomi, Tables of Integral Transforms, Vol. I, McGraw Hill Book Co., New York, 1954.

where $G_o^{(o)}(\rho,k|\rho',z')$ is the original infinite domain Green's function, and $G^{(o)}(\rho,k|\rho',z';\sigma,u)$ is a perturbation term given below in Eqn. (15). The inverse transform is written

$$\delta G^{(o)}(\rho,z|\rho',z';\sigma,u) = \frac{1}{4\pi^2}\int_{\infty}^{\infty} K_1(k\rho')K_1(k\rho)\frac{I_1(kR)}{K_1(kR)}\xi(\sigma,u)e^{-ik(z-z')} \qquad (15)$$

where

$$\xi(\sigma,u) = \frac{k\dfrac{I_1(kR)}{I_1(kR)\sqrt{2}\left(1+\frac{uk}{2\omega}\right)J_o\left[i^{3/2}\frac{\sqrt{2R}}{\delta}\left(1+\frac{uk}{2\omega}\right)\right]}\dfrac{i^{-3/2}}{\delta}\dfrac{J_1\left[i^{3/2}\frac{\sqrt{2R}}{\delta}\left(1+\frac{uk}{2\omega}\right)\right]}{}-1}{k\dfrac{K_o(kR)}{K_1(kR)\sqrt{2}\left(1+\frac{uk}{2\omega}\right)J_o\left[i^{3/2}\frac{\sqrt{2R}}{\delta}\left(1+\frac{uk}{2\omega}\right)\right]}\dfrac{i^{-3/2}}{\delta}\dfrac{J_1\left[i^{3/2}\frac{\sqrt{2R}}{\delta}\left(1+\frac{uk}{2\omega}\right)\right]}{}+1}.$$

It will be recognized that for $k \to 0$, $K_1(o)$ and $K_o(o) \to \infty$, while $I_1(o)$, $I_o(o) \to 0$. The principal values for this integral must occur near $k = 0$. Thus, in evaluating β, k^2 was neglected in comparison with k. Eqn. (15) is suitable for numerical evaluation, and a similar expression could be derived for $G^{(i)}(\rho,z|\rho',z';\sigma,u)$. Further manipulation of this expression is not necessary, however, since Eqn. (15) already demonstrates the order of the flow effect on the field distribution. This effect appears in the $(1 + uk/2\omega)$ term. For simplicity k will be assigned unit value, then for $u = 10^3$ m/sec and $f = 10^6$ cps such that $\omega = 6.28 \times 10^6$, $uk/2\omega \approx 10^{-4}$. The remaining term $\sqrt{2}R/\delta$ therefore has a value of 2.5 and the flow cannot appreciably perturn the field distribution.

Case #4 Small Argument Expansion

In the limit where αR, $\beta R \ll 1$ the various functions can be expanded. This has been done to order four in kR. The vector potential outside the plasma

in this case is approximately

$$A^{(\vec{o})}(\rho,z)= \hat{\phi}\ \frac{\mu I e^{i\omega t}}{32(a^2+z^2)^{3/2}}\ \left(\frac{a}{\rho}\right)\left\{\rho^2\left[8+\frac{24\ a\rho}{(a^2+z^2)}\right]-R^4\left[i\sigma\mu\omega+\frac{3\sigma\mu_o z}{(a^2+z^2)}\right]\right\}, \quad (16)$$

The hydrodynamic interaction is seen to vary as $z/(a^2 + z^2)^{5/2}$ while the ohmic dissipation varies as $1/(a^2 + z^2)^{3/2}$. The magnitudes compare according to

$$\frac{\text{OHMIC}}{\text{HYDROMAGNETIC}} \approx 2 \times 10^3\ \frac{a^2 + z^2}{z}\ ,$$

for a single loop. For a long solenoid the hydromagnetic effects are even less important, as these effects appear only in the neighborhood of the ends of the induction solenoid where $\vec{u} \times \vec{B} \neq 0$.

Finally, the magnetic Reynolds number and the hydromagnetic interaction parameter are estimated. The magnetic Reynolds number is

$$R_M = \sigma\mu_o uL \approx 10^{-1}.$$

The interaction parameter is

$$N = \frac{\sigma B^2 L}{\rho u} \approx 10^{-3}\ ;$$

where the following nominal values have been assumed:

$\sigma = 10^3$ mhos/meter.

$u = 10^3$ meters/sec

$L = 10^{-1}$ meters

$B = 10^{-1}$ webers/meter^2 (= 1000 gauss)

ρ = 1 kilogram/meter^3 (~ atm density)

C. CONCLUSIONS

It is apparently quite safe to assume that the spatial distributions of the electromagnetic field quantities (i.e., $\vec{E}$, $\vec{B}$, $\vec{j}$) are not appreciably disturbed by the flowing plasma in the electrodeless arc discharge for cases of interest in the present analysis. These cases include those examples of magnetic Reynolds number and interaction parameter with magnitude less than unity.

APPENDIX IV

ENERGY BALANCE IN THE ELECTRODELESS ARC

A. NOMENCLATURE

In this Appendix the following notations are employed:

a_R	-	Radiation constant = 7.569×10^{-16} (joule/meter^3/$^oK^4$)
$\vec{A}$	-	Magnetic vector potential (Webers/meter)
$\vec{B}$	-	Magnetic induction (webers/meter^2)
c	-	Velocity of light (3×10^8 m/sec)
C	-	Capacitance (farads)
$\vec{E}$	-	Electric field strength (volts/meter)
f	-	Circular frequency (sec^{-1})
h_o	-	Stagnation enthalpy (joules/kg)
$\vec{j}$	-	Current density (amperes/m^2)
L	-	Inductance (henry)
p	-	Pressure (n/m^2)
$\vec{q}_{rad}$	-	Radiation flux including absorption (w/m^2/sec)

T	-	Temperature (^{o}K)
$\vec{u}$	-	Mass-average convective velocity (m/sec)
U	-	Internal energy per unit mass
δ	-	Electromagnetic skin depth = $[2/\sigma\mu_o\omega]^{\frac{1}{2}}$(meters)
ϵ_o	-	Permittivity of free space = 8.85×10^{-12}(fd/meter)
$\eta(T)$	-	Viscosity (kg/m/sec)
$K(T)$	-	Thermal conductivity coefficient, including the effects of ambipolar diffusion (joule/m^2/sec/^{o}K)
λ_o	-	Debye shielding distance (meters)
λ_R	-	Rosseland mean free path for absorption (meters)
μ_o	-	Permeability of free space = $4\pi \times 10^{-7}$(h/m)
ρ	-	Mass density (kg/m^3)
$\sigma(T)$	-	Electrical conductivity (mhos/meter)
$\tilde{\sigma}$	-	Stephen Boltzman Constant = 5.6686×10^{-8} joules/meter^2 sec^{o}K.
$\overline{\overline{\tau}}$	-	Viscous stress tensor (kg/m)
ψ	-	Electric scalar potential (volts)
ω	-	Angular frequency = $2\pi f(sec^{-1})$

The rationalized Meter-Kilogram-Second (MKS) system of units is used throughout this analysis.

B. DERIVATION OF THE ENERGY BALANCE EQUATION

The most important part of any theoretical study is the initial formulation of a problem. In the following study therefore, an effort is made to treat the entire problem while setting up the functional energy balance equation. A macroscopic (i.e., continuum) treatment of the

electrodeless arc energy balance is chosen because only the high pressure case is of interest here, and the additional complexities of a general microscopic* analysis appear unwarranted at this time.

The basic continuum hydromagnetic** equations are:

Conservation of momentum:

$$\rho\frac{D\vec{u}}{Dt} = -\vec{\nabla}p - \vec{\nabla}\cdot\overline{\overline{\tau}} + \vec{j} \times \vec{B}; \qquad (1)$$

Conservation of energy:

$$\rho\frac{DU}{Dt} = \vec{\nabla}\cdot K\vec{\nabla}T - \rho\vec{\nabla}\cdot\vec{u} - \vec{\nabla}\cdot\vec{q}_{rad} + \vec{j}\cdot(\vec{E} + \vec{u} \times \vec{B}) - \overline{\overline{\tau}}:\vec{\nabla}\vec{u}; \qquad (2)$$

Conservation of mass:

$$\frac{D\rho}{Dt} = -\rho\vec{\nabla}\cdot\vec{u}; \qquad (3)$$

and the convective derivative operator is defined:

$$\frac{D}{Dt} = \frac{\partial}{\partial t} + (\vec{u}\cdot\vec{\nabla})$$

The scalar product of $\vec{u}$ and Equation (1), when added to Equation (2) gives

$$\rho\frac{D}{Dt}\left[\frac{1}{2}u^2 + U\right] = -\vec{u}\cdot\vec{\nabla}p + \vec{\nabla}\cdot[K\vec{\nabla}T - \vec{q}_{rad} - \overline{\overline{\tau}}\cdot\vec{u}] - \rho\vec{\nabla}\cdot\vec{u} + \vec{j}\cdot\vec{E} \ .$$

The convective pressure derivative is

---

*Jancel, R., and Kahan, T., Electrodynamics of Plasmas, John Wiley and Sons, Ltd., New York 1966 Chapters 5 and 6.
**Drummond, J. E., Plasma Physics McGraw-Hill Book Co., New York 1961 Chapter 6.

$$\frac{Dp}{Dt} = \frac{\partial p}{\partial t} + \vec{u}\cdot\vec{\nabla}p$$

Thus

$$\vec{u}\cdot\vec{\nabla}p = \frac{Dp}{Dt} - \frac{\partial p}{\partial t} \quad .$$

Also

$$\frac{D}{Dt}\left(\frac{p}{\rho}\right) = \frac{1}{\rho}\frac{Dp}{Dt} - \frac{p}{\rho^2}\frac{D\rho}{Dt};$$

from Equation (3)

$$\frac{D\rho}{Dt} = -\rho\vec{\nabla}\cdot\vec{u} \quad .$$

Finally

$$\frac{D}{Dt}\left(\frac{p}{\rho}\right) = \frac{1}{\rho}\frac{\partial p}{\partial t} + \frac{1}{\rho}\vec{u}\cdot\vec{\nabla}p + \frac{p}{\rho}\vec{\nabla}\cdot\vec{u}$$

gives

$$\vec{u}\cdot\vec{\nabla}p + p\vec{\nabla}\cdot\vec{u} = \rho\frac{D}{Dt}\left(\frac{p}{\rho}\right) - \frac{\partial t}{\partial t},$$

hence, the energy balance is given by

$$\rho\frac{D}{Dt}\left[\frac{1}{2}u^2 + U + \frac{p}{\rho}\right] = \frac{\partial p}{\partial t} + \vec{\nabla}\cdot\left[K\vec{\nabla}T - \vec{q}_{rad} - \vec{\tau}\cdot\vec{u}\right] + \vec{j}\cdot\vec{E}.$$

The stagnation enthalpy of this system is

$$h_o = h + \frac{1}{2}u^2$$

The free stream enthalpy is

$$h = U + \frac{p}{\rho}$$

Thus $h_o = \frac{1}{2}u^2 + U + p/\rho$, and the energy balance can be written

$$\rho\frac{Dh_o}{Dt} = \frac{\partial p}{\partial t} + \vec{\nabla}\cdot\left[K\vec{\nabla}T - \vec{q}_{rad} - \vec{\vec{\tau}}\cdot\vec{u}\right] + \vec{j}\cdot\vec{E}. \qquad (4)$$

Some mathematical insight can be gained by inspecting the form of each term in Equation (4). These terms are therefore expanded in a cylindrical coordinate system and presented in the following paragraphs. Because of the symmetry of this discharge about the z = 0 axis, all azimuthal gradients are seen to vanish. In a subsequent section several simplifications will be rigorously justified and incorporated into the theory, and the initial set of working equations for this analysis will be developed.

C. EXPANSION AND EVALUATION OF TERMS IN THE ENERGY BALANCE EQUATION

The bracketed terms in Equation (4) give the rates of energy change per unit volume through the respective mechanisms of conduction (including ambipolar diffusion), radiation (emission and absorption) and viscosity. Noting that $\partial/\partial\varphi = 0$, Equation (4) is written

$$\rho\left[u_r\frac{\partial h_o}{\partial r} + u_z\frac{\partial h_o}{\partial z}\right] = \vec{j}\cdot\vec{E} + \frac{1}{r}\frac{\partial}{\partial r}\left[r\left(K\vec{\nabla}T - \vec{\vec{\tau}}\cdot\vec{u} - \vec{q}_{rad}\right)\right]_r + \frac{\partial}{\partial z}\left[K\vec{\nabla}T - \vec{\vec{\tau}}\cdot\vec{u} - \vec{q}_{rad}\right]_z \qquad (5)$$

Since the flow is primarily in the axial direction a good initial assumption is $u_z \gg u_r$, such that for non-turbulent subsonic flow $u_r \approx 0$. The term involving the viscous stress tensor becomes

$$(\bar{\bar{\tau}}\cdot\vec{u}) = -\eta \begin{vmatrix} -2/3\dfrac{\partial u_z}{\partial z} & 0 & \dfrac{\partial u_z}{\partial r} \\ 0 & -2/3\dfrac{\partial u_z}{\partial z} & 0 \\ \dfrac{\partial u_z}{\partial r} & 0 & +4/3\dfrac{\partial u_z}{\partial z} \end{vmatrix} \cdot \begin{pmatrix} 0 \\ 0 \\ u_z \end{pmatrix}$$

which reduces to

$$(\bar{\bar{\tau}}\cdot\vec{u}) = -\eta u_z \left[\hat{r}\frac{\partial}{\partial r} + \hat{k}\,\frac{4}{3}\,\frac{\partial}{\partial z}\right]u_z \quad . \tag{6}$$

In an optically thin discharge

$$\nabla\cdot\vec{q}_{rad} = 4\tilde{\sigma}K_p(T)T^4, \tag{7}$$

where $\tilde{\sigma}$ is the Stephen-Boltzmann constant and $K_p(T)$ is the Planck mean absorption coefficient.

In the optically thick regime

$$\vec{q}_{rad} = -\frac{16\tilde{\sigma}}{3}\,\lambda_R T^3\nabla\vec{T}, \tag{8}$$

where λ_R is the Rosseland mean free path.

The enthalpy derivative can be manipulated for simplification.

Since $h_o = \frac{1}{2}u^2 + U + p/\rho$,

$$\rho u_z \frac{\partial h_o}{\partial z} = \rho u_z^2 \frac{\partial u_z}{\partial z} + \rho u_z Cv \frac{\partial T}{\partial z} + \rho u_z R \frac{\partial T}{\partial z} + \rho u_z T \frac{\partial R}{\partial z}$$

$$\rho u_z \frac{\partial h_o}{\partial z} = \rho u_z \left[u_z \frac{\partial u_z}{\partial z} + \left(Cp - \frac{R}{M} \frac{dM}{dT}\right) \frac{\partial T}{\partial z} \right], \qquad (9)$$

where M is the mass-average molecular weight $\left(= \frac{R_o}{R}\right)$.

Assuming an ideal gas law:

$$p = \rho RT = \rho \frac{R_o}{M} T ,$$

the following relation is obtained:

$$\frac{1}{M} \frac{dM}{dT} = \frac{1}{\rho} \frac{d\rho}{dT} + \frac{1}{T} - \frac{1}{p} \frac{dp}{dT} \quad . \qquad (10)$$

From the data of Gilmore* the magnitudes of the terms in Equation (7) can be estimated. Noting that at low temperatures $\frac{dM}{dT} = 0$, a high temperature is assumed: $t \sim 1.5$ ev. Letting $\Delta T = T_2 - T_1 = 2ev - 1ev$, and picking $\rho = \text{const} = 10^{-1}\rho_o$ for $p = \text{const} = 50$ atm, the following approximate values are found:

$$\Delta p = p(T_2) - p(T_1) = [3.1661 \times 10^1 - 9.062] \text{ (atm)}$$

$$\Delta\rho = \rho(T_2) - \rho(T_1) = [1.5 \times 10^{-1} - 6 \times 10^{-1}]\rho_o$$

$$p(T = 1.5ev) \sim 20 \text{ atm}, \rho(T = 1.5ev) \sim 2 \times 10^{-1}\rho_o$$

Then

$$\frac{1}{p} \frac{dp}{dT} \approx \frac{1}{p} \frac{\Delta p}{\Delta T} = \frac{31{,}661 - 9.062}{11{,}600} \cdot \frac{1}{20} \approx 9.74 \times 10^{-5}$$

*Gilmore, F. R., Equilibrium Composition and Thermodynamic Properties of Air to 24,000°K. Rand Report RM 1543, 24 August 1955, Figure 4, p. 65.

$$\frac{1}{\rho}\frac{d\rho}{dT} \approx \frac{1}{\rho}\frac{\Delta\rho}{\Delta T} = \frac{(1.5 \times 10^{-1} - 6 \times 10^{-1})\rho_o}{11{,}600} \cdot \frac{1}{2 \times 10^{-1}\rho_o} \approx -1.94 \times 10^{-4}.$$

Finally

$$\frac{1}{M}\frac{dM}{dT} \approx 9.74 \times 10^{-5} + 5.75 \times 10^{-5} - 19.4 \times 10^{-5} \approx 4 \times 10^{-5}.$$

The value for C_p can be obtained from Fenter**

$$10 < Cp/R \text{ [for } p/\rho_o \sim 10^{-1} \text{ and } (10^4 < T < 2 \times 10^4)] < 50.$$

Inserting the smallest value for Cp into (9) and noting the above evaluation of Equation (10) gives an estimate of the maximum effect that the term $\frac{1}{M}\frac{dM}{dT}$ can have on the energy balance in the regime of interest:

$$\left(\frac{Cp}{R} - \frac{1}{M}\frac{dM}{dT}\right) R \sim (10 - 4 \times 10^{-5})\, R \approx 10R \approx Cp \quad .$$

The term $\frac{1}{M}\frac{dM}{dT}$ is therefore of minor importance to the energy balance for the regime considered in this analysis, and can therefore be neglected.

The enthalpy derivative is now written

$$\rho u_z \left[u_z \frac{\partial u_z}{\partial z} + Cp \frac{\partial T}{\partial z} \right] . \qquad (11)$$

A comparison is made between the magnitudes of the viscous and conductive contributions to heat transfer. Let $K(T)\, \partial T/\partial r + \eta u_z \partial u_z/\partial r = \Phi$.

A linear temperature profile is assumed, to give

$$\frac{\partial T}{\partial r} \approx \frac{T(R) - T(0)}{R - 0}$$

**Fenter, F. W., The Thermodynamic Properties of High Temperature Air Chance Vought Report No. RE-IR-14 28 June 1961, Figure 11b.

where R is the outer plasma radius. For $T_{center} \sim 10^4$, $T_R \sim 1000^o$ and $R \sim 10$ cm:

$$\frac{\partial T}{\partial r} \approx -9 \times 10^4$$

From Yos,** $K(T) \sim 1$ w/m^{o}K for $1 < P < 30$ atm and $T \sim 10^4$, hence

$$K\frac{\partial T}{\partial r} \approx -9 \times 10^4$$

Let $u_o \approx 400$ m/sec at the center and let the radial velocity distribution be parabolic such that $\partial u/\partial r = -u_o r/R^2$.

From Yos (Figure 19) $\eta < 3 \times 10^{-3}$ poise $\sim 3 \times 10^{-4}$(mks).

Letting $r = R/2$ and again letting $R \sim 10$ cm gives

$$\eta u_z \frac{\partial u_z}{\partial r} \approx -2.4 \times 10^2 .$$

Then $\Phi = K(T)\frac{\partial T}{\partial r} + \eta u_z \frac{\partial u_z}{\partial r} \approx -9 \times 10^4 - 0.024 \times 10^4$

and

$$\Phi \approx K(T)\frac{\partial T}{\partial r} .$$

The effect of viscous transfer in the discharge region is seen to be negligibly small compared with the effects of thermal conduction. The effect of viscosity in the axial direction is less easy to determine rigorously because of the coupling between the convective enthalpy loss

**Yos, J. M., Transport Properties of Nitrogen, Hydrogen, Oxygen, and Air to 30,000^{o}K, Avco Report RAD-TM-63-7, 22 March 1963, Figure 20.

and the viscous term through $\partial u/\partial z$. If a thought experiment is constructed in which the viscous effects are maximized while the thermal transfer is held constant (or minimized), a crude estimate of the relative importance of viscosity in the axial direction can be obtained. Let $\partial u/\partial z$ be maximized by assuming that the gas flow is accelerated from zero to sonic velocity in the region of space containing the discharge. Then

$$\frac{4}{3}\eta u_z \frac{\partial u}{\partial z} \approx \frac{4}{3} \cdot 3 \times 10^{-4} \times (4 \times 10^2)^2 \approx 64,$$

where the acceleration path has been taken to be a meter in length, and the velocity and viscosity have the same values as in the preceeding example. The conductive contribution in this case is essentially equal to the temperature drop across the discharge. If a discharge exists at all, this drop must numerically exceed 64. Thus, under nearly any circumstances

$$K \frac{\partial T}{\partial z} >> \frac{4}{3}\eta u_z \frac{\partial u_z}{\partial z} \quad .$$

Apparently the effect of viscosity is very small in terms of its contribution to the overall energy balance. In general, the provision of a mechanism for the establishment of a velocity profile appears to be the extent of the requirement for a viscous term in such an analysis as this. Thus, so long as no drastic changes in velocity take place within the discharge itself, the energy balance in the discharge can be established without the rigorous inclusion of a viscous transfer mechanism if a reasonably accurate velocity profile is chosen.

D. THEORETICAL SIMPLIFICATIONS AND THEIR JUSTIFICATIONS

(1) Local Thermodynamic Equilibrium. In the preceding equations the plasma temperature T has been introduced. The parameters $K(T)$, $\lambda_R(T)$, $\eta(T)$ and $\sigma(T)$ are stated functions of temperature in this analysis. The assumption of local thermodynamic equilibrium (L.T.E.) is clearly implied, and must be justified. The high pressure induced discharge is characterized by large plasma currents and high levels of ohmic dissipation, and as such, has been classified* as an arc type of discharge (i.e., in contrast to the relatively low energy "glow" discharge). High pressure arc discharges are known** to equilibrate in a time on the order of 10^{-3} sec or less, and the assumption of LTE is probably justified for the case of a CW induced discharge. Equilibrium can be rigorously demonstrated by showing that the temperature of the plasma electrons equals the temperature of the plasma ions and/or neutral particles. This can be accomplished by showing that the mechanism for energy transfer from the electric field to the plasma is predominately through elastic collisions between electrons and heavy particles, and that the rate of energy transfer from the plasma electrons to the heavy particles equals the rate of energy transfer from the electric field to the electrons. Such a scheme has been reported by Cambel*** who gives the following expression for the relative temperature difference between the electron gas (i.e., T_e) and the heavy particle gas

---

* Babat, G. J., J. Inst. Elect. Engr. (London 94, 27, 1947.)

** Cobine, J. D., Gaseous Conductors, Dover Publications, New York, 1958, p. 335.

*** Cambel, Ali Bulent, Plasma Physics and Magnetofluidmechanics, McGraw-Hill Book Co., New York, 1963, Chapter 6, pp. 143-145.

(i.e., T_g):

$$\frac{T_e - T_g}{T_e} = \frac{m_H}{8m_e}\left(\frac{eE\lambda}{3/2kT_e}\right)^2, \qquad (12)$$

where λ is the electron mean free path in the plasma, and is given by Sutherland's* formula

$$\frac{\lambda_1}{\lambda_2} = \frac{(1 + T'/T_2)}{(1 + T'/T_1)} .$$

For an electron in air at atmospheric density the following values obtain: $\lambda_1 = 54.1 \times 10^{-6}$cm, $T_1 = 273^oK$ and $T' = 111^oK$. Thus, for a plasma temperature $T_2 \gg T_1$:

$$\lambda_2 \approx 7.5 \times 10^{-5}\text{cm}.$$

Assuming that $T_e \approx 10^{4o}K$, $m_H \approx 2.5 \times 10^{-23}$ and that $E < 20$ v/cm $= 6.7 \times 10^2$ stat volts/cm, the left hand side of Equation (12) becomes

$$\frac{T_e - T_g}{T_e} \approx 4.6 \times 10^{-3} ,$$

hence

$$T_g \approx 9.954 \times 10^3\ ^oK \approx T_e . \qquad (13)$$

*Cobine, J. D., Gaseous Conductors, Dover Publications, New York, 1958 P. 22.

Finally, Compton* shows that the collisions between electrons and heavy particles are substantially elastic if

$$E/p < 1$$

where the electric field strength is given in volts per centimeter (in contrast with Equation (12)) and the pressure is given in mm Hg. Again assuming atmospheric pressure (= 760 mm Hg) and $E \approx 20$ volts/cm, $E/p < 1$ for any case of practical interest. Thus, the existence of L. T. E. is established in the electrodeless arc at atmospheric pressure and above.

It is mentioned in passing that the value $E \approx 20$ volts/cm was derived from Thomson's eddy current model of the electrodeless discharge where

$$|E_\varphi(r)| = \frac{1}{2}\,\delta\omega B(R)\,[M_1(\sqrt{2}R/\delta)/M_o(\sqrt{2}R/\delta)],$$

and nominal values were were chosen for a solenoid of 20 cm diameter, and E(r) is evaluated near the outer plasma boundary.

(2) Ohms Law, Electric Scalar and Magnetic Vector Potentials, and Charge Neutrality in the Electrodeless Arc Plasma. In a gaseous plasma, a scalar relation (i.e., the neglecting of Hall currents) can be assumed to exist between the current density $\vec{j}$ and the electric field $\vec{E}$ if $\omega_c\tau < 1$, where $\omega_c = eB/m_e$ is the electron cyclotron frequency and τ is the average momentum transfer collision time for electrons. For the case of the

*Compton, K. T., Phys. Rev., 22 (1923).

atmospheric plasma previously considered, $\tau < 10^{-11}$ sec and B < 1 kilogauss = $10^{-1} w/m^2$. Then $\omega_c \tau = eB\tau/m_e < 1.7 \times 10^{-1} < 1$, and the scalar form of Ohms law applies. Clearly, Hall currents become vanishingly small at higher pressures.

Additionally, for the sample plasma, the electron plasma frequency $\omega_p = [n_e e^2/\varepsilon_o m_e]^{1/2} \approx 10^{12} \gg \omega$, where ω is the frequency of the induction field. The corresponding ion frequency $\omega_1 \approx (m_e/m_i)^{\frac{1}{2}} \omega p \approx 10^{10} \gg \omega$. Thus, plasma oscillations and all allied effects can be neglected in this analysis.

In the high pressure electrodeless arc, Ohm's law is written

$$\vec{j} = \sigma(T) [\vec{E} + \vec{u} \times \vec{B}] \tag{14}$$

The electric field is derived from the magnetic vector potential $\vec{A}$ and an electric scalar potential ψ according to

$$\vec{E} = - \vec{\nabla}\psi - \frac{\partial}{\partial t} \vec{A}, \tag{15}$$

where the Lorentz gauge has been chosen for the sake of generality, relating the potentials through

$$\nabla \cdot \vec{A} = -\sigma \mu_o \psi - \varepsilon_o \mu_o \partial\psi/\partial t. \tag{16}$$

It will now be shown that a substitution of the Coulomb gauge $\nabla \cdot A = 0$ for Equation (16) introduces no appreciable error in the analysis of the energy balance in the high pressure electrodeless arc, and such substitution will be shown to add considerable strength to the analysis.

The debye shielding length λ_D is a measure of the magnitude of charge separation in a plasma for which the resulting electrostatic energy density equals the particle thermal energy density* The magnitude of the debye length is given by

$$\lambda_D = 7.43 \times 10^{12} \left[\frac{kT(ev)}{n_e(cm^{-3})}\right]^{\frac{1}{2}} cm.$$

In the sample plasma previously discussed, $kT \approx$ lev (i.e., $T \approx 10^4$) and $n_e \approx 10^{16} cm^{-3}$, thus in this plasma $\lambda_D \approx 10^{-5} cm$. At the outer boundary of this plasma the temperature will reduce to $\approx 7000 \sim 0.6ev$, $n_e \approx 10^{15} cm^{-3}$ and $\lambda_{D\ sheath} \approx 3 \times 10^{-5} cm$.

This is the order of distance into the plasma over which a static potential has a non-zero gradient. In the electrodeless discharge ψ arises from the large voltage drop $L \frac{dI}{dt}$ across the induction solenoid. Since this represents a very large potential gradient $(\nabla\psi)_z$ in the axial direction, and since the conductivity σ of the plasma is high, the effects of any interaction between $(\nabla\psi)_z$ and σ must be carefully considered, as large axial surface currents which could violently affect the overall energy balance appear to be possible.

There are several methods for treating this problem. The method to be presented, while lacking much mathematical elegance, appeals directly to

*Heald, M. A., and Wharton, C. B., Plasma Diagnostics with Microwaves, John Wiley and Sons, Inc., New York, 1965, p. 77-79.

the intuition and seems to be the method most directly related to the actual problem. Consider a solenoid of radius R and inductance L carrying a large high frequency current $Ie^{i\omega t}$. The voltage drop across this solenoid is $i\omega L\, Ie^{i\omega t}$. Let a hot coaxial plasma of radius R be induced by eddy currents, and let it occupy the central volume of the solenoid. The equivalent circuit of this situation appears in Figure A-3, where the inductive branch on the left represents the induced discharge and the capacitive branch on the right represents the quasi-electrostatic coupling between the solenoid and the plasma. The values of the capacitors C are approximately given by the values for the capacitance of coaxial cylinders

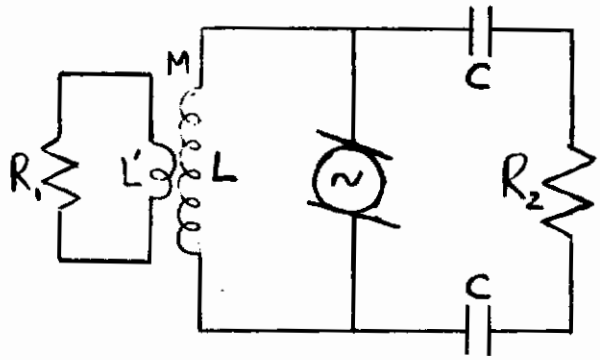

Figure 19

$$C = 2\pi\epsilon_o \ell [\log_e A/R]^{-1},$$

where ℓ is the length of the cylinder. In the usual case, the solenoid is part of a resonant circuit, and a ground plane* exists somewhere along its length. If this nodal plane bisects the solenoid the capacitors C are equal and the total series capacity in the right hand branch is

*Hollister, D. D., IEEE Trans. PTGAP, AP 13, 134 (1965)

$$C = \pi\epsilon_o \ell [\log_e A/R]^{-1}.$$

The resistance R_2 of the right hand branch is the resistance of an annular cylinder of diameter 2R, wall thickness λ_D, length ℓ, and electrical conductivity σ (i.e., R_2 is the plasma resistance as seen by the static potential of the solenoid). Thus,

$$R_2 \approx \frac{1}{\sigma} \frac{\ell}{2\pi R\lambda_D}$$

The voltage across the circuit is V, so the current through the right hand branch is V/Z_2, where $Z_2 = R_2 + X_c = \frac{1}{2\pi}\left(\frac{\ell}{\sigma R\lambda_D} + \frac{2 \log A/R}{j\omega\epsilon_o \ell}\right)$.

Nominal values for the circuit parameters are as follows:

σ_{sheath}	3×10^2 mhos/meter
ℓ	0.5 meter
R	0.10 meter
λ_D	3×10^{-7} meter
ϵ_o	10^{-11} fd/meter
A	0.20 meter

Then

$R_2 \approx 8.85 \times 10^3$ ohms,

$C_2 \approx 2 \times 10^{-11}$ fd.;

for a frequency of 1 MC/sec, $\omega = 6.28 \times 10^6$ and $X_c = 1/6.28 \times 10^6 \times 2 \times 10^{-11}$ $\approx 0.8 \times 10^4$ ohms. Therefore $Z_2 \approx 2 \times 10^4$ and $I_2 \approx V/2 \times 10^4 \approx 5 \times 10^{-5} V$.

The power lost in the right hand circuit is therefore

$I_2^2 R_2 \approx 2.5 \times 10^{-9} V^2 \cdot 10^4$, or roughly $2.5 \times 10^{-5} V^2$ watts.

The left hand circuit has the same voltage drop as the right hand circuit: $V = L\, dI/dt = j\omega IL$. This circuit when under load is characterized by a Q which is within a factor of two of 5. Thus, $Q = \omega L/R_1 \approx 5$, where R_1 is the effective series resistance of the plasma in the inductive branch. Thus $I_1 = V/\omega L = V/5R_1$. The reflected resistance R_1 also is usually within a factor or two of 5, hence $I_1 \approx 4 \times 10^{-2} V$, and the power delivered to this circuit is $I_1^2 R_1 \approx 1.6 \times 10^{-3} V^2 \cdot 5 \approx 8 \times 10^{-3} V^2$.

The net contribution of the capacitive circuit to the energy (i.e. power) of the system, hence to the energy balance, is seen to be on the order of a third of one percent, and is therefore neglected.

It is stated without further proof that this conclusion is valid in general for electrodeless discharges at high powers. In the low power, low density regime the opposite is true, as evidenced by the growth curves presented in Figures 9 and 10 of the preceding reference. Additionally, the capacitive mechanisms are definitely not to be neglected in breakdown studies, as $\nabla\psi$ is the initial breakdown field.

Since the capacitive effects are negligibly small in the case being treated, it is possible to modify Equation (15) to read

$$\vec{E} = -\frac{\partial \vec{A}}{\partial t} \qquad (17)$$

In addition, $\nabla\psi$ must vanish within a few debye lengths of the plasma surface. Hence, within the plasma ψ must have a constant value. Electric neutrality requires that no free charge exist in the plasma, and the plasma is known not*to contact the discharge tube wall, thus preventing an

*Dymshits, B. M. and Koretskii, Ya. P., Sov. Phys.-Tech. Phys. 9, 1294 (1966).

appreciable charge build up at the wall.

Since no other source for Ψ exists, this potential must vanish in the plasma. Therefore Equation (16) can be written

$$\nabla\cdot\vec{A} = 0 \tag{18}$$

as in the Coulomb gauge.

Radial components of the induction field of the solenoid exist only near its end and are very small in the plasma region of this fringing field. The main contribution to Lorentz currents will be the field component given by $u_z B_r$. It is evident from the geometry that this component must add to the total current density at one end of the solenoid and subtract from the total current density at the other end of the solenoid. Any net induced current differential can arise only from a difference in the electrical conductivity at the ends of the discharge. While this difference exists, the Lorentz field is at most several volts/meter, and is not considered important* to the overall energy balance. Equation (14) is then written

$$\vec{j} = \sigma(T)\vec{E}. \tag{19}$$

From Equations (17) and (18) is obtained

$$\nabla\cdot\vec{E} = -\frac{\partial}{\partial t}\nabla\cdot\vec{A} = 0. \tag{20}$$

---

*This question is treated in full in Appendix III of this report.

The divergence of Equation (19) is substituted in Equation (20) to give

$$\nabla \cdot \vec{j} = (\vec{E} \cdot \nabla \vec{T}) \frac{d\sigma(T)}{dT} , \tag{21}$$

which is the desired relation between the electric field and the temperature gradient. Since the net plasma charge is zero, the divergence of the plasma current density vanishes and

$$\vec{E} \cdot \nabla \vec{T} = 0; \tag{22}$$

thus demonstrating that, in the high pressure electrodeless arc, as in the DC arc at high pressures, the isothermal and equipotential surfaces are orthogonal, and the current flows on the isothermal surfaces.*

E. THE GENERAL WORKING EQUATIONS

Referring back to the energy balance equation, the driving term is $\vec{j} \cdot \vec{E}$. Taking a scalar conductivity gives

$$\vec{j} = \sigma(T)\vec{E},$$

where $\sigma(T)$ denotes the dependence of the electrical conductivity on temperature. In the Coulomb gauge $\vec{E} = -\partial\vec{A}/\partial t = -i\omega\vec{A}$, hence,

$$\vec{j} \cdot \vec{E} = (-i\omega\vec{A})\sigma(T) \cdot (-i\omega\vec{A}).$$

Noting that $\vec{A} = \vec{A}_r + i\vec{A}_i$ is a complex quantity, the dissipation is $(\vec{j} \cdot \vec{E}^*)$, hence

$$\vec{j} \cdot \vec{E}^* = \frac{1}{2}\sigma(T)\omega^2[A_r^2 + A_i^2], \tag{23}$$

*Thiene, P. G., Phys. Fluids 6, 1319 (1963).

where the factor ½ on the right occurs because peak values of the field quantities have been employed.

Finally, the argument used to discard the viscous term is employed to show that $u_z \partial u_z/\partial z \ll C_p \partial T/\partial z$. Then $\rho Dh_o/Dt \approx C_p \rho u_z \partial T/\partial z$ is essentially the convective loss from the electrodeless arc. Energy balance for the optically thin electrodeless arc is now written:

$$\frac{1}{2}\sigma(T)\omega^2[A_r^2 + A_i^2] + \frac{1}{r}\frac{\partial}{\partial r}\left(rK(T)\frac{\partial T}{\partial r}\right) + \frac{\partial}{\partial z}K(T)\frac{\partial T}{\partial z} - \rho C_p u_z \frac{\partial T}{\partial z} - 4K_p(T)\tilde{\sigma}T^4 = 0 \quad (24)$$

where the axial dependence of A has been neglected. This is:

Rate of energy input to volume by ohmic heating	+	Rate of energy input to volume by conduction	-	Rate of energy loss to volume via forced convection	-	Rate of energy loss to volume via radiation	=	0

In the limit of an optically <u>thick</u> plasma, the radiant flux vector $\vec{q}_{rad}$ is given by

$$\vec{q}_{rad} = -\frac{16}{3}\tilde{\sigma}\lambda_R T^3 \vec{\nabla} T,$$

where λ_R is the Rosseland mean free path. The energy balance equation is then written

$$\frac{1}{2}\sigma(T)\omega^2[A_r^2 + A_i^2] + \frac{1}{r}\frac{\partial}{\partial r}\left(r\tilde{K}\frac{\partial T}{\partial r}\right) + \frac{\partial}{\partial z}\tilde{K}\frac{\partial T}{\partial z} - \rho C_p u_z \frac{\partial T}{\partial z} = 0, \quad (25)$$

where

$$\tilde{K} = \left(K(T) + \frac{16}{3}\tilde{\sigma}\lambda_R T^3\right)$$

is a radiation enhanced coefficient of heat conductivity valid for the optically thick limit.

APPENDIX V

PROGRAM DOCUMENTATION

IDENTIFICATION

Name: LITTLE CHARYBDIS

FM39F - Electrodeless Arc

Philco 2000, FORTRAN IV

Aeronutronic Division, Philco-Ford Corporation

Newport Beach, California 92663

PURPOSE

The purpose of the program is to investigate the energy balance of an electrodeless arc discharging in air. This is done by integrating six first order differential equations which describe the properties of the discharge. All initial values for the equations are known except temperature, which must be guessed. An incorrect guess yields a solution in which there is no energy balance, in which case the program must be rerun with a better guess. The independent variable of the equations is the radius of

discharge. Integration begins at the center of the discharge and continues outward.

RESTRICTIONS

None.

METHOD

The equations are integrated using RKS3, the Runge-Kutta library integration routine.

FORMULATION

The following are constants in the integration:

$\omega = 2\pi f$, where f is input frequency.

$\mu_o = 4\pi \times 10^{-7}$

$\tilde{\sigma} = 0.5668 \times 10^{-7}$

The tables used for interpolation purposes are $\sigma(T,P)$ and AKC (T,P).

The input variables are:

P = pressure in atmospheres.

DELRC = step size of first step (adjusted automatically) (meters).

DELRP = lower limit on step size to be printed (meters).

T - temperature in degrees Kelvin.

f = frequency in cycles per second.

FLD = magnetic field (gauss).

The initial conditions of the system are:

r = 0

Ar = 0

$Br = FLD^* .17517 \times 10^{-4}$

$A_I = 0.$

$B_I = FLD^* - .63817 \times 10^{-4}$

$S = 0.$

T = input temperature.

The equations are integrated from r = 0 to r = r*, where r* is the point where $T < 1000^{o}K$, or $T > 30{,}000^{o}K$, or Deriv count > 4000. If none of these happen, the integration is stopped when r = .35 meters.

The differential equations are:

$$\dot{A}_r = B_r - \frac{A_r}{r} \qquad \text{if } r = 0 \quad \dot{A}_r = \frac{1}{2} B_r$$

$$\dot{B}_r = - \omega\sigma(T)\mu_o A_i$$

where $\sigma(T) = 0$ if $T < 2000$, or $\sigma(T)$ is interpolated quadratically from a table. $\sigma(T)$ and AKC(T) depend on T and P, however, at this point we know the value of P from input, and we need only T to proceed with interpolation.

If the quadratic interpolation returns a negative value, linear interpolation is used; likewise linear interpolation is used around the peak of the curve.

$$\dot{A}_i = B_i - \frac{A_i}{r} \qquad \text{if } r = 0 \quad \dot{A}_i = \frac{1}{2} B_i$$

$$\dot{B}_i = \omega\sigma(T)\mu_o A_r$$

$$AKR = 4.52 \times 10^{-5} \, p^{1.31_e} \, (5.18 \times 10^{-4} T - 7.13 \times 10^{-9} T^2)$$

$$\lambda_R = \left[AKR \right]^{-1}$$

then AKC is a quadratic table lookup, except for $T < 500^{o}K$.

$$AKC(T) = .04 \left(\frac{T}{500}\right)^{.75}$$

$$AKPP = 8.3\ AKR$$

There are two versions of subroutine DERIV. One contains the Planck formulas for S and T, the other version contains the Rosseland formulas. The Planck formulas are the following

$$\dot{S} = -1/2\ r\ \omega^2\ \sigma(T)\ (A_r^2 + A_i^2) + 4r\ AKPP\ \tilde{\sigma}\ T^4$$

$$\dot{T} = S\left[r\ AKC(T)\right]^{-1}$$

The Rosseland formulas are:

$$\dot{S} = -1/2\ r\ \omega^2 \sigma(T)(A_r^2 + A_i^2)$$

$$\dot{T} = S\left[r\ AKC(T) + 1\ 6/3\ \tilde{\sigma}\ T^3)\lambda_R\right]^{-1}$$

Auxiliar computations at each integration step.

$$RAD = 2\pi r\tilde{\sigma}T^4$$

$$CØND = 2\pi r\dot{T}\ AKC(T)$$

$$SIGER - \omega A_i \sigma(T)$$

$$SIGEI = \omega\ A_r \sigma(T)$$

$$SIGE{*}{*}2 = \frac{1}{2}\sigma(T)\omega^2(A_r^2 + A_i^2)$$

Two power integrations are made in the CNTRL routine, using a modified Euler scheme.

$$\text{Power out} = \int_{r=0}^{r=r^*} 2\pi\omega^2\sigma(T)r(A_r^2+A_i^2)dr$$

$$\text{Power in} = -2\pi S_{r^*} + 8\pi\tilde{\sigma} \int_{r=0}^{r=r^*} AKPP^* \, T^{4*} \, r \, dr$$

The following are also computed.

$$E(r) = -\omega \, (A_r^2 + A_i^2)^{\frac{1}{2}}$$

$$I/\ell = \sigma(T,P) \int_{r=o}^{r=r^*} E(r)dr$$

$$\text{B Magnitude} = (\beta_r^2 + \beta_i^2)^{\frac{1}{2}}$$

Power Ratio = Power Out/Power In

$$R = 8\pi\tilde{\sigma} \int_{r=o}^{r=r^*} AKPP * T^4 * rdr$$

$$J(r) = \sigma(T,P)E(r)$$

$$F = \frac{R}{\text{Power Out}}$$

The energy balance is achieved when the Power Ratio is close to 1.

As mentioned earlier, this is dependent on the initial temperature value, which is input. The user may input a table of trial temperature values, and the program will compute one integration per temperature. If the power balance is bracketed by two of the temperatures, the user must then refine the trial temperature then rerun the program. The program is designed so that the user may also input a table of frequencies for which he desires a solution.

Input Data

Card	Column	Format	Name, Definition
1,2	1-72	12A6	Title

If the auxiliary output tape is desired for possible plotting, write PLOT in column 61 of card 2. If it is the last such case write END in column 67 of card 2. If both of these are entered in card 2, the case must be stacked last. See description of tape in output section.

3	1-12	E12.8	P, pressure in atmospheres.
"	13-24	"	Not used
"	25-36	"	"
"	37-48	"	AMUO, $4\pi x10^{-7}$
"	49-60	"	SIGMA (σ), $.5668x10^{-7}$
"	61-72	"	DELRC, delta r for first step (computed thereafter)
4	1-12	E12.8	DELRP, lower limit on step size to be printed. (If DELRP = 0, every integration step is printed.)
5	1-2	I2	N1 (1), number of frequencies ($\geq$1)
"	3-4	"	N1 (2), number of field values ($\geq$1)
"	5-6	"	N1 (3) = 1
"	7-8	"	N1 (4) = 1
"	9-10	"	N1 (5) = 1
"	11-12	"	N1 (6) = 1
"	13-14	"	N1 (7), number of temperatures ($\geq$1)
6	1-72	6E12.8	Frequency table, 6 fields of 12.*
7	1-72	6E12.8	Field value table, 6 fields of 12.*

* up to 24 values, or 2 cards.

8	1-72	6E12.8	Temperature table, 6 fields of 12.*

This concludes the input. Cases may be stacked. The following data is output at each printed r value:

First line of output: r, B magnitude, B_r^2, B_I^2, RAD, CØND, SIGER, SIGEI, SIGE**2, Total Deriv Count (number of times Deriv routine has been entered).

Second line: Ar, Br, A_I, B_I, S, T.

Third line: $\dot{A}r$, $\dot{B}r$, $\dot{A}_I$, $\dot{B}_I$, $\dot{S}$, $\dot{T}$.

Fourth line: λr, Power out, Power in, Power ratio. (The last 3 items appear on the fourth line only if $T < 4200^{\circ}K$).

Fifth line: E(r), J(r), $\sigma(T,P)$, AKC(T)

After r = r" is reached the integration is concluded, then quantities I/L, F and R are printed.

In addition to the printed output, there is also binary tape output which is used as input to a plot program, FM39FA. For each integration, two records are put on the auxiliary tape (logical 10).

First record:

NPLØT	Plot number
IPFLAG	Number of points in the plot
P	Pressure in atmospheres
f	Frequency in cycles per second
B	Field value
TW	Initial temperature, deg. K.

* up to 24 values, or 2 cards.

The second record is a two-dimensional array of nine columns and IPFLAG rows. The dimension statement limits its size to 150x9. There is one row for each data point taken from the integration. Each row consists of the variables r, Ar, Br, A_I, B_I, S, T, plus two extra dummy variables which are used to fill up the nine columns. This allows addition of two new variables at a later date without disrupting the dimensions and the record length. The end of data is signaled by NPLØT = -7.

SUBPROGRAMS

The subprograms used in the program are the standard ones used with RKS3, namely a CNTRL subroutine and a DERIV subroutine. There are three interpolation routines referenced in the program. INT7 (NM58F) interpolates using a first or second degree Lagrange polynominal. L1INT (NM36F) is first order Lagrangian interpolation from a singly-dimensioned array. L2INT (NM37F) is first order Lagrangian interpolation from a doubly-dimensioned array. There is also a block data subprogram which contains all tables used for interpolation.

APPENDIX TO FM39F PROGRAM DOCUMENTATION

The following additions to the program were made after the program was documented. The user may input a table of field values for which integration is desired. The table may be input in two different ways.

1. Input the number of values in table on card 5, column 3-4. Input the field values in gauss on card 7. The program will convert each value to real and imaginary parts in webers per square meter.

2. Input the number of values in the table on card 5, column 3-4. Input the real and imaginary parts of the field in webers per square meter on successive fields of the card; e.g., columns 1-12 will contain the real part of the first value, columns 13-24 will contain the imaginary part of the first value, etc. If this method is used, input -1 in columns 5-6 of card 5. This is the variable N1(3) in the program.

PROGRAM

A complete listing of this program is included in the compilation presented the numerical data read-out.

APPENDIX VI

THEORETICAL TEMPERATURE PROFILES FOR THE ELECTRODELESS ARC IN HIGH PRESSURE AIR

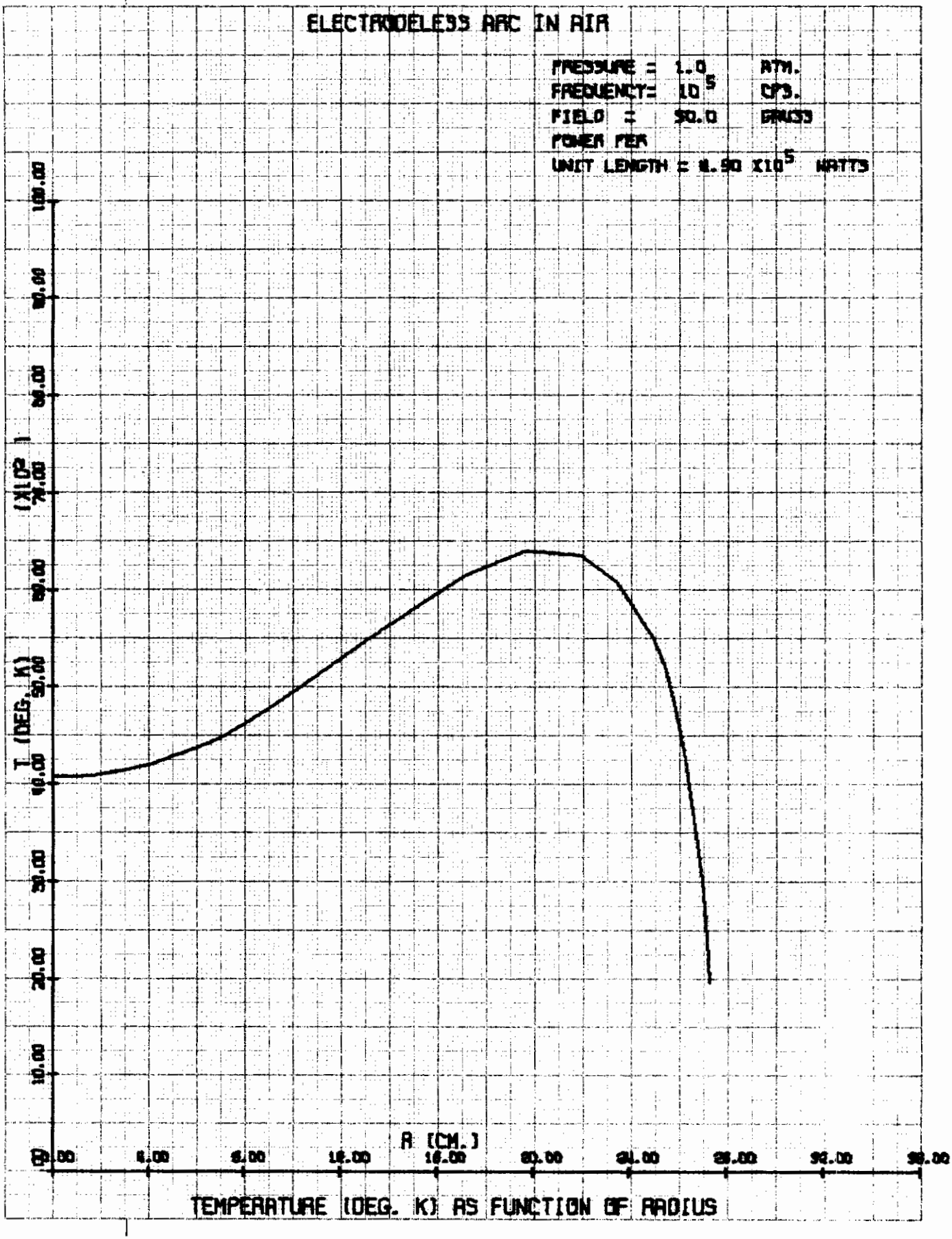

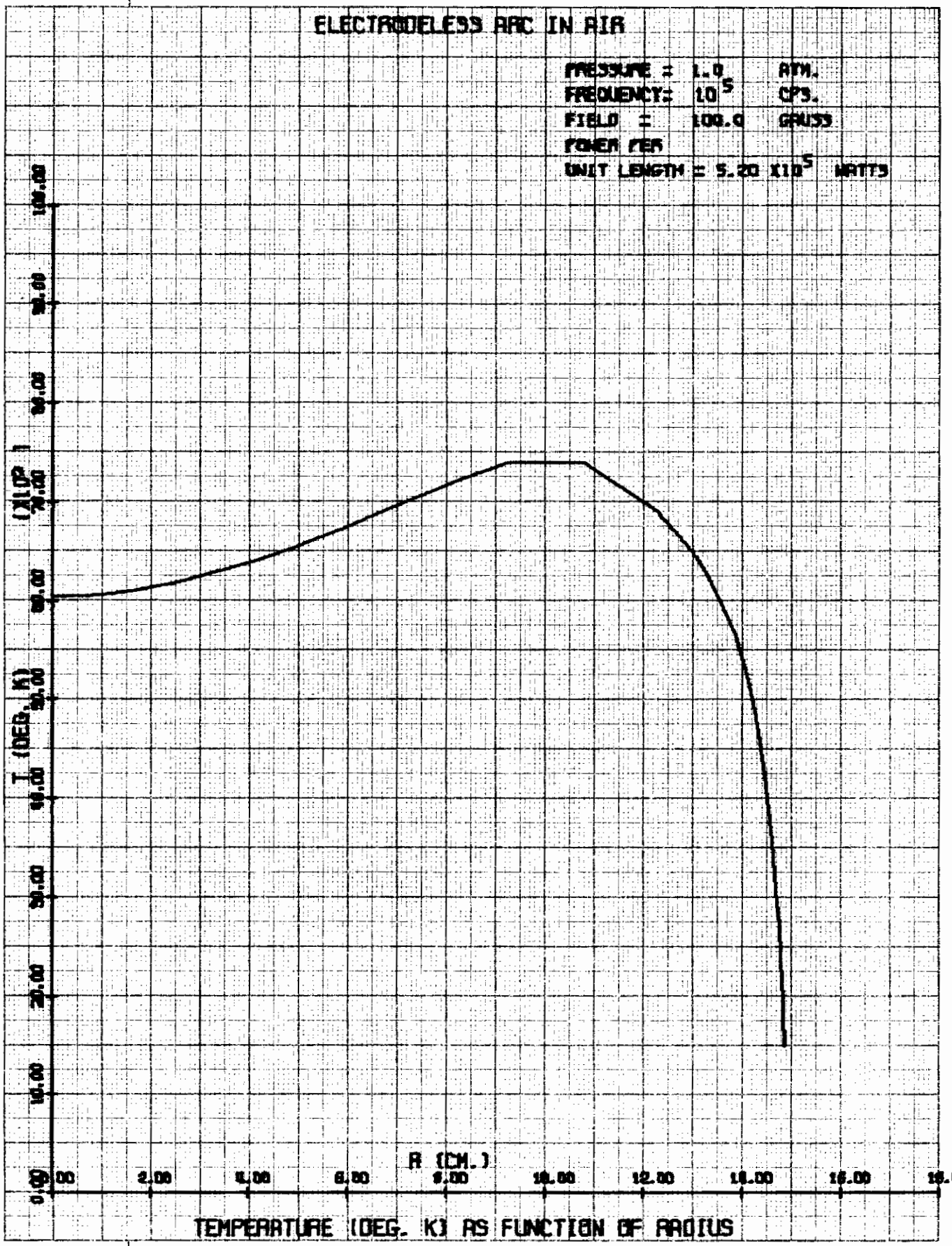

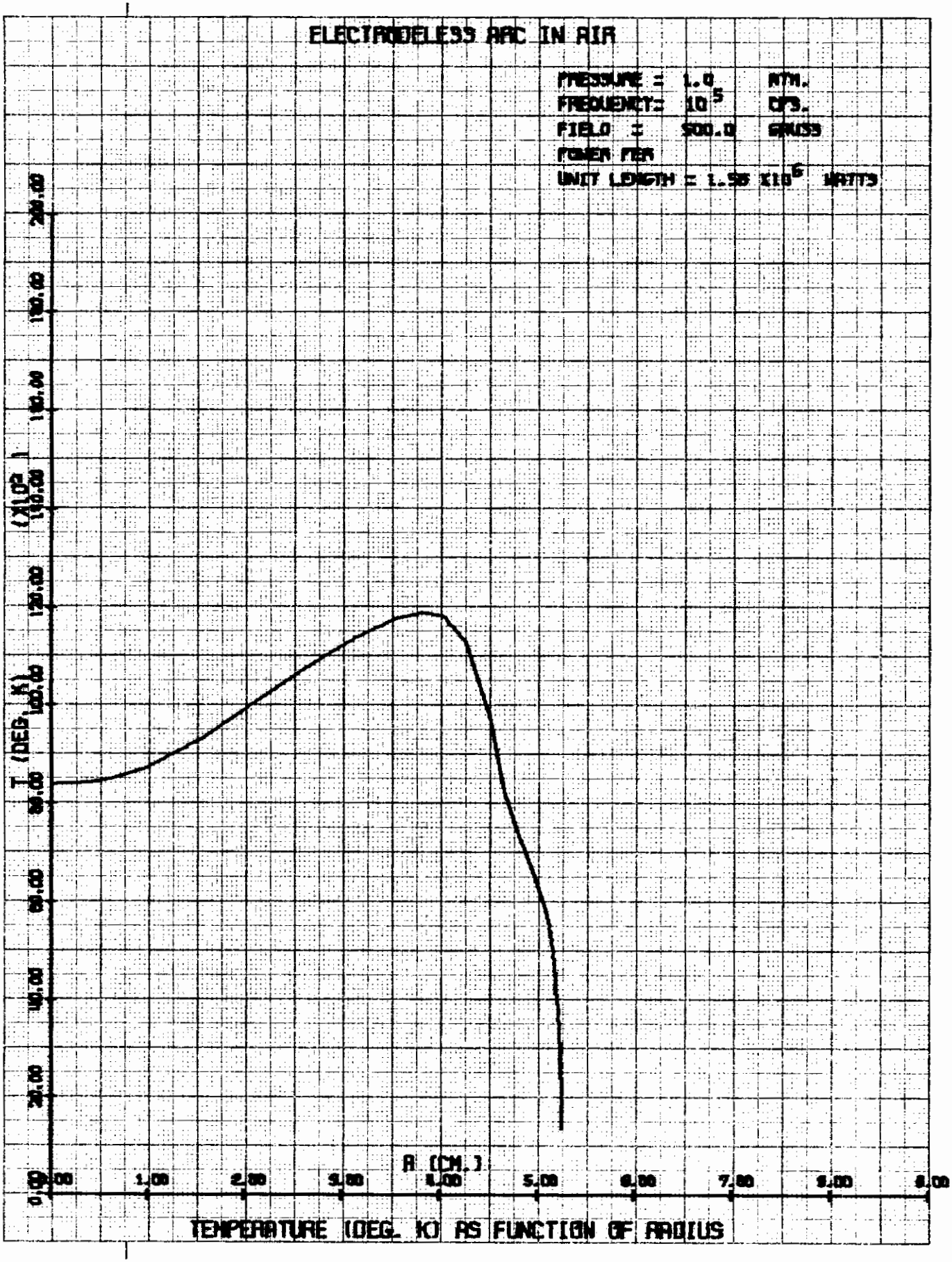

TEMPERATURE (DEG. K) AS FUNCTION OF RADIUS

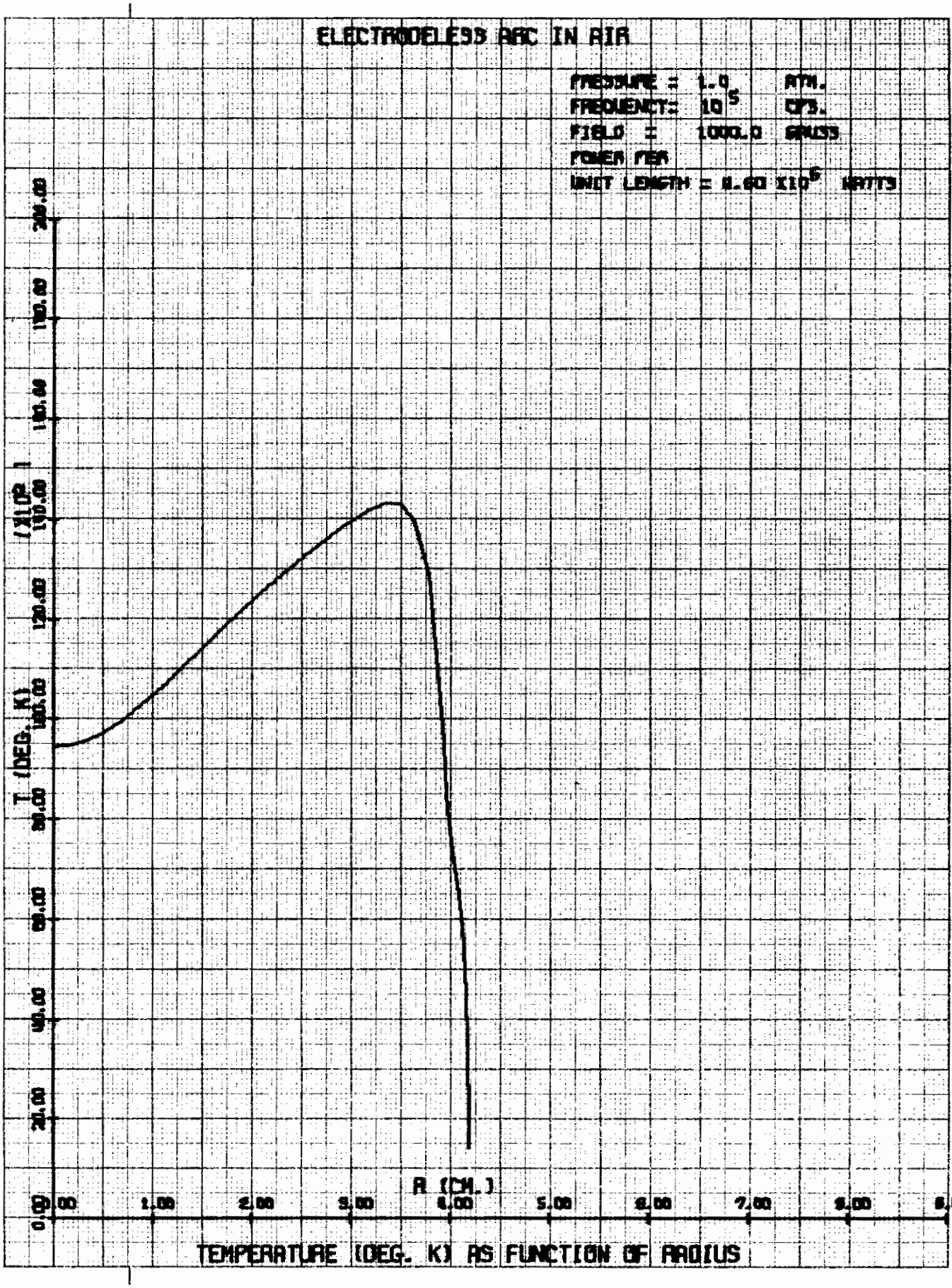

TEMPERATURE (DEG. K) AS FUNCTION OF RADIUS

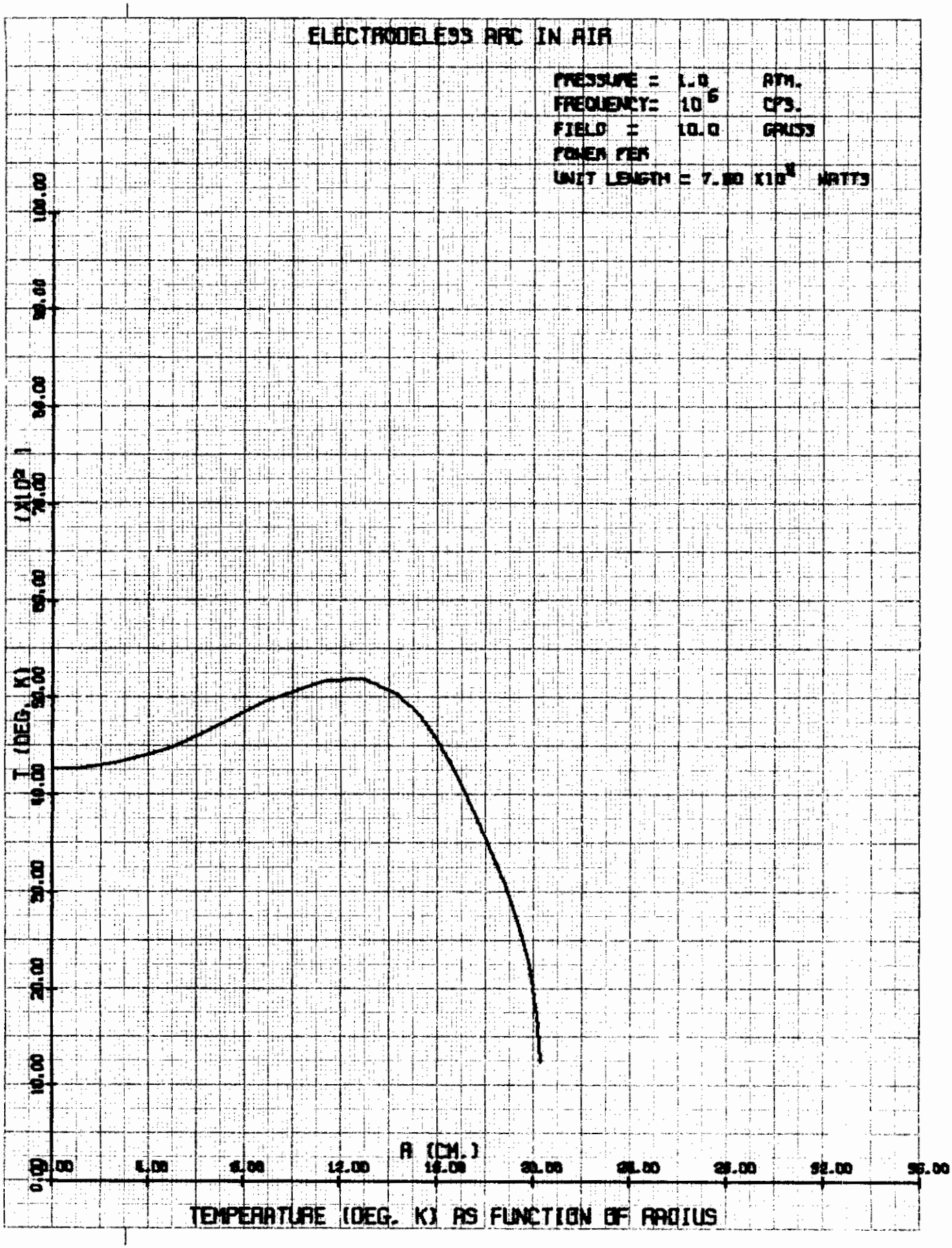

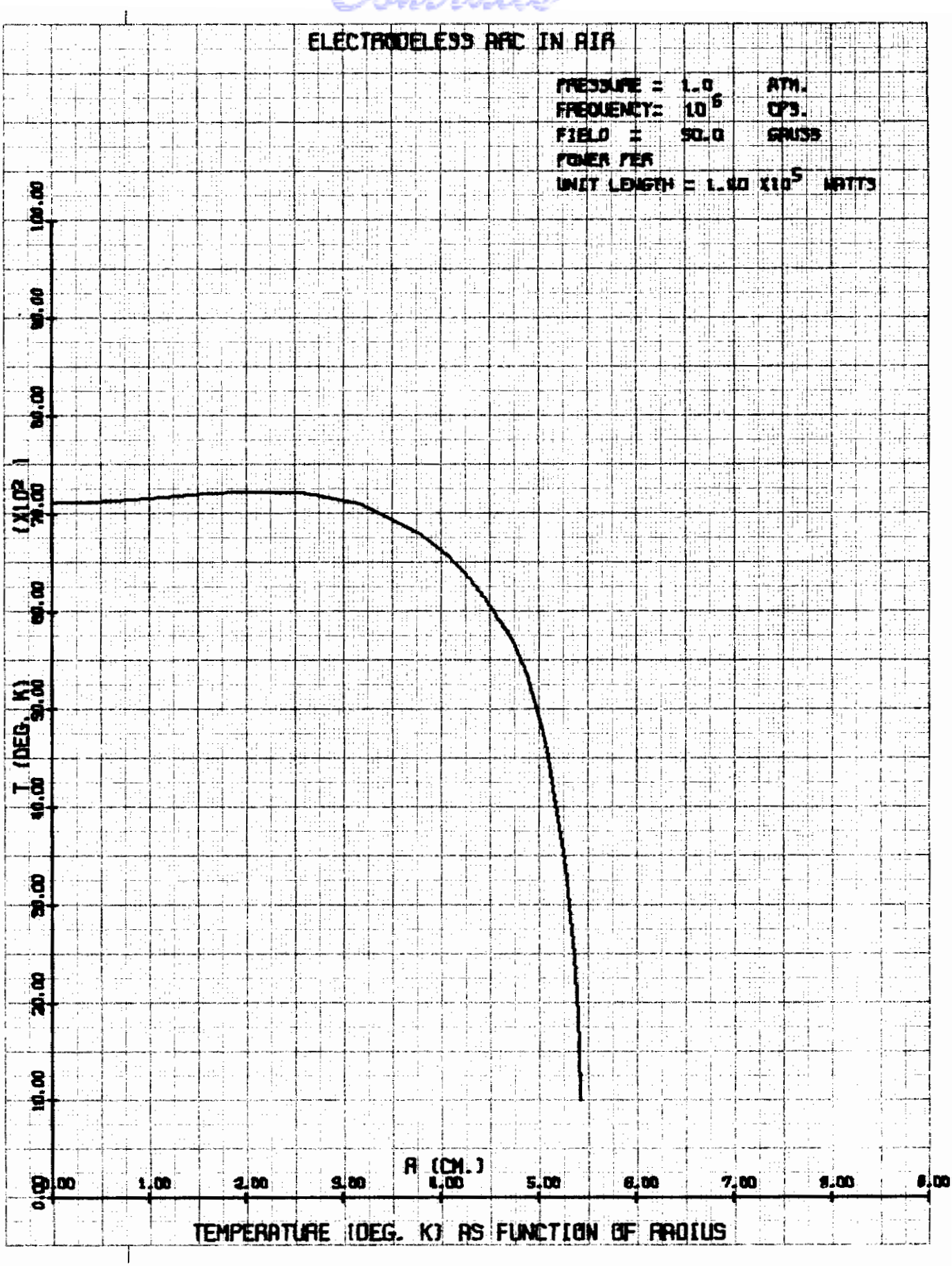

TEMPERATURE (DEG. K) AS FUNCTION OF RADIUS

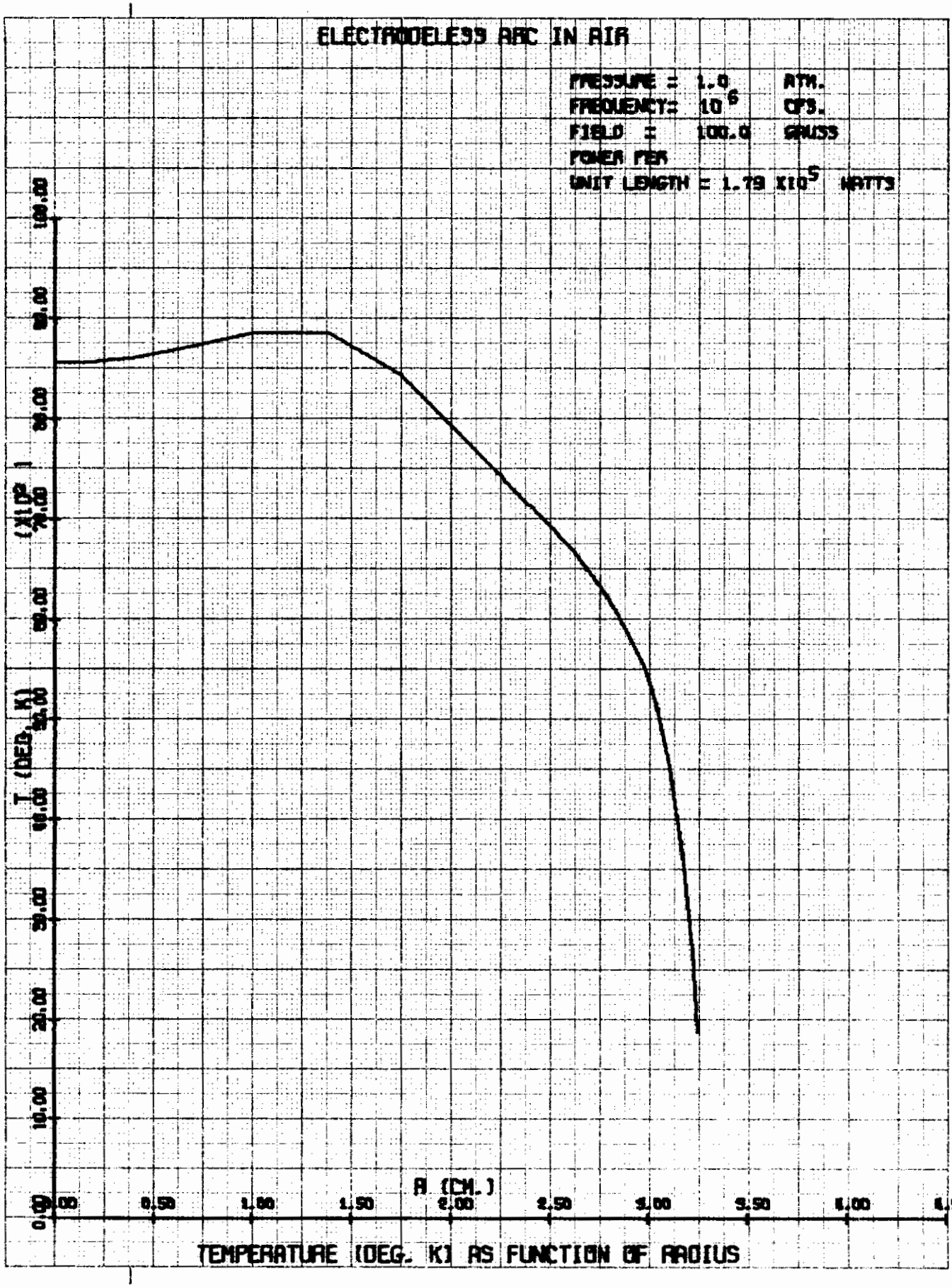

TEMPERATURE (DEG. K) AS FUNCTION OF RADIUS

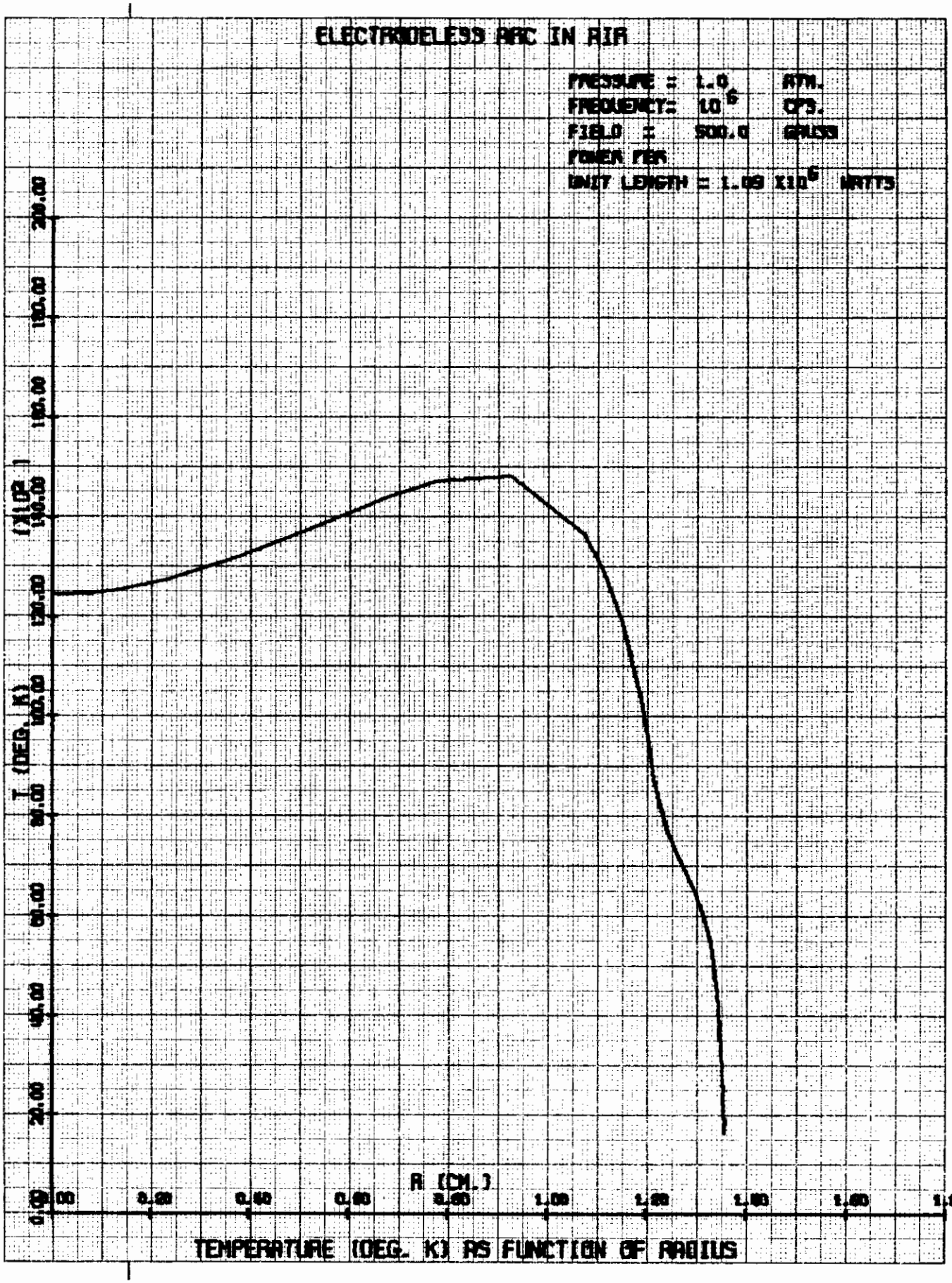

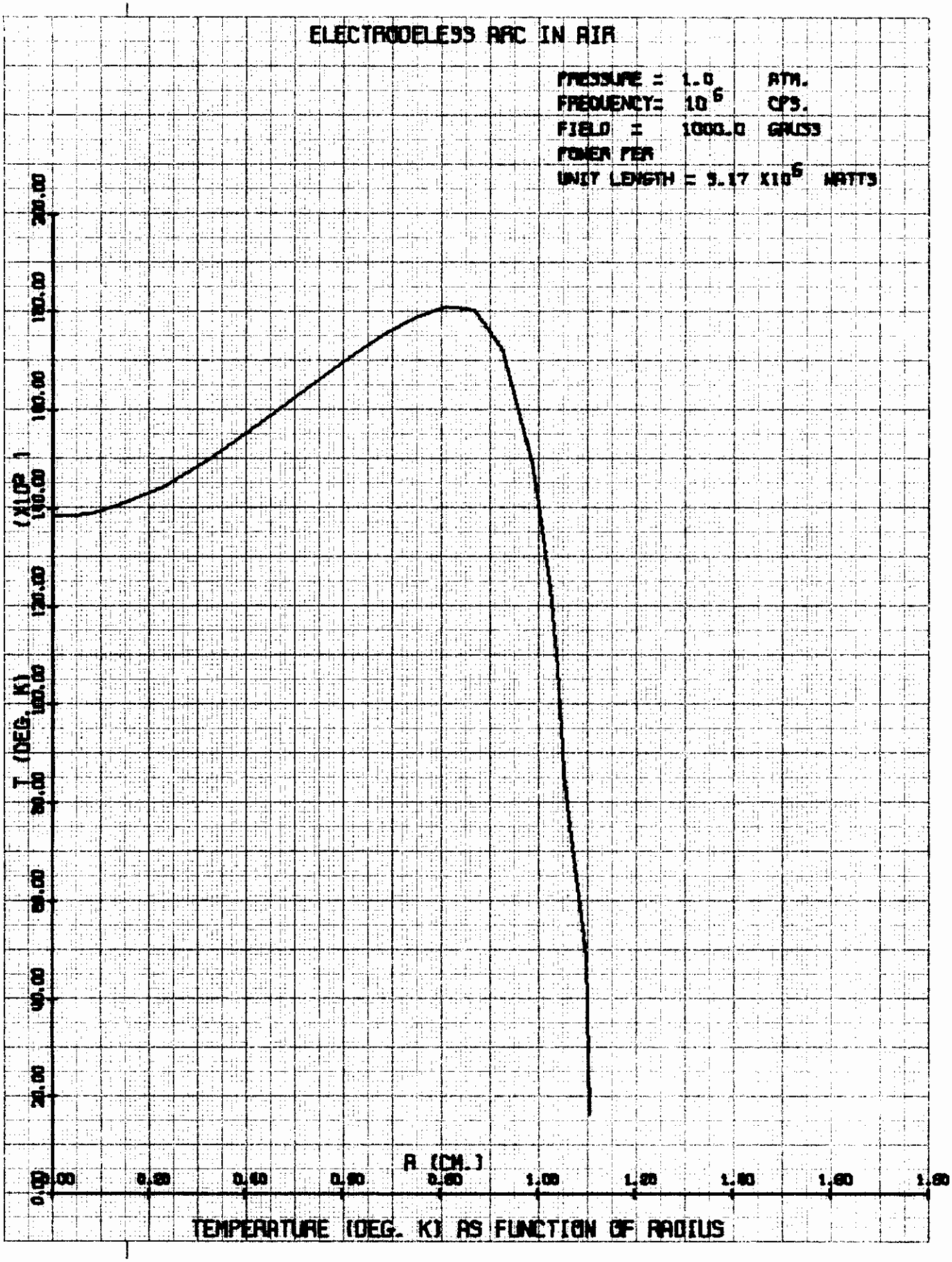

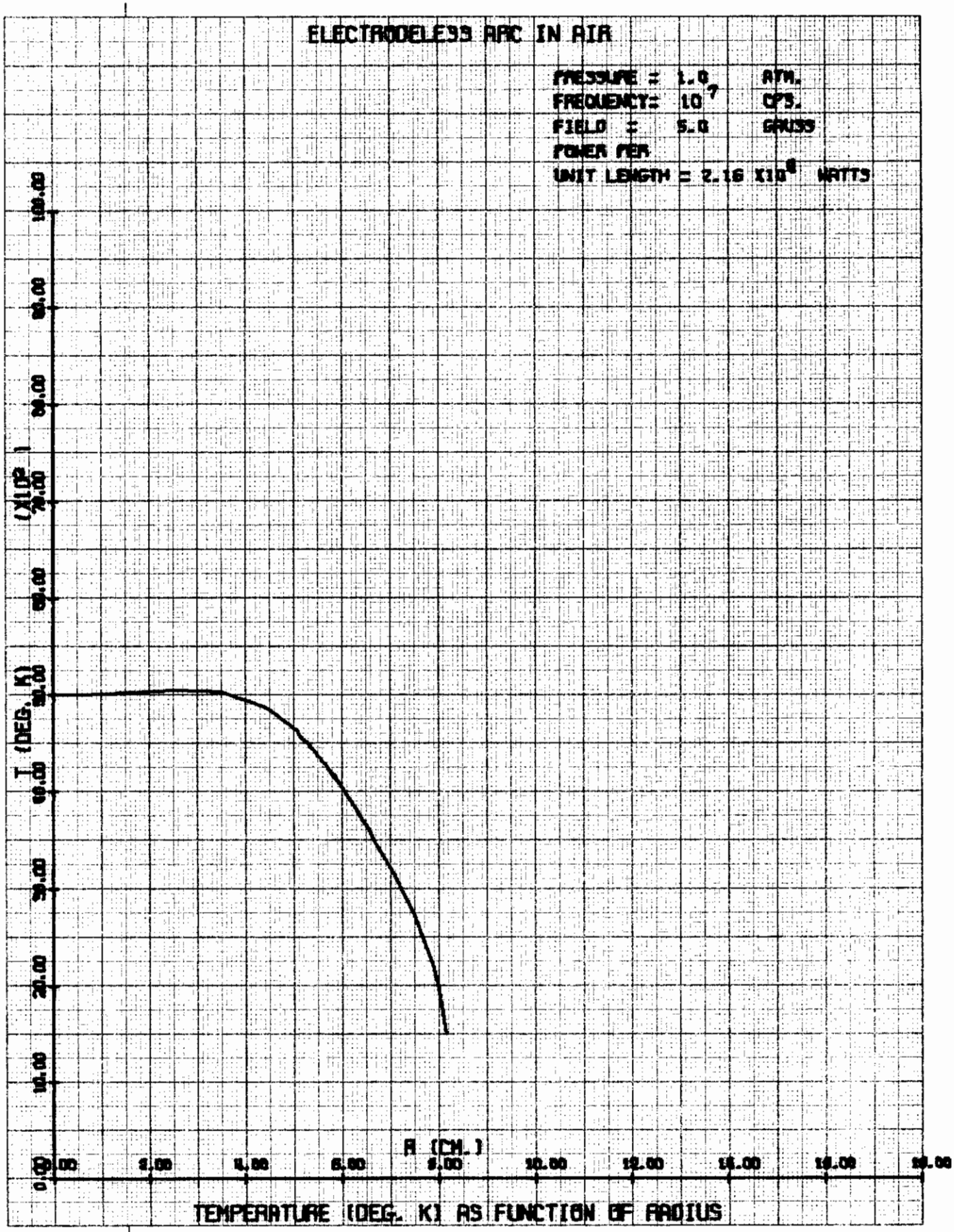

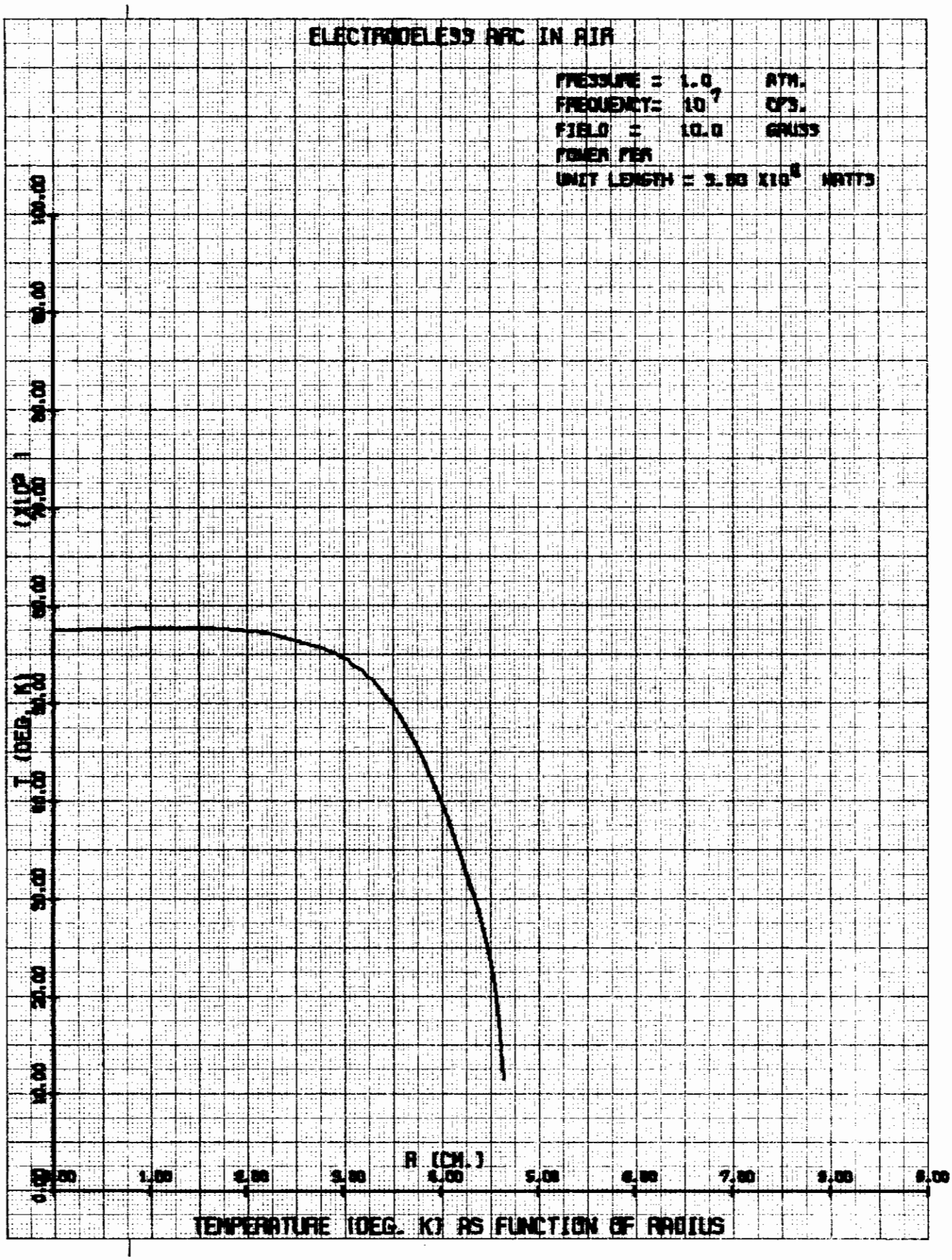

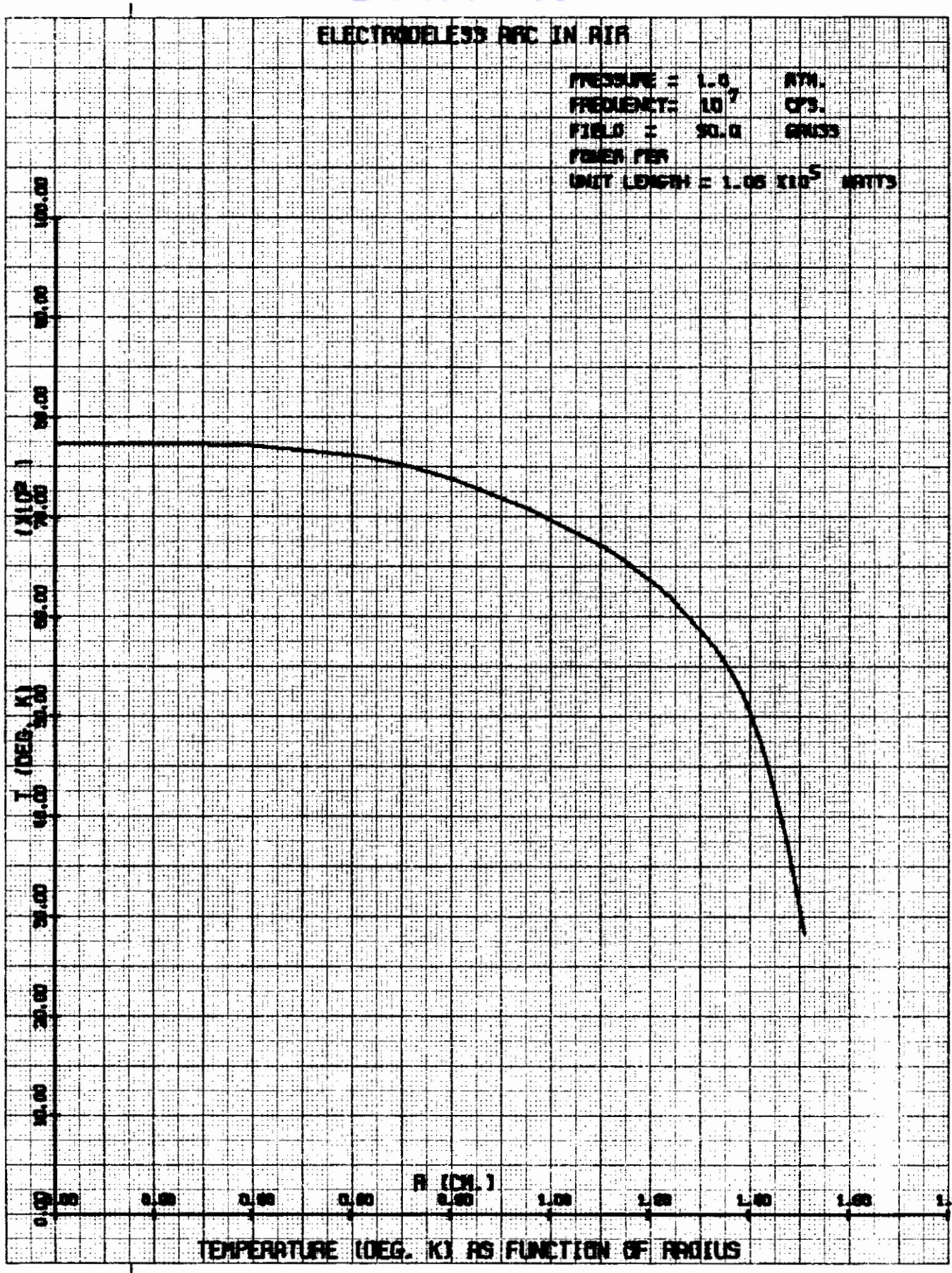

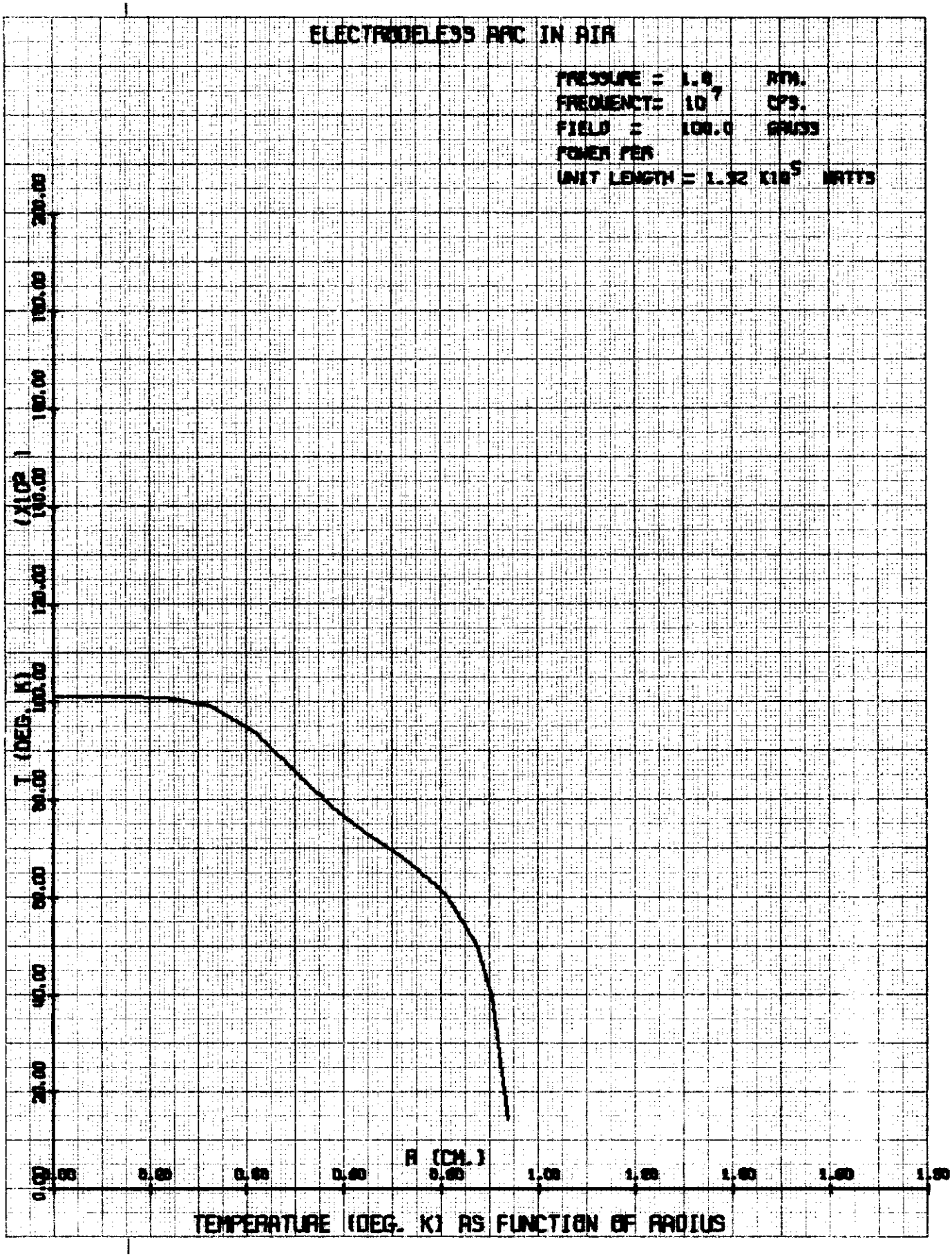

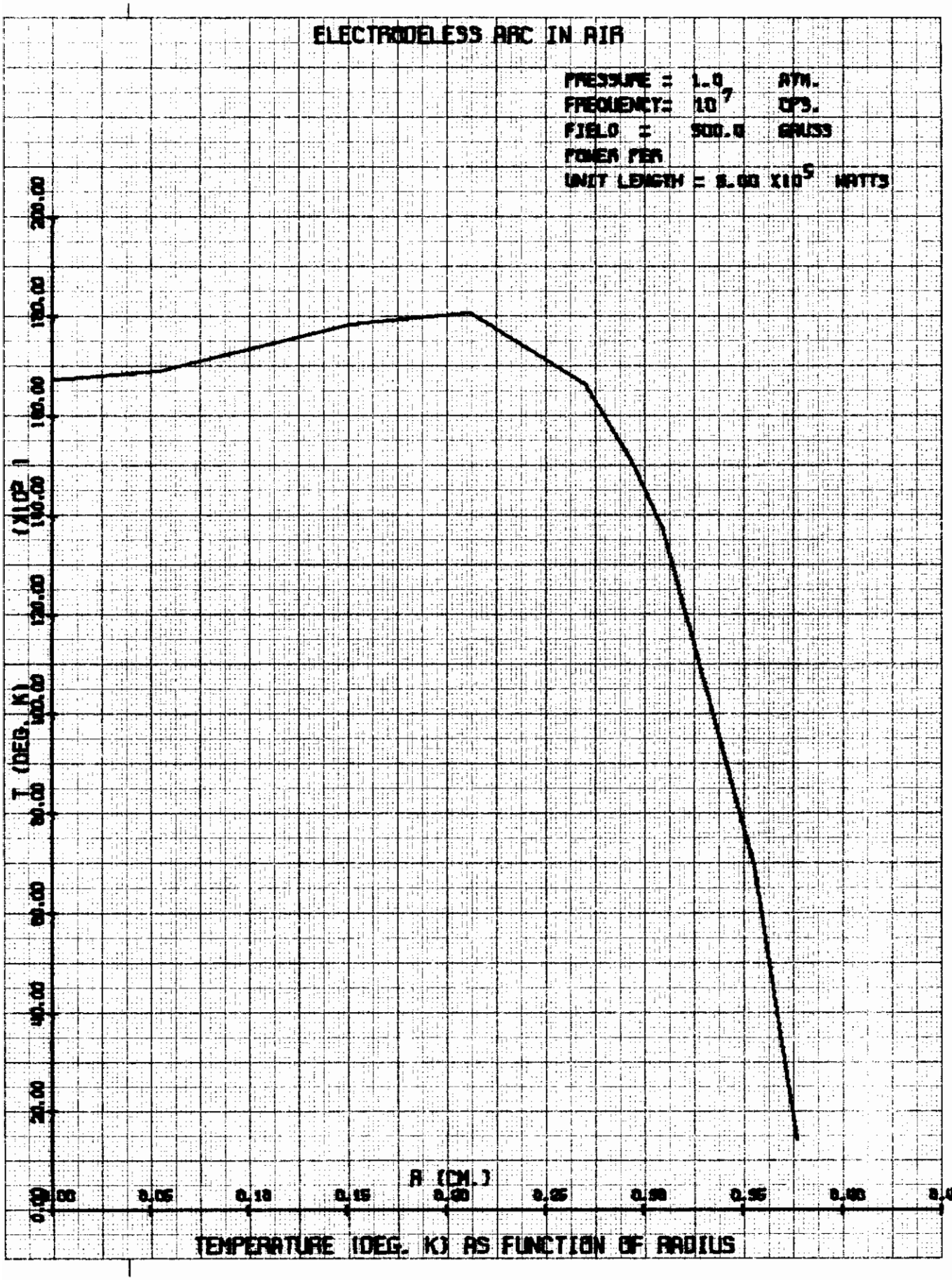

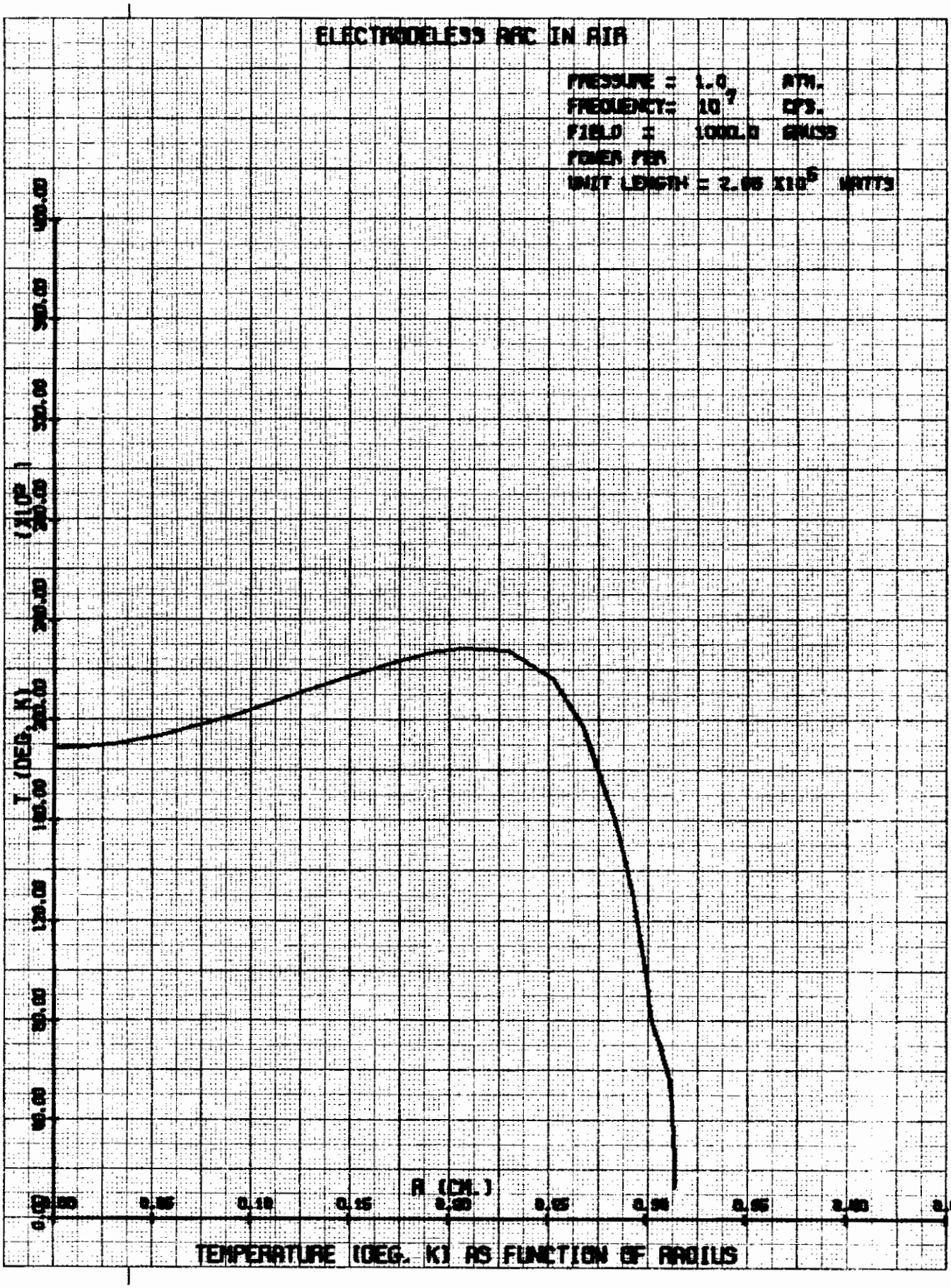

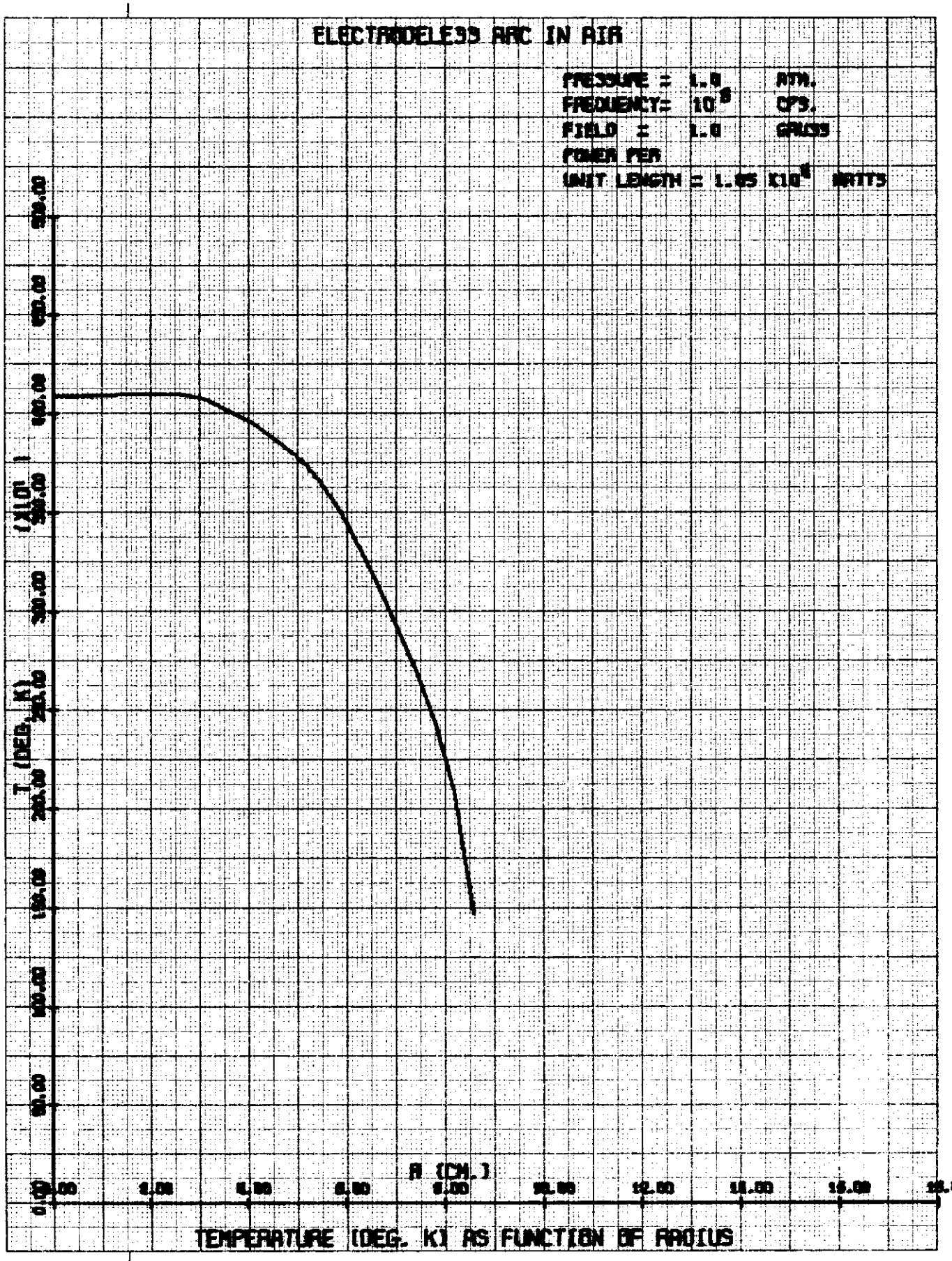

TEMPERATURE (DEG. K) AS FUNCTION OF RADIUS

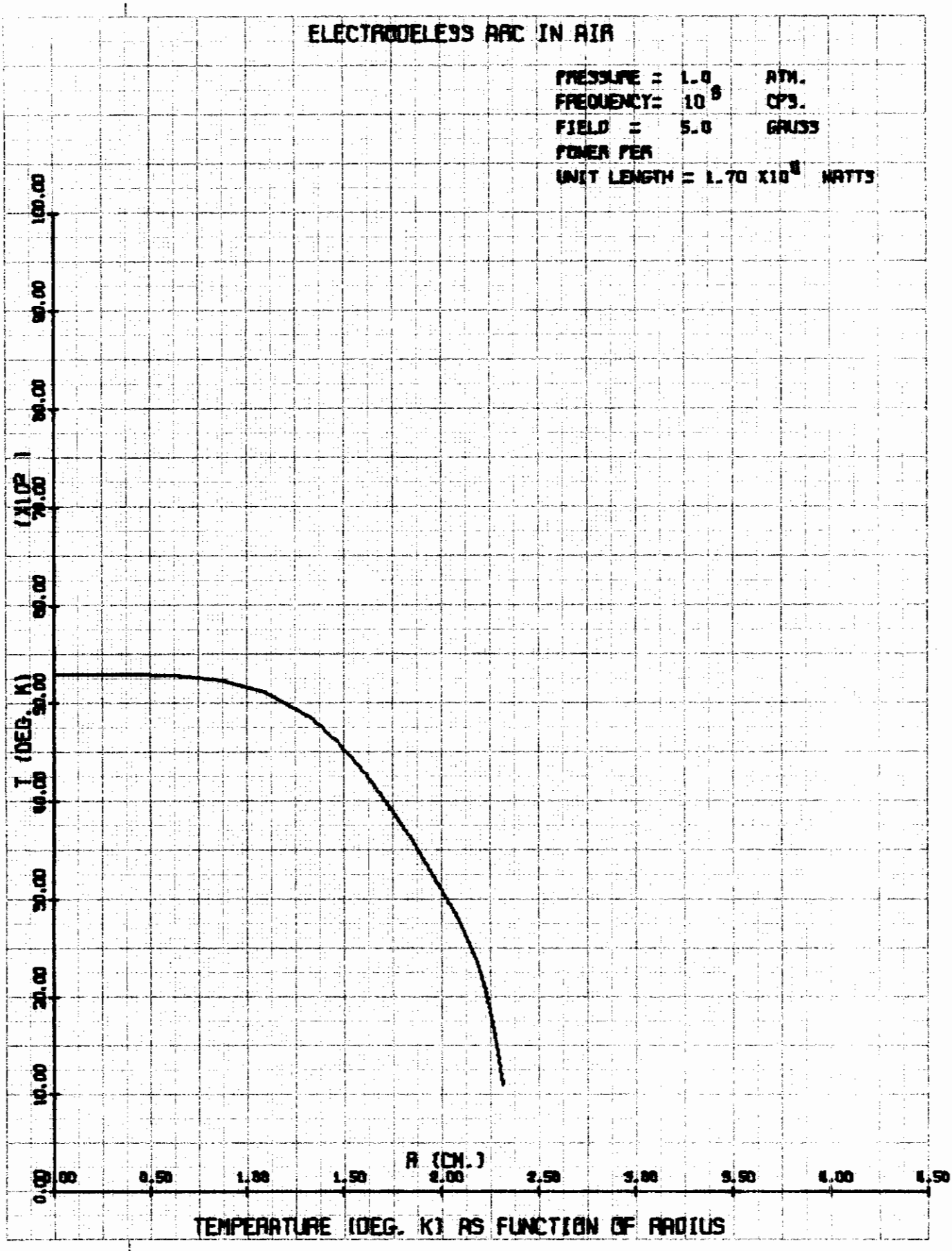

TEMPERATURE (DEG. K) AS FUNCTION OF RADIUS

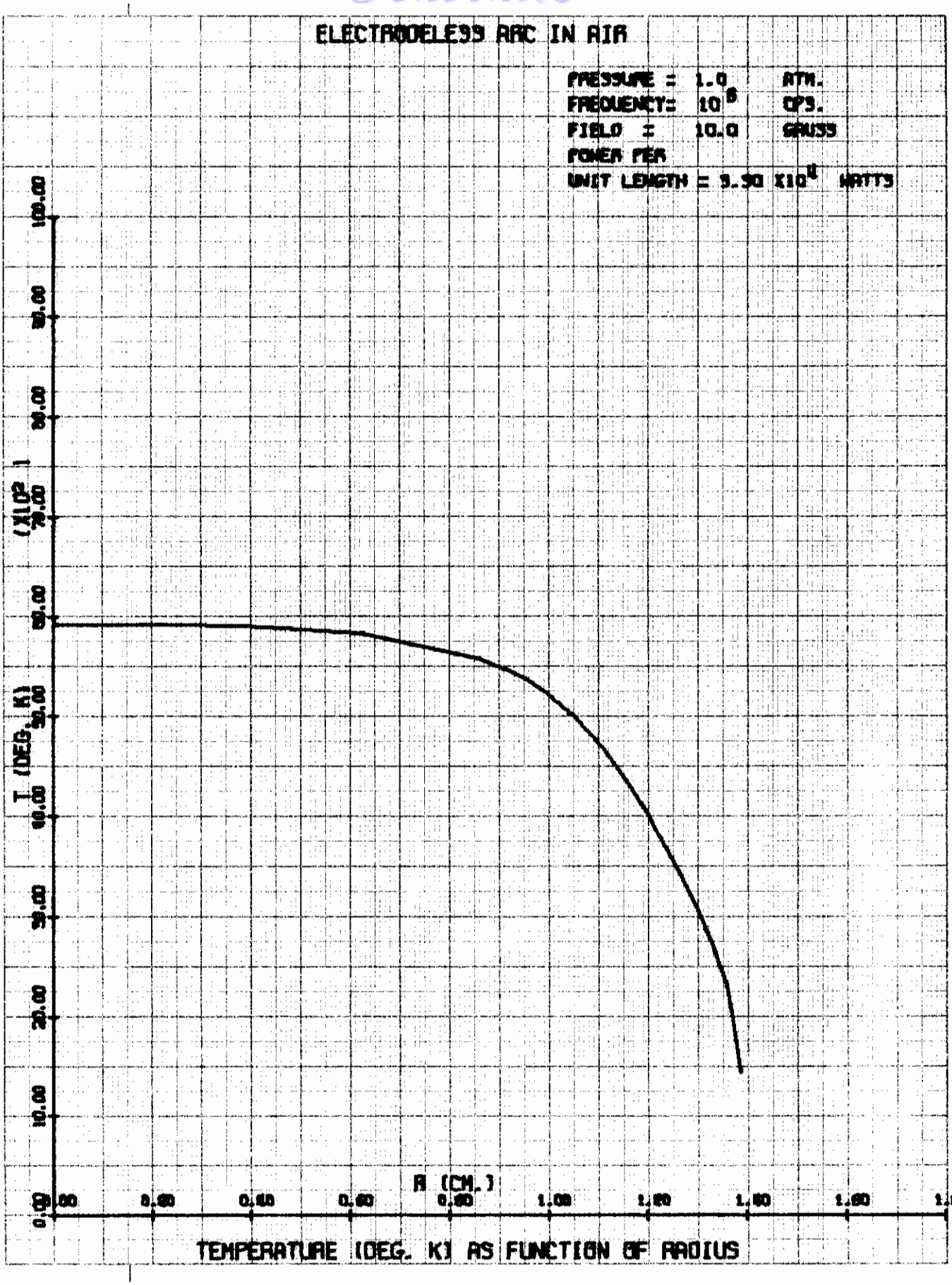

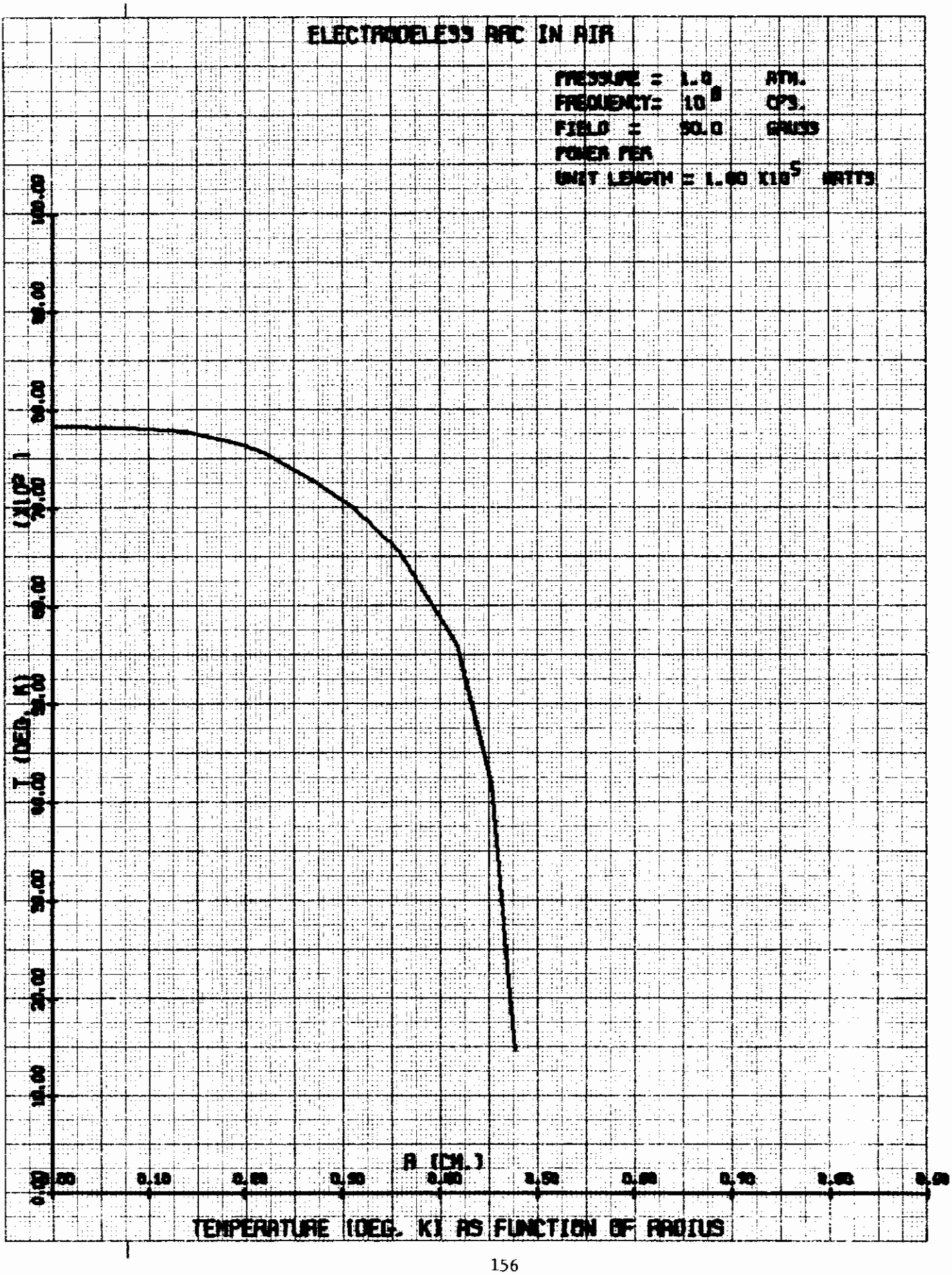

TEMPERATURE (DEG. K) AS FUNCTION OF RADIUS

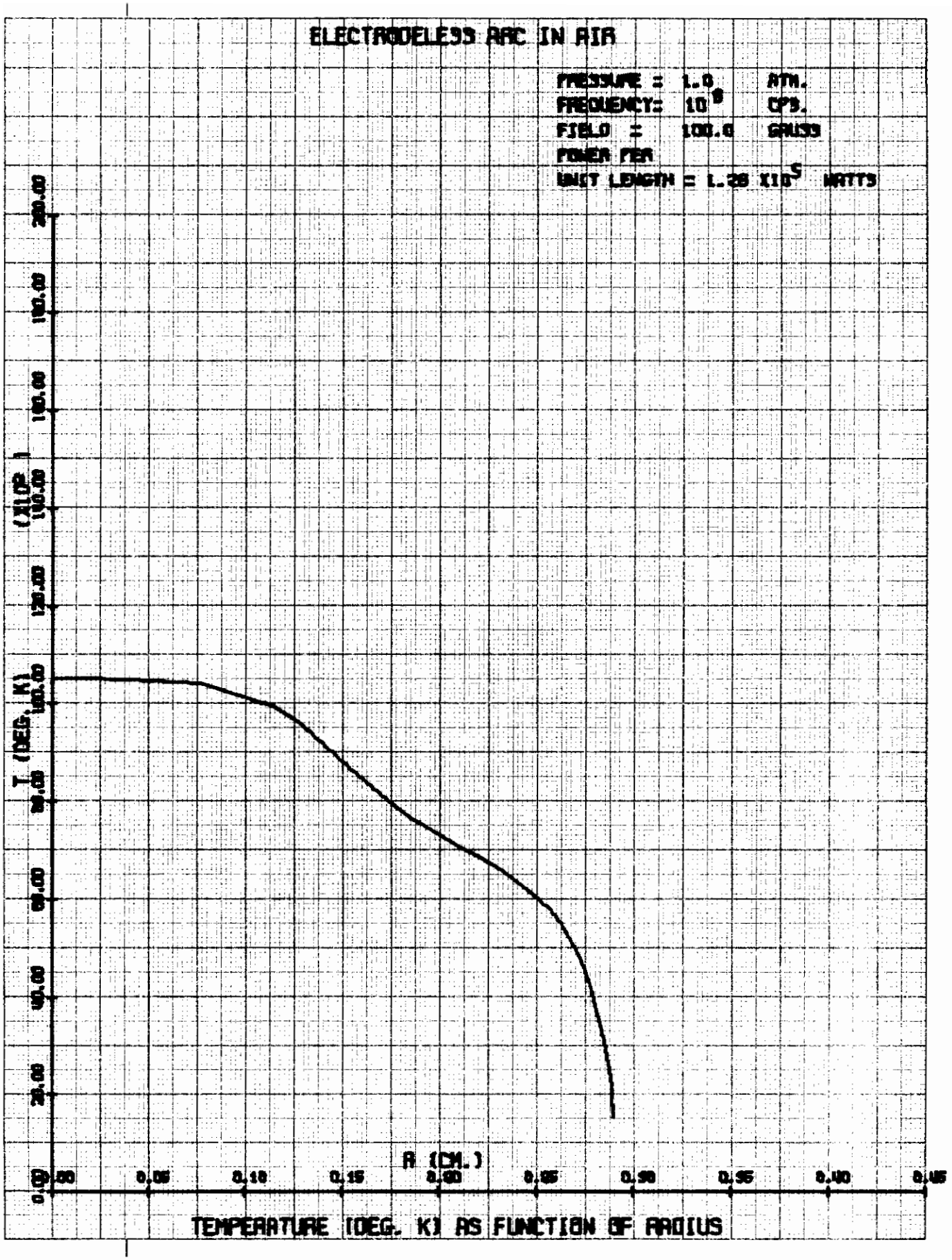

TEMPERATURE (DEG. K) AS FUNCTION OF RADIUS

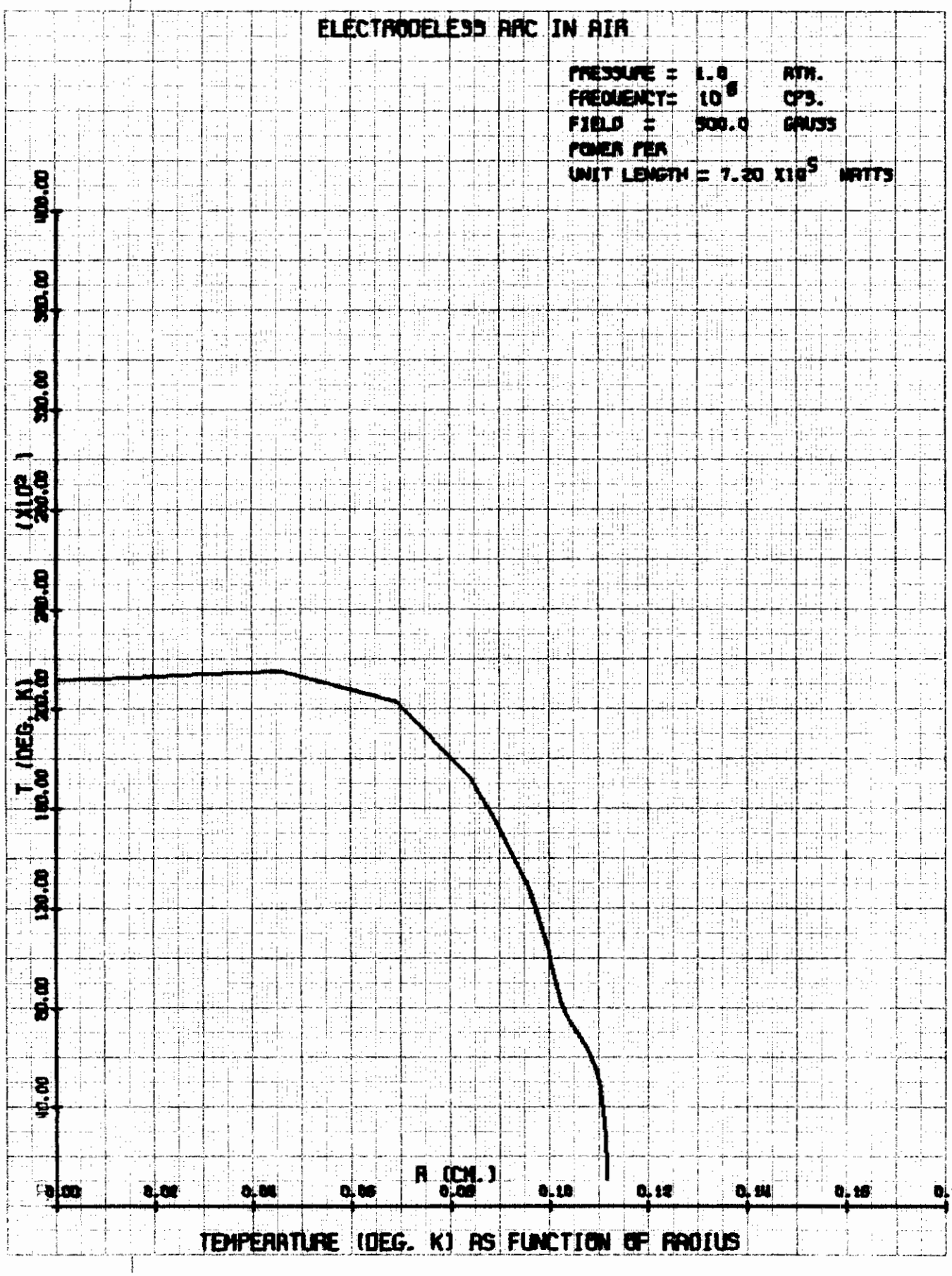

TEMPERATURE (DEG. K) AS FUNCTION OF RADIUS

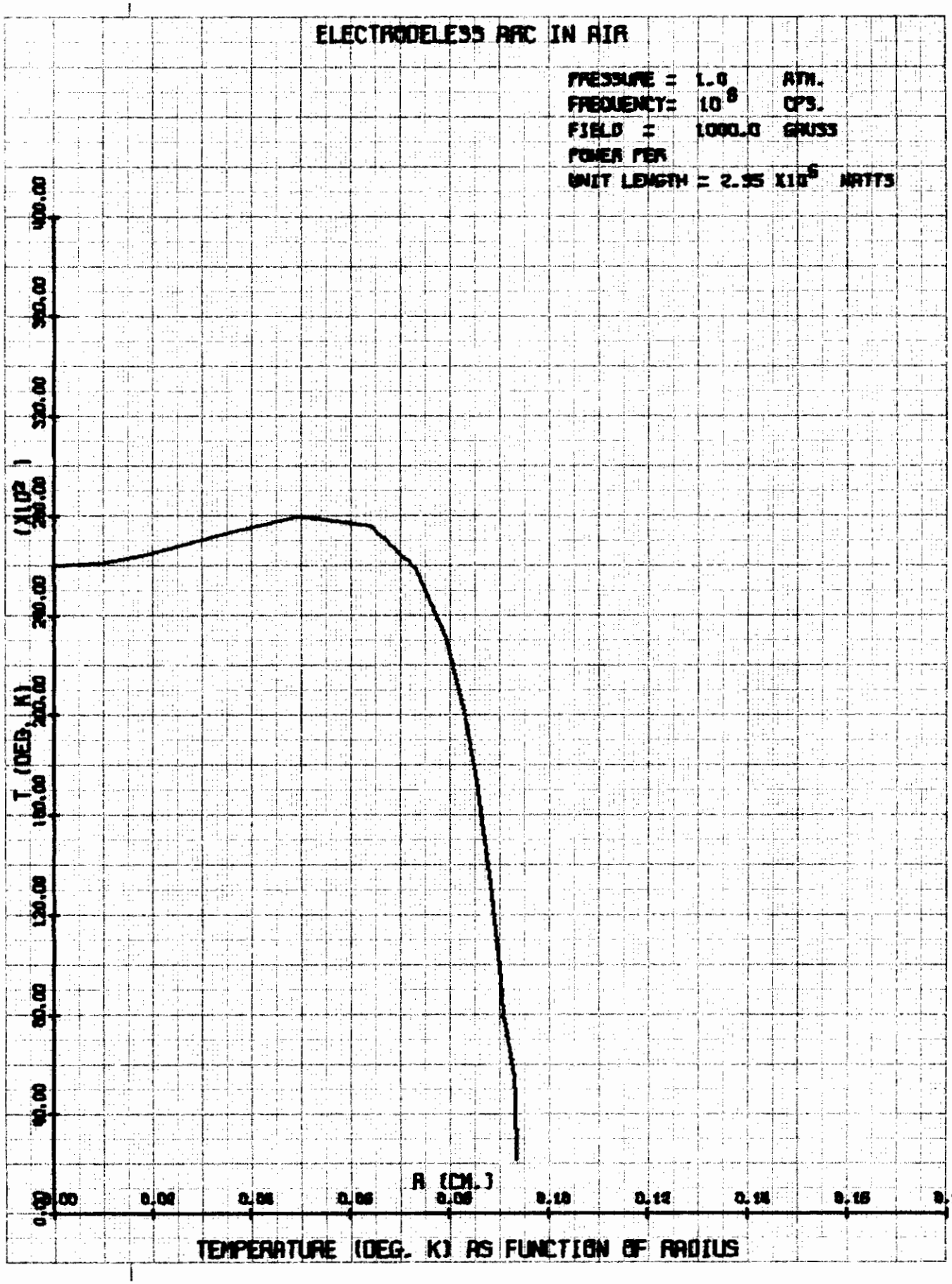

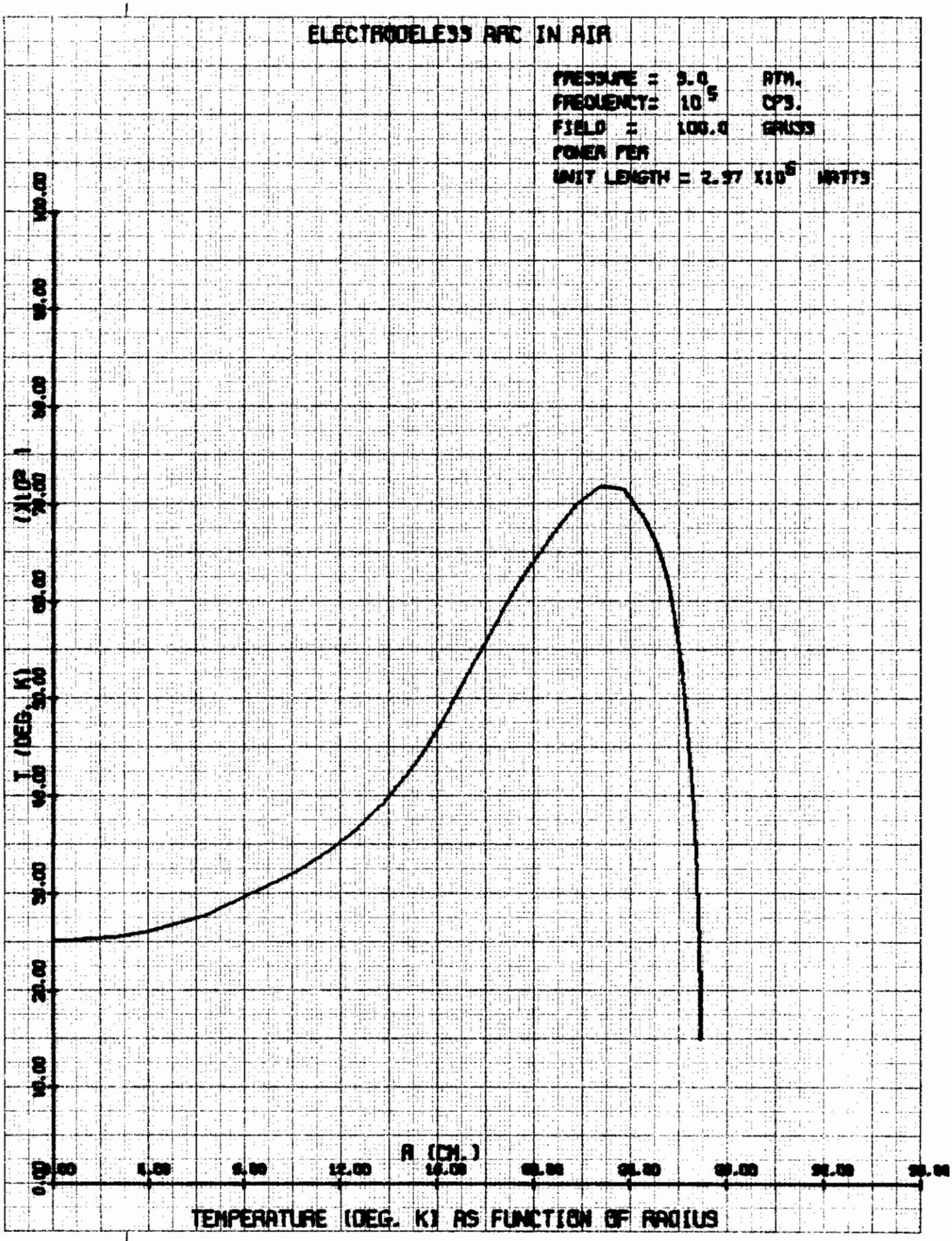

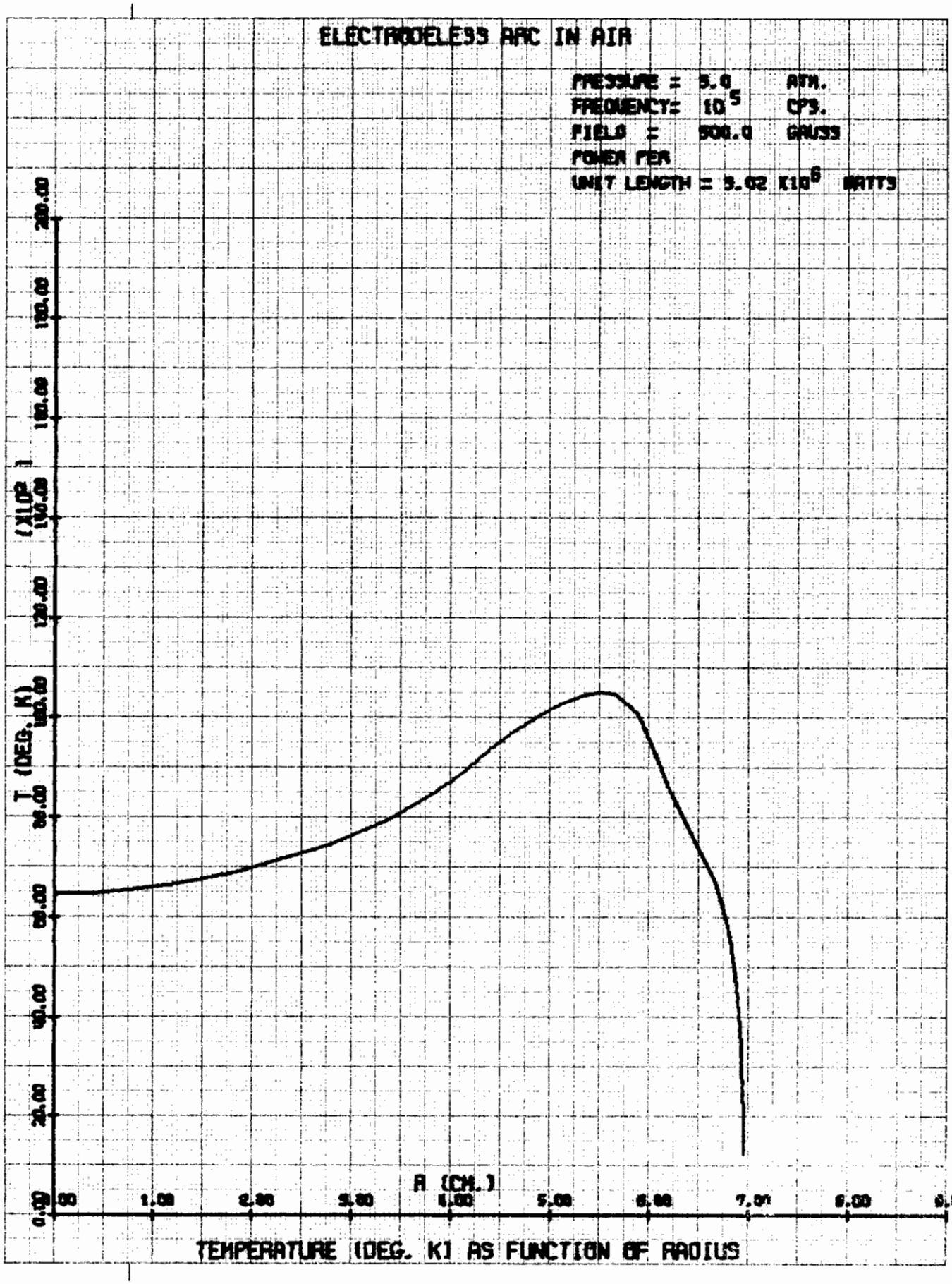

TEMPERATURE (DEG. K) AS FUNCTION OF RADIUS

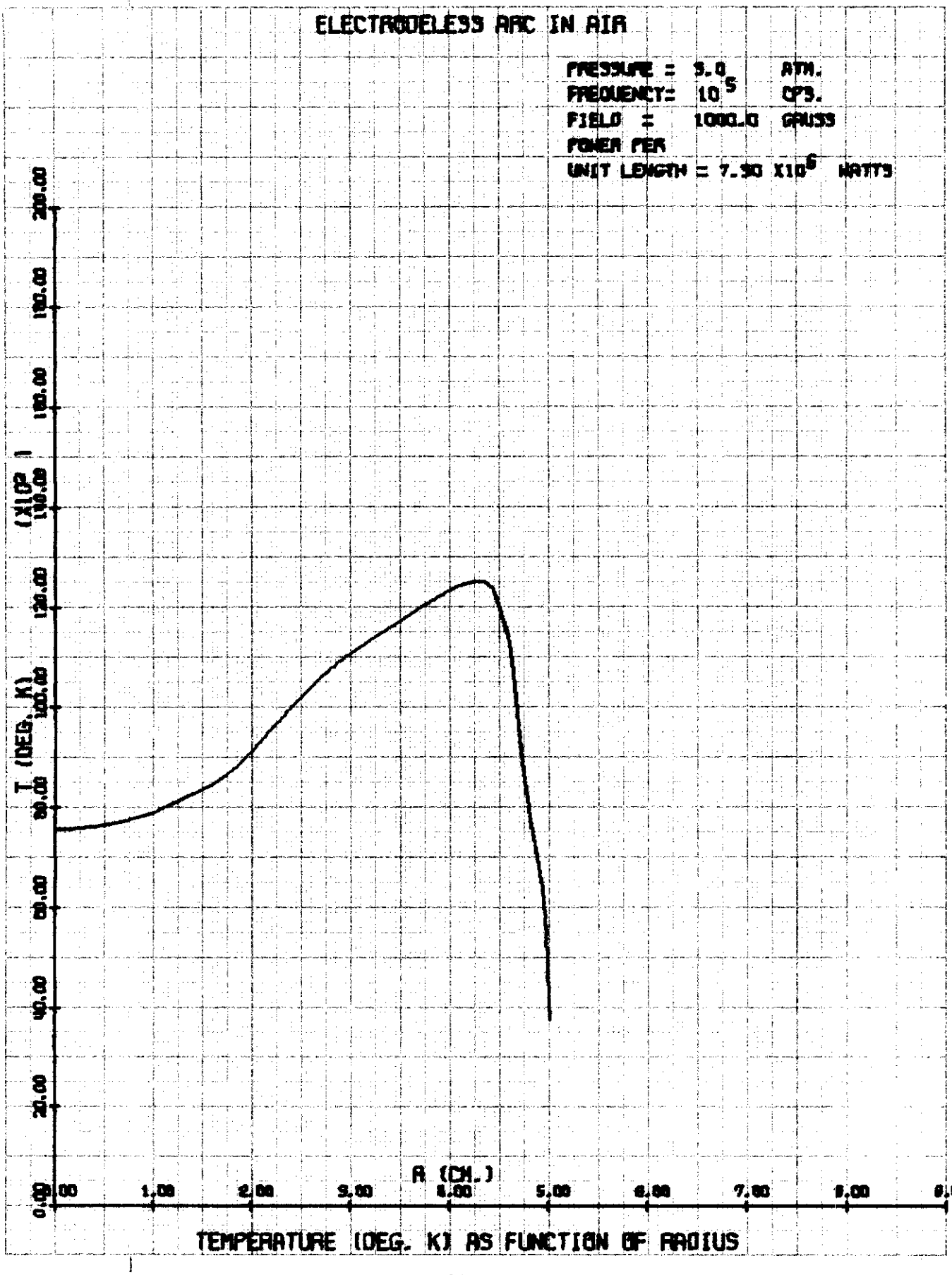

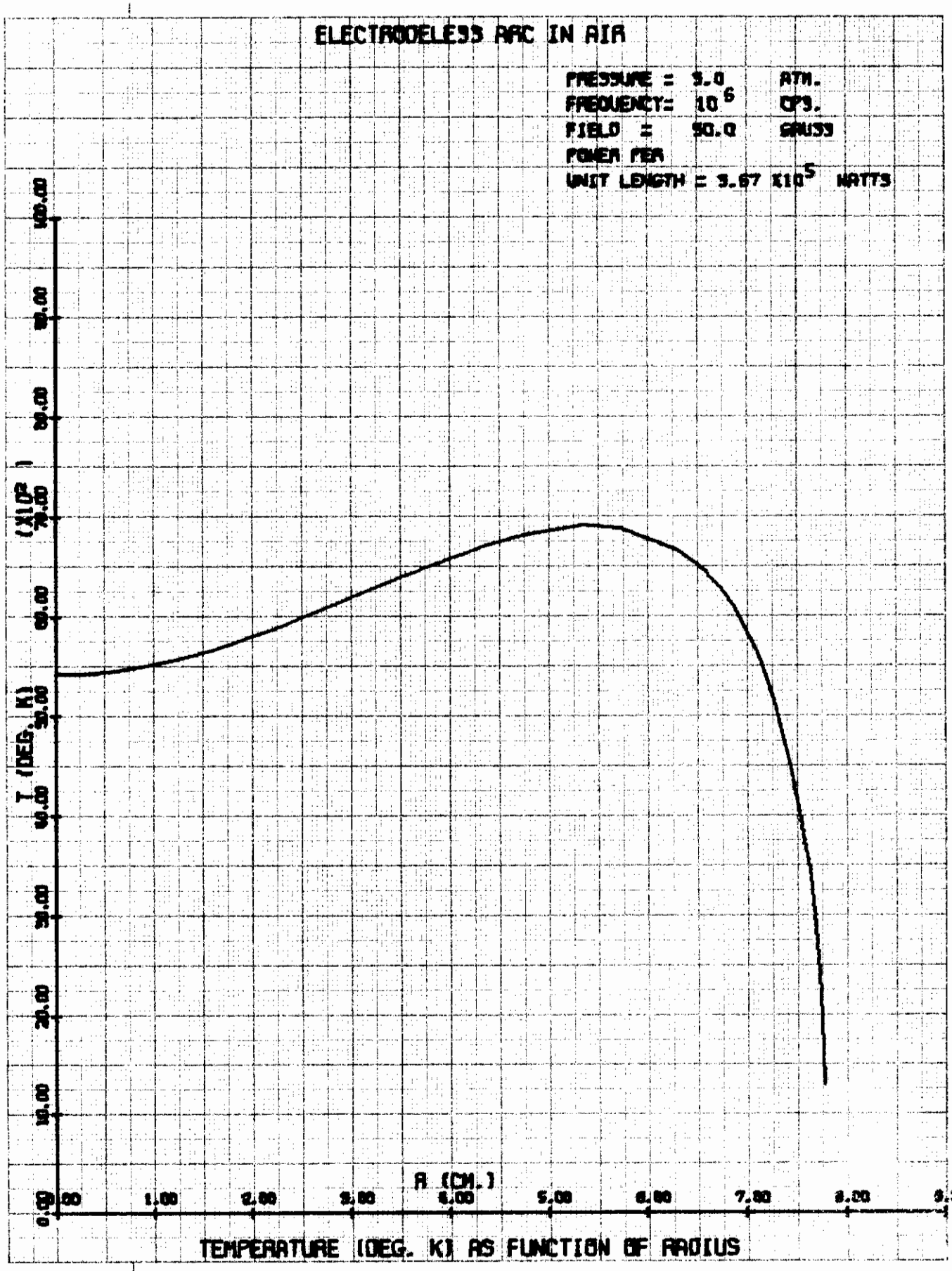

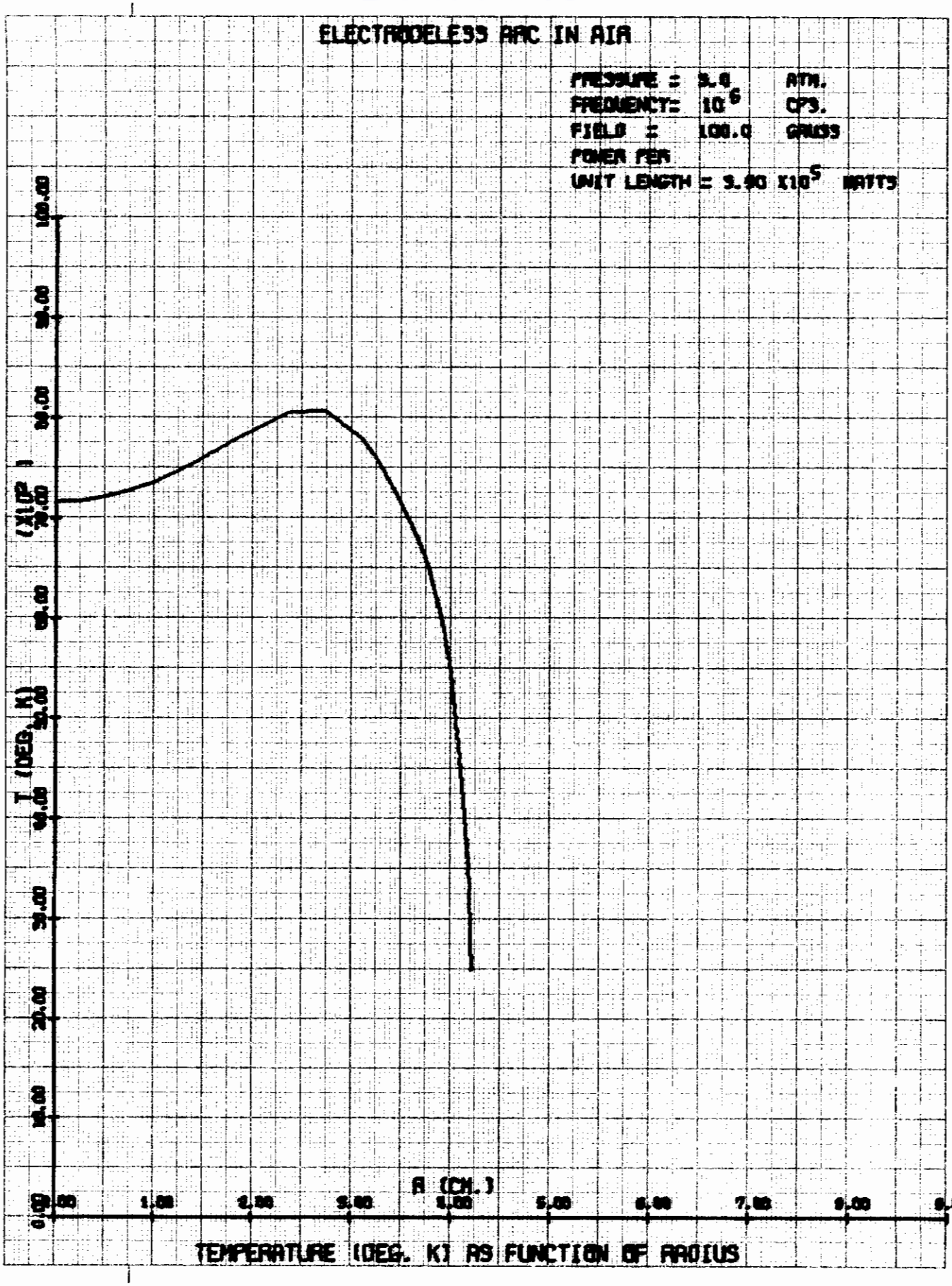

TEMPERATURE (DEG. K) AS FUNCTION OF RADIUS

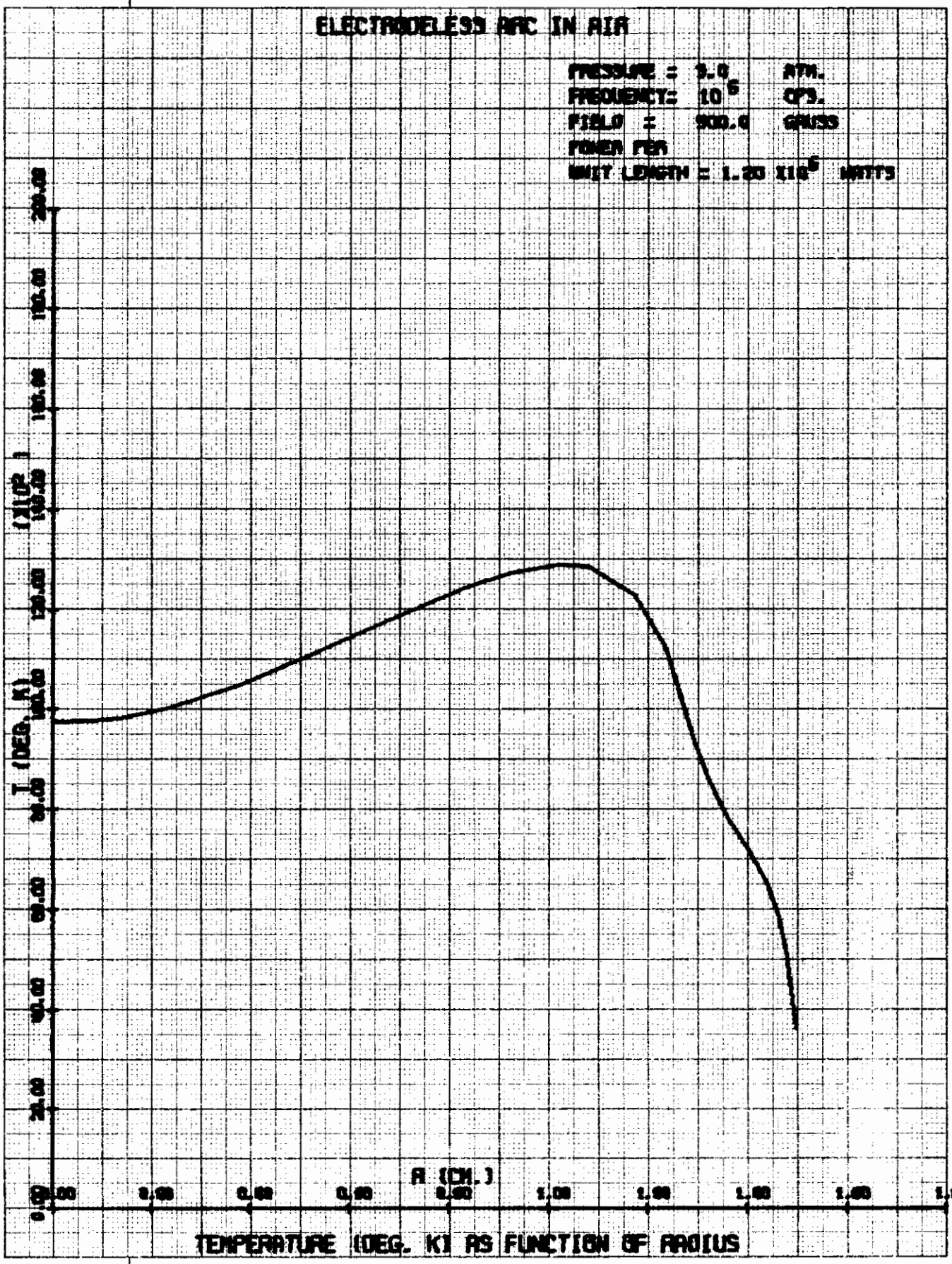

TEMPERATURE (DEG. K) AS FUNCTION OF RADIUS

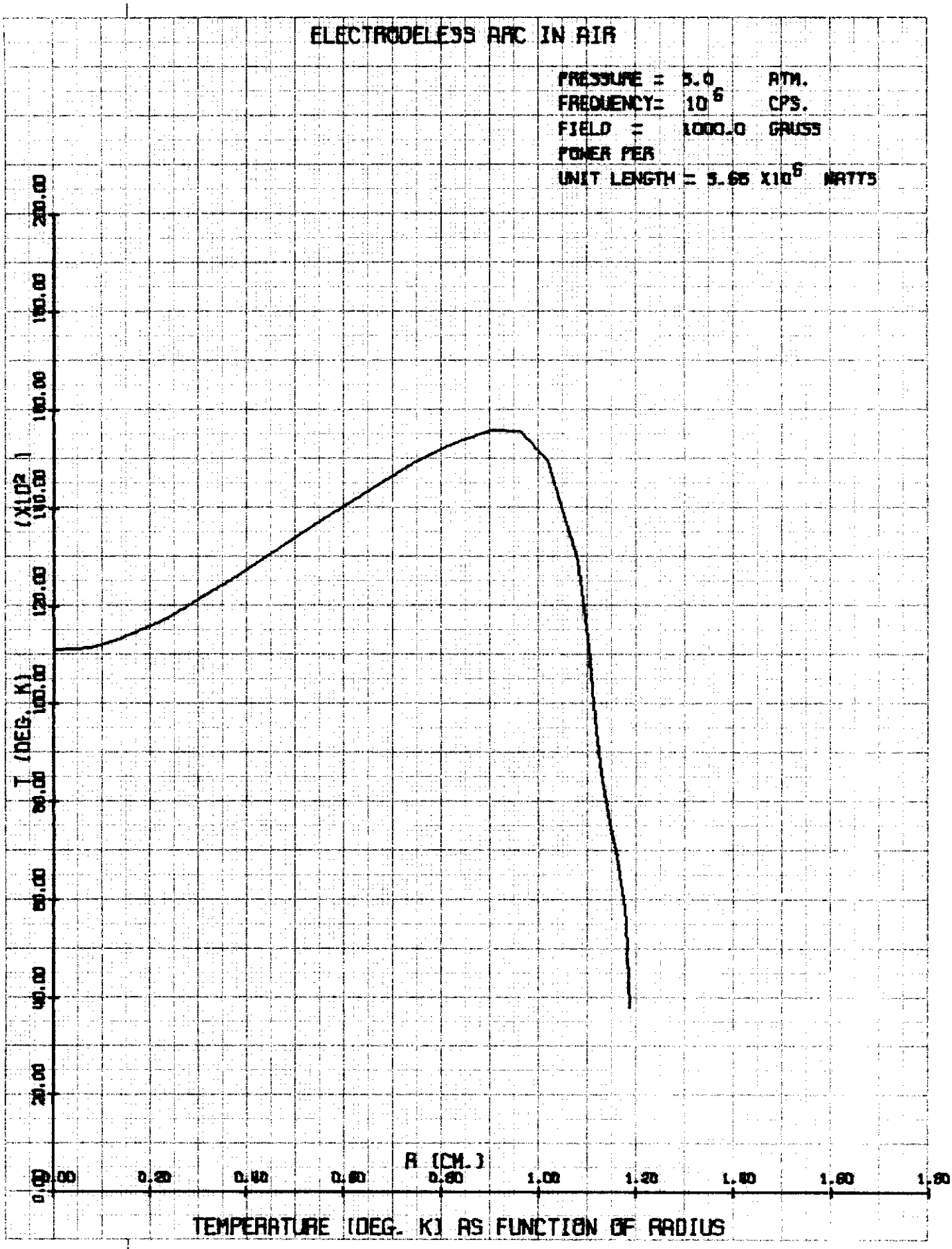

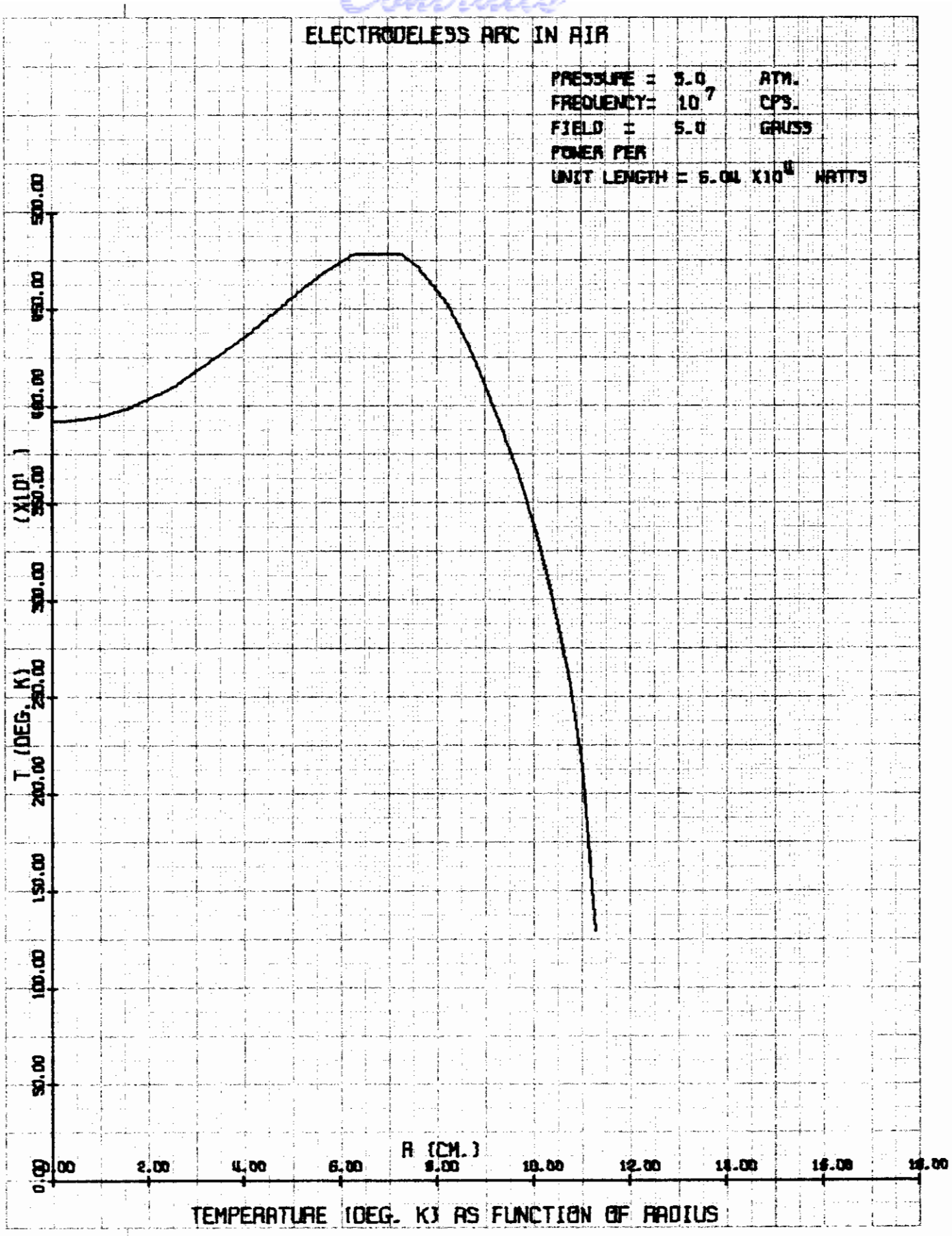

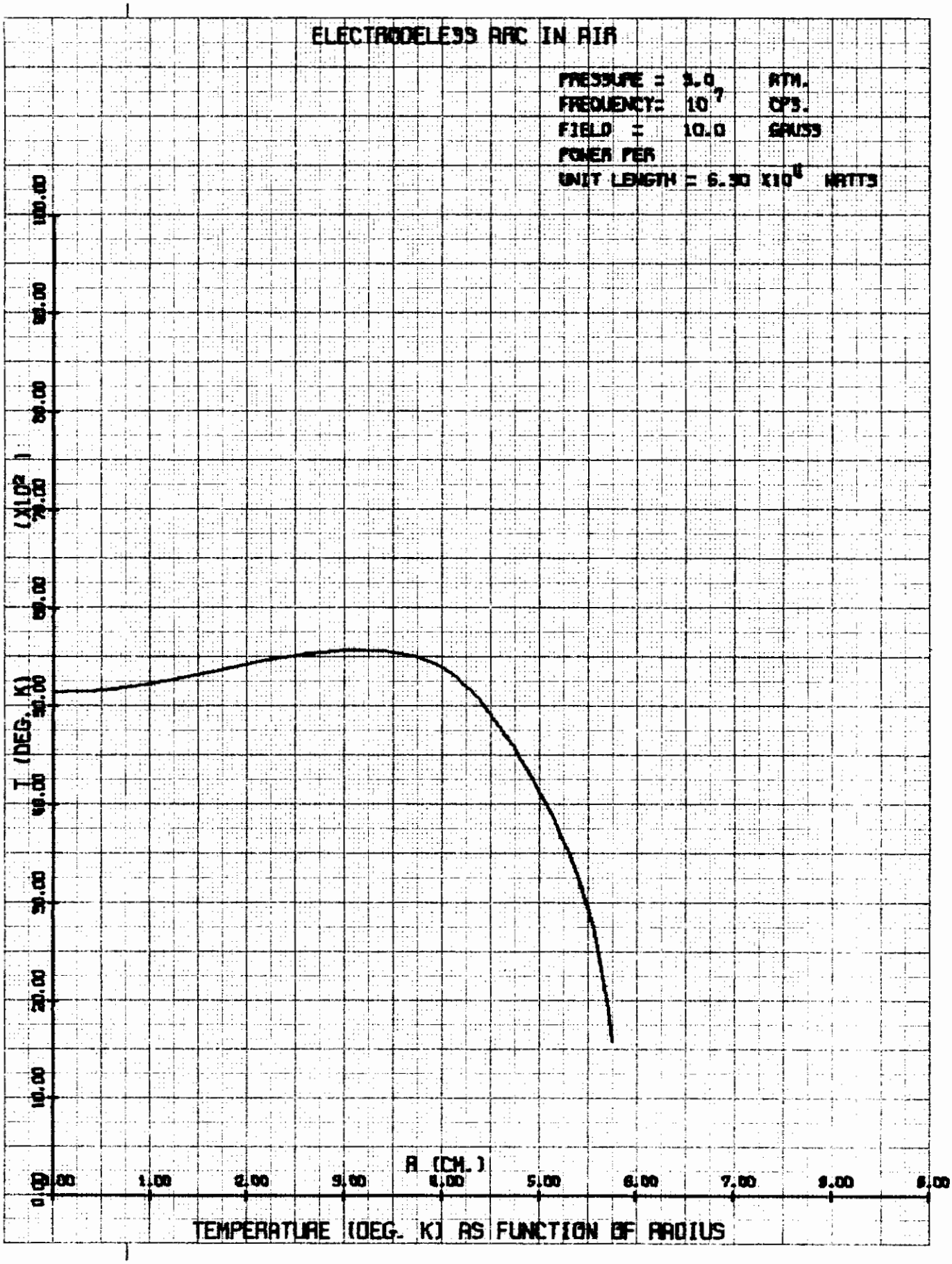

TEMPERATURE (DEG. K) AS FUNCTION OF RADIUS

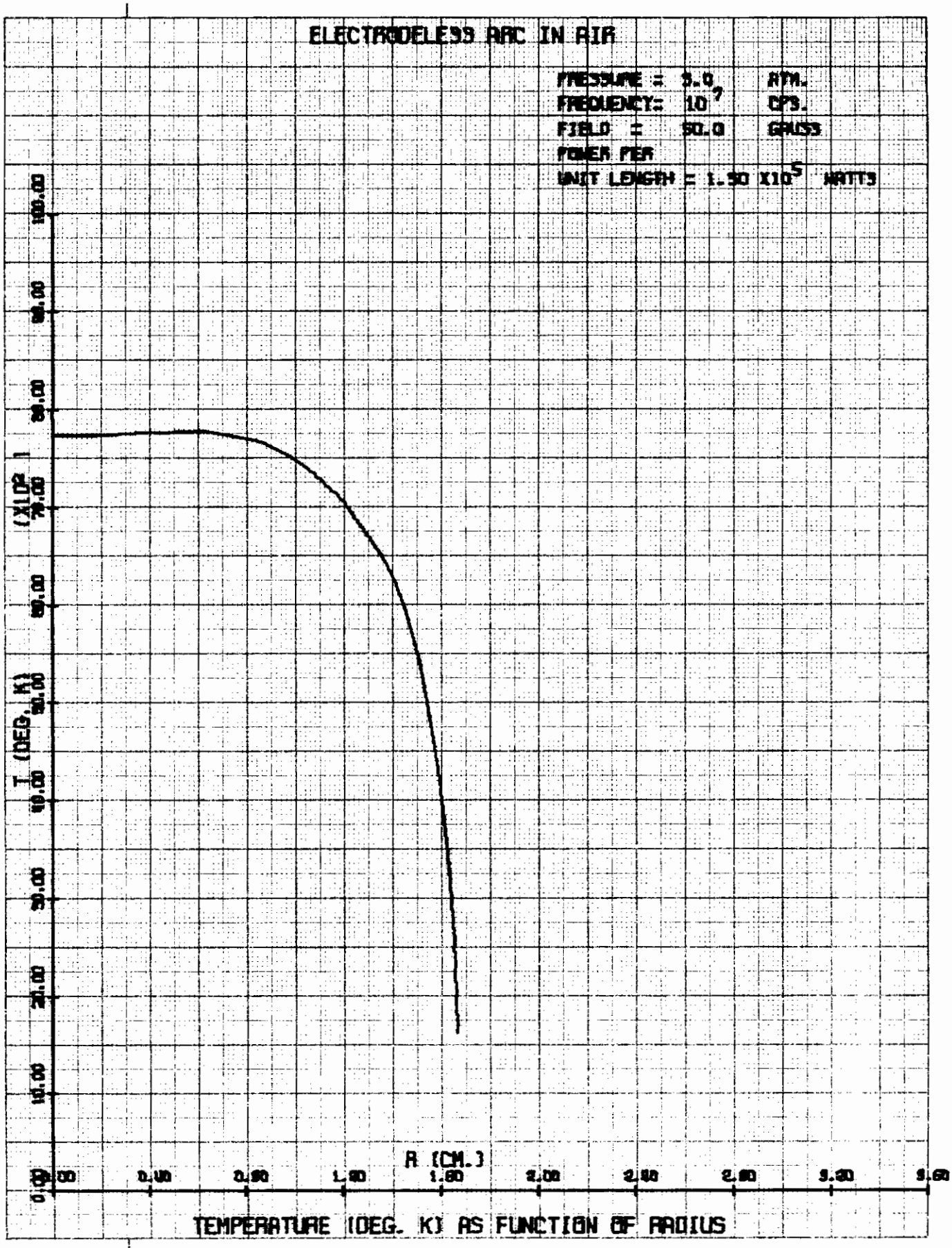

TEMPERATURE (DEG. K) AS FUNCTION OF RADIUS

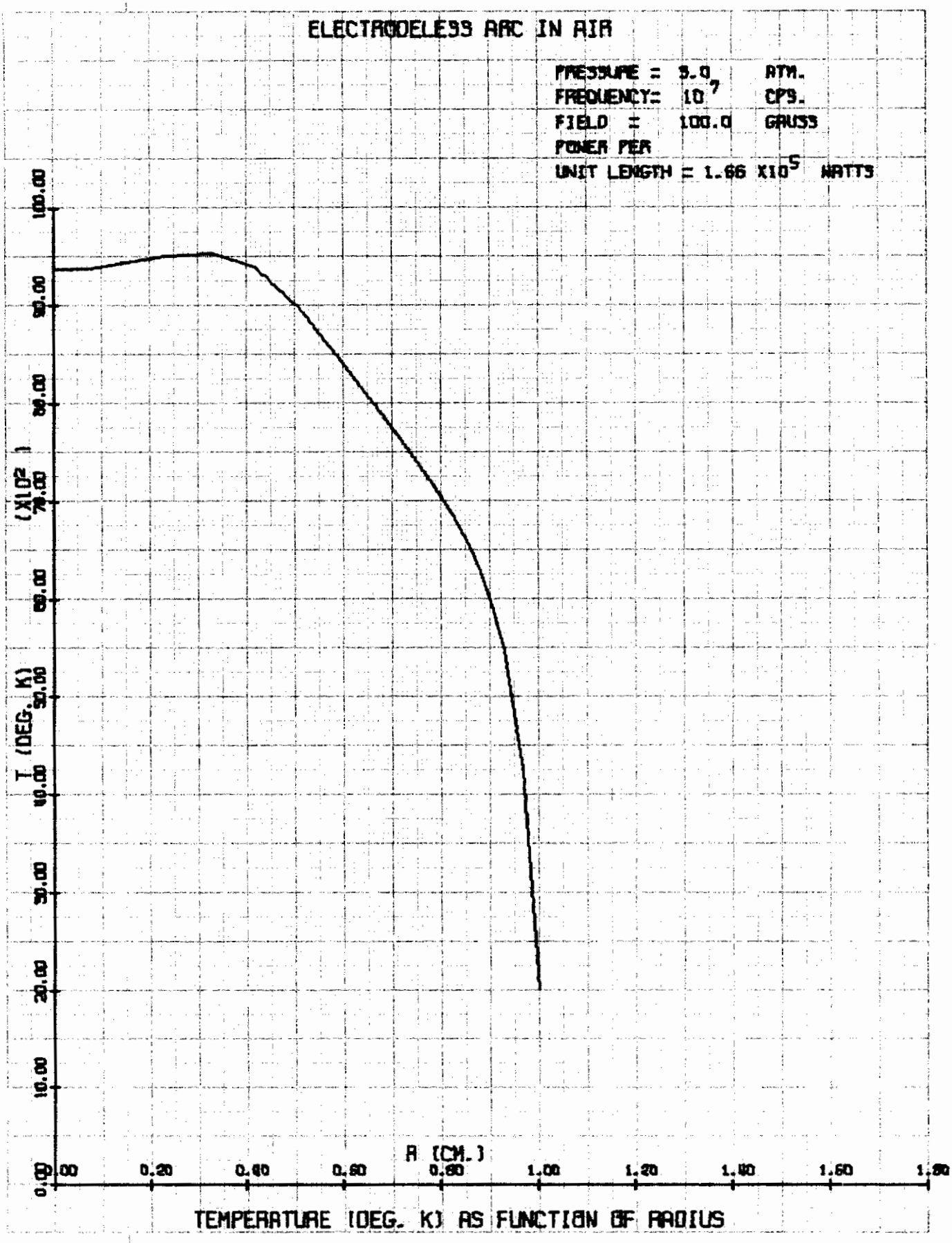

TEMPERATURE (DEG. K) AS FUNCTION OF RADIUS

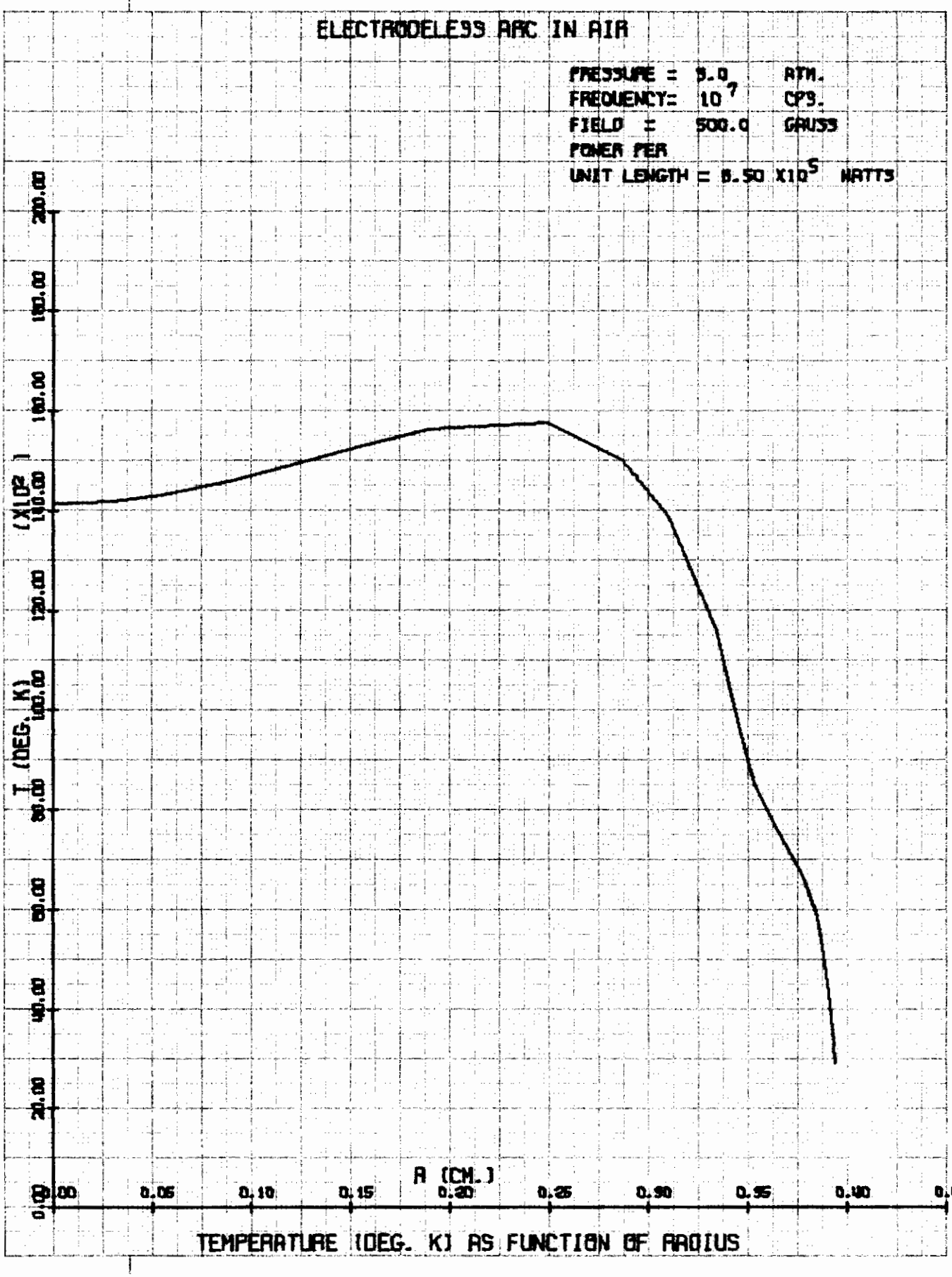

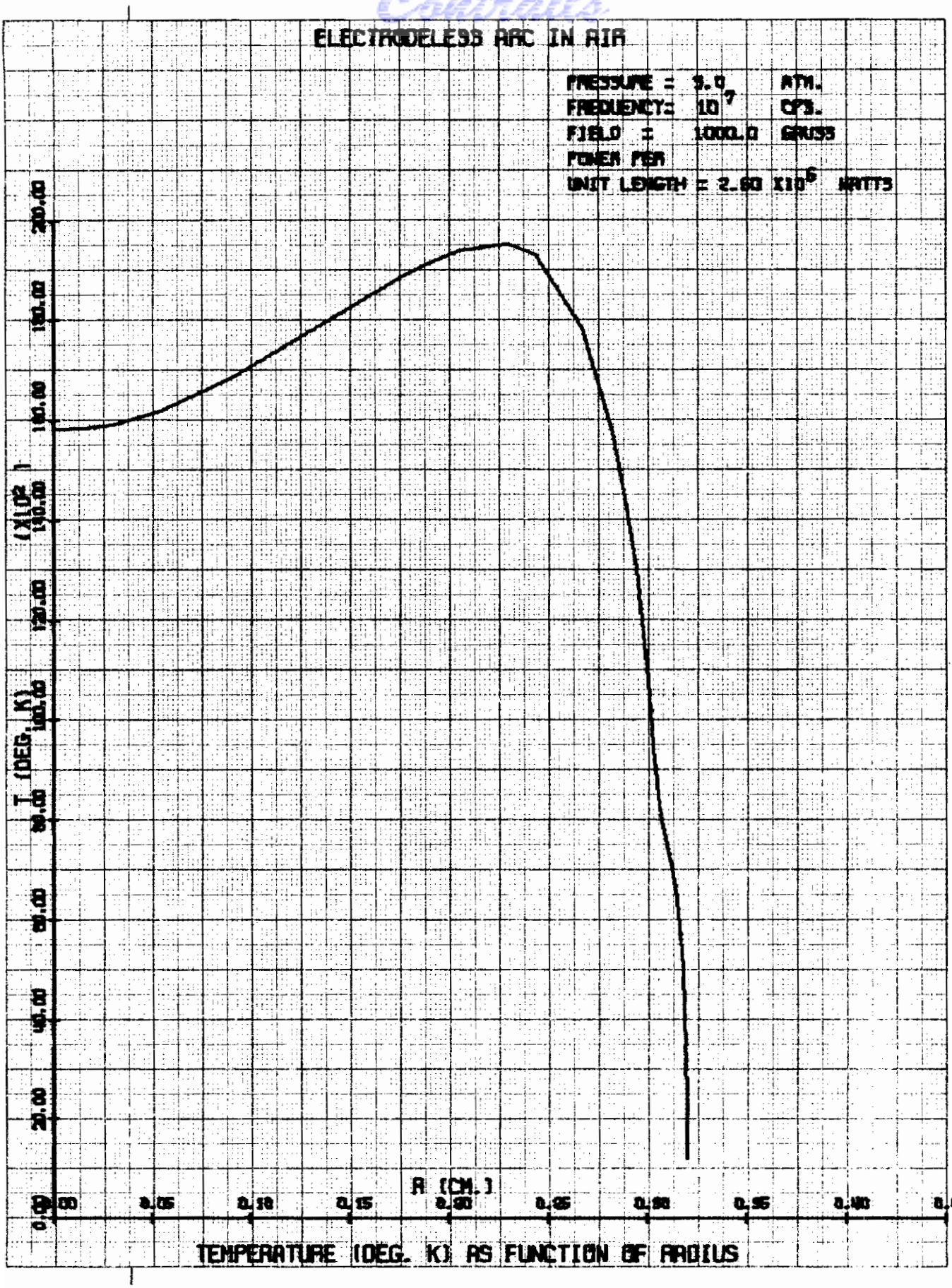

TEMPERATURE (DEG. K) AS FUNCTION OF RADIUS

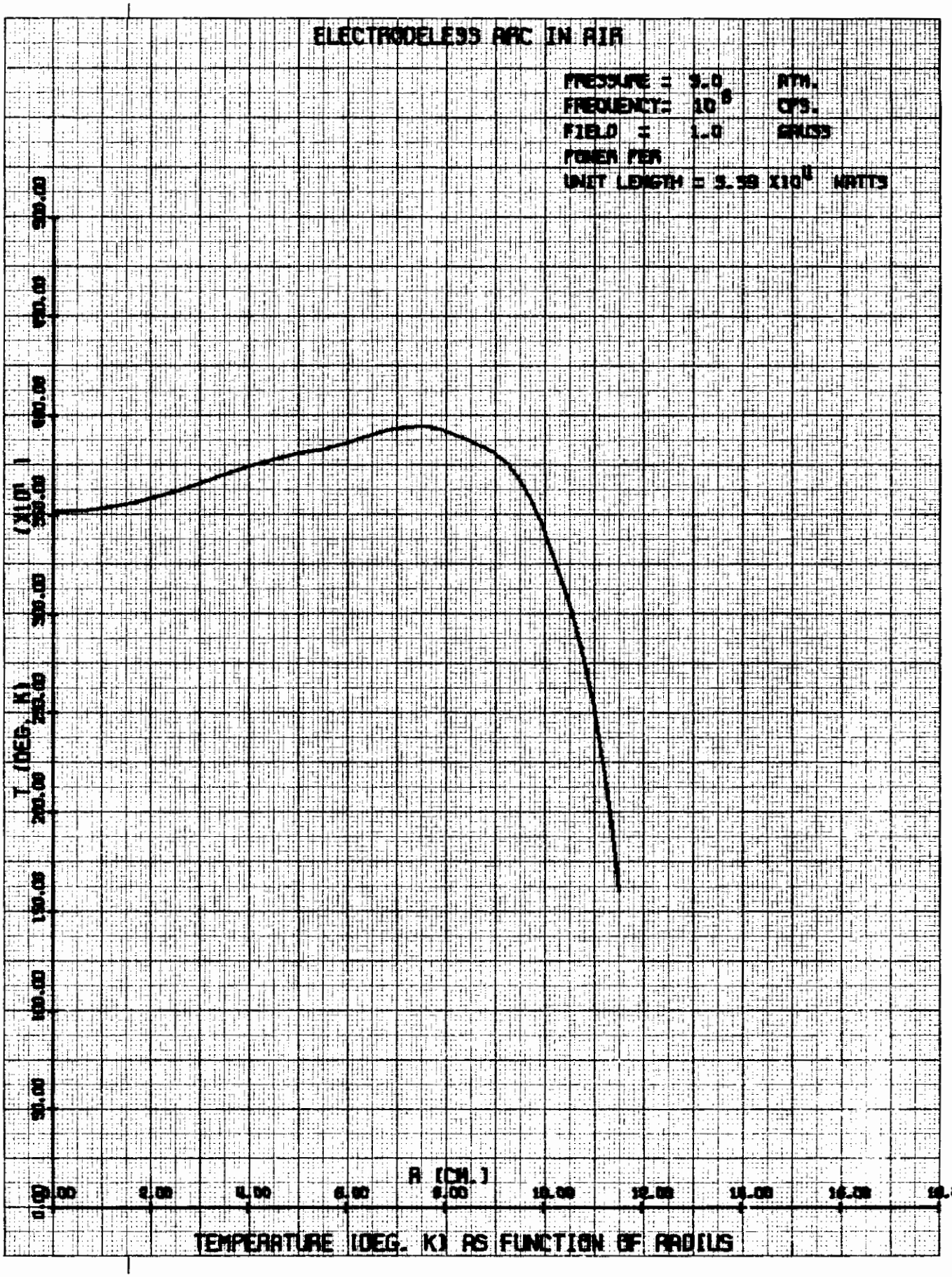

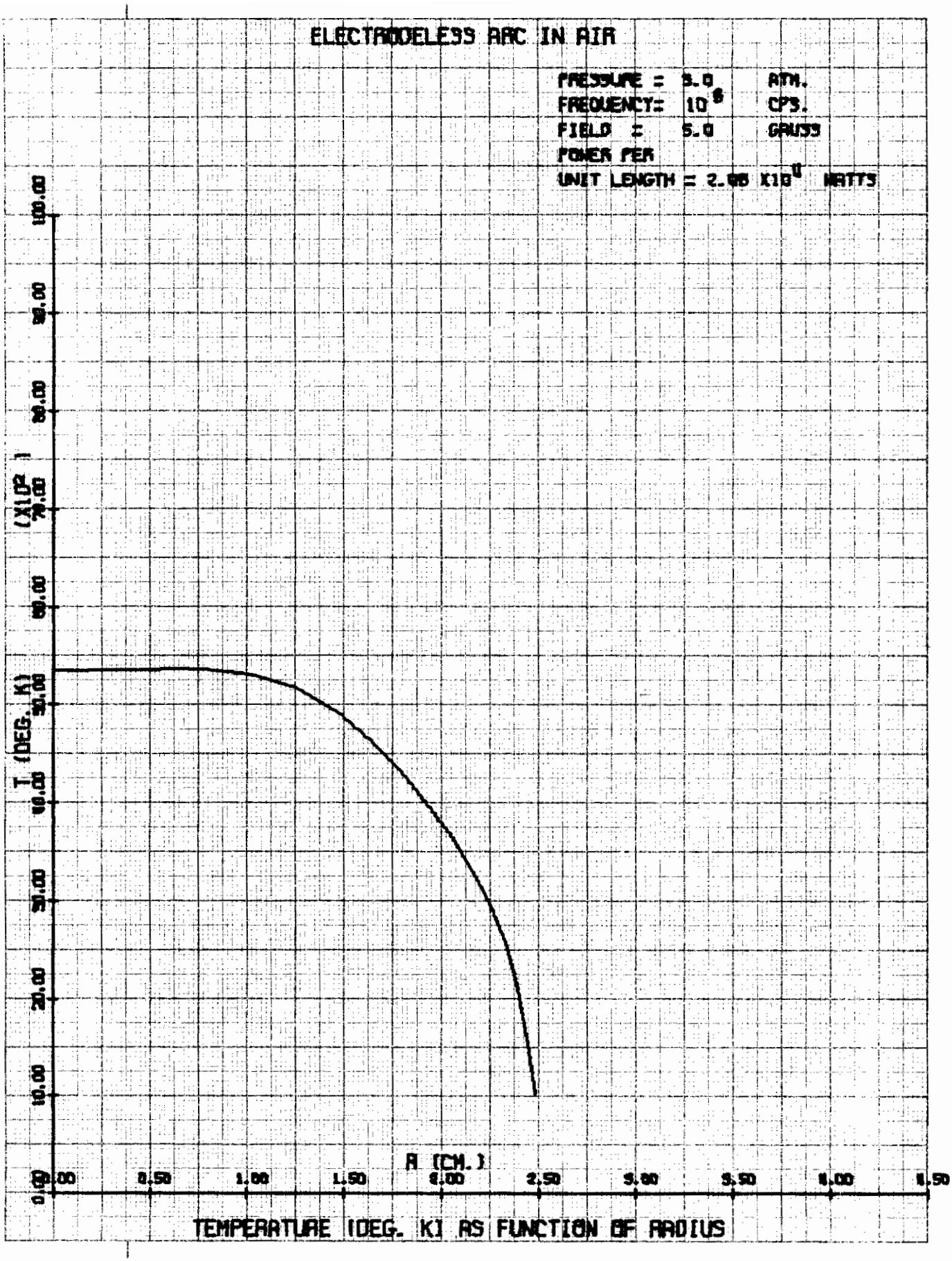

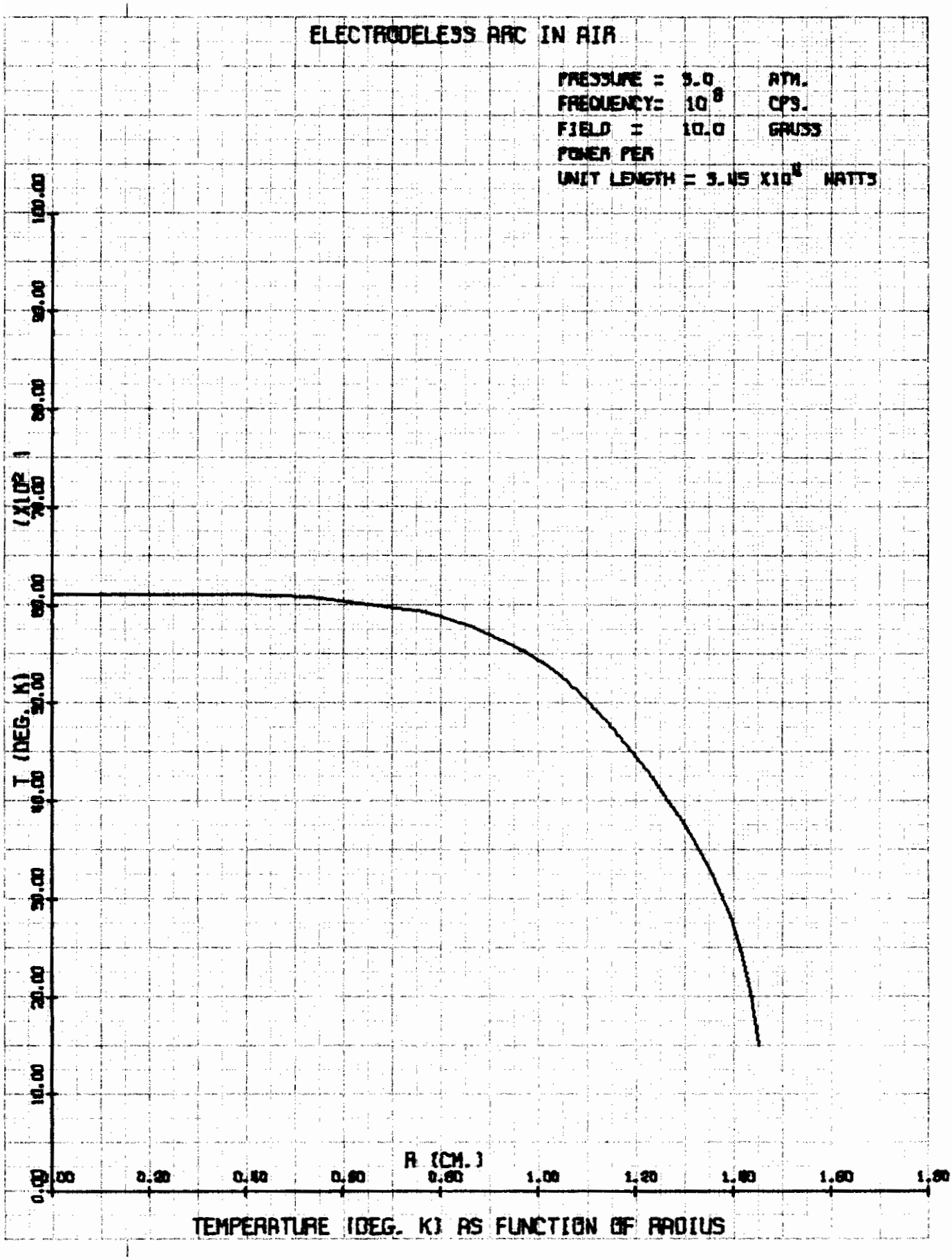

TEMPERATURE (DEG. K) AS FUNCTION OF RADIUS

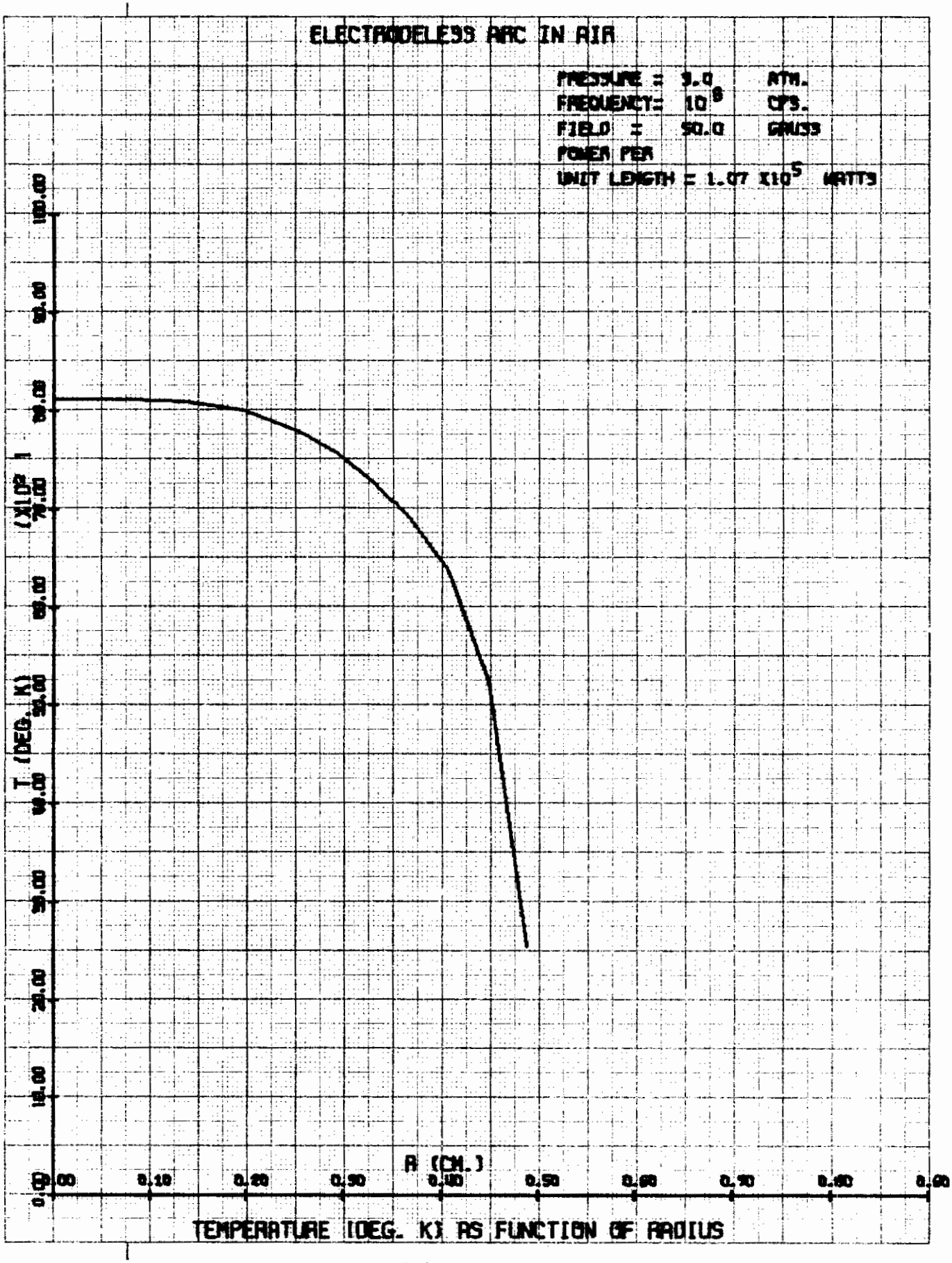

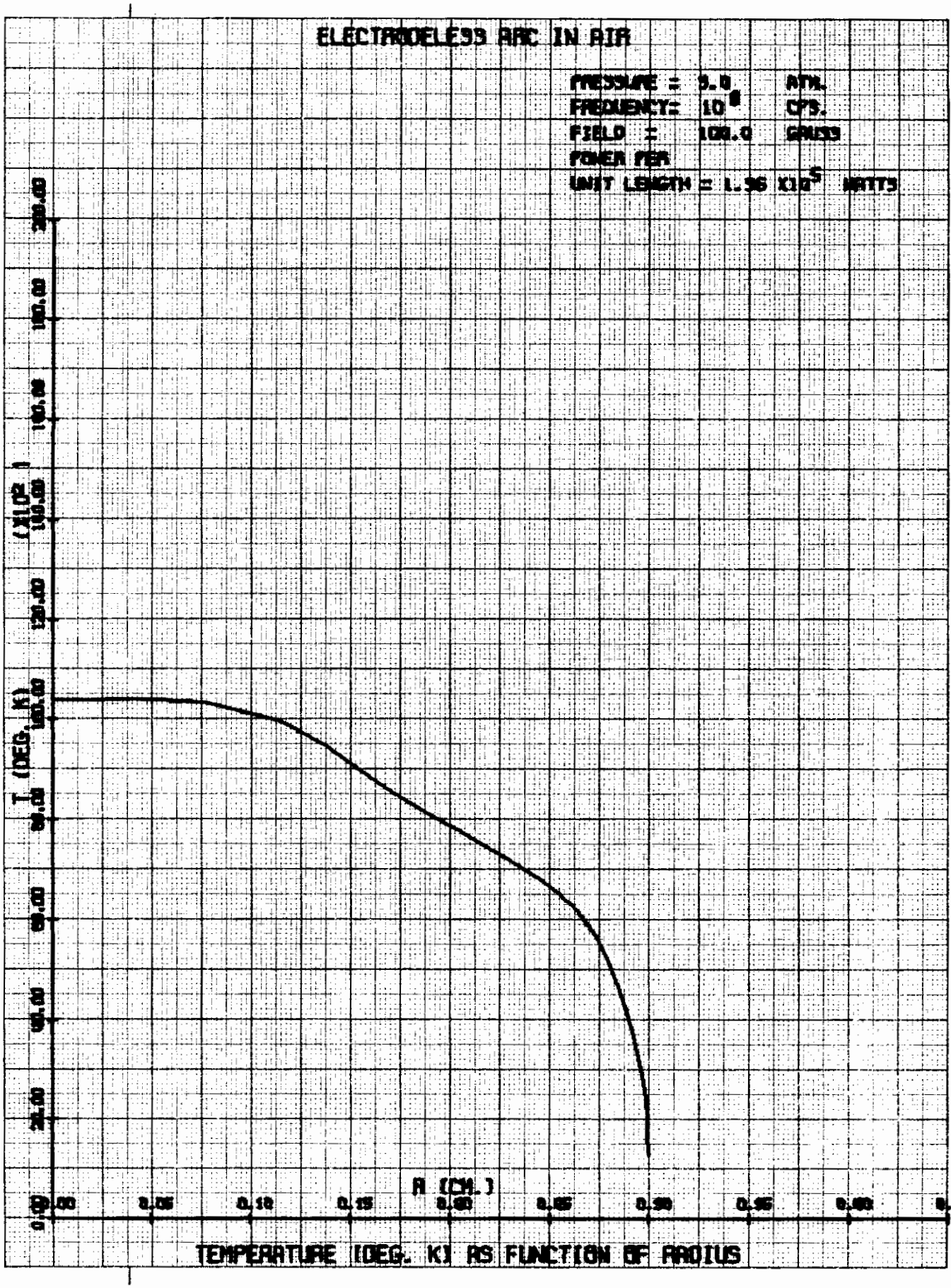

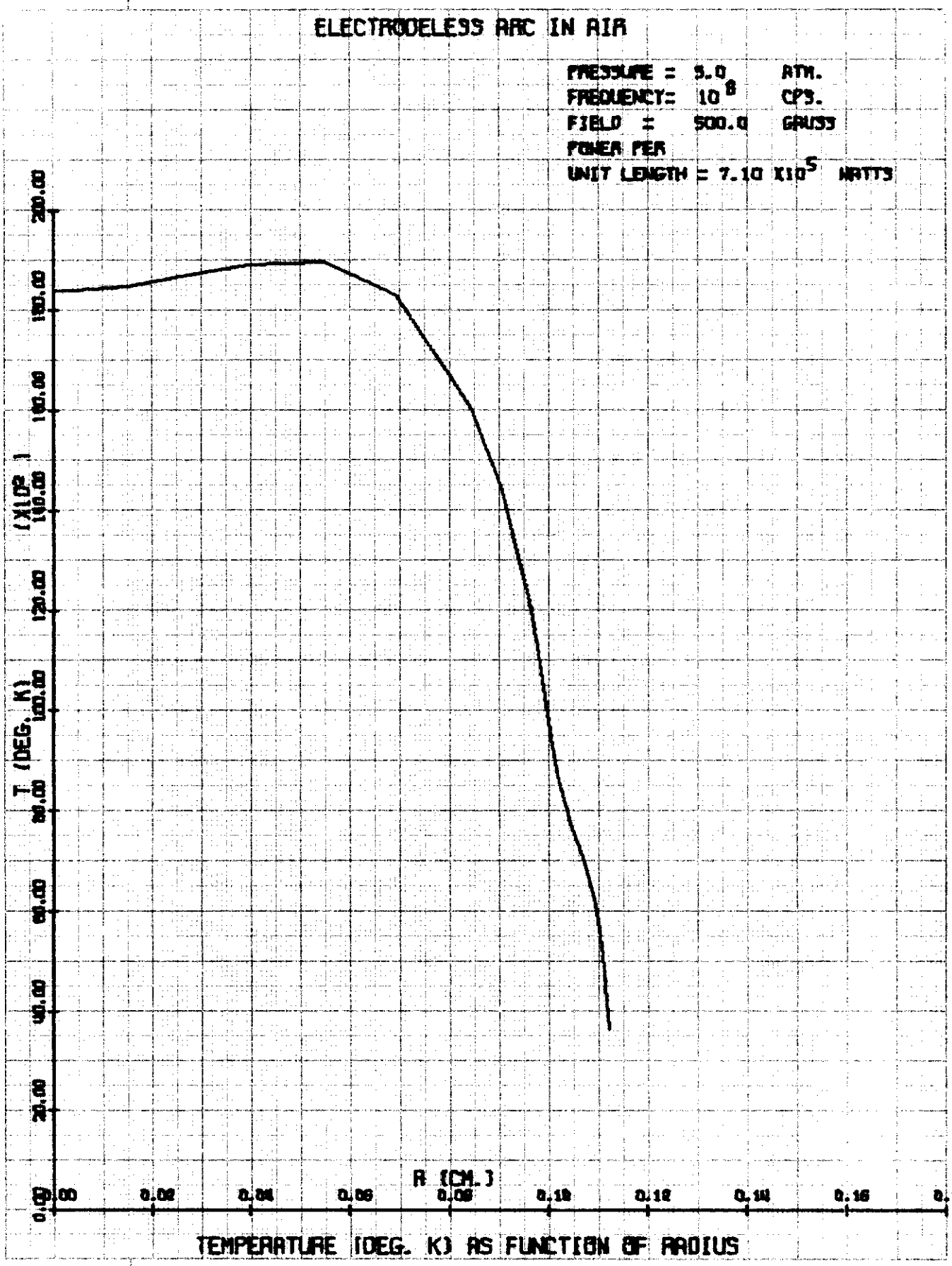

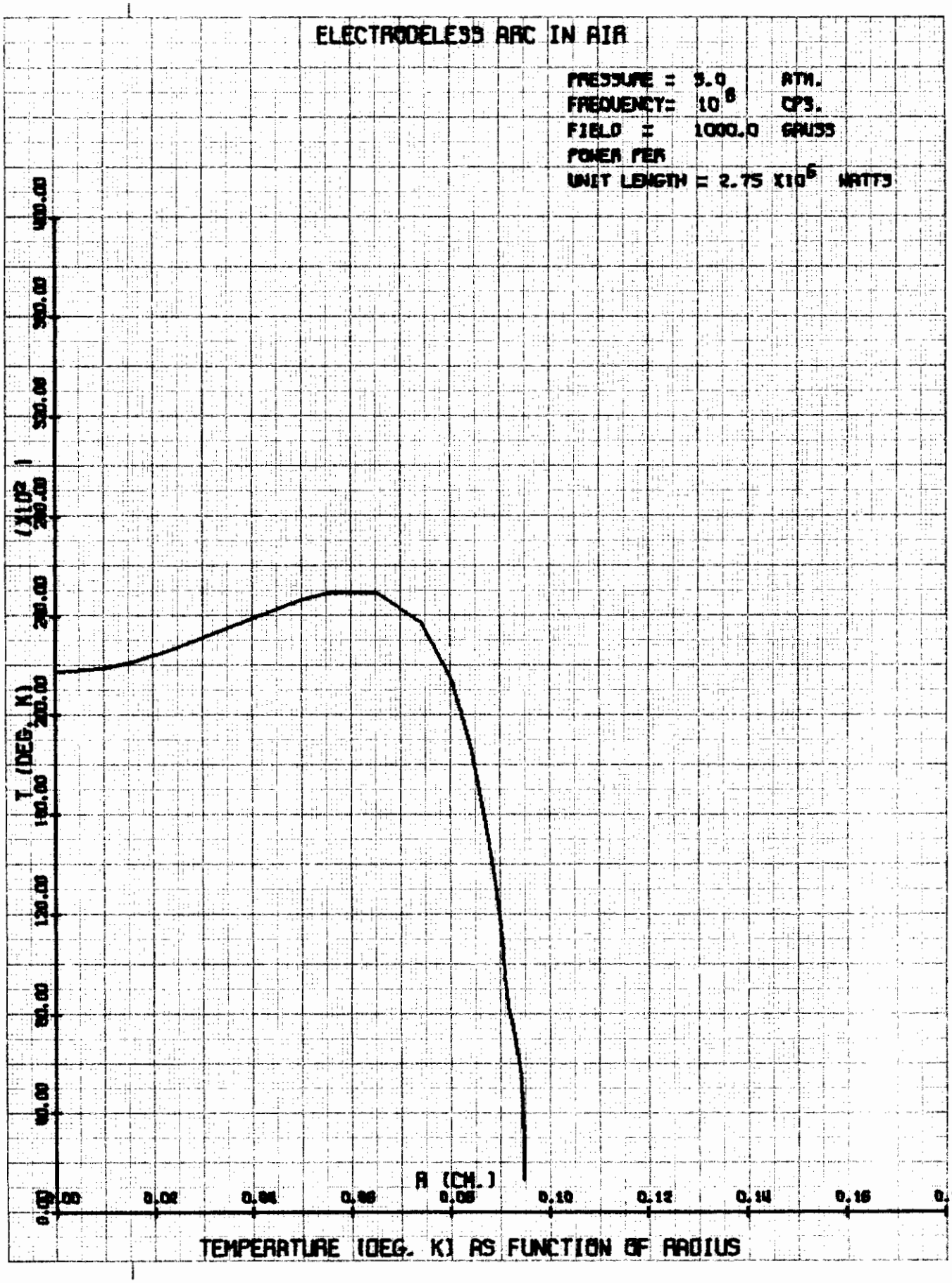

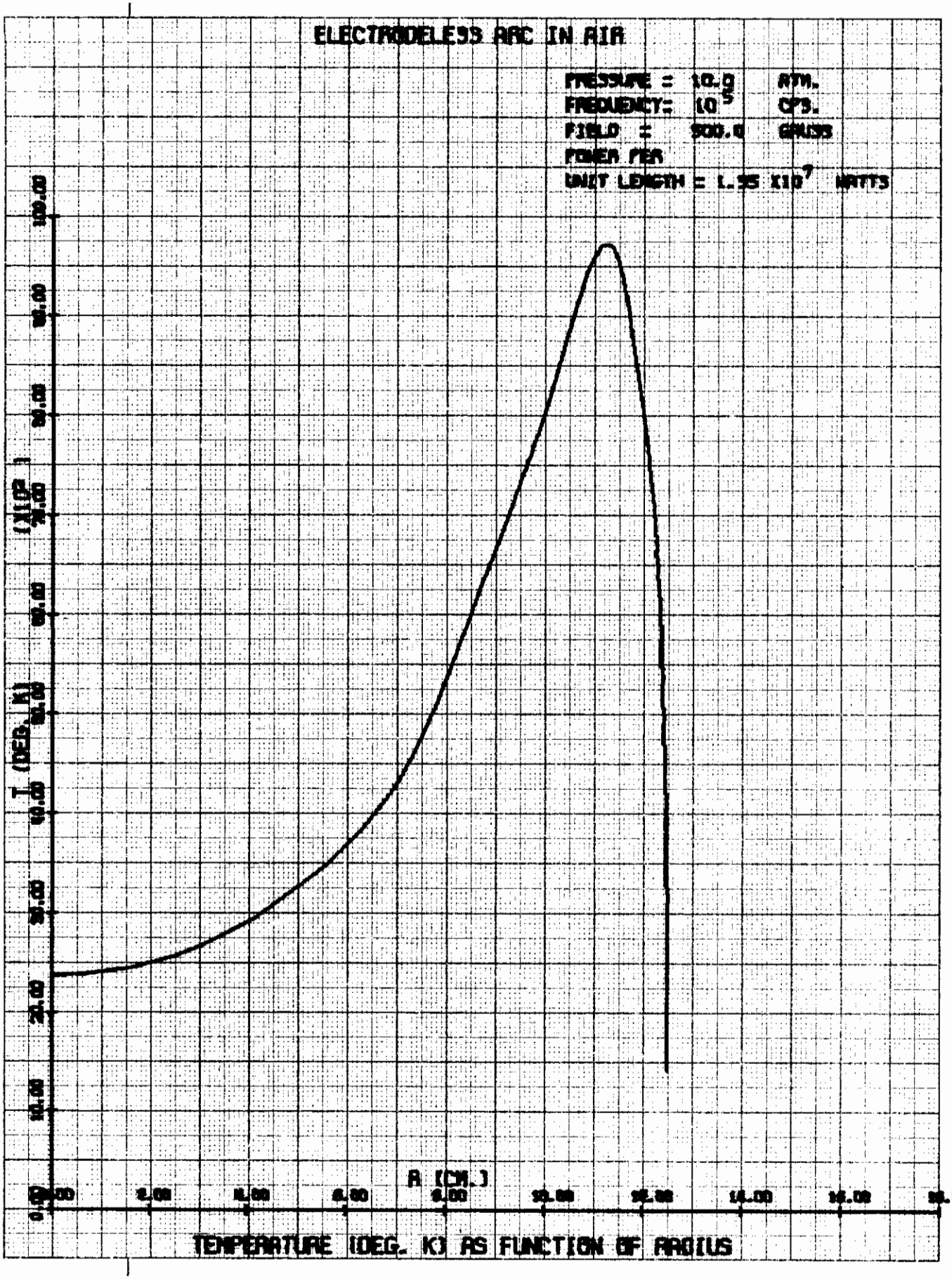

TEMPERATURE (DEG. K) AS FUNCTION OF RADIUS

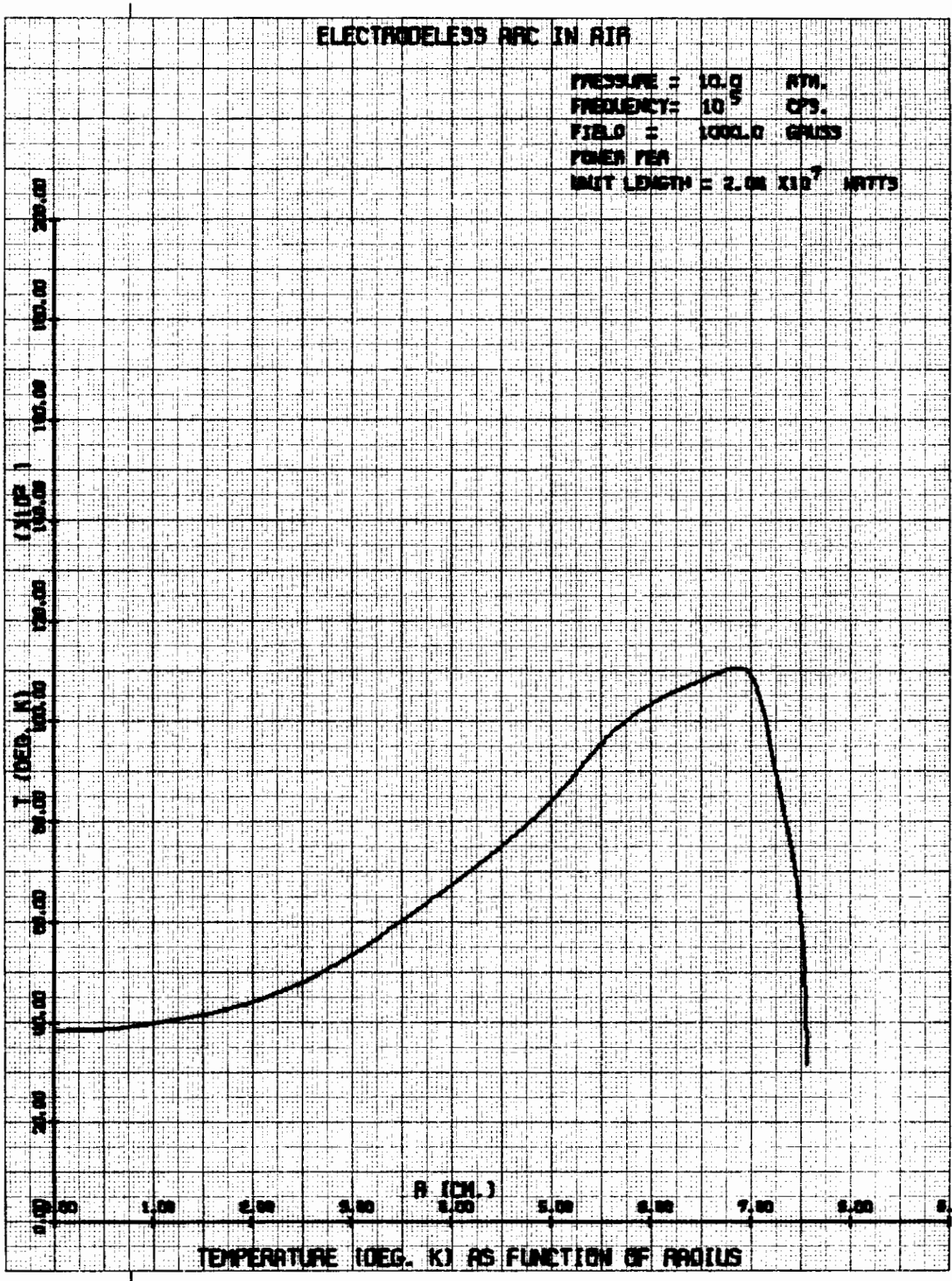

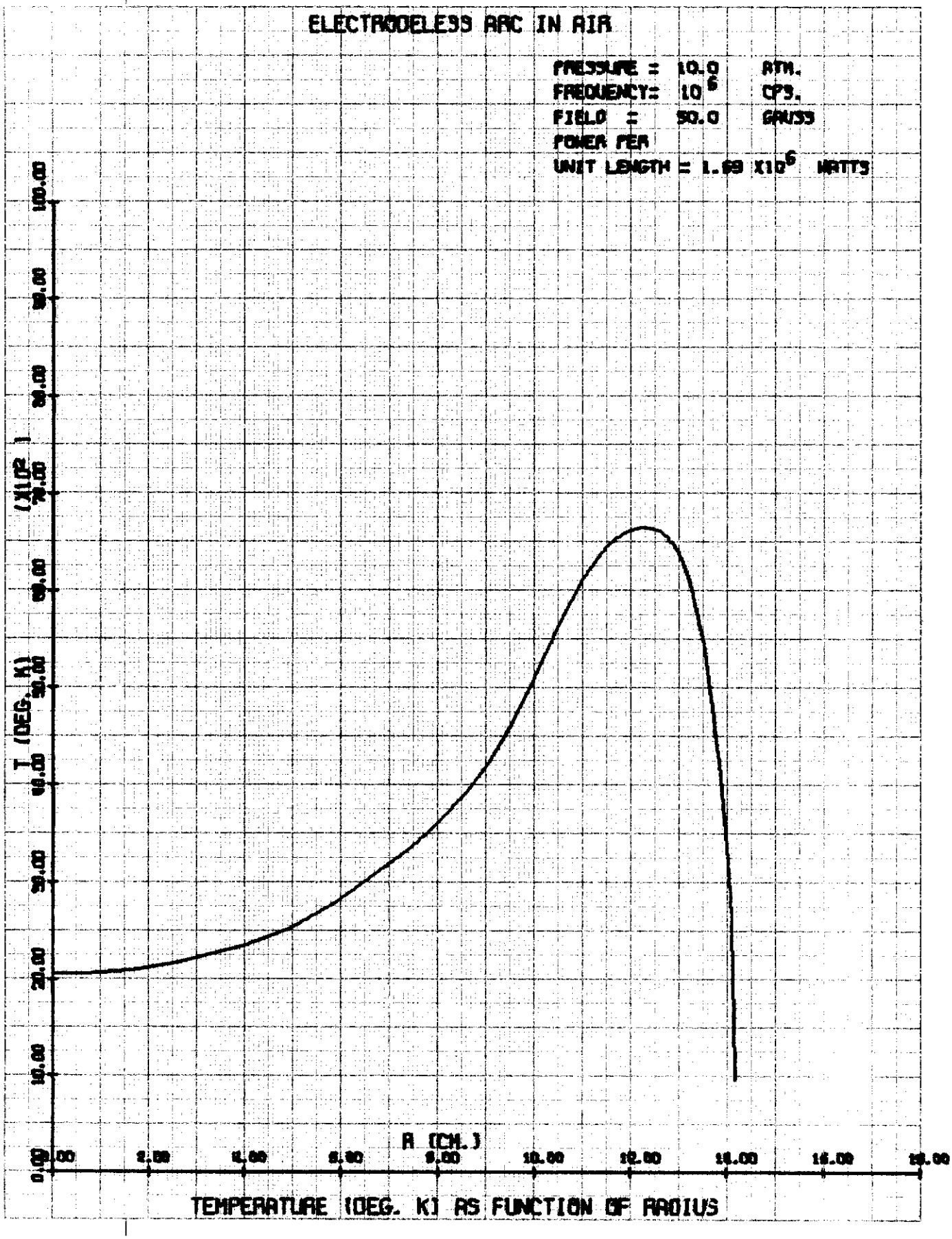

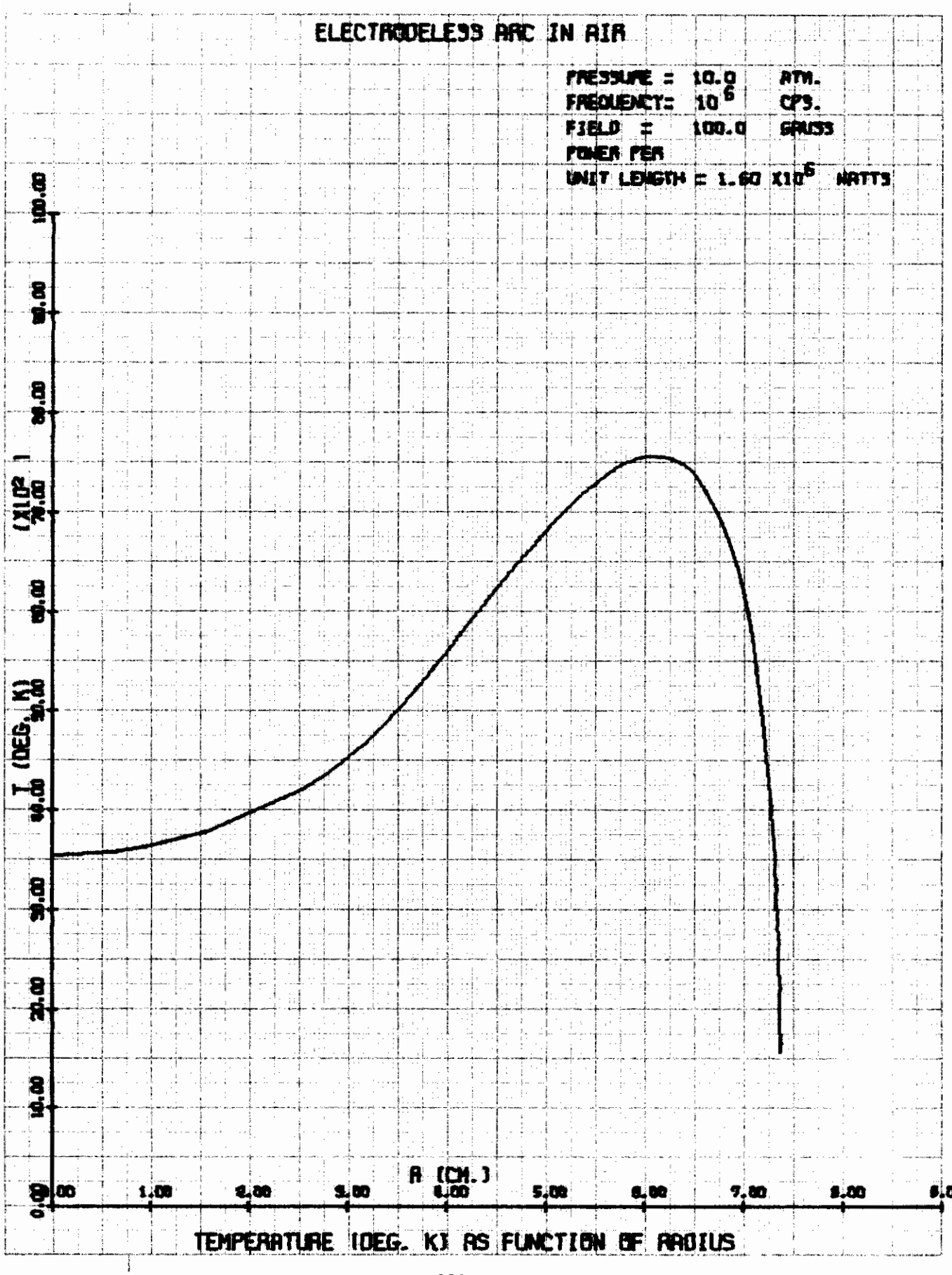

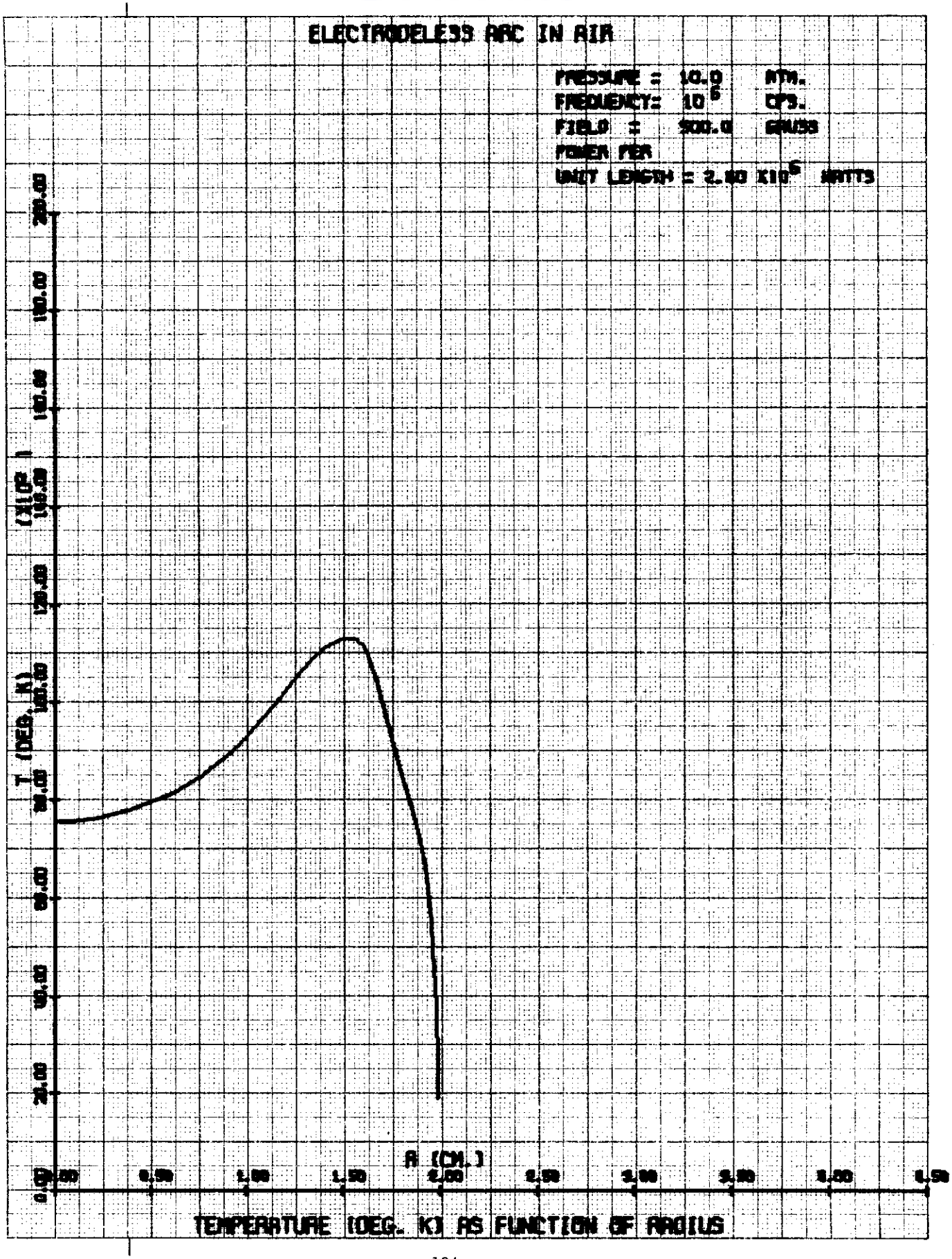

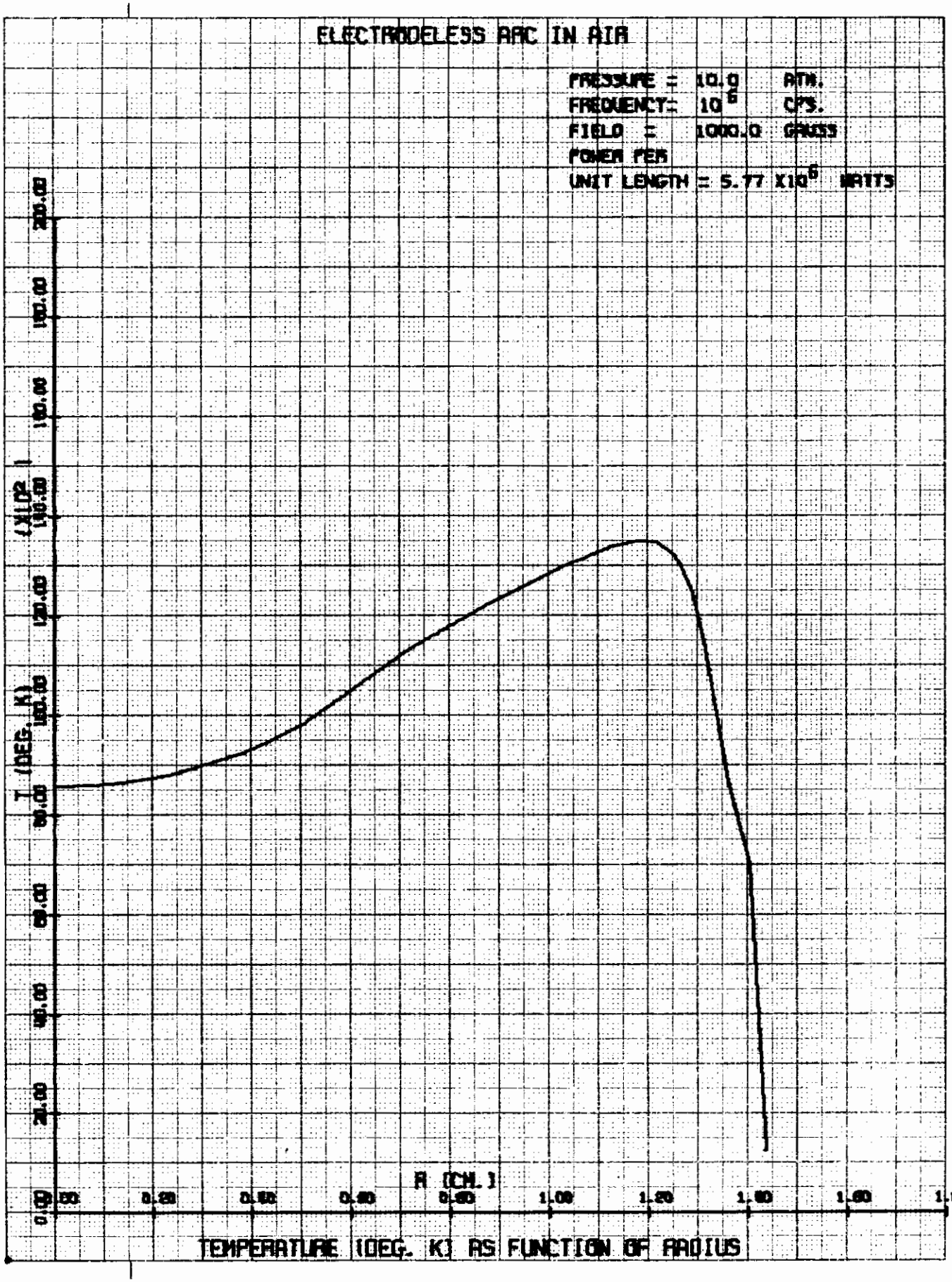

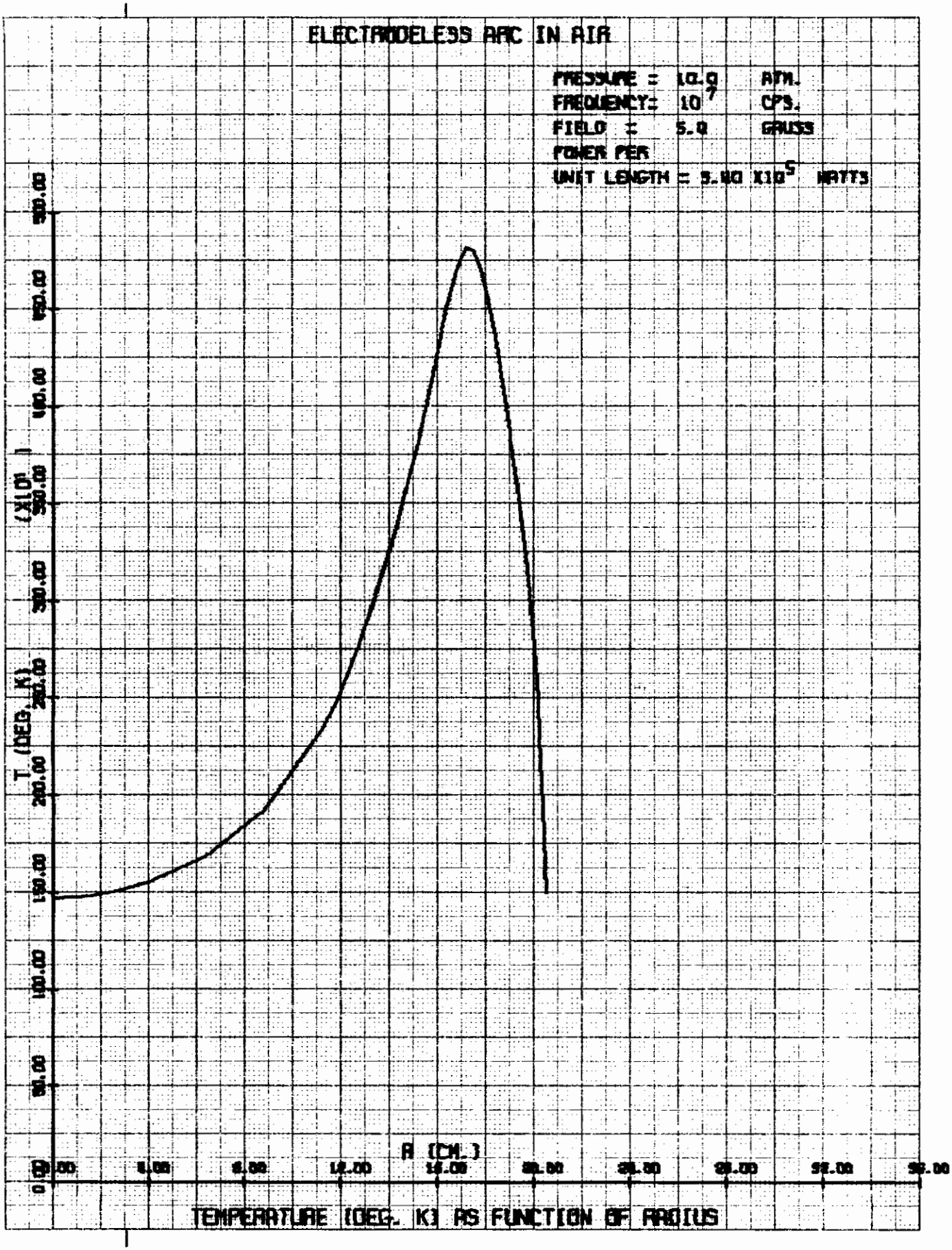

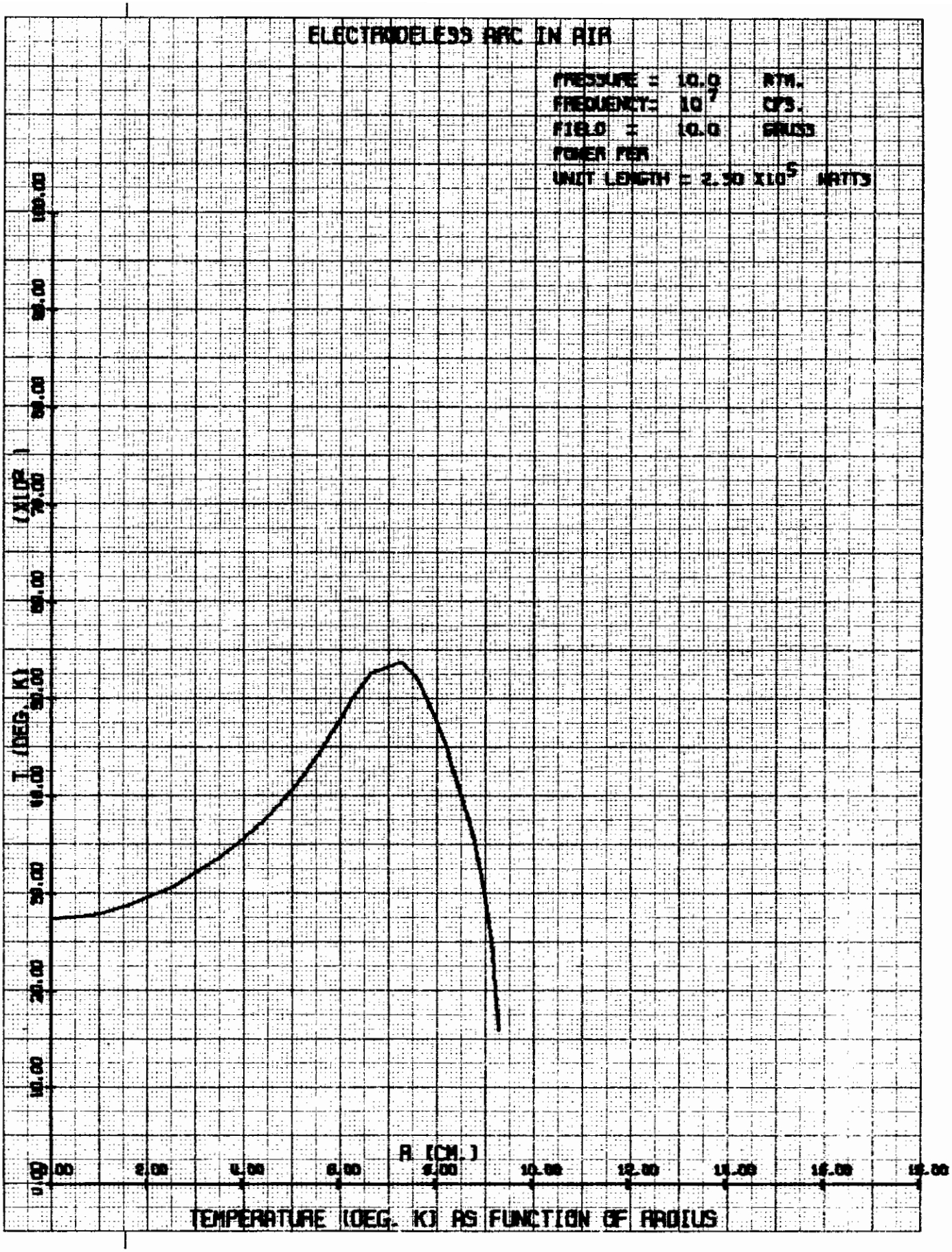

TEMPERATURE (DEG. K) AS FUNCTION OF RADIUS

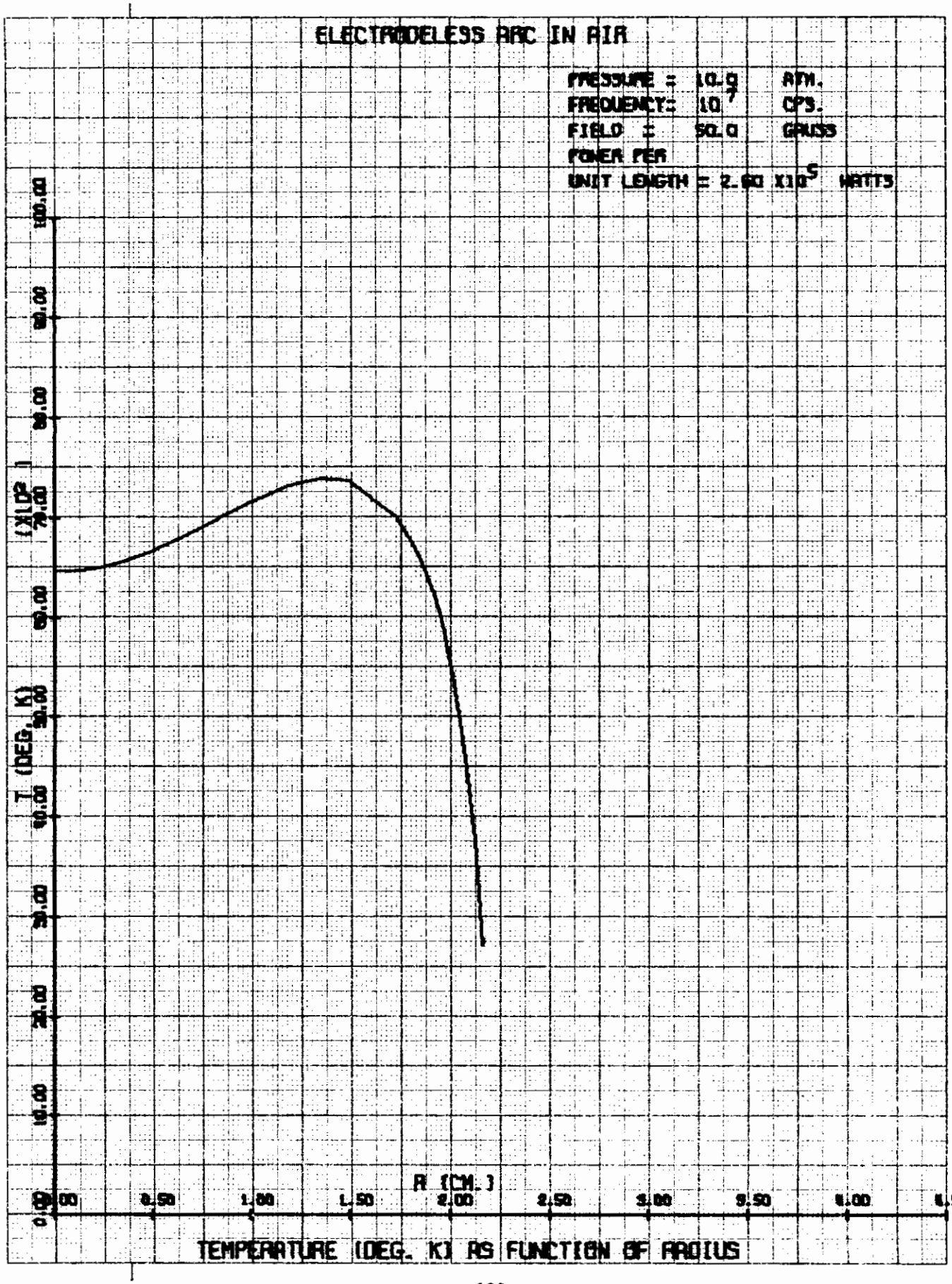

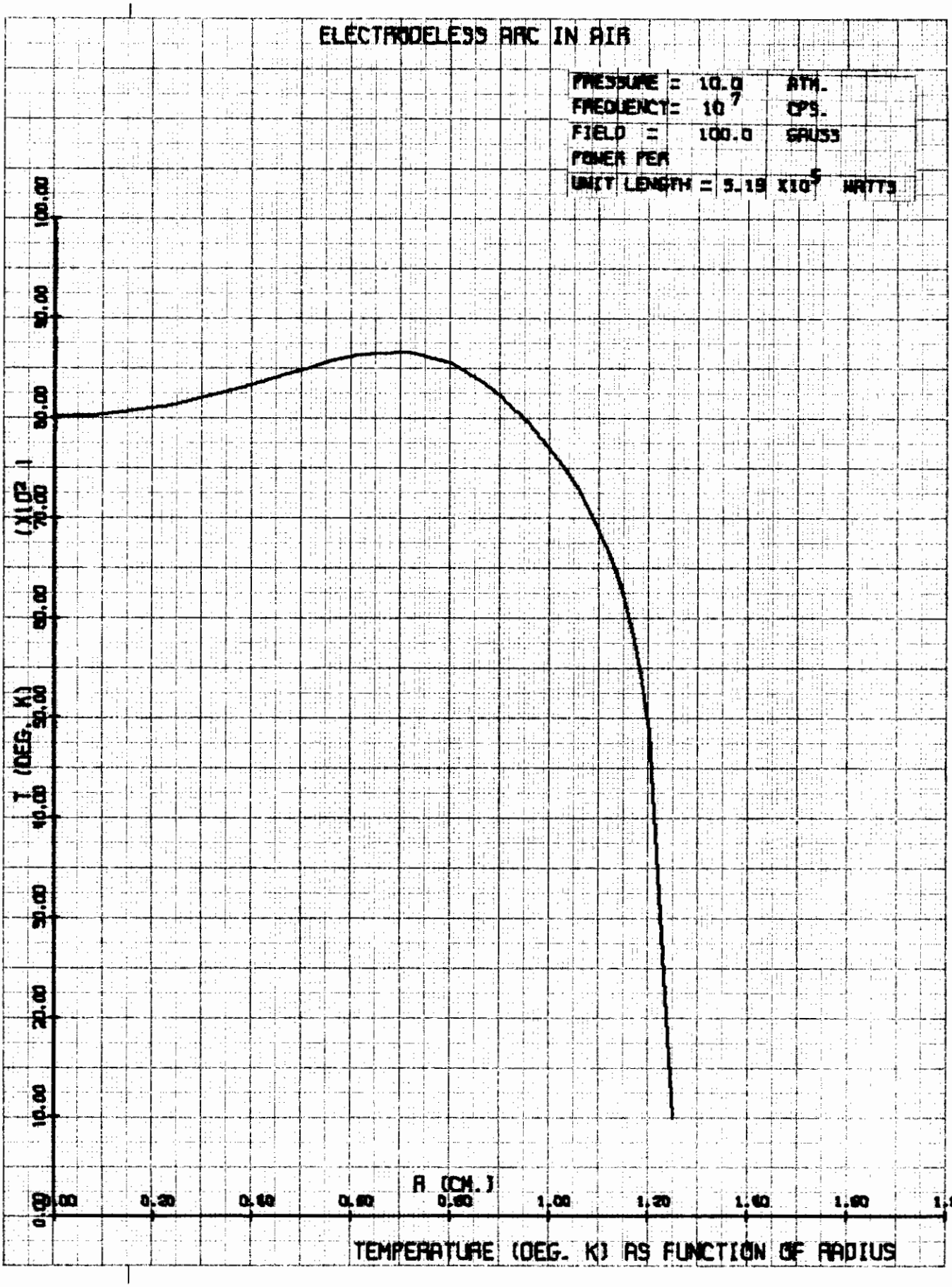

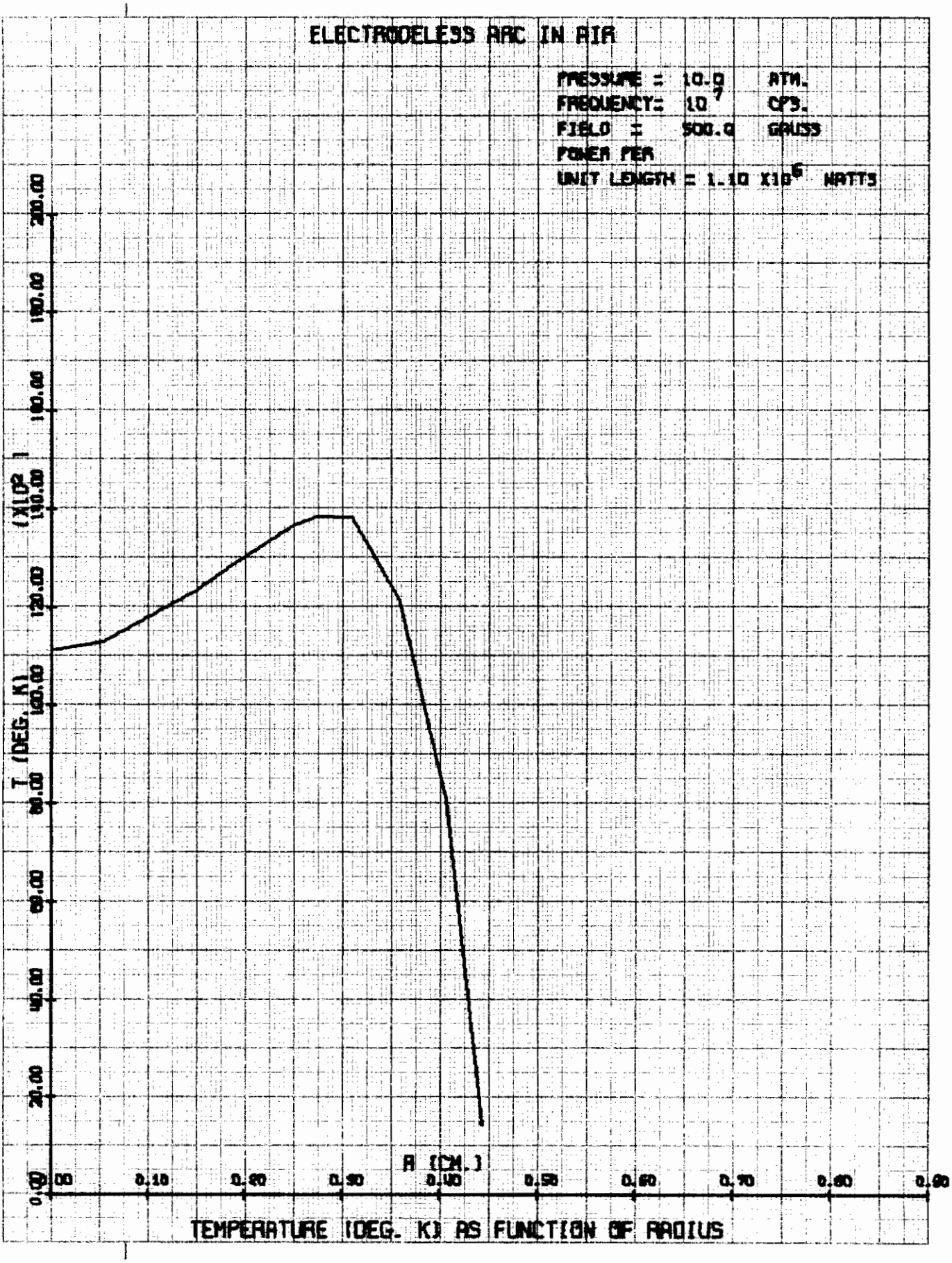

TEMPERATURE (DEG. K) AS FUNCTION OF RADIUS

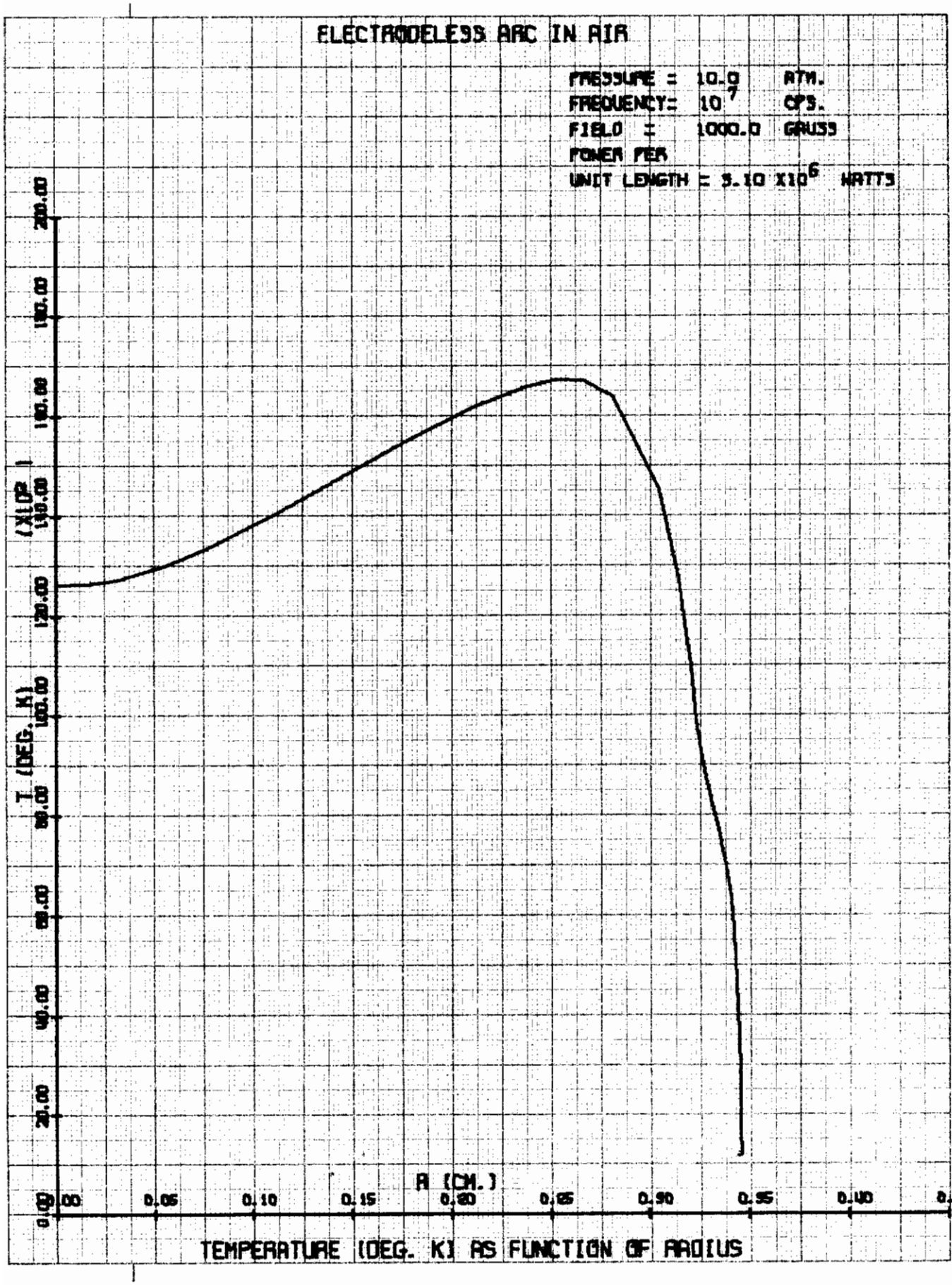

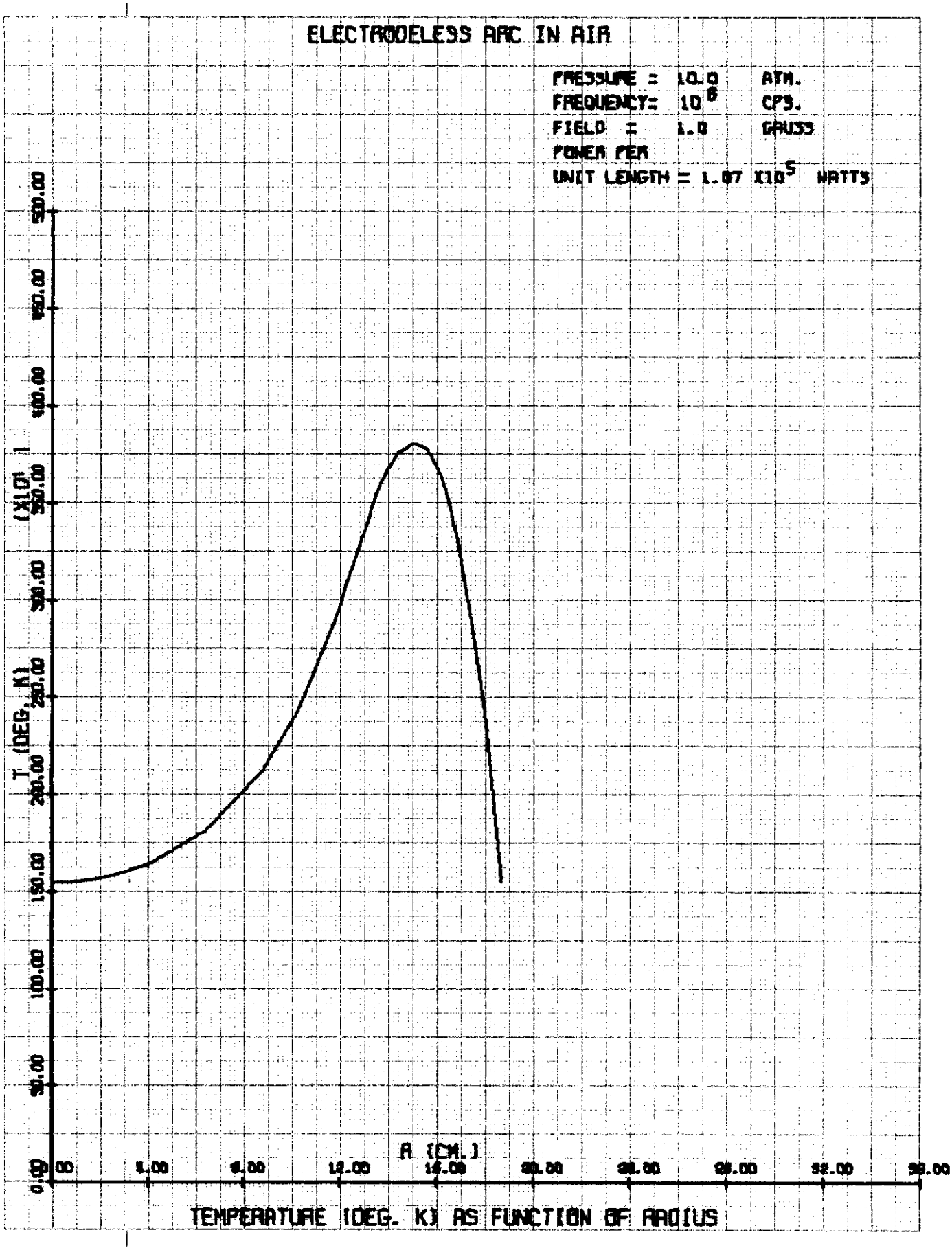

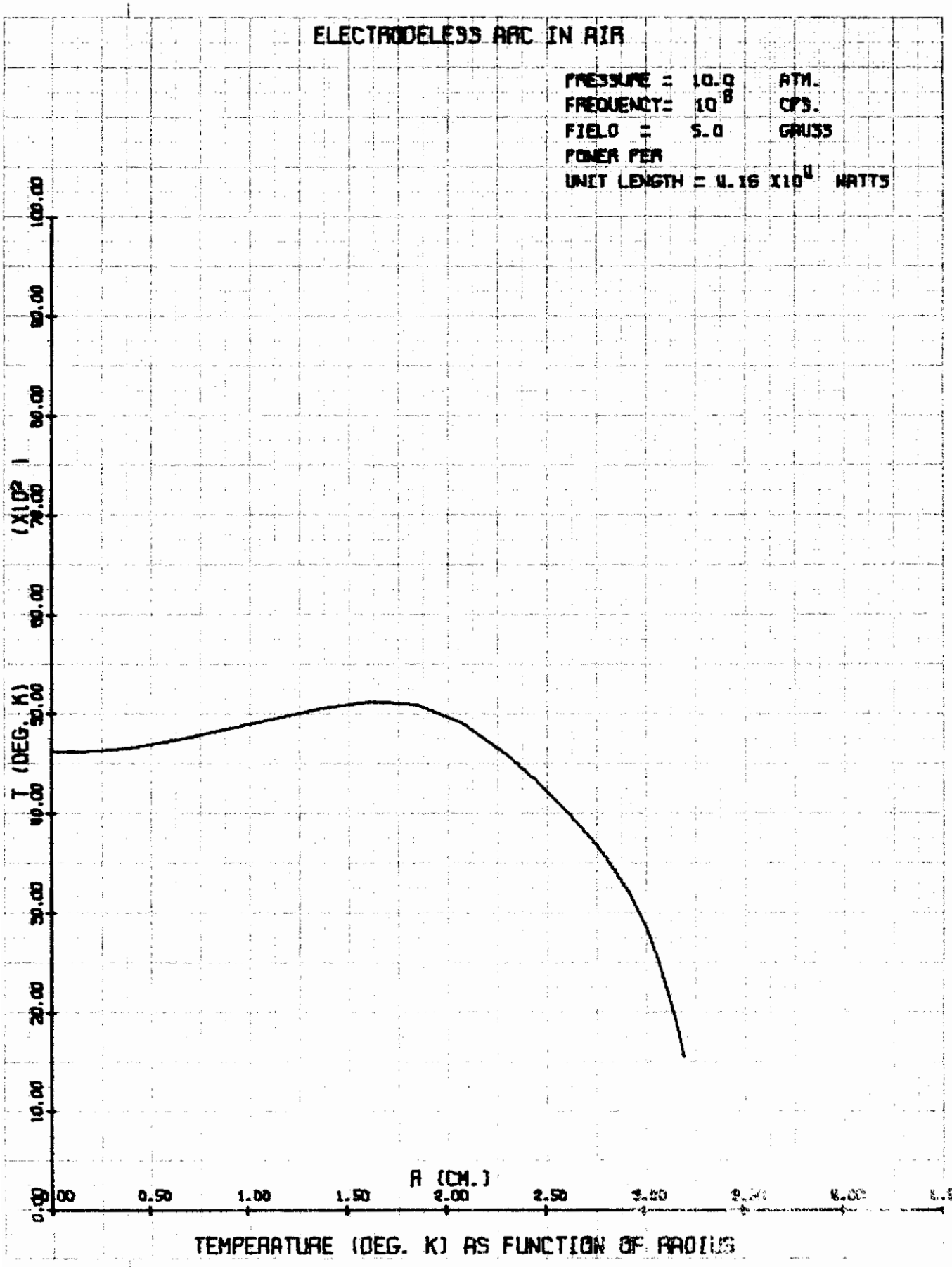

TEMPERATURE (DEG. K) AS FUNCTION OF RADIUS

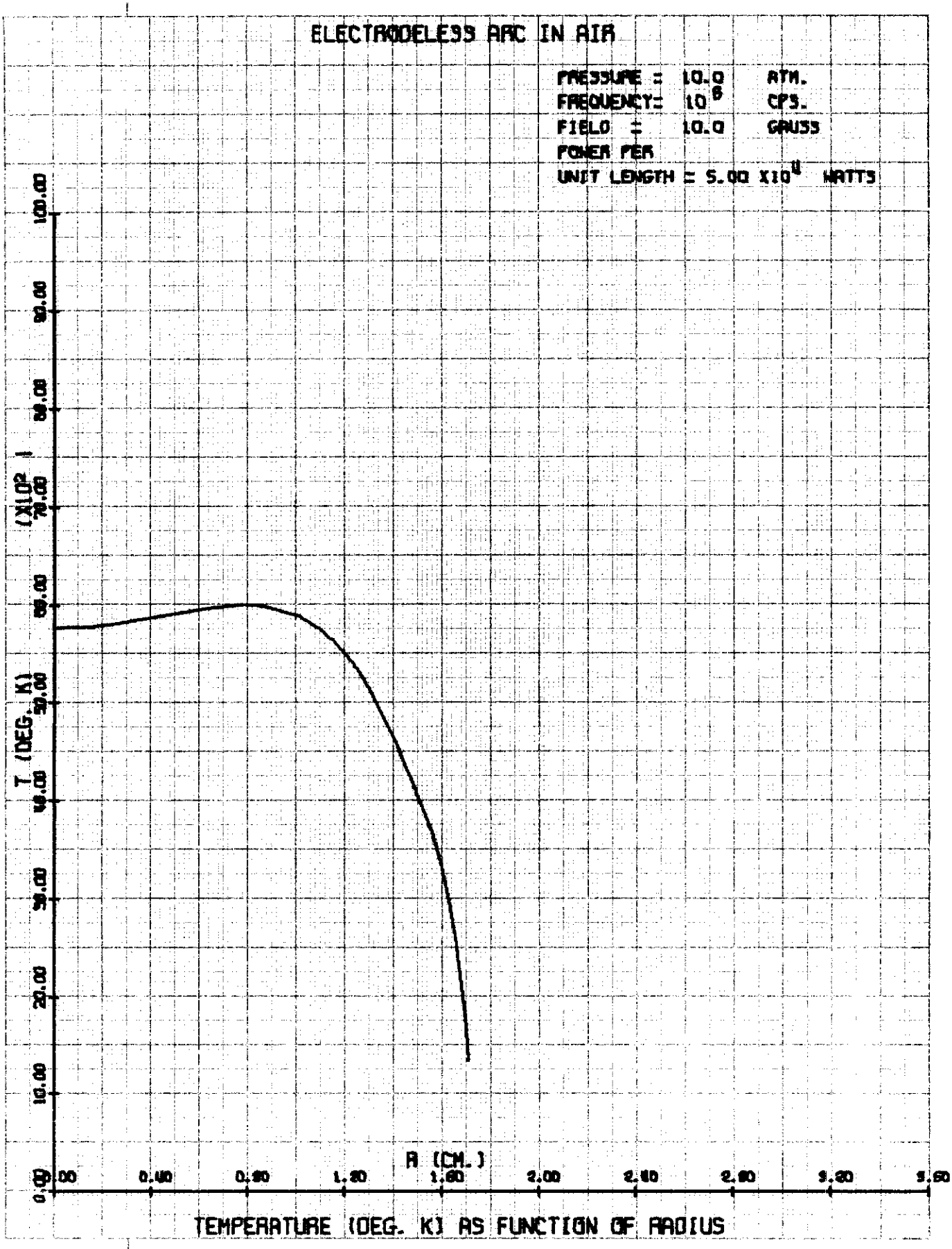

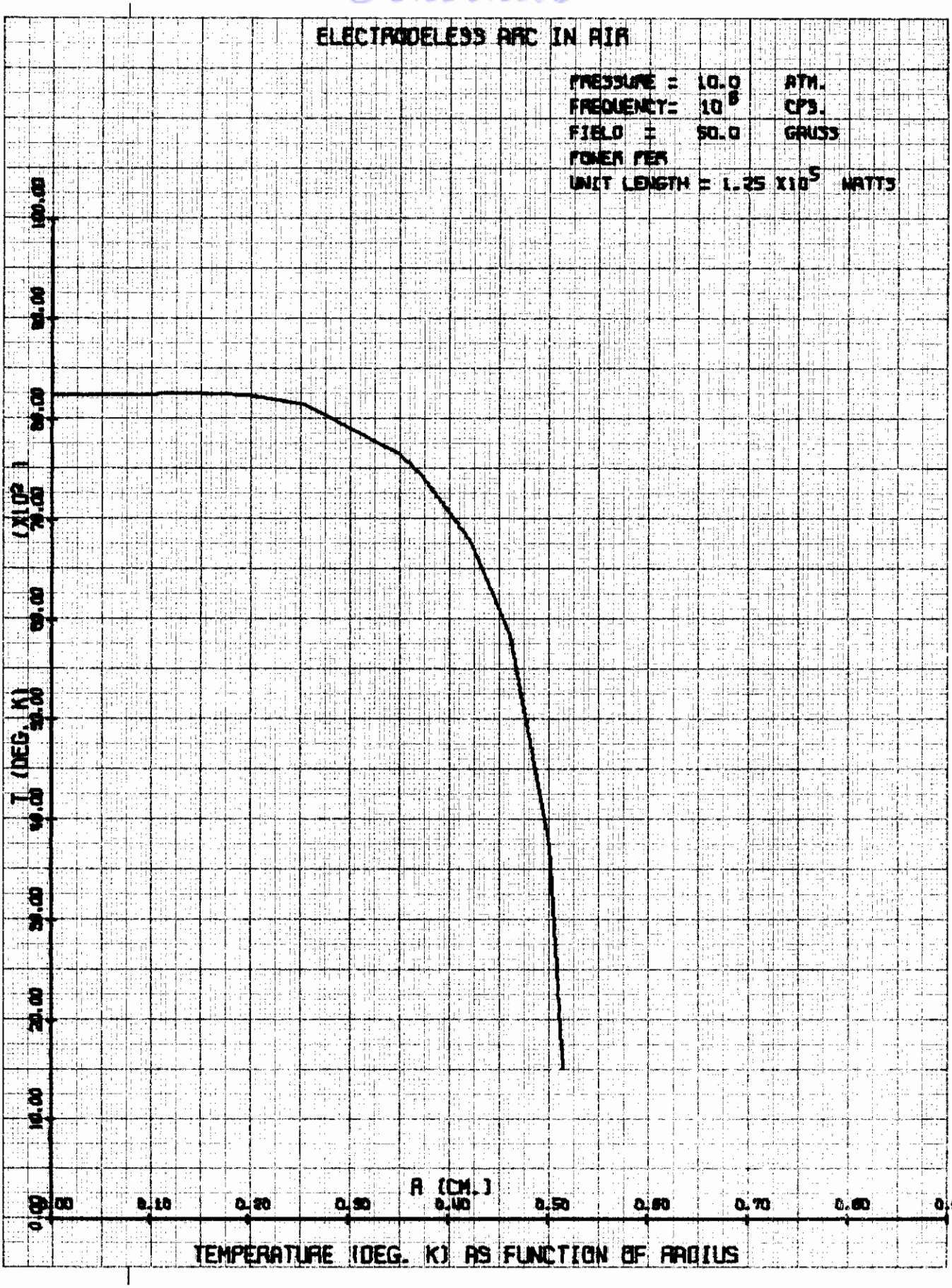

TEMPERATURE (DEG. K) AS FUNCTION OF RADIUS

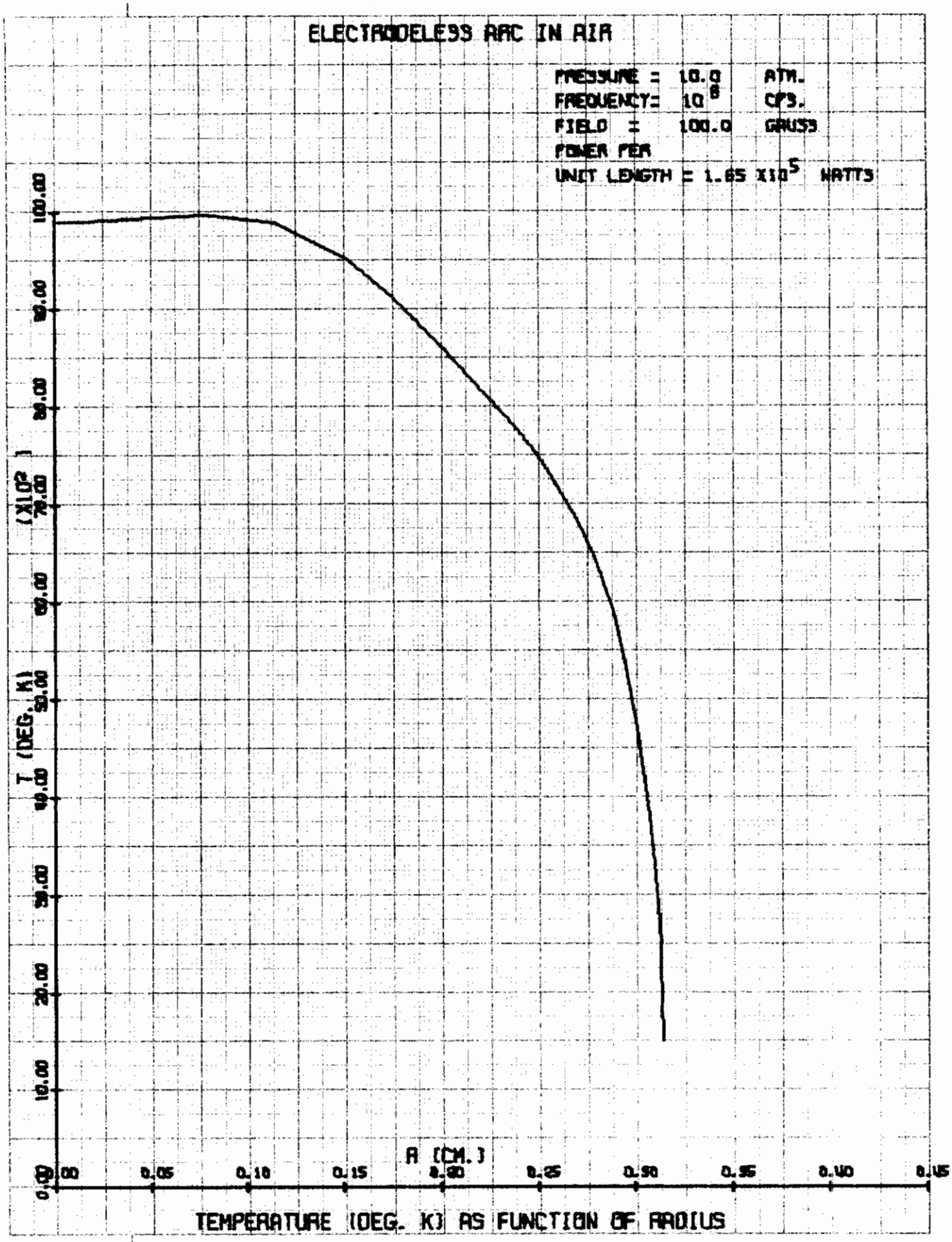

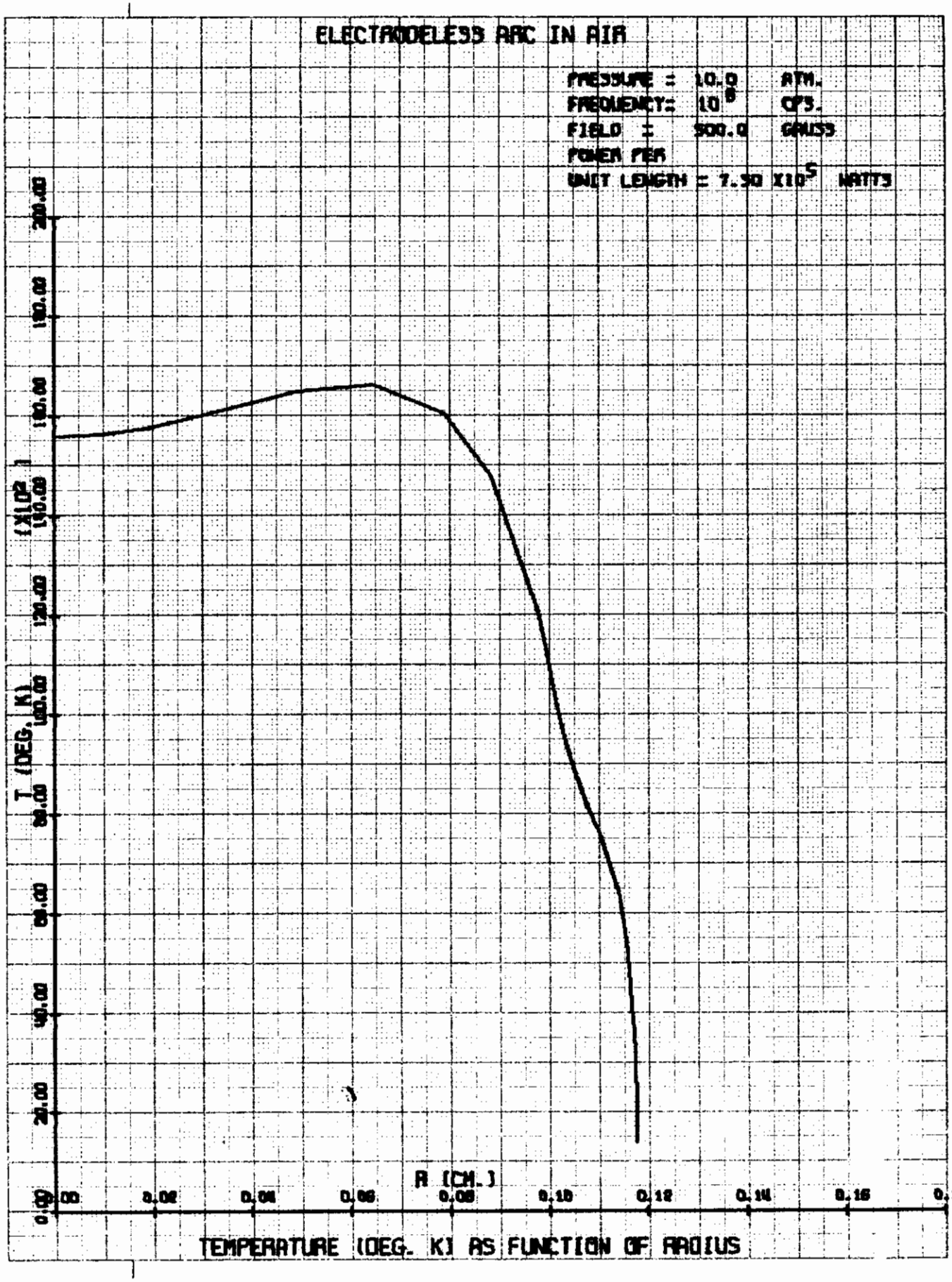

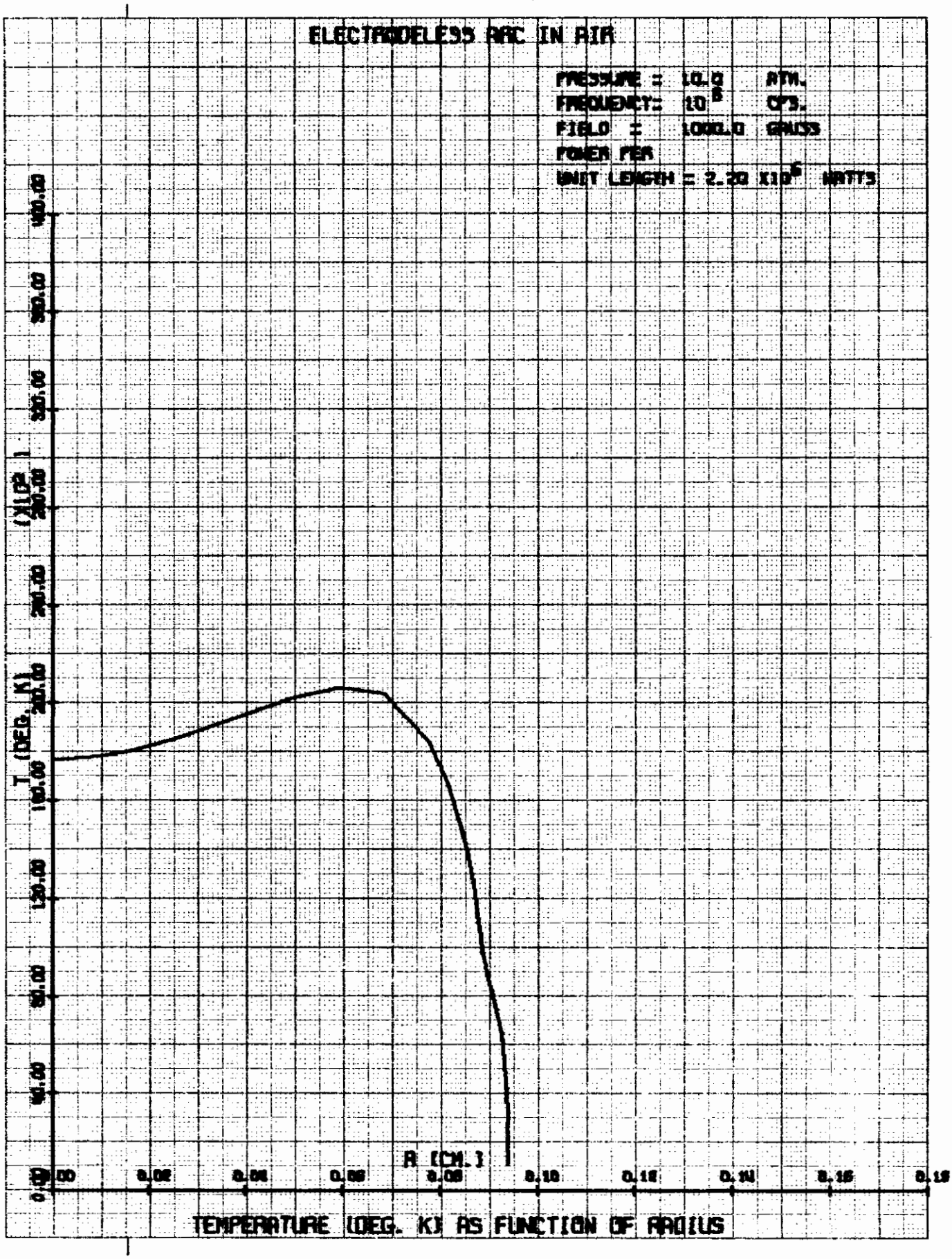

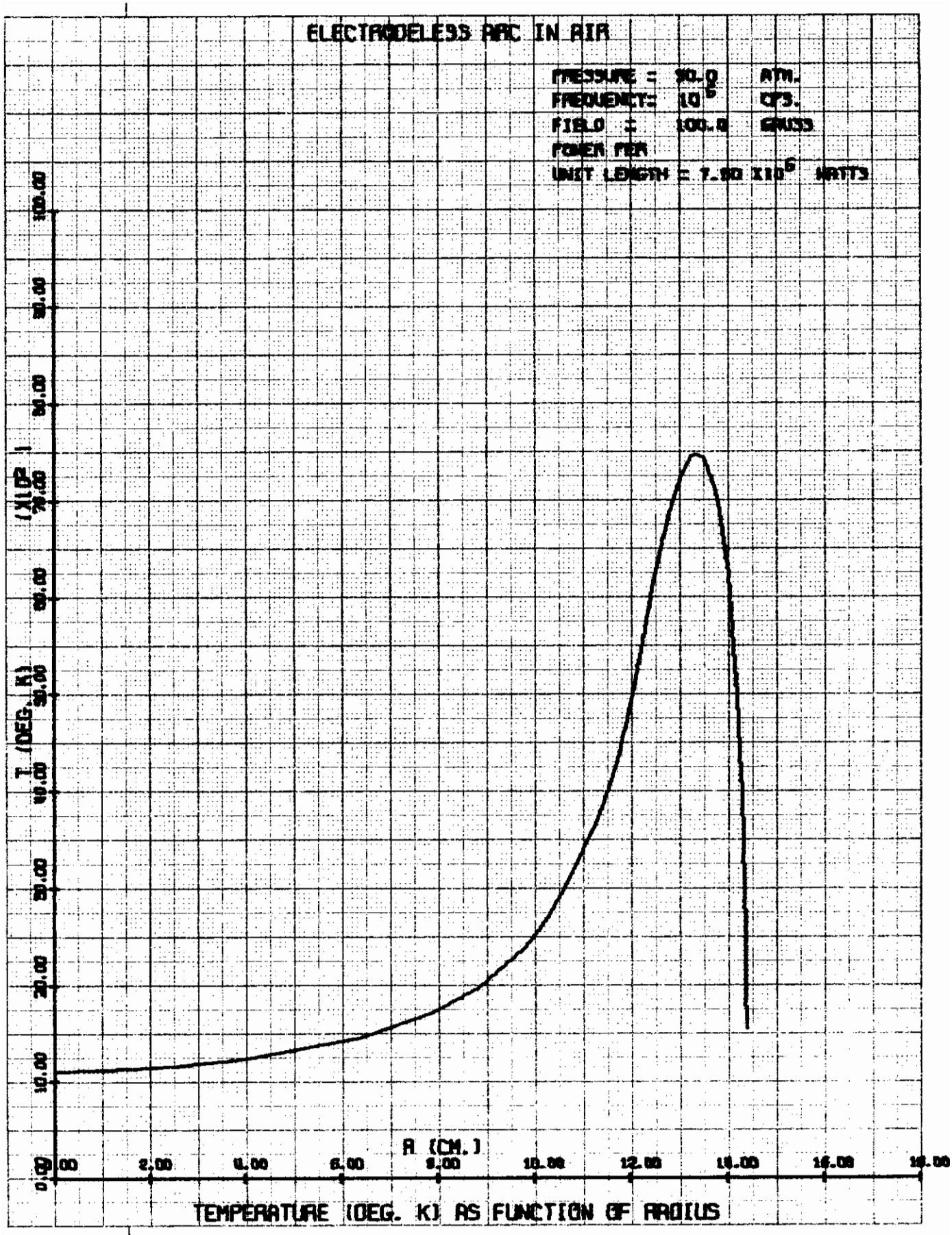

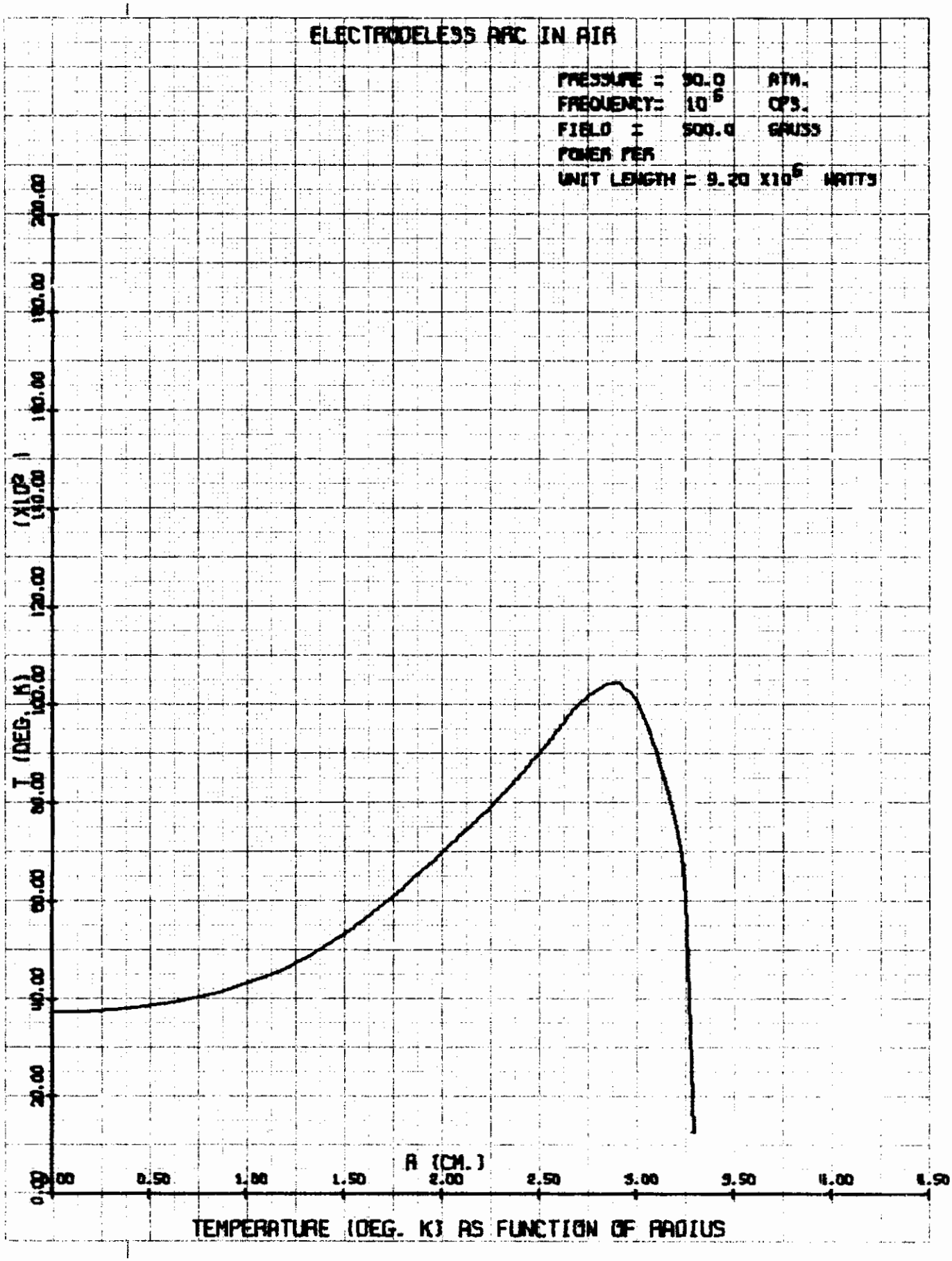

TEMPERATURE (DEG. K) AS FUNCTION OF RADIUS

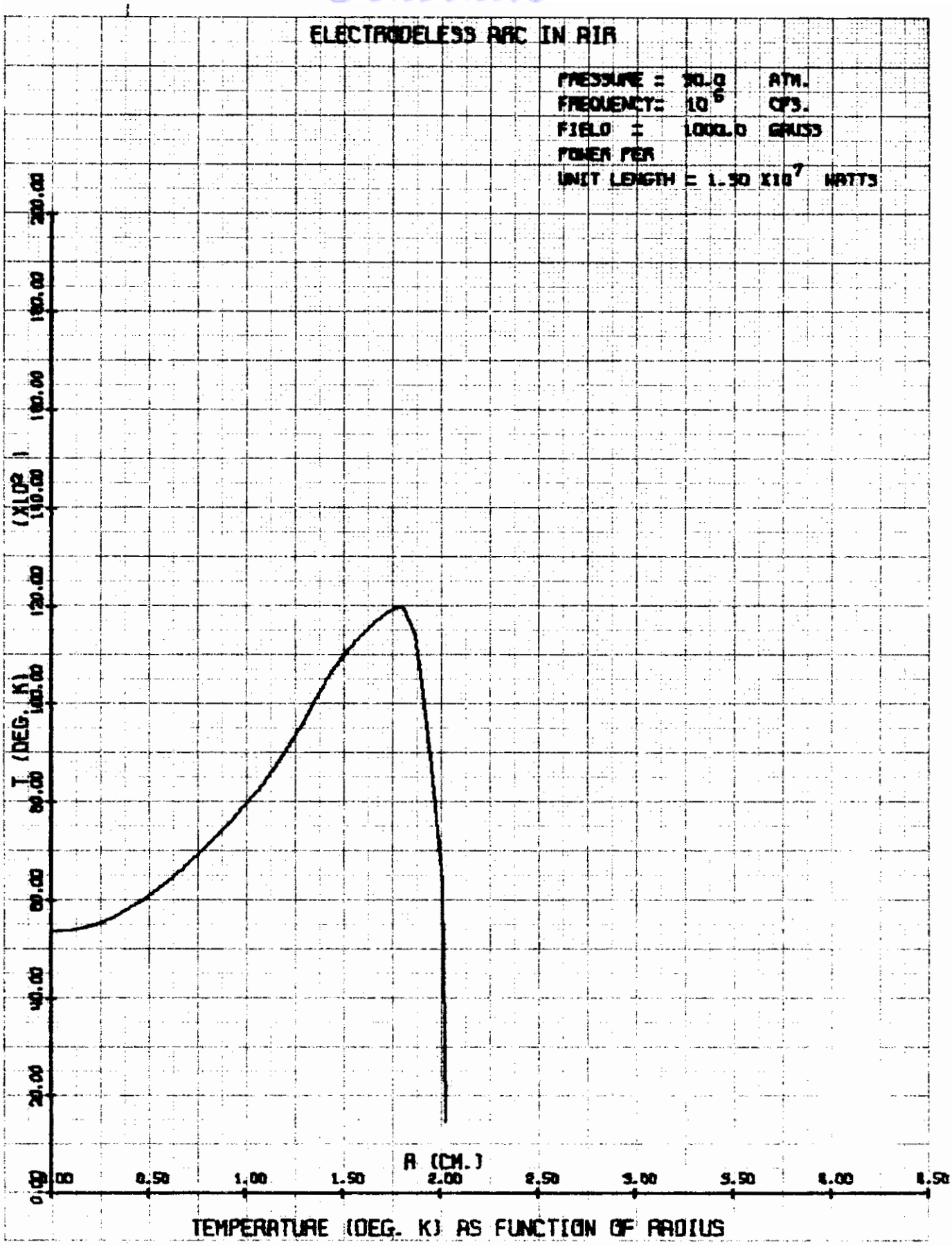

TEMPERATURE (DEG. K) AS FUNCTION OF RADIUS

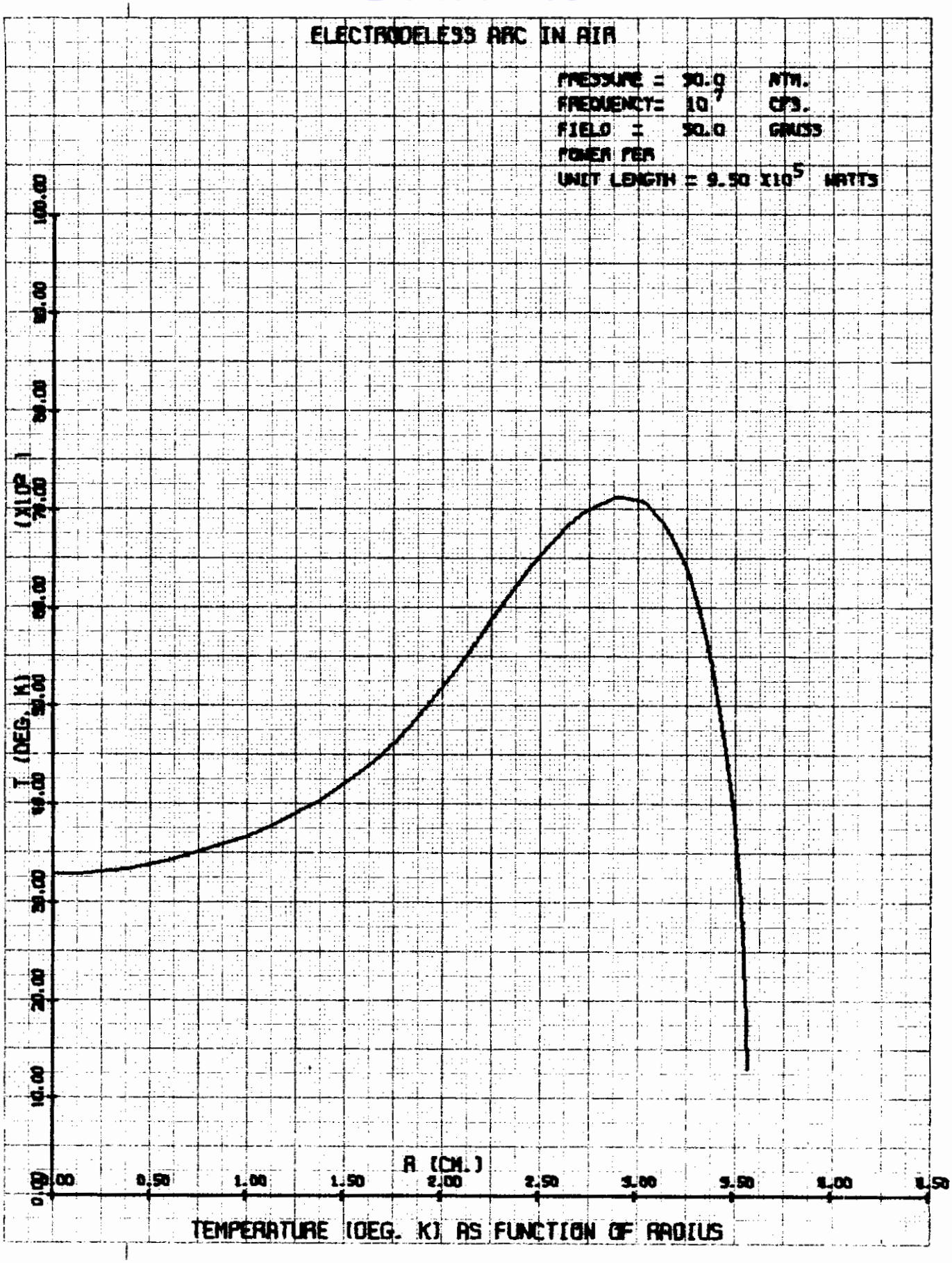

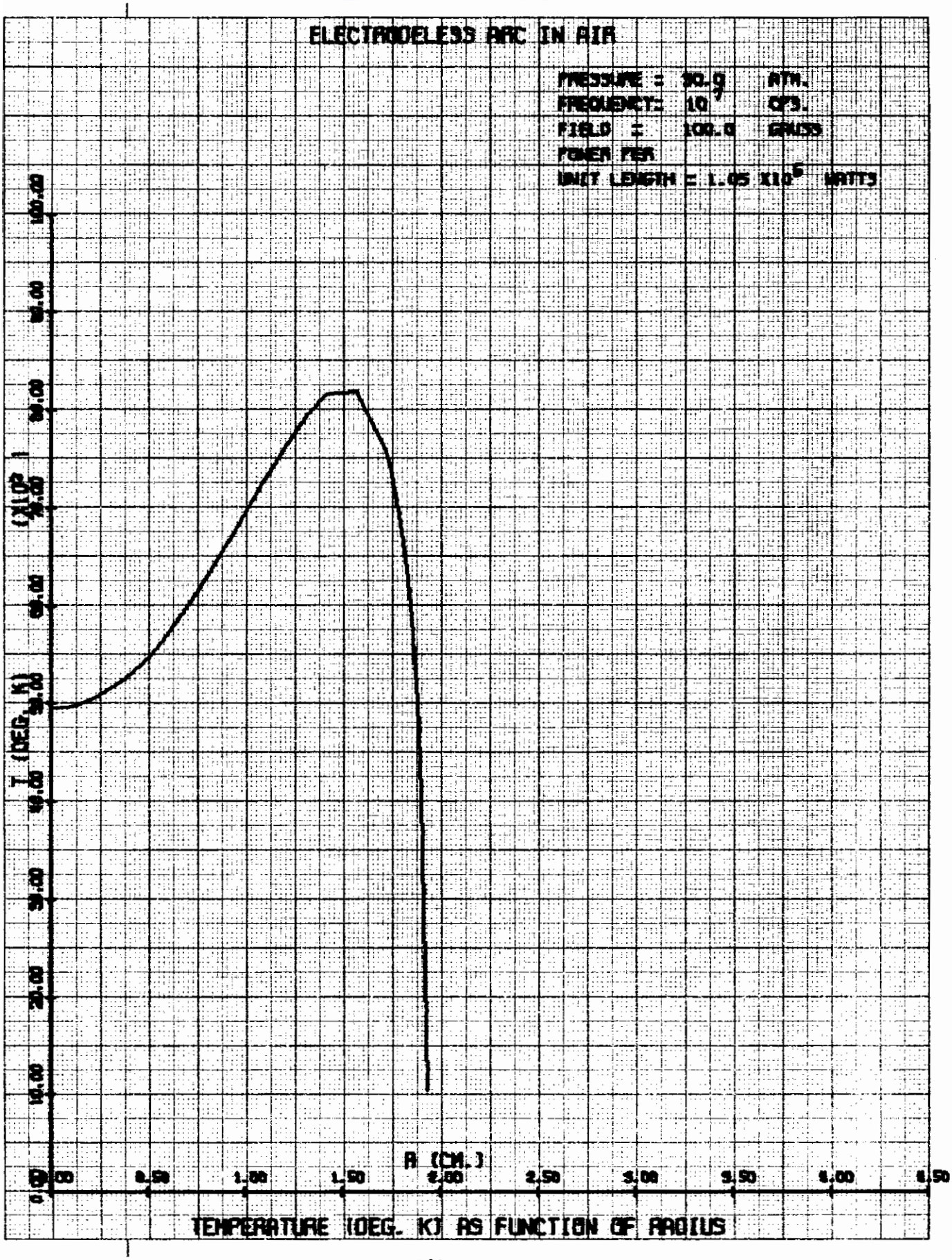

TEMPERATURE (DEG. K) AS FUNCTION OF RADIUS

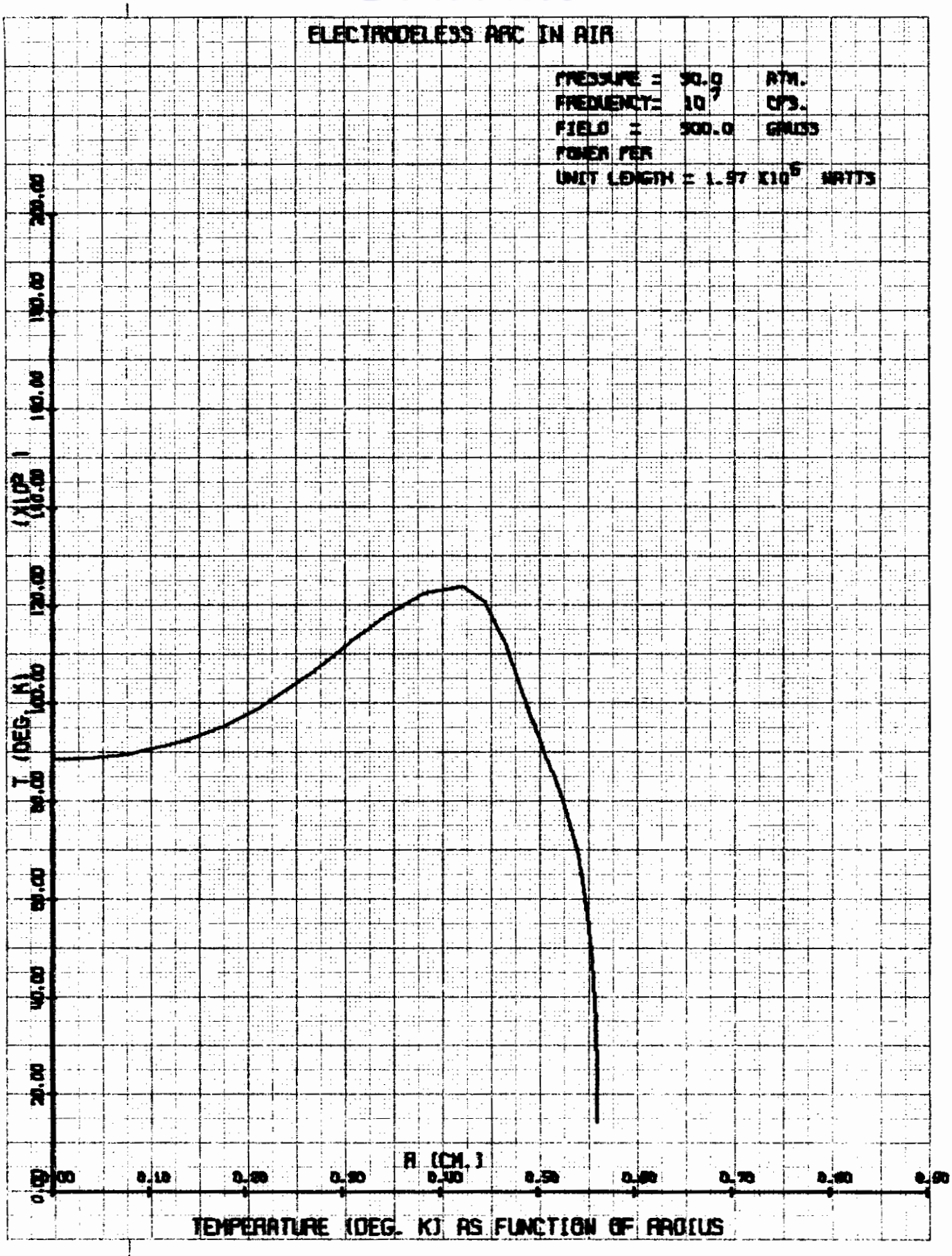

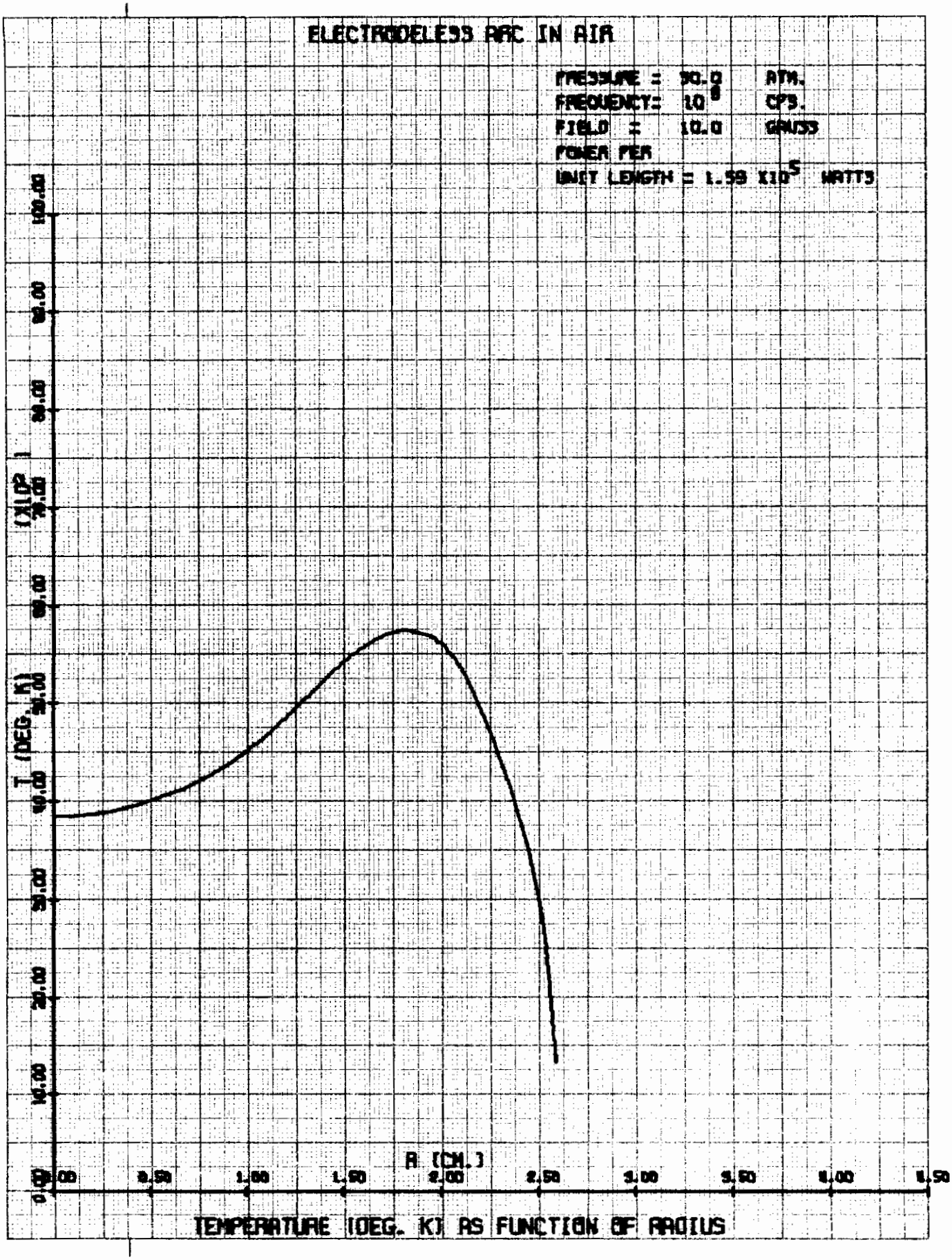

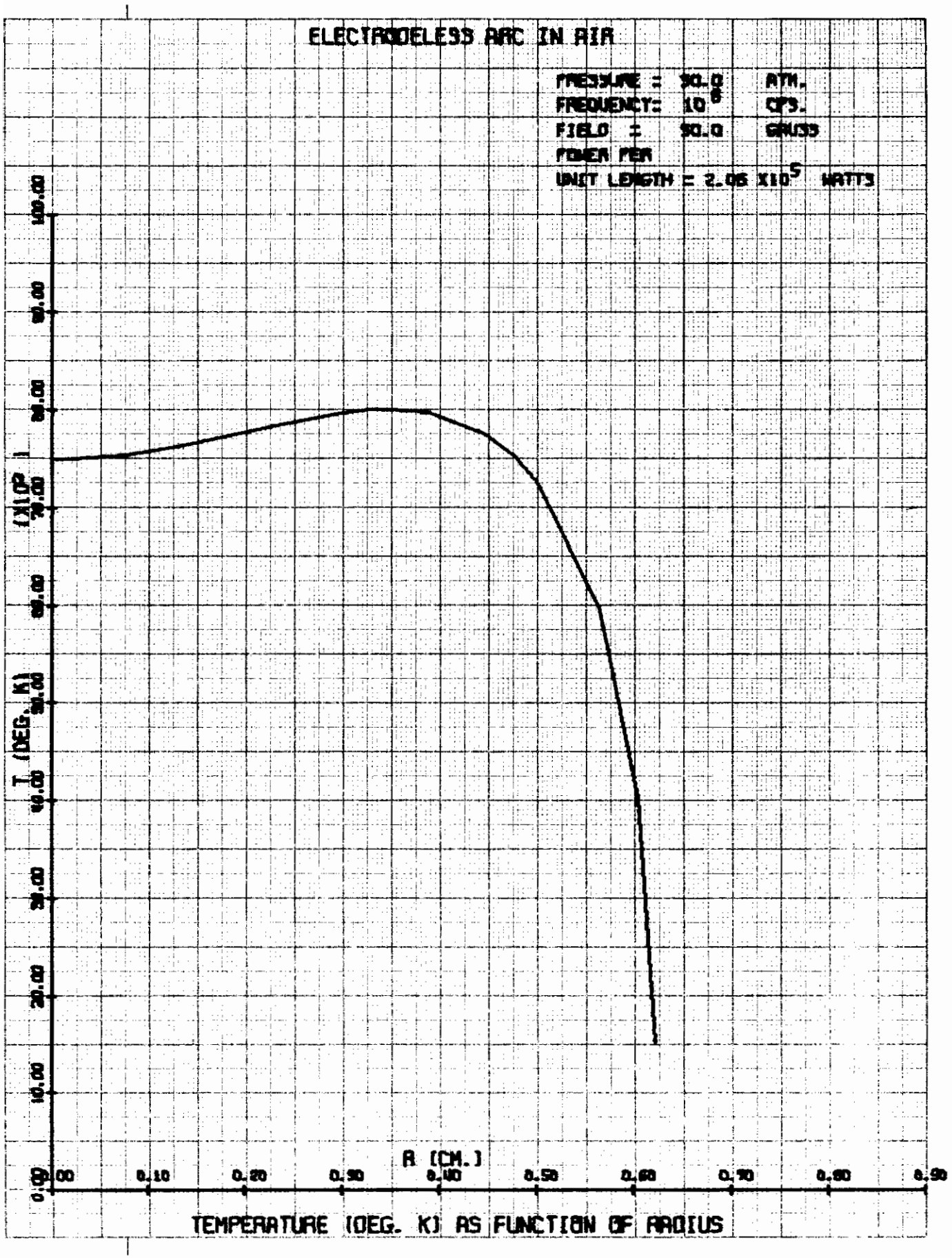

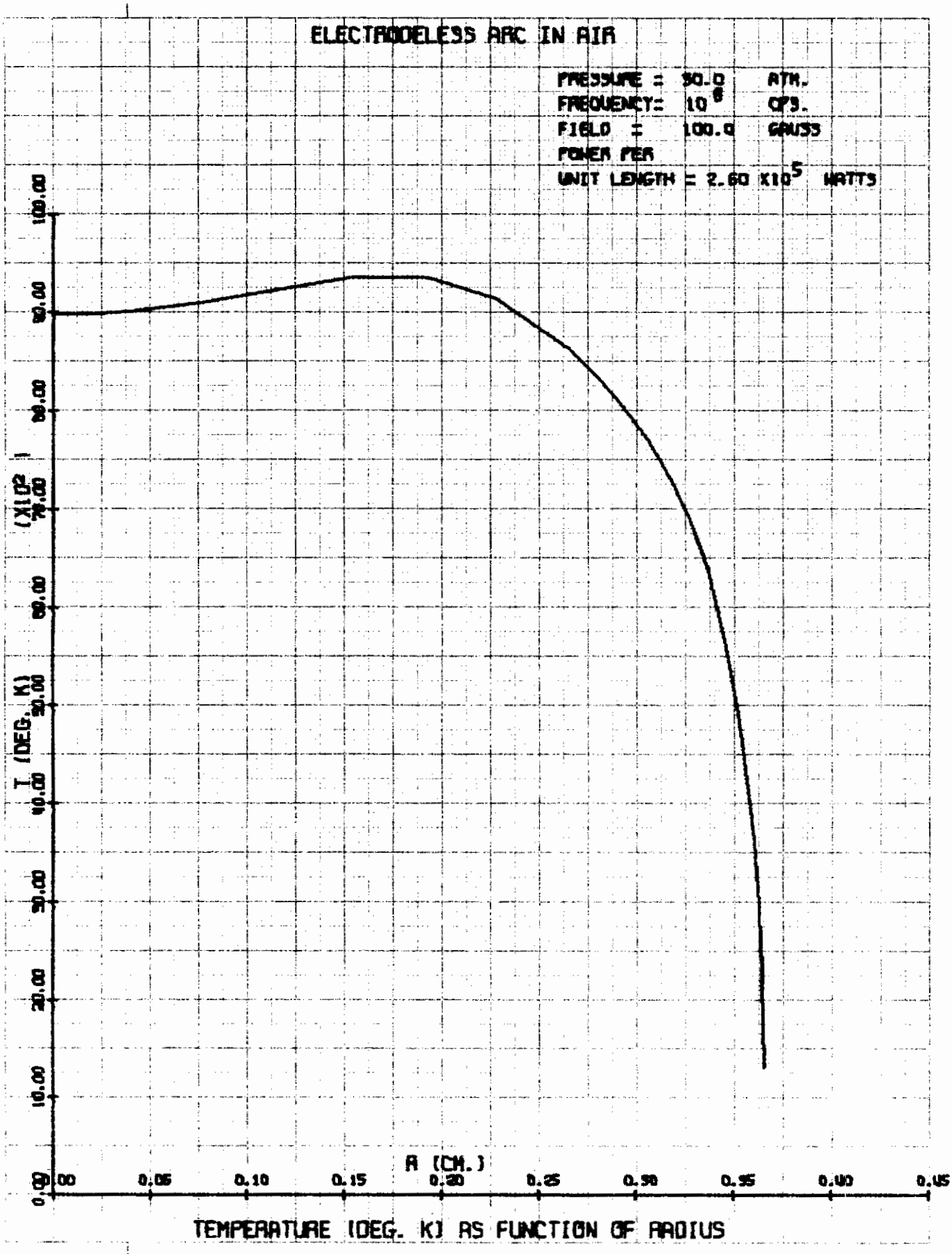

TEMPERATURE (DEG. K) AS FUNCTION OF RADIUS

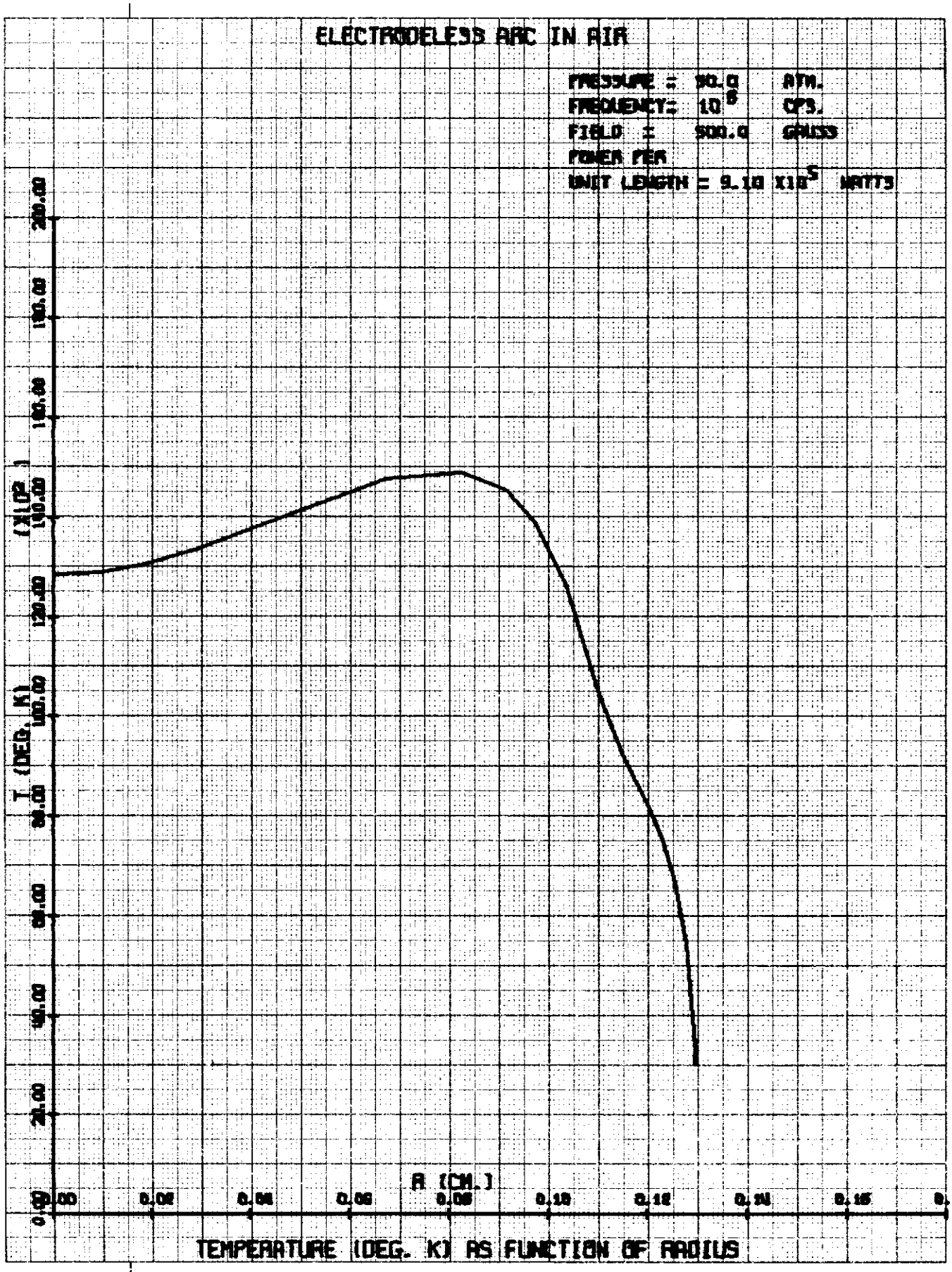

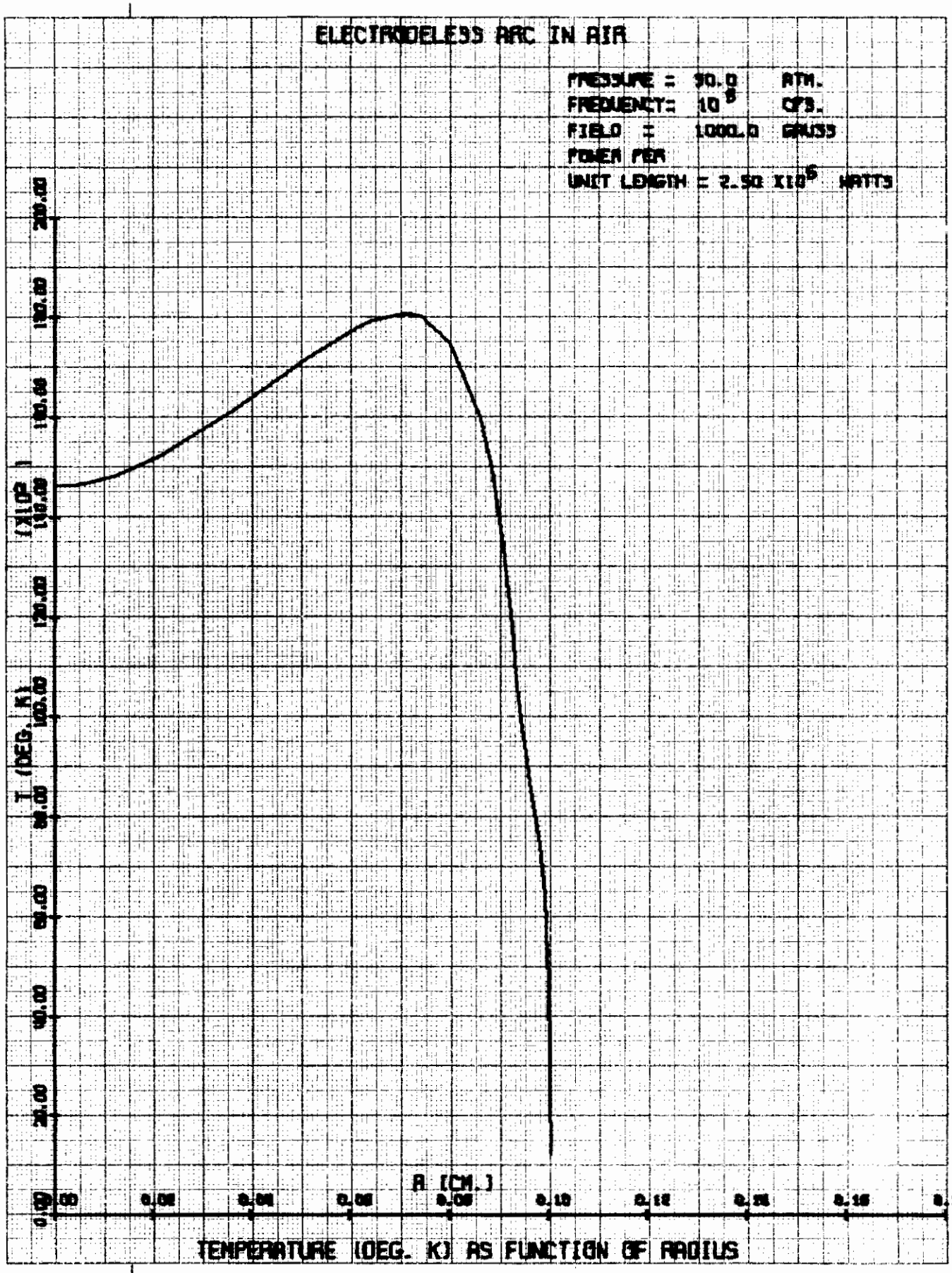

TEMPERATURE (DEG. K) AS FUNCTION OF RADIUS

APPENDIX VII

SUMMARY OF ENERGY BALANCE CALCULATIONS

Case	Pressure (Atm)	Freq. (Hz)	B(gauss)	B^2[w/m]^2	P/ℓ[w/m]	Radiation [w/m]	Radiation Fraction F	R(m)	σ_{eff} = [$2.38\times10^{12} B^2/P/\ell$] [mhos/m]	T_{eff} [°K]	H/RT_o
1	1	10^5	50	2.5×10^{-5}	4.89×10^5	3.58×10^5	0.731	2.55×10^{-1}	1.215×10^2	6,050	1.85×10^2
2	1	10^5	100	10^{-4}	5.15×10^5	3.21×10^5	0.624	1.31×10^{-1}	4.62×10^2	7,150	3.4×10^2
3	1	10^5	500	2.5×10^{-3}	1.58×10^6	1.09×10^6	0.694	4.58×10^{-2}	3.77×10^3	11,320	6.7×10^2
4	1	10^5	1000	10^{-2}	4.63×10^6	3.57×10^6	0.770	3.923×10^{-2}	5.14×10^3	13,300	1×10^3
5	1	10^6	10	10^{-6}	7.89×10^4	4.97×10^4	0.629	1.62×10^{-1}	3.01×10^1	5,000	1.23×10^2
6	1	10^6	50	2.5×10^{-5}	1.42×10^5	3.55×10^4	0.250	4.35×10^{-2}	4.18×10^2	7,050	3.2×10^2
7	1	10^6	100	10^{-4}	1.79×10^5	3.90×10^4	0.218	2.44×10^{-2}	1.33×10^3	8,300	4.82×10^2
8	1	10^6	500	2.5×10^{-3}	1.099×10^6	5.22×10^5	0.475	1.21×10^{-2}	5.41×10^3	13,700	1.05×10^3
9	1	10^6	1000	10^{-2}	3.17×10^6	1.96×10^6	0.617	1.03×10^{-2}	7.51×10^3	17,100	1.85×10^3
10	1	10^7	5	2.5×10^{-7}	2.16×10^4	5.77×10^3	0.267	5.36×10^{-2}	2.75×10^1	4,950	1.20×10^2
11	1	10^7	10	10^{-6}	3.80×10^4	5.15×10^3	0.136	3.55×10^{-2}	6.26×10^1	5,600	1.54×10^2
12	1	10^7	50	2.5×10^{-5}	1.06×10^5	3.53×10^3	0.0334	1.186×10^{-2}	5.61×10^2	7,300	3.6×10^2
13	1	10^7	100	10^{-4}	1.32×10^5	5.60×10^3	0.0123	6.63×10^{-3}	1.80×10^3	8,900	5.2×10^2
14	1	10^7	500	2.5×10^{-3}	8.17×10^5	2.08×10^5	0.255	3.30×10^{-3}	7.27×10^3	16,700	1.77×10^3
15	1	10^7	1000	10^{-2}	2.68×10^6	1.24×10^6	0.464	2.98×10^{-3}	8.89×10^3	19,950	2.16×10^3
16	1	10^8	1	10^{-8}	1.05×10^4	1.78×10^3	0.170	5.905×10^{-2}	2.26×10^0	4,000	9.4×10^1
17	1	10^8	5	2.5×10^{-7}	1.69×10^4	5.44×10^2	0.0322	1.499×10^{-2}	3.52×10^1	5,100	1.26×10^2
18	1	10^8	10	10^{-6}	3.31×10^4	4.995×10^2	0.0149	1.054×10^{-2}	7.13×10^1	5,750	1.65×10^2
19	1	10^8	50	2.5×10^{-5}	1.02×10^5	3.579×10^2	0.00352	3.678×10^{-3}	5.83×10^2	7,350	3.7×10^2
20	1	10^8	100	10^{-4}	1.262×10^5	6.36×10^2	0.00504	2.047×10^{-3}	1.88×10^3	9,000	5.2×10^2
21	1	10^8	500	2.5×10^{-3}	7.294×10^5	7.276×10^4	0.0998	9.85×10^{-4}	8.16×10^3	18,400	2.02×10^2
22	1	10^8	1000	10^{-2}	2.39×10^6	6.035×10^5	0.252	8.92×10^{-4}	9.96×10^3	21,950	2.3×10^3
23	3	10^5	100	10^{-4}	2.36×10^6	2.043×10^6	0.865	2.801×10^{-1}	1.02×10^2	6,200	1.75×10^2
24	3	10^5	500	2.5×10^{-3}	3.02×10^6	2.465×10^6	0.816	6.336×10^{-2}	1.97×10^3	9,400	5.3×10^2
25	3	10^5	1000	10^{-2}	7.33×10^6	6.245×10^6	0.853	4.93×10^{-2}	3.25×10^3	10,750	5.95×10^2
26	3	10^6	50	2.5×10^{-5}	3.667×10^5	2.31×10^5	0.632	6.98×10^{-2}	1.62×10^2	6,700	2.26×10^2
27	3	10^6	100	10^{-4}	3.91×10^5	2.03×10^5	0.520	3.602×10^{-2}	6.08×10^2	7,800	3.7×10^2
28	3	10^6	500	2.5×10^{-3}	1.22×10^6	7.546×10^5	0.621	1.27×10^{-2}	4.88×10^3	12,600	7.5×10^2
29	3	10^6	1000	10^{-2}	3.68×10^6	2.60×10^6	0.706	1.11×10^{-2}	6.47×10^3	14,550	1×10^3
30	3	10^7	5	2.5×10^{-7}	6.023×10^4	3.93×10^4	0.653	8.95×10^{-2}	9.88×10^0	4,600	1.07×10^2
31	3	10^7	10	10^{-6}	6.31×10^4	2.945×10^4	0.467	4.577×10^{-2}	3.77×10^1	5,350	1.33×10^2
32	3	10^7	50	2.5×10^{-5}	1.32×10^5	2.205×10^4	0.1677	1.32×10^{-2}	4.51×10^2	7,500	3.3×10^2
33	3	10^7	100	10^{-4}	1.665×10^5	2.44×10^4	0.1466	7.44×10^{-3}	1.43×10^3	8,800	4.8×10^2
34	3	10^7	500	2.5×10^{-3}	8.58×10^5	3.21×10^5	0.304	3.377×10^{-3}	6.93×10^3	15,200	1.16×10^3

Case	Pressure (Atm)	Freq. (Hz)	B(gauss)	B^2[w/m]^2	P/ℓ[w/m]	Radiation [w/m]	Radiation Fraction F	R(m)	$\sigma_{eff} = [2.38\times10^{12} B^2/P/\ell]$ [mhos/m]	T_{eff}[°K]	H/RT_o
35	3	10^7	1000	10^{-2}	2.62×10^6	1.377×10^6	0.527	2.948×10^{-3}	9.09×10^3	18,500	1.85×10^3
36	3	10^8	1	10^{-8}	3.38×10^4	1.65×10^4	0.487	1.06×10^{-1}	7.04×10^{-1}	3,900	8.1×10^1
37	3	10^8	5	2.5×10^{-7}	2.05×10^4	3.11×10^2	0.151	1.65×10^{-2}	2.91×10^1	5,200	1.26×10^2
38	3	10^8	10	10^{-6}	3.47×10^4	2.78×10^3	0.0800	1.07×10^{-2}	6.86×10^1	5,900	1.55×10^2
39	3	10^8	50	2.5×10^{-5}	1.07×10^5	2.19×10^3	0.0204	3.78×10^{-3}	5.56×10^2	7,700	3.55×10^2
40	3	10^8	100	10^{-4}	1.359×10^5	2.96×10^3	0.0217	2.12×10^{-3}	1.75×10^3	9,200	5.15×10^2
41	3	10^8	500	2.5×10^{-3}	7.13×10^5	1.18×10^5	0.166	9.73×10^{-4}	8.35×10^3	17,300	1.63×10^3
42	3	10^8	1000	10^{-2}	2.76×10^6	1.04×10^6	0.377	9.58×10^{-4}	8.63×10^3	17,750	1.72×10^3
43	10	10^5	500	2.5×10^{-3}	1.35×10^7	1.244×10^7	0.922	1.34×10^{-1}	4.41×10^2	7,900	3.2×10^2
44	10	10^5	1000	10^{-2}	1.995×10^7	1.85×10^7	0.926	8.14×10^{-2}	1.19×10^3	9,000	4.5×10^2
45	10	10^6	50	2.5×10^{-5}	1.69×10^6	1.485×10^6	0.879	1.499×10^{-1}	3.52×10^1	5,700	1.37×10^2
46	10	10^6	100	10^{-4}	1.61×10^6	1.32×10^6	0.821	7.303×10^{-2}	1.48×10^2	6,850	2×10^2
47	10	10^6	500	2.5×10^{-3}	2.49×10^6	1.894×10^6	0.777	1.80×10^{-2}	2.44×10^3	10,250	5.3×10^2
48	10	10^6	1000	10^{-2}	5.78×10^6	4.73×10^6	0.819	1.386×10^{-2}	4.12×10^3	11,900	6.5×10^2
49	10	10^7	5	2.5×10^{-7}	3.41×10^5	3.02×10^5	0.886	2.13×10^{-1}	1.745×10^0	4,100	8×10^1
50	10	10^7	10	10^{-6}	2.293×10^5	1.886×10^5	0.822	8.73×10^{-2}	1.04×10^1	4,850	1.1×10^2
51	10	10^7	50	2.5×10^{-5}	2.63×10^5	1.44×10^5	0.549	1.869×10^{-2}	2.26×10^2	7,200	2.26×10^2
52	10	10^7	100	10^{-4}	3.19×10^5	1.400×10^5	0.439	1.03×10^{-2}	7.46×10^2	8,450	3.85×10^2
53	10	10^7	500	2.5×10^{-3}	1.11×10^6	6.115×10^5	0.553	3.83×10^{-3}	5.36×10^3	13,000	7×10^2
54	10	10^7	1000	10^{-2}	3.09×10^6	2.00×10^6	0.647	3.20×10^{-3}	7.70×10^3	15,500	1×10^3
55	10	10^8	1	10^{-8}	1.07×10^5	9.099×10^4	0.849	1.89×10^{-1}	2.22×10^{-1}	3,350	5.5×10^1
56	10	10^8	5	2.5×10^{-7}	4.16×10^4	2.27×10^4	0.545	2.35×10^{-2}	1.43×10^1	5,000	1.14×10^2
57	10	10^8	10	10^{-6}	5.04×10^4	1.85×10^4	0.368	1.29×10^{-2}	4.72×10^1	5,900	1.45×10^2
58	10	10^8	50	2.5×10^{-5}	1.25×10^5	1.511×10^4	0.121	4.08×10^{-3}	4.76×10^2	8,000	3.3×10^2
59	10	10^8	100	10^{-4}	1.66×10^5	1.64×10^4	0.0989	2.35×10^{-3}	1.43×10^3	9,300	4.8×10^2
60	10	10^8	500	2.5×10^{-3}	7.30×10^5	2.12×10^5	0.290	9.85×10^{-4}	8.15×10^3	16,000	1.08×10^3
61	10	10^8	1000	10^{-2}	2.21×10^6	9.45×10^5	0.428	8.56×10^{-4}	1.08×10^4	19,900	1.81×10^3
62	30	10^6	100	10^{-4}	7.81×10^6	7.34×10^6	0.940	1.61×10^{-1}	3.04×10^1	5,800	1.32×10^2
63	30	10^6	500	2.5×10^{-3}	9.21×10^6	8.24×10^6	0.894	3.50×10^{-2}	6.45×10^2	8,720	3.6×10^2
64	30	10^6	1000	10^{-2}	1.31×10^7	1.18×10^6	0.899	2.08×10^{-2}	1.815×10^3	10,100	5×10^2
65	30	10^7	50	2.5×10^{-5}	9.49×10^5	7.87×10^5	0.830	3.55×10^{-2}	6.27×10^1	6,300	1.5×10^2
66	30	10^7	100	10^{-4}	1.05×10^6	7.98×10^5	0.762	1.87×10^{-2}	2.25×10^2	7,620	2.33×10^2
67	30	10^7	500	2.5×10^{-3}	1.98×10^6	1.42×10^6	0.720	5.12×10^{-3}	3×10^3	11,150	5.7×10^2
68	30	10^7	1000	10^{-2}	3.77×10^6	2.85×10^6	0.756	3.54×10^{-3}	6.31×10^3	13,810	7.3×10^2
69	30	10^8	10	10^{-6}	1.586×10^5	1.18×10^5	0.745	3.296×10^{-2}	1.498×10^1	5,285	1.15×10^2
70	30	10^8	50	2.5×10^{-5}	2.067×10^5	8.89×10^4	0.430	5.24×10^{-3}	2.88×10^2	7,840	2.5×10^2
71	30	10^8	100	10^{-4}	2.60×10^5	8.73×10^4	0.336	2.94×10^{-3}	9.15×10^2	9,130	4×10^2
72	30	10^8	500	2.5×10^{-3}	9.19×10^5	4.21×10^5	0.458	1.11×10^{-3}	6.475×10^3	13,940	7.4×10^2
73	30	10^8	1000	10^{-2}	2.58×10^6	1.44×10^6	0.557	9.26×10^{-4}	9.24×10^3	16,900	1×10^3

APPENDIX VIII

BIBLIOGRAPHY ON RF DISCHARGES *

The references contained herein have been organized according to the following categories:

I. General Information (RF Discharges)

II. Capacitive RF Discharges

III. Inductive RF Discharges

- A. Low Pressure
- B. High Pressure
- C. Pulsed

IV. Microwave Discharges

*This bibliography was assembled in part from information generously provided by Hans U. Eckert, Aerospace Corporation, El Segundo, California.

BIBLIOGRAPHY ON RF DISCHARGES

I. GENERAL INFORMATION

	Author	Title	Originating Agency	Remarks
1.	M. F. Romig	Steady State Solutions of the Radio-Frequency Discharge with Flow	Physics of Fluids, 3, 129 (1960)	
2.	H. Rother	Massentrennungs-und Einschnürungseffekte in HF-Plasmen	Zeitschrift für	18a, 300, (1963)
3.	P. Maroni R. Jancel T. Kahan	Analyse de la Fonction de Distribution Electronique dans une Descharge Haute Frequence (Premiere Partie)	Institut H.-Poincare (Sorbonne), Laboratoire de Theories Physiques	Journal de Physique 23, 425, (1962)
4.	M. Erickson C. S. Ward S. C. Brown S. J. Buchsbaum	Containment of Plasmas by High Frequency Electric Fields	Dept. Physics & Res. Lab.of Elec.,MIT Cambridge, Mass., Bell. Tel.Lab.Inc., Murray Hill, N. J.	Journal Appl. Phys. 33, 2429 (1962)
5.	S. C. Brown	High-Frequency Gas-Discharge Breakdown	Tech. Rpt-301 (1955) Res.Lab.Elec., MIT Cambridge, Mass.	
6.	L. Biberman B. Panin	Measurement of the Parameters of a High-Frequency Electrodeless Discharge by Means of Two Probes	Convair-S.C. L-59-3-43 Transl.by W.R. Eichler (1959)	Zhurn.Tekhn.Fix.21, 12, (1951)
7.	F. Ciorascu	Energy Distribution of Electrons in Very High Frequency Discharges in Hydrogen	Transl. fr. Rumanian by G. Duffy, Convair AEC2-0003-1 (1962)	Studii si Cercetari de Fisica 8, 1, (1957)
8.	A. Dzherpetov A. A. Zaitsev	Striated High Frequency Discharge	Doklady Adademii (1963) Nauk SSSR, 89, 825-28	
9.	C. E. Muehe	AC Breakdown in Gases	Lincoln Lab, TR 380	26 Feb. 1965

I. GENERAL INFORMATION (cont'd)

	Author	Title	Originating Agency	Remarks
10.	R. B. Hall S. C. Brown	Reflection of an Electron Beam from High-Frequency Fields	Mass. Inst. of Tech.	Jour.Apl.Phys. 32, 1835, (1961)
11.	T. W. Karras B. Lindman	RF Breakdown in a DC Parabolic Potential Field	Univ. of Calif.	Unpublished
12.	A. D. MacDonald	High-Frequency Breakdown in Air at High Altitudes		Proc. IRE, March 1959, pp 435-41
13.	D. J. Rose S. C. Brown	High-Frequency Gas Discharge Plasma in Hydrogen	Mass. Inst. of Tech.	Phys. Rev. 98, 310-66 (1955)
14.	W. P. Allis S. C. Brown	High Frequency Electrical Breakdown of Gases		Phys. Rev. 87, 419-24 (1952)
15.	S. C. Brown A. D. MacDonald	Limits for the Diffusion Theory of High Frequency Gas Discharge Breakdown	Mass. Inst. of Tech.	Phys.Rev.76, 1629-33 (1949)
16.	S. Aisenberg	Multiple Probe Measurements in High-Frequency Plasma Lasers	Mass. Inst. of Tech.	Jour.Appl.Phys.35, 130-34 (1964)
17.	G. I. Babat	Electrodeless Discharge and Some Allied Problems	1947	Jour.Inst.Elec.Eng. (London)94, 27-37
18.	J. S. Townsend R. H. Donaldson	Electrodeless Discharges	Oxford	Philos.Mag.5, 178-91 (1926)
19.	K. A. MacKinnon	On the Origin of the Electrodeless Discharge		Philos.Mag.8, 605-16 (1929)
20.	J. Tykocinski Tykociner	Measurement of Current in Electrodeless Discharges	Univ. of Ill.	Philos.Mag.13, 953-63 (1932)
21	O. Sherman J. F. McCov	Minimum Sustaining Field Strength for Radio-Frequency Plasmas		Jour.Appl.Phys.35, 2080, (1964)
22	D. D. Hollister	An Electrodeless Technique for Full Scale Simulation of the Re-entry Environment	Aeronutronic Div., Philco-Ford Corp.	Prod. Second Space Congress, April '65 pp 549-574

	Author	Title	Originating Agency	Remarks
23.	S. I. Andreev M. P. Vanyukov A. A. Egorova	Efficiency of Energy Transfer to an Electrodeless High-Frequency Discharge		Soviet Phys.Tech. Phys.12, 910-913 (1968)
24.	E. S. Weibel R. Keller	On the Design of a Rotating Field Pinched Discharge	Laboratoire de Recherches en Physique des Plasmas, Lausanne,	Plasma Physics 9, 401-414 (1967) Switzerland
25.	J. S. Townsend W. Nethercot	High Frequency Discharges in Gases		Philos.Mag.Ser.7, Vol.7, 600-616 (1929)
26.	J. S. Townsend	Generalization of the Theory of Electrical Discharges		Philos.Mag.Vol.26 290-311 (1936)
27.	E. A. Bamberg S. V. Dresvin	Determination of Certain Parameters of a High-Frequency Ring Discharge		Sov.Phys.Tech.Phys. 8, 43-48 (1963)
28.	A. Mironer	Design of a High Enthalpy Radio Frequency Gas Discharge	Allied Research Assoc., Inc.	AIAA Jour.1,2638-2639 (1963)
29.	P. J. Huffman E. J. Rolinski	Prelininary Study of a Radio Frequency Plasma		Tech.Doc.Rept No. ML-TDR-64-317 (1964)
30.	J. Pomerantz	The Influence of the Absorption of Radiation in Shock Tube Phenomena		J.Quant.Spectrosc. Radiat.Transfer,Vol.1, 185-248 (1961)
21	J.Besombes-Vailhe	Etude de la Repartition de la Temperature Movenne dans le Jet D'une Torche a Plasma D'argon Haute Frequence	Centre de Spectrographie, Nouvelle Faculte des Sciences, Institut du Genie Chimique, Toulouse	Report No. 18
32.	D. B. Henderson	Aerodynamic Study of an Argon Plasma		Physics of Fluids, Vol.10, 1692-7(1967)
33.	H. V. Eckert	Equations of the Electrodeless Ring Discharge and their Solution for the Breakdown Criterion	Convair Scientific Res. Lab, San Diego, Calif.	Rept. No. 5, Convair (1959)

	Author	Title	Originating Agency	Remarks
34.	H. V. Eckert F. L. Kelly H. N. Olsen	Spectroscopic Observations on Induction-Coupled Plasma Flames in Air and Argon	Lockheed Calif.Co. Burbank, Calif., & Plasma Sciences Labs., Inc., Van Nuys, Calif.	Jour.Appl.Phys.39, 1846 (1968)
35.	V. V. Dolgopolov	Plasma Absorption of Energy from a High-Frequency Field through Multiple Ion Gyroresonance		Sov.Phys.Tech.Phys. 8, 893-5 (1964)
36.	S. D. Vagner N. A. Krylov	Effects of a Magnetic Field on the Parameters of a High-Frequency Discharge		Sov.Phys.Tech.Phys. 10, 1105-8 (1966)
37.	V. I. Solunskii B. L. Timan	Volume Recombination in the Presence of Ambipolar Diffusion in a Gas-Discharge Plasma		Soviet Phys.Tech. Phys. 9, 207-9 (1964)
38.	D. H. Hale	The Breakdown of Gases in High Frequency Electrical Fields		Phys.Rev.73, 1046-52 (1948)
39.	M. J. Kofoid J. M. Dawson	Anamalous Skin Depth in a Gaseous Plasma		Phys.Rev. 17, 1086-8 (1966)
40.	S. V. Dresvin A. V. Donskoi	Determination of the Conductivity of a High-Frequency Induction Discharge in Argon by Calorimetric and Spectral Methods		Sov.Phys.Tech.Phys. 10, 1270-4 (1966)
41.	H. W. Emmons	Magnetohydrodynamics		Prod. 8th Midwestern Mechanics Conf.,April 1963, pp 71-82
42.	N. A. Bobyrev	Localization of a Linear High-Frequency Discharge		Sov.Phys.Tech.Phys 11, 308-15 (1966)
43.	I. Michiyoski M. Namano	Performance Characteristics of a Vortex-Type MHD Power Generator		Plasma Phys. 9, 939-48 (1967)

I. GENERAL INFORMATION (Cont'd)

	Author	Title	Originating Agency	Remarks
44.	L. E. Belousova	Relation of Radius to Power for a Thermal Plasma of Spherical Shape		Teplofizika Vysokikh Temp.4, 499-502 (1966)
45.	R. Carruthers	Skin Effect in Gas Discharges		Appl.Sci.Res. B,5, 135-8 (1955)
46.	H. V. Eckert	Measurement of Maintenance Fields in Electrodeless Ring Discharges and Correlation with Uniform Field Data	Lockheed-California Co.	Plasma Phys.Rept. No. 5, LR16397 (1962)
47.	G. L. Cann J. M. Teem R. D. Buhler L. K. Branson	Magnetogasdynamics Accelerator Techniques		Report AEDC-TDR-62-145, ASTIA Doc. No. 277 954 (1964)
48.	V. W. Hertz A. Koller	Elektrodenlose Dreispulenplasmakanone		Zeitschrift fur Naturforschung

II. CAPACITIVE RF DISCHARGES

	Author	Title	Originating Agency	Remarks
1.	Golovanivskii/ Kuzovnikov	Effect of Compression of the Positive Column of a Gas Discharge by an Inhomogeneous High-Frequency Field	Soviet Physics	1962
2.	M. Chenot	Effects Polarises Dans Une Decharge H.F.	Ecole Normale Super-Ieure des Jeunes Filles, Paris, France	1955
3.	M. Chenot	Recherches Experimentales Sur La Decharge En Haute Frequence Theses	Paris, France, Annales de Physique Tome 3, pp 277-375	1948
4.	M. M. Chenot	Proprietes Generales de La Decharge En Haute Frequence Comme Source de Courant Continu	Ecole Normale Superieue des Jeunes Filles, Paris, France	1957
5.	M. M. Chenot	Effets De Charge D'Espace Dans Une Decharge En Haute Frequence.I	" "	1955
6.	M. M. Chenot	Effets De Charge D'Espace Dans Une Decharge En Haute Frequence.II	" "	1955
7.	M. M. Chenot	Production De Courant Continu Par Une Decharge En Haute Frequence. I	" "	1956
8.	M. M. Chenot	Production De Courant Continu Par Une Decharge En Haute Frequence. II	" "	1957
9.	M. M. Chenot	Decharge Dans Les Gaz.-Pile a Gaz Ionise En Haute Frequence	Extrait des Comptes des Seances de 1'	1952
10.	M. M. Chenot	Decharge Dans Les Gaz.-Characteristiques En Debit Continu D'une Decharge En Haute Frequence	" "	1952

II. CAPACITIVE RF DISCHARGES (Cont'd)

	Author	Title	Originating Agency	Remarks
11.	M. M. Chenot	Decharge Electrique-Production D'une Tension Constante Par Une Decharge Excitee En Haute Frequence	Extrait des Comptes des Seances de 1'	1948
12.	G. Francis	The Growth of Electrodeless Discharge in Hydrogen	Proc. of the Phys. Soc.	Aug. 1954
13.	E. J. Powers	Evidence of Anomalous Diffusion in an RF Discharge in a Magnetic Field	Stanford University	
14.	O. M. Shvets S.S.Ovchinnikov V.F.Tarasenko O.S.Pavlochenko V.T.Tolok	High Frequency Method for Producing a Dense Plasma in a Metallic Chamber	Sov. Phys. Tech. Phys. 10 1675-77 (1966)	
15.	J. R. Trimmier A. Miller	Doppler Measurements of the Kinetic Energies Produced in Radio Frequency Plasmoids	Dept. of Phys., New Mexico State Univ., University Park, N. M.	Unpublished
16.	K.S.Golovanivski V.D.Dugar-Zabon A.A.Kuzovnikov	Space Charge in a Stationary Plasma Disturbed by an Inhomogeneous High-Frequency Field	Sov.Phys.Tech.Phys. 9, pp 355-7	1964
17.	R. L. Chuan		Univ. of Southern Calif.	Phys. Fluids 1, 4521 (1958)
18.	A. I. Carswell			Rev. Sci. Inst. 34, 1015(1963)

III. INDUCTIVE RF DISCHARGES

	Author	Title	Originating Agency	Remarks
1.	R. L. Barger J. D. Brooks W. D. Beasley	An Experimental Study of the Ionization of Low-Density Gas Flows by Induced Discharges	Langley Res. Center Langley Field, Va.	NASA TN D-431, 1960
2.	B. I. Davydov	The Ignition of an Electrodeless Discharge		1951
3.	R.A.Dimirkhanov I.D.Khodyrev N.I.Leont'ev T.I.Gutkin	Interaction of High Frequency Electromagnetic Fields with Plasma	Internat'l Atomic Energy Agcy,Salzburg Conf.Preprint No. CN-10/233	Translated from the Russian by G.Duffy, Cnvair AE61 0003-12
4.	M. C. Gourdine D. Hollister	A Study of Some of the Properties of an RF Generated Plasma	Plasmadyne Report No. PLR-105	1961
5.	Degeilh D. Blanc	Etude De La Decharge Par Induction Dans Les Sources D'ions Posities a Excitation Electque De Haute Frequence	Laboratoire d'Optique Electronique du C.N.R.S. Toulouse/Centre de Physique Nuclear	Jour.de Physique 24, 187, (1963)
6.	S. Kubota	Study of Breakdown of Gases by Purely Azimuthal Electric Fields	Inst. of Physical & Chem. Res.	J.Phys.Soc.Japan, 1314-5 (1962)
7.	H. U. Eckert	Transition from Free to Ambipolar Diffusion in an Electrodeless Discharge	North Holland, Amsterdam	Proc.Fifth Interna'l Conf. Ioniz.Phen. Gases, I, 537 (1962)
8.	V. H. Schluter	Rekombination und Ionisation in Einer Stationaren Hochfrequenzentladung		Zeitschr.f.Natforschung 18a 439-46 (1963)
9.	C. C. Goodyear	Dissociation and Ionization of Hydrogen in High Frequency Discharges	Clarendon Lab.,Oxford	Proc.Phys.Soc.79, 732-40 (1962)

III. INDUCTIVE RF DISCHARGES (Cont'd)

	Author	Title	Originating Agency	Remarks
10.	I. A. Kossyi	Radial Charged Particle Flux in a Discharge Excited by a High Frequency Traveling Wave		Sov.Phys.Tech.Phys. 10, 1678-81 (1966)
11.	A. D. Andreev Y. N. Lobanov	Special Features of the Electrodeless Ring Discharge		Sov.Phys.Tech.Phys. 9, 1437-9 (1965)
12.	B. M. Dymshits Y.P.Koretskii	An Experimental Investigation of Induced Discharges		Sov.Phys.Tech.Phys. 9, 1294-8 (1965)
13.	L. R. Boedeker C. W. Haldemen	Initial Experimental Results on the Operating Modes and Electrical Conductivity in an RF Plasma Flow Device	AIAA Plasmadynamics Conf. March 2-4, 1966	AIAA Paper, 66-165
14.	R. C. Jones F. E. Nagel	Field Strengths for Prebreakdown Magnetic Induction Discharge	Melpar, Inc.	Proc.IEEE 52, 625 (1964)
15.	D. R. Keefer M. H. Clarkson B. E. Mathews	Probe Measurements in an Electrodeless Discharge	AIAA Plasmadynamics Conf. March 2-4, 1966	AIAA Plasmadynamics Paper 66-194
16.	M. H. Clarkson R. E. Field Jr. D. R. Keefer	Electron Temperatures in Several RF-Generated Plasmas		AIAA Jour. 4, 546-7 (1966)
17.	D. B. Henriksen	Analysis of Field Distributions in an Electrodeless Discharge	University of Florida	MS Thesis
18.	H. Schluter	Untersuchungen an Einer Hochfrequenzapparatur Mit Statischem Magnetfeld	Max-Planck-Inst. fur Physik	Zeitschr.f.Naturforschg. 15a, 3, 281 (1960)
19.	V. H. Schluter	Uber Hochfrequenzetladungen Mit Statischem Magnetfeld	Max-Planck-Inst. fur Physik	

III. INDUCTIVE RF DISCHARGES (Cont'd)

	Author	Title	Originating Agency	Remarks
20.	G. Lisitano M. Tutter	Mickrowellenmessungen an Einer Hochfrequenzerregten Gasentladung		Zeitschr.f.Naturfor. 16a, 692-9 (1961)
21.	H. J. Strausz	Untersuchungen Uber Den Existenzebereich der Elektrodenlosen Ringentladung		Ann.Physik Ser. 7, Vol.1, 281-95 (1958)
22.	H. Hausler	Der Einflusz Einer Hochfrequenz Gasentladung auf die Frequenz einer Selbsterregten Kurzwellenschwingstufe		Zeitschr.f.Angew. Physik 9, 60-68 (1957)
23.	G. Birkhoff	Messung der Elektrischen Vorgange Innerhalf einer Hochfrequenz-Ringentladung		Zeitschr.f.Angew. Physik.10, 204-6 (1958)
24.	J. J. Thomson	The Electrodeless Discharge through Gases		Philos.Mag.Ser. 7, Vol.4, 1128-60 (1927)
25.	V. H. Fetz H. Oechsner	Uber die Untersuchung eines Hochfrequenzplasmas mit Hilfe einer Gleichstromsonde		Zeitschr.f.Angew. Physik 12, 250-53 (1960)
26.	A. V. Donskoi S. V. Dresvin D. G. Ratnikow	High Frequency Induction Discharge in a Chamber with Water-Cooled Metal Walls		Teplofiz.Vysokikh Temp.3, 922-3 (1965)
27.	H. V. Eckert	Diffusion Theory of the Electrodeless Ring Discharge		Jour.Appl.Phys.33, 2788- (1962)
28.	D. D. Hollister	Self-Diagnosing Electrodeless Plasma Generator	Aeronutronic Div., Philco-Ford Corp.	IEEE Trans.,Antennas & Propagation, Vol. AP-13, 134-40 (1965)
29.	T. B. Reed	The Induction-Coupled Plasma Torch	Lincoln Laboratory Mass.Inst.of Tech.	Jour.Appl.Phys.32, 821-4 (1961)
30.	J. J. Thomson	On the Discharge of Electricity through Exhausted Tubes without Electrons		Philos.Mag.Ser. 5, Vol. 32, 320-464 (1891)

III. INDUCTIVE RF DISCHARGES (Cont'd)

	Author	Title	Orginating Agency	Remarks
31.	R. L. Chuan	Plasma Heating of Supersonic Airstream	Univ. of Southern Calif.	Phys. of Fluids, Vol. 1, (1958)
32.	M. D. Raizer A. G. Frank V. F. Kitaeva	Localization of a High-Frequency Induction Discharge		Sov.Phys.Tech.Phys. 8, 752-8 (1964)
33.	N. A. Bobyrev	Dynamic Stabilization of a Current-Carrying Plasma Cylinder		Sov.Phys.Tech.Phys. 11, 316-23 (1966)
34.	E.D.Andryukhina S.E.Grebenshchikov M.S.Rabinovich M.D.Raizer A.Ya.Safronov I.S.Shpigel'	Certain Features of Induction Gaseous Discharges		Sov.Phys.Tech.Phys. 5, 497-505 (1960)
35.	N.A.Bobyrev O.I.Fedyanin	A Study of the Initial Stage of a High-Current Electrodeless Discharge		Sov.Phys.Tech.Phys. 6, 959-64 (1962)
36.	J. Kunz	Theory of Electromagnetic and Electrostatic Induction in Electrodeless Discharge		Philos.Mag. 13, 964-75 (1932)
37.	T.A.El-Khalafawy V.A.Souprunenko A.M.Ternopole M.A.Bourham	Plasma Wave Excitation and Thermalization in an Electrodeless Induction Discharge		Phys. Letters, Vol. 24A, 233-4 (1967)
38.	R.E.Rovinskii L.E.Belousova V.A.Gruzdev	The Geometry of Electrodeless Discharges Induced in Inert Gases		Teplofizika Vysokikh Temp.4, 328-35 (1966)
39.	R.E.Rovinskii V. A. Gruzdev I.P.Shirokova	Energy Balance of a Stationary Induced Discharge		Teplofizika Vysokikh Temp.4, 35-9 (1966)

III. INDUCTIVE RF DISCHARGES (Cont'd)

	Author	Title	Originating Agency	Remarks
40.	D.D.Hollister	A Study of Some of the Properties of an RF Generated Plasma		Bull.Am.Phys.Soc.7, 373 (1962)
41.	D.D.Hollister	The Electrodeless Ring Discharge in Gases		Bull.Am.Phys.Soc.7, 441 (1962)
42.	V.K.Goykhman V.M.Gol'dfarb Z.S.Tsukernik	Radiation of Argon, Oxygen, Nitrogen and Air High-Frequency Discharge Plasmas at Atmospheric Pressure		Vsesoyuznaya Konferentsiya po Fizike Nizkotemperaturnoy Plazmy,Kiev (1966)
43.	D.D.Hollister	On the Electrodeless Arc in High Pressure Air		Phys.Letters Sept(1968)
44.	H.V.Eckert	Analytical Solution of the Energy Balance Equation for Thermal Induction Plasmas in Argon		AIAA Fluid & Plasma Dynamics Conf. June (1968)
45.	J.A.Sprouse	Coupling Mechanism Between RF Excited Coils and Conductive Media		AIAA Fluid & Plasma Dynamics Conf. June (1968)

III-A. LOW PRESSURE INDUCTIVE RF DISCHARGES

	Author	Title	Originating Agency	Remarks
1.	R.L.Barger J.D.Brooks W.D.Beasley	The Design and Operation of a Continuous Flow Electrodeless Plasma Accelerator	Langley Res. Ctr.	Feb. 1962
2.	D.B.Miller	Acceleration of Plasmas by Inductively Generated Electro-Magnetic Fields	Univ. of Michigan Dept.of Elec.Engrg.	Final Rept.Contr.No. AF 19(604)-4557 USAF Bedford, Mass.April(1961)
3.	F.Cabannes	Etude de la Decharge Electrique par Induction dans les Gaz Rares	Annales de Physique	Annales de Physique, Vol.10,1026-78(1955)
4.	V.G.Lisitano M.Tutter	Mikrowellenmessungen an einer Hochfrequenzerregten Gasentladung	Aus dem Max-Planck Inst. fur Physik und Astrophysik, Muchen	Zs.f.Naturforschg. 16a, 692-9 (1961)
5.	H.Schluter	Rekombination und Ionisation in einer Stationaren Hochfrequenzentladung		Zs.f.Naturforschg. 18a,439-46 (1963)
6.	J.R.Peterson C.J.Cook O.Heinz	Beam Extraction from an RF Ion Source	Stanford Res. Inst. Menlo Park, Calif.	(1960)
7.	K.Korper	Hochfrequenzheizung eines Plasmazylinders in einem Axialen Magnetfeld		Zeit.fur.Naturforschg. 15a,235-43 (1960)
8.	G.Birkhoff	Messung der Elektrischen Vorgange Innerhalf einer Hochfrequenz-Ringentladung		As.f.Angew Physik, 10, 204-6 (1958)
9.	E.Hausler	Der Einflusz einer Hochfrequenz-Gasentlandung auf die Frequenz einer Selbsterregten Kurzwellenschwingstufe		Zs.f.Angew.Physik, 9, 60-8 (1957)
10.	H.Schulter	Untersuchungen an Balmerspektrem Bei einer Hockfrequenzentladung	Max-Planck-Institute fur Physik und Astro-Physik, Munchen 23	Phd.Dissertation, Univ. of Munich (1960)

III-A. LOW PRESSURE INDUCTIVE RF DISCHARGES (Cont'd)

	Author	Title	Originating Agency	Remarks
11.	M.C.Gourdine D.D.Hollister	Investigation of the Conductivity of a Ring Discharge	Plasmadyne Corp., Santa Ana, Calif.	
12.	V.K.Korper	Hochfrequenzheizung eines Plasmazylinders in einem Axialen Magnetfeld		Zs.f.Naturforschg. 15a, 235-43 (1960)
13.	K.Chandraker A.Von Engel	The Starting Mechanism of the First Stage of the Ring Discharge		Proc.Royal Soc.A, 284, 442-54 (1965)
14.	K.Chandraker A.Von Engel	Evolution of the High Frequency Ring Discharge	Clarendon Lab, Oxford Univ.	Paper at VII Conf. on Phen.in Ion Gases, Belgrad (1965)
15.	H.H.Bromer F.Dobler	Elektronendichtenbestimmunger mit einer Mikrowellenbrucke in Schwach Ionislerten Plasmen		Zs.f.Naturforschg. 20a, 599-606 (1965)
16.	B.Pfeiffer	Skin Effect in Anisotropic Plasmas and Resonance Excitation of Electron-Cyclotron Waves I, Theory	Swiss Fed. Inst. of Tech.	Jour.Appl.Phys.37, 1624-27 (1966)
17.	B.Pfeiffer	Skin Effect in Anisotropic Plasmas and Resonance Excitation of Electron-Cyclotron Waves II, Experiments	Swiss Fed.Inst. of Tech.	Jour.Appl.Phys.37, 1628-33 (1966)
18.	H.Schluter C.J.Ransom	Radio Frequency Plasmas at Hybrid Ion-Electron Resonance	Dept.of Physics, The Univ. of Texas,Austin	Annals of Phys.33, 360-80, (1965)
19.	K.Chandraker S.M.Deval	Electron Temperature in a High Frequency Ring Discharge		Proc.8th Int'l.Conf. Phen.in Ionized Gases, Vienna (1967)
20.	A.D.Stokes	The Ring Discharge Environment for Total Radiation Intensity and Thermal Conductivity Measurements		Proc.8th Int'l.Conf. Phen.in Ionized Gases, Vienna (1967)
21.	C.G.Smith	Studies of a Ring Discharge		Phys.Rev.59,997-1004(1941)

III-B. HIGH PRESSURE INDUCTIVE RF DISCHARGES

	Author	Title	Originating Agency	Remarks
1.	A.A.Duzonvanikov	An Investigation of High Frequency Discharge in the Bands from 1.5 to 15 MC III	News of the Inst. of Higher Learning, Phys. No.6,	Transl.by McGraw-Hill (1960) pp 64-70
2.	M.Clement T.Consoli C.Gormezano R.Ricateau M.Weill	Experimental Study of an RF Argon	Vie Conf.Intern.sur les Phen.d'Ion dans les Gaz, Paris 8	Juillet 1963
3.	T.B.Reed	Heat-Transfer Intensity from Induction Plasma Flames and Oxy-Hydrogen Flames		J. Appl.Phys.34, 2266-9 (1963)
4.	R.V.Mitin K.K.Pryadkin	A High-Pressure Electrodeless Discharge		Sov.Phys.Tech.Phys. 10, 933-6 (1966)
5.	A.V.Donskoi S.V.Dresvin K.K.Voronin F.K.Volynets	Some Features of the Processes of Growth of Refractory Crystals in High-Frequency Plasma Torches		Teplofizika Vysokikh Temp.3, 627-31 (1965)
6.	P.D.Johnston	Temperature and Electron Density Measurements in an RF Discharge in Argon		Phys.Letters 20, 499-500 (1966)
7.	V.M.Gol'dfarb S.V.Dresvin	Optical Investigation of the Distribution of Temperature and Electron Density in an Argon Plasma		Teplofizika Vysokikh Temp.3, 333-9 (1965)
8.	R.V.Mitin K.K.Pryadkin	Magnetic Properties of a High Pressure Electrodeless Discharge		Sov.Phys.Tech.Phys. 11, 672-6 (1966)
9.	M.P.Freeman J.D.Chase	Energy Transfer Mechanism and Typical Operating Characteristics for the Thermal Radio Frequency Plasma Generator	Central Res. Div. American Cyanamid Co.	

III-B. HIGH PRESSURE INDUCTIVE RF DISCHARGES (Cont'd)

	Author	Title	Originating Agency	Remarks
10.	R.V.Mitin K.K.Pryadkin	Magnetic Field Influence on High-Pressure Electrodeless Discharge Plasma		Proc.8th Int'l Conf. Phen.in Ionized Gases 249, (1967) Vienna
11.	D.W.Hughes E.R.Wooding	Electrical Conductivity of the Plasma in a H-Mode RF Plasma Torch		Proc.8th Int'l Conf. Phen.in Ionized Gases 238, (1967) Vienna
12.	D.W.Hughes E.R.Wooding	Temperature Distribution in an H-Mode RF Plasma Torch		Phys.Letters, Vol.24A 70-71 (1967)
13.	H.W.Emmons	Experiments on High Pressure Plasmas		Proc.11th Int'l Cong. Appl.Mechanics, 933-9 (1964)Munich
14.	V.N.Soshnikov E.S.Trekhov	The Theory of High-Frequency Vortex Discharges at High Pressure		Teplofizika Vysokikh Temp.4, 166-72(1966)

III-C. PULSED INDUCTIVE RF DISCHARGES

	Author	Title	Originating Agency	Remarks
1.	Zaidel, Malyshev, Shreider	Spectroscopic Diagnostic Techniques for Hot Plasmas		Sov.Phys.Tech.Phys. 6, (1961)
2.	Stepanov Kitsenko	Excitation of Electromagnetic Waves in a Magnetoactive Plasma by a Beam of Charged Particles		" "
3.	Stepanov Kitsenko	Cyclotron Instability in a Plasma		" "
4.	Velikhov	Stability of a Plasma-Vacuum Boundary		" "
5.	Sanochkin	Thermal Ionization and Electrical Conductivity of Gas Mixtures		" "
6.	Lubanov Tulinova	On the Behavior of an Electron Beam Within a Betatron during the Injection Period		" "
7.	Popov	Investigation of Current Density Distribution over the Cross Section of an Ion Beam		" "
8.	Fateev	Free Motion of Particles in Fixed-Field Alternating-Gradient Accelerators		" "
9.	Nazarov	Propagation of Ion Cyclotron Waves in a Plasma		" "
10.	Volkov/Tolok/ Sinel'nikov	Investigation of Electrodeless Discharge in a Mirror System with a Supplementary Azimuthal Magnetic Field		" " pp 185-7

III-C. PULSED INDUCTIVE RF DISCHARGES (Cont'd)

	Author	Title	Originating Agency	Remarks
11.	Demirkhanov Khodyrev Leont'ev T.I.Gutkin	Interaction of High Frequency Electromagnetic Fields with Plasma	Translated at Convair Library by G.Duffy AE 61-0003-12	Conf.Plasma Phys. & Thermon.Reactions, Salzburg, 1961
12.	H.Beerwald	Untersuchung des Aufbaues einer Elektrodenlosen Ringentladung mit Hilfe von Mikrowellen	Inst.fur Plasma Physik Kernforschungsanlage, Julich, Deutschland	Proc.5th Int'l Conf. Ionization Phenom. in Gases
13.	R.Treat	Ionization in an Electrodeless Discharge	ASD-ASTIA 256 216 AFOSR	TN-031-655, Contr. AF 49(638)-655 (1961)
14.	G.Malesani	Experiments on Breakdown Phenomena in Theta-Pinch	Univ. of Padua, Italy	6th Int'l Conf. on Ioniz.Phen.in Gases, Paris, 1963
15.	V.W.Hertz A.Koller A.Michel H.Schindler	Elecktrodenlose Drei-Spulenplasmakanone		Zs.f.Naturforschg. 18a, 1237-9 (1963)
16.	P.Bogen E.Hintz	Investigations on a Pulsed Electrodeless Ring Discharge with Magnetic Bias Fields of Different Amplitudes		5th Int'l Conf. on Ioniz.Phen.in Gases, Munich, 1961

IV. MICROWAVE DISCHARGES

	Author	Title	Originating Agency	Remarks
1.	W.Scharfman T.Morita	Focused Microwave Technique for Measurement of the Ionization Rate and Collision Frequency	Stanford Res.Inst.	Feb. 1964
2.	W.B.Cottingham S.J.Buchsbaum	Diffusion in a Microwave Plasma in the Presence of Turbulent Flow	Bell Telephone Lab	Oct. 1964
3.	P.P.Keenan	Microwave Breakdown of Antenna Radomes at High Altitudes	G.E.Elect. Eff. of Re-entry	1961
4.	A.V.Phelps O.T.Fundingsland	Microwave Determination of the Probability of Collision of Slow Electrons in Gases	Mass. Inst. of Tech.	Phys.Rev. July 1951
5.	B.Lax W.P.Allis S.C.Brown	The Effect of Magnetic Field on the Breakdown of Gases at Microwave Frequencies	" "	" " Dec. 1950
6.	A.D.MacDonald S.C.Brown	Electron Diffusion in a Spherical Cavity	" "	" " Mar. 1950
7.	L.J.Varnerin S.C.Brown	Microwave Determinations of Average Electron Energies and the First Townsend Coefficient in Hydrogen	" "	" " Sept. 1950
8.	J.W.Lathrop S. C. Brown	The Relationship of Pulsed to C-W Breakdown of Gas at Microwave Frequencies	" "	" " Dec. 1949
9.	A.D.MacDonald D.D.Betts	High Frequency Gas Discharge Breakdown in Neon	" "	" " May 1952
10.	A.D.MacDonald S.C.Brown	High Frequency Gas Discharge Breakdown in Hydrogen	" "	" " Aug. 1949

IV. MICROWAVE DISCHARGES (Cont'd)

	Author	Title	Originating Agency	Remarks
11.	E.Everhart S.C.Brown	The Admittance of High Frequency Gas Discharges	Mass. Inst. of Tech.	Phys.Rev., May 1949
12.	A.D.MacDonald S.C.Brown	High Frequency Gas Discharge Breakdown in Helium	" "	" " Oct. 1948
13.	M.A.Herlin	Electrical Breakdown of a Gas between Coaxial Cylinders at Microwave Frequencies	" "	" " June 1948
14.	M.A.Herlin S.C.Brown	Microwave Breakdown of a Gas in a Cylindrical Cavity of Arbitrary Length	" "	" " Aug. 1948
15.	M.A.Herlin S.C.Brown	Breakdown of a Gas at Microwave Frequencies	" "	" " April 1948
16.	J.L.Hirshfield S.C.Brown	Microwave Method for Measuring the Probability of Electrons in a Gas	" "	" " June 1958
17.	K.B.Persson	Limitations of the Microwave Cavity Method of Measuring Electron Densities in a Plasma	General Electric Co.	" " Jan. 1957

Unclassified
Security Classification

DOCUMENT CONTROL DATA - R & D

(Security classification of title, body of abstract and indexing annotation must be entered when the overall report is classified)

1. ORIGINATING ACTIVITY (Corporate author) Aeronutronic Division Philco-Ford Corporation Newport Beach, California 92663	2a. REPORT SECURITY CLASSIFICATION Unclassified 2b. GROUP

3. REPORT TITLE

AN INVESTIGATION OF THE HIGH PRESSURE RLECTRODELESS ARC IN AIR

4. DESCRIPTIVE NOTES (Type of report and inclusive dates)

5. AUTHOR(S) (First name, middle initial, last name)

Donald D. Hollister

6. REPORT DATE February 1969	7a. TOTAL NO. OF PAGES	7b. NO. OF REFS
8a. CONTRACT OR GRANT NO. F33615-68-C-1137 b. PROJECT NO. C018 c. d.	9a. ORIGINATOR'S REPORT NUMBER(S) 9b. OTHER REPORT NO(S) (Any other numbers that may be assigned this report) AFFDL-TR-68-160	

10. DISTRIBUTION STATEMENT This document has been approved for public release and sale; its distribution is unlimited.

11. SUPPLEMENTARY NOTES	12. SPONSORING MILITARY ACTIVITY Air Force Flight Dynamics Laboratory Wright-Patterson AFB, Ohio 45433

13. ABSTRACT

The equation of energy balance for the high pressure electrodeless arc in air is numerically integrated and agreement with the Thomason Eddy Current theory is found. Scaling laws are derived for purposes of engineering analysis and design. Conceptual designs for high pressure electrodeless and DC arc heaters are compared at the fifty megawatt level in a flowing plasma system. The electrodeless technique is found to be somewhat more efficient than the DC technique in this comparison.

DD FORM 1 NOV 65 1473

Unclassified
Security Classification

Security Classification

14. KEY WORDS	LINK A		LINK B		LINK C	
	ROLE	WT	ROLE	WT	ROLE	WT

Security Classification